

Historic, Archive Document

Do not assume content reflects current scientific knowledge, policies, or practices.

Reserve
aM911
.15

INVESTIGATION OF RHEOLOGICAL PROPERTIES OF AERIAL-DELIVERED FIRE RETARDANT

Final Report

to

UNITED STATES DEPARTMENT OF AGRICULTURE
FOREST SERVICE

U.S. INTERMOUNTAIN FOREST & RANGE EXPERIMENT STATION

A report of research performed under the
auspices of the Intermountain Forest and
Range Experiment Station, Ogden, Utah.



Shock Hydrodynamics

A DIVISION OF **Whittaker**
CORPORATION

AD-33 Bookplate
(1-63)

NATIONAL

A
G
R
I
C
U
L
T
U
R
A
L



LIBRARY

24510

INVESTIGATION OF RHEOLOGICAL PROPERTIES
OF AERIAL-DELIVERED FIRE RETARDANT *(D:D #6)*

FINAL REPORT

(8890-04) *(D:D #C)*

by

W.H. Anderson

R.E. Brown

K.G. Kato

N.A. Louie

et al. *J*

500 Contract 26-3198,

Period Covered: 26 June 1973 Through 25 June 1974.

25 June 1974

Intermountain Forest & Range Experiment Station

USDA Forest Service

Ogden, Utah 84401

The research conducted under this contract is a part of a program to improve fire control technology, specifically through the use of fire retardant chemicals and delivery systems whose chemical and/or design characteristics are tailored to fuel and fire situation needs. This program is being conducted at the Northern Forest Fire Laboratory. Information or questions regarding these studies should be directed to the:

Northern Forest Fire Laboratory
Drawer G
Missoula, Montana 59801

SHOCK HYDRODYNAMICS DIVISION, WHITTAKER CORPORATION U. S. DEPT. OF AGRICULTURE
15010 Ventura Boulevard, Sherman Oaks, California 91403 NATIONAL AGRICULTURAL LIBRARY

SEP 28 1977

CATALOGING - PREP.

ACKNOWLEDGEMENT

The authors wish to acknowledge Dr. P. J. Blatz who derived Eq. (31) and (34), Mr. R. R. Randall who conducted the gas gun experiments, Mr. G. E. Taylor and Mr. J. Dalby who conducted many of the rheological property measurements, Mrs. Connie Oh who performed the computer computations, and Mr. Charles W. George, Contract Monitor, for several helpful comments.

TABLE OF CONTENTS

	Page
SUMMARY	xi
1. INTRODUCTION	1
2. NATURE OF THE PROBLEM	3
2.1 Background	3
2.2 Fire Suppression by Chemical Retardants	4
2.2.1 Water-Modifying Additives	4
2.2.2 Mechanism of Cellulose Ignition	4
2.2.3 Flame-Inhibiting Additives	5
2.3 Dissemination Sequence of Aerial-Delivered Retardant .	5
3. LIQUID BREAKUP THEORY	7
3.1 Drop Breakup Mechanism and Breakup Time	8
3.2 Droplet Size	11
3.3 Effect of Geometry and Nonidealized Fluid Properties .	14
4. BREAKUP THEORY OF LIQUID RETARDANTS	16
4.1 Surface Erosion Breakup	16
4.1.1 Effect of Non-Newtonian Viscosity	19
4.1.2 Effect of Fluid Elasticity	20
4.1.3 Secondary Droplet Breakup	23
4.2 Deformation (Taylor Instability) Breakup	23
4.2.1 Deformation Rate of the Liquid	24
4.2.2 Growth Rate of the Instabilities	26
4.2.3 Solution of the Equations	28
5. MEASUREMENT OF RHEOLOGICAL PROPERTIES	32
5.1 Rotational Viscometer Technique	32
5.2 Experimental Results	34
5.2.1 Data Correction	34
5.3 Discussion of Experimental Results	40
5.3.1 Effect of Shear Rate	48
5.3.2 Estimated Yield Stress	48

TABLE OF CONTENTS (Continued)

		Page
5.4	Capillary Viscometer Technique	50
5.5	Experimental Results and Discussion	51
	5.5.1 Phos-Chek XA Solution	51
	5.5.2 Fire-Trol Solutions	55
	5.5.3 Comparison of Data	60
5.6	Effective Viscosity of Fire Retardant Solutions	60
5.7	Surface Tension Measurements	64
5.8	Effect of Retardant Concentration on Rheological Properties	65
	5.8.1 Effect on Viscosity and Yield Stress	65
	5.8.2 Effect on Surface Tension	69
6.	SHOCK TUBE STUDIES	70
6.1	Introduction	70
6.2	Design of the Shock Tube	70
	6.2.1 Shock Tube Instrumentation	72
	6.2.2 Calculation of Wind Velocity	73
6.3	Experimental Results	75
	6.3.1 General Behavior of Drop Deformation and Breakup	77
	6.3.2 Breakup Time Initiation	84
6.4	Correlation With Theory	85
6.5	Droplet Size Studies	87
	6.5.1 Test Results	88
7.	CONTROLLED LIQUID INJECTION STUDIES	90
7.1	Experimental Technique	90
7.2	Observations	90
8.	LIQUID BREAKUP ANALYSIS AND CORRELATION	93
8.1	Initial Breakup by Taylor Instability	94
	8.1.1 Evaluation of the Breakup Equation Constants	94

TABLE OF CONTENTS (Continued)

	Page
8.1.2 Computational Results	98
8.2 Liquid Breakup by Surface Erosion	108
8.2.1 Average Droplet Size	108
8.2.2 Particle Size Distribution	111
8.3 Further Discussion	111
8.3.1 Droplet Settling	113
8.3.2 Effect of Atmospheric Properties	114
8.3.3 Ground Contour Pattern	114
9. DISTRIBUTION OF FIRE RETARDANTS ON FUELS	118
9.1 Wetting of Fuels by Water and Retardants	118
9.1.1 Fuel Characteristics	118
9.1.2 General Mechanism of Fuel Wetting	119
9.1.3 Effect of Drop Size and Impact Velocity	121
9.1.4 Effects of Physical and Rheological Properties	123
9.1.5 Vertical Fuel Coverage	124
9.2 Experimental Studies	125
9.2.1 Static Drop Spread	125
9.2.2 Drop Spread from Impact	126
9.2.3 Effect of Drop Size	130
9.2.4 Wetting Out of Fuels by Retardants	134
10. CONCLUSIONS AND RECOMMENDATIONS	135
10.1 Test Planning	137
10.1.1 Particle Size Measurement	138
REFERENCES	139
APPENDIX I. GLOSSARY OF TERMS	143
APPENDIX II. DERIVATION OF EFFECTIVE VISCOSITY EQUATION	146
APPENDIX III. DERIVATION OF LIQUID CYLINDER DEFORMATION RATE EQUATIONS	148

FIGURE	TITLE	PAGE
1	Comparison of Experiment Drop Breakup Times With the Andersen-Wolfe Equation	10
2	Cumulative Percent Mass vs Mass Median Diameter for Liquid Drop Breakup	12
3	Comparison of Experimental Average Mass Droplet Sizes With the Andersen-Wolfe Theory	13
4	Apparent Viscosity of Phos-Chek XA as a Function of Shear Rate (Uncorrected)	35
5	Apparent Viscosity of Fire-Trol 100 as a Function of Shear Rate (Uncorrected)	36
6	Apparent Viscosity of Fire-Trol 931 as a Function of Shear Rate (Uncorrected)	37
7	Apparent Viscosity of Phos-Chek XA Retardant Solutions as a Function of Shear Rate	38
8	Apparent Viscosity of Fire-Trol 100 Retardant Solutions as a Function of Shear Rate	39
9	Model of Concentric Cylinder Viscometer	40
10	Corrected Apparent Viscosity vs Shear Rate for Phos-Chek XA at 20° C and 30° C	41
11	Corrected Apparent Viscosity vs Shear Rate for Fire-Trol 100 at 20° C and 30° C	42
12	Corrected Apparent Viscosity vs Shear Rate for Fire-Trol 931 at 20° C	43
13	Comparison of the Corrected Viscosity as a Function of Shear Rate of the Three Fire Retardant Solutions	44
14	Power Law Plot of Shear Stress vs Shear Rate for Phos-Chek XA at 20° C	45
15	Power Law Plot of Shear Stress vs Shear Rate for Fire-Trol 100 at 20° C	46
16	Power Law Plot of Shear Stress vs Shear Rate for Fire-Trol 931 at 20° C	47
17	Experimental Viscosity vs Shear Rate for Phos-Chek XA at 25° C Determined by the High Pressure Capillary Tube Technique	53

FIGURE	TITLE	PAGE
18	Viscosity vs Shear Rate for Phos-Chek XA at Various Temperatures from High Pressure Capillary Viscometer Experiments	54
19	Plot of Pressure vs L/R Ratio for Phos-Chek XA at 25° C at Various Shear Rates	56
20	Recoverable Shear of Phos-Chek XA as a Function of Shear Rate at 25° C	57
21	Viscosity vs Shear Rate for Fire-Trol 100 at 25° C from High Pressure Capillary Viscometer Experiments . . .	58
22	Viscosity vs Shear Rate for Fire-Trol 931 at 25° C from High Pressure Capillary Viscometer Experiments . . .	59
23	Comparison of the Viscosity vs Shear Rate Curves of the Fire Retardant Solutions at 25° C	61
24	Effective Viscosity vs Shear Rate of Phos-Chek XA	63
25	Corrected Viscosity of Phos-Chek XA as a Function of Concentration and Shear Rate	66
26	Shear Stress as a Function of Corrected Shear Rate for Five Aqueous Concentrations of Phos-Chek XA	67
27	Shock Tube Used to Study the Aerodynamic Breakup of Liquid Fire Retardants	71
28	Shock Tube Instrumentation	74
29	Oscilloscope Record of Pressure Transducer Signal	74
30	Shock Wave Flow Velocity vs Shock Overpressure for Air . .	76
31	Aerodynamic Breakup Sequence of Liquid Retardant Drops in a Shock Tube with Average Wind Velocity of 89 ft/sec	78
32	Aerodynamic Breakup at 146 ft/sec	80
33	Aerodynamic Breakup at 284 ft/sec	82
34	Experimental Time to Initiate Drop Breakup in the Shock Tube	86
35	Test Setup for Liquid Jet Experiments	91

FIGURE	TITLE	PAGE
36	Liquid Jet Injected Into Air Through a 30mm Orifice	92
37	Computed Taylor Breakup Characteristics of Liquid Retardants in the CL-215 Aircraft	100
38	Computed Effect of Aircraft Velocity on the Taylor Breakup Characteristics of Phos-Chek XA from the CL-215 Aircraft	101
39	Computed Effect of Tank Length on the Liquid Breakup Characteristics	102
40	Computed Effect of Tank Radius on the Liquid Breakup Characteristics	103
41	Computed Effect of Tank Dimensions on the Taylor Breakup Characteristics of 2000 gallons of Phos-Chek XA	105
42	Computed Effect of Deformation Viscosity on the Liquid Breakup Characteristics	106
43	Computed Effect of Liquid Instability Viscosity on the Liquid Breakup Characteristics	107
44	Preliminary Theoretical Estimate of the Final Average Diameter of the Droplets Produced by the Aerodynamic Breakup of Liquid Fire Retardants	110
45	Preliminary Theoretical Estimate of the Final Size Distribution of the Droplets Produced by the Aerodynamic Breakup of Liquid Fire Retardants	112
46	Correlation Between Ground Pattern and Effective Viscosity of Retardants Dropped from the TBM Aircraft	117
47	Static Spread of Liquid Retardant Drops Over Various Flat Material Surfaces	127
48	Static Spread of Liquid Retardant Drops Over Various Flat Material Surfaces	128
49	Static Spread of Liquid Retardant Over Flat and Inclined Plywood Surface	131
50	Dynamic Spread of Liquid Retardant Over Flat and Inclined Plywood Surface	131

FIGURE	TITLE	PAGE
51	Static and Dynamic Spread of Large Drops of Fire-Trol 100 Over Flat and Inclined Plywood Surface	132
52	Splotch Patterns of Single Drops of Fire Retardant on Plywood	133
53	Results of a Grah-Wilson Experiment on a Common Oak Branch	136

TABLE	TITLE	PAGE
I	Instrument Constants for the Haake Rotoviscometer	33
II	Corrected Surface Tension Estimates	64
III	Estimated Yield Stresses for Phos-Chek XA Mixtures in Water	68
IV	Surface Tension of Phos-Chek XA - Water Mixtures at 20° C	69
V	Computed Taylor Instability Breakup Characteristics of Phos-Chek XA	96
VI	Preliminary Computed Final Average Droplet Sizes Produced by the Surface Stripping of Liquid Retardants	109

Use of trade or firm names is for reader information only, and does not constitute endorsement by the U. S. Department of Agriculture of any commercial product or service.

SUMMARY

This report describes the results of an investigation whose purpose was to establish the relationships between the rheological properties of a liquid fire retardant and the aerial drop behavior, dispersion characteristics, and wetting-out properties of the retardant. Previous studies by the Forest Service and others have demonstrated that retardant rheology can have a significant effect on the behavior of the retardant in use.

The results of a literature survey on the current understanding of the aerodynamic breakup of liquids are summarized. It is shown that present understanding is largely limited to small drops and jets of Newtonian liquids, and has only limited applicability to the aerial breakup of large quantities of real retardants. The breakup of aerial delivered fire retardants is then discussed. The breakup occurs both by Taylor instability growth (following deformation) and surface erosion (peripheral stripping), and the retardants may be non-Newtonian and/or elastic in their flow behavior. Analytical models are developed that describe the aerodynamic deformation and breakup of the liquid in terms of the important system parameters and fluid properties-including aircraft velocity, tank and gating system and retardant rheology. The effects of non-Newtonian viscosity and fluid elasticity are contained in these models. It is shown that the combined effects of viscosity and fluid elasticity can be expressed in terms of an effective viscosity that controls the flow behavior of the liquid.

Experimental studies were conducted to measure the physical and rheological properties of the liquid retardants Phos-Chek XA, Fire-Trol 100 and Fire-Trol 931. Viscosity was measured as a function of shear rate using both a rotational viscometer, and a high pressure capillary tube viscometer. Fluid elasticity was measured using the capillary tube technique. It was found that the retardants all undergo shear thinning, i.e., their viscosity decreases with increase in shear rate up to some limiting value. Thus the normal (Brookfield) viscosity is not a reliable basis for judging the potential relative breakup characteristics (rate and particle size) of various retardants since aerodynamic breakup occurs at higher shear rates. However Phos-Chek-which is a gum thickened retardant - exhibits considerable elasticity while undergoing shear, and this causes its effective viscosity to remain high during breakup (the elastic stress increases with increasing shear rate). Gum thickened retardants thus differ significantly from clay thickened retardants - such as Fire-Trol 100-which are essentially non-elastic and shear thin to a relatively small viscosity while undergoing aerodynamic breakup. The effects of temperature, retardant mix concentration, and sample preparation on measured viscosity were also investigated, and measurements made of surface tension and yield strength of the retardants.

The aerodynamic breakup characteristics of the preceding three retardants and water were studied using shock tube and gas gun techniques. It was found that the ease of breakup (breakup rate) of the liquids increased in the order: Phos-Chek XA, Fire-Trol 100, Fire-Trol 931 and water. This order is in agreement with the order for decreasing effective liquid viscosity. The photographic sequences of the breakup process showed that Phos-Chek exhibits considerable stability toward aerodynamic breakup compared to the other liquids, and this increased stability is attributable to its elasticity.

An analysis was made of the breakup characteristics of the preceding chemical retardants and water under a variety of conditions, using the developed breakup models and experimental rheological property measurements. The effects of the controlling parameters such as aircraft velocity, tank and gating system, and rheological properties of the fuel are discussed in detail. It is shown that the aerodynamic deformation of the liquid preceding its Taylor breakup both increases the lateral extent of the liquid and gives an initial lateral velocity to the particles produced by Taylor breakup. The ground path width of the disseminated liquid particles should thus increase with increase in drop height-up to a limiting value. The Taylor breakup time of the ejected liquid decreases with increase in aircraft velocity and decrease in load size (particularly tank length), deformation viscosity and Taylor instability viscosity. The size of the particles produced by the Taylor breakup and surface erosion of the liquid decreases with increase in aircraft velocity and decrease in effective fluid viscosity (at the appropriate shear rate). Ground path length and area increase with increase in particle size. The relative ordering of the liquids for decreasing final particle size is Phos-Chek, Fire-Trol 100, Fire-Trol 931 and water. The effective viscosity for both Taylor breakup and surface erosion decreases in the same order. Small particles have smaller settling velocities and hence remain airborne for a longer time period than do larger particles. Thus evaporation rates are greater for small particles. Consequently the relative ordering of the liquids for increase in droplet impaction time and cloud settling time, and decrease in retardant recovery for the preceding retardants is the same as for decreasing particle size.

The results of a brief literature survey on fuel wetting by rain and fire retardants are summarized. The wetting of a fuel by aerial delivered fire retardant involves the impaction and splattering of individual liquid droplets or particles on portions of the fuel, followed by run (flow) and drip of the liquid over other portions of the fuel. Experimental studies were conducted to obtain information regarding the spreading and storage of fire retardants on typical fuels by both dynamic and static liquid droplet impaction. It is shown that the rheological properties of retardants can have a significant effect on both fuel wetting by impaction and subsequent liquid storage by the fuel.

On the basis of the results of the studies, it is concluded that the rheological properties can have a significant effect on aerial breakup and dispersion of fire retardants, and on their fuel-wetting characteristics. The models developed on the program appear to be adequate to explain most of the important aspects of the aerial dissemination of bulk fire retardant. A brief discussion is presented of recommended studies that could potentially improve the models and present understanding of aerial dissemination - including the measurement of the droplet sizes produced by various retardants under various dissemination conditions.

1. INTRODUCTION

Although the use of aircraft to deliver water or water-based retardants to large forest or other fires dates back only about 20 years, the advantages of such a delivery system were soon recognized and the airtanker drop of retardant rapidly became an important method of fire suppression. It was early known that the incorporation of various additives such as borate with the water could significantly increase the local efficiency of fire suppression, and it was rapidly found that the additives also had important effects on the breakup characteristics and dispersion behavior of the free-falling mass of liquid dropped from the aircraft. Since that time a variety of studies have been conducted by the Forest Service and others in an effort to develop better fire suppression additive materials, and improve the delivery of the retardant from the aircraft to the fire area. These studies have encompassed such things as mechanism studies of how retardants suppress fires, determination of the local physical form and specific quantity of the retardant needed to suppress various kinds of fires, effects of additive composition on fire suppression effectiveness, and effects of aircraft velocity, altitude and the method and rate of releasing the retardant on the dispersion pattern and ultimate ground recovery of the retardant.

The results of the preceding studies have been quite fruitful with regard to enhancing the effectiveness of suppressing fires by aircraft drops of retardants. For example, the studies have led to the development of improved retardant additives for use in suppressing fires, and have determined some of the better techniques for the release of the retardant from the aircraft. The studies have also helped to define the proper operating conditions (velocity and altitude) for the aircraft (within safety limits) at the time of the drop. However, although the studies have elucidated various ways of enhancing the effectiveness of suppressing fires by aircraft drops of retardants, they have also shown that in actuality many of the processes that occur from the time of drop of the retardant from the aircraft until its final settling on the fuel complex - including its distribution and retention on the fuel - are coupled and ultimately depend on the rheological properties of the retardant.

It is thus evident that further progress in the art of suppressing fires by the aerial drop of fire retardants including

- a. the development of improved retardants,
- b. design of better drop techniques (tank and gating systems),
- c. control of dispersion pattern,
- d. control of retardant distribution,
- e. retention and recovery,
- f. system and dispersion optimization, and
- g. ability for higher altitude drop

requires a knowledge of the pertinent rheological properties of fire retardants and an understanding of how these properties affect the various processes that occur from the time of drop until the dispersed retardant settles out on the fuel complex.

Recognizing this need, the U.S. Forest Service has sponsored a program with Shock Hydrodynamics, whose overall purpose was to establish the relationships between the rheological properties of a liquid fire retardant and the drop behavior, breakup and dispersion characteristics, and wetting-out properties of the retardant. This report describes the results of these studies.

In the succeeding sections-following a summary of the nature of the problem - there is first presented the results of a literature survey on current knowledge regarding the theory of the aerodynamic breakup of liquids. Theoretical studies are then described in which equations are developed for calculating the breakup characteristics of liquid fire retardant when dropped from an aircraft.* This is followed by sections which describe measurements which were made of various physical and rheological properties of conventional fire retardant solutions, and the aerodynamic breakup characteristics of these solutions using shock tube and gas gun techniques. The developed theory is then used to estimate the aerodynamic breakup characteristics of the various fire retardant solutions and water under various drop conditions, and the effects of the various system parameters and fluid properties examined in detail. A preliminary discussion is presented relating the liquid breakup and dispersion characteristics to the final ground pattern produced. The results of a brief literature review on the wetting out characteristics of typical fuels by rain and retardant solutions are then summarized, and the results of studies that were conducted to further understand the wetting out of fuels by retardants described. The report concludes with a brief discussion of further studies that could usefully be conducted to extend and test the developed concepts.

*The more important terms used throughout the report are summarized in Appendix I.

2. NATURE OF THE PROBLEM

2.1 BACKGROUND

The use of aircraft to deliver water or fire retardant chemicals on large fires was first instituted in the middle 1950's, and by 1960 the airtanker drop of retardant on inaccessible fires was a common practice. In the early drops ordinary water was primarily used as the fire retardant, but it was rapidly found that the addition of various substances, particularly borate, to the water could significantly increase the effectiveness of the retardant in suppressing the fire on a local level, as well as reduce evaporative loss of the water during its dispersion by increasing the particle size. Since that time there has been a more-or-less continuing effort to improve firefighting techniques using the airtanker drop, and there have been numerous revisions of mixture compositions and dissemination techniques in bringing the airtanker drop to its present relatively high degree of perfection. The use of aerial-delivered retardants steadily increased during that time. For example, it is reported¹ that in 1970 the USDA Forest Service, Bureau of Land Management and California Division of Forestry alone applied aerially about 17 million gallons of fire retardant whose raw cost was about 3.5 million dollars, and whose cost with mixing and delivery costs added was about 20 million dollars, or more than a dollar a gallon.

It is evident that with expenditures of this magnitude it is desirable that ultimately the most efficient additives be used in the retardant, and that the dissemination of the retardant be accomplished in the optimum manner with respect to its overall fire suppression ability. This requires information regarding the various processes that occur during the dissemination of the retardant and its suppression of a fire under various conditions. Over the years a variety of studies have been conducted that have helped to provide this information. It has been found for example, that certain fertilizer solutions have very good properties, both with respect to fire suppression and their aerial dissemination. The use of fertilizer solutions as fire retardants is of special importance since their use can simultaneously have beneficial effects on plant growth. Studies have also been conducted on the mechanism of fire suppression by retardant mixtures, and on the effects of various controllable parameters such as aircraft speed and altitude and the method and rate of the release of the retardant from the aircraft on the dissemination characteristics and ultimate ground recovery of the retardant. These latter studies have shown that the rheological properties of the retardant play a significant and in some cases dominant role in controlling the aerial dispersion of the retardant, and consequently the concentration and physical properties of the retardant as it interacts with the fuel complex on the ground.

It is evident then that in order to optimize the aerial dissemination of fire retardants currently in use, information must be acquired on the pertinent rheological properties of these retardants under the shear stress conditions experienced in free fall from an aircraft, and on the relationship of these properties to the various processes that control the breakup and dissemination behavior of the retardants. Future development of new additives would thus require consideration of the rheological properties of the retardant in conjunction with the fire suppression effectiveness of the material.

2.2 FIRE SUPPRESSION BY CHEMICAL RETARDANTS

The suppression of fire in a fuel complex by a chemical retardant consisting of water that contains various additives can be a very complex event, but the general principles are understood to some extent. The fire can either be extinguished directly by the retardant, or the retardant can be applied to fuel ahead of the advancing fire front and prevent or retard the burning. The direct extinguishment depends heavily on the conventional mechanisms by which water puts out a fire, i.e., cooling of the burning material, absorbing heat energy from the heat source, preventing heat from reaching the fuel, diluting the combustible gases around the fuel (with steam), etc. Various additives can influence extinguishment in this manner as well as in water retardment of the advancing fire front, while other additives can retard fire advancement irrespective of whether water is present when the fire reaches the area that has been treated with the retardant.

2.2.1 Water-Modifying Additives

Various substances can be added to the water that can make the water more efficient in suppressing fire. Retardants made up of water and these types of additives are called "short-term" retardants, in that their effectiveness depends largely on the extinguishing properties of water. The additives can act in various ways. Wetting agent additives such as certain detergents lower the surface tension of water so that the water can spread easier on a surface and also penetrate into smaller cracks. The water will also (undesirably) foam more easily. Water containing a wetting agent is sometimes called "wet water". Additives such as certain polymers and gums that increase the viscosity of water causes the water to stick or adhere more easily to the fuel, and to be retained in greater thickness. Water thickened with additives that increase the viscosity of the water is sometimes called "viscous water", "thickened water", "sticky water" or "slippery water". Some thickening additives in addition retain moisture and coat the fuel, while additives such as bentonite merely coat the fuel to exclude oxygen and retard the escape of the fuel pyrolysis products.

2.2.2 Mechanism of Cellulose Ignition

Although a variety of water-modifying additives are available and used in fire suppression work, some of the most important fire retardants in use today contain large amounts of fertilizer materials such as ammonium sulfate and ammonium phosphates. These materials suppress fires by an additional mechanism than the water-modifying additives, and their method is based on the alteration of the pyrolysis products formed when the fuel is heated.

Consider briefly the ignition of cellulosic-type of materials such as various woods. A recent literature review of the subject is given in reference 2, and a paper in reference 3 discusses certain particularly pertinent aspects of the subject. When such a material is subjected to an external heat source such as the hot gas flame and radiation from an adjacent fire, the surface temperature of the material begins to rise and moisture is driven out from near the surface of the material. As the surface temperature continues to rise, heat is slowly conducted into the interior of the material. When the surface temperature becomes greater than about 100°C , pyrolysis reactions begin to occur in the material, and small amounts of combustible gaseous products start to be evolved, together with water vapor and carbon dioxide. The pyrolysis reaction at this point is endothermic however and the gaseous products are largely non-combustible. During the endothermic surface pyrolysis, the wood slowly undergoes charring as the volatiles are driven from the material. As the surface temperature is further increased, the concentration of combustible gases and tars caused by pyrolysis increases, and when the temperature reaches about 350 to 600°C , depending on the material, the reaction in the evolving gases suddenly become exothermic - with the subsequent increase in temperature leading to ignition as the gases mix with and undergo further reaction with air.

The endothermic pyrolysis reactions preceding ignition drive off volatiles which causes the material to undergo charring, and the rate of heating can consequently affect the ignition characteristics of the material. Slow heating allows the material to be decomposed in a manner that the volatiles produced are relatively non-combustible, and this eventually results in a relatively thick char layer being produced. Ignition becomes more difficult as time proceeds in this case due to the loss of combustible volatiles, and the presence of the char layer which lowers the heat conduction rate into the material. On the other hand rapid heating causes rapid formation of combustible volatiles with consequent ignition occurring before the formation of extensive charring.

2.2.3 Flame-Inhibiting Additives

The manner in which the ammonium sulfate and ammonium phosphate materials suppress fire then, is based on their ability to cause pyrolysis to occur at a lower temperature so that the fuel undergoes charring without ignition. The overall effect is the formation of more char and less volatiles. The method of doing this is believed to result largely from chemical reaction between the solid retardants and the fuel pyrolysis products causing incombustible products to be formed, although there are also probably other mechanisms involved. Since the effectiveness of these kinds of additives depends on the composition of the additive and not on the presence of water they are called "long-term" retardants. However, the best results are obtained when the materials are applied in water solution and not in dry powder form, possibly because the material can coat the fuel complex more efficiently in this manner. The suppression effectiveness of the material depends both on the amount of material deposited on a unit area of the fuel, and on the amount of fuel coated by the material and the type of retardant.

2.3 DISSEMINATION SEQUENCE OF AERIAL-DELIVERED RETARDANT

The sequence of events that occur when a chemical retardant is delivered and applied to a fire by aircraft (e.g., an airtanker) is relatively straightforward, and its examination can serve to point out the inter-relation between the various events. Briefly, the tanker carries a load (e.g., 1400

gallons) of the premixed retardant to the fire area, the retardant being contained in one or more (usually 2-8) tanks or compartments. If two tanks are used the loads can be dropped either separately, sequentially, or together. The tanks can have various shapes and sizes, as well as various sized gates through which the retardant is dropped, and different mechanisms for operating the gate. Depending then on the dimensions of the tank and gating system and on the speed of the aircraft, the aircraft will travel for some distance during the release of the retardant from the aircraft, and this distance will help determine the pattern and area of the dispersed retardant when it reaches the ground. The speed and altitude of the aircraft during drop normally range between 90-150 knots and 75-300 feet, respectively, depending on the aircraft involved and the flying conditions. The attitude of the aircraft at the time of load release can also affect the trajectory of the free-falling retardant, and hence also the dispersion area and pattern.

As the gate is opened the bulk liquid retardant begins to undergo free-fall toward the ground, but with a trajectory whose initial angle is determined by the speed and attitude of the aircraft. As the moving liquid interacts with the atmosphere it is subjected to aerodynamic forces which deform (flatten) the liquid and simultaneously erodes (breaks) the liquid at its free surface into droplets (particles). The deforming bulk liquid subsequently breaks into many relatively large particles (globs), and these globs also undergo surface erosion as they continue their trajectory toward the ground. Depending on conditions, the larger droplets formed by surface erosion may subsequently undergo further breakup. In any event, however, as the eroded droplets are formed their forward motion is greatly retarded (due to increase in drag) so that their subsequent fall is usually close to vertical in the absence of a wind (the smaller eroded particles are carried by the wind). Both the breakup characteristics of the deforming liquid and the rate of surface erosion depend on the rheological properties of the liquid, particularly its effective viscosity under the local shear rate conditions.

During the breakup of the drop (bulk liquid) into globs, the trajectory of the drop may change to some extent due to increase in initial vertical velocity as the liquid exits the gate and to slight decrease in horizontal velocity due to frontal drag on the drop by aerodynamic forces. The subsequent trajectory of falling globs may likewise change with time, due to that fact that as a liquid glob proceeds through the atmosphere it gets smaller (which may decrease its velocity) until it either impacts the ground or all of the glob has been broken (eroded) into droplets. In any event the path length of the disseminated liquid will depend primarily on the exit time of the liquid from the aircraft, and the rate of aerodynamic breakup of the falling liquid - which depends on the rheological properties of the liquid. The concentration of disseminated liquid is not uniform over the entire path length, which in typical cases may be about 300 to 800 feet, depending on various factors. The concentration is usually lowest over about the first third of the dispersion path length, due to the fact that a finite time is required for all of the liquid to leave the aircraft and the amount of liquid surface exposed to erosion is initially relatively small. The concentration then increases to a maximum value, and then drops off sharply as the last remainder of the individual globs is broken up. The concentration of dispersed retardant needed in fire fighting application depends on several factors, but in a typical case may be two or more gallons per one hundred square feet of ground area.

The droplets formed by the surface erosion reach their terminal vertical fall velocity rapidly, and as they descend the droplet cloud undergoes spreading due to diffusion, downwash of the aircraft and wind. It has been found that wind speed and the settling time of the droplets are usually the strongest lateral area coverage parameters. The settling time depends on drop height, and also on particle size, shape and density. Thickened and elastic (gummed) materials reach the ground in a more coherent mass and in a shorter time than plain water. Thus gum thickened retardants can be used to permit higher and therefore safer drops without decreasing the effectiveness (concentration) of the dispersed retardant. The extent of evaporation of the dispersed liquid also depends on the settling time of the droplets, as well as on their size and viscosity.

The aerodynamic breakup of a liquid retardant glob produces a distribution of droplet sizes, and these different sized droplets descent at different rates. In general, large particles travel faster than smaller ones, but the extent that the particles undergo deformation (flattening) during descent also enters in since particle shape helps determine the value of the drag coefficient of the particle. The extent of deformation of a droplet of a specified size will depend on the physical properties of the droplet, particularly its surface tension and viscosity. Since the droplets descend at different rates, the settling of the dispersed liquid cloud occurs over a finite time, e.g., 5 to 30 seconds after the first particles reach the ground. As the retardant droplets settle they interact with and coat the fuel complex, and the nature of this interaction and coating depends both on the rheological properties of the retardant and on the particle size. The nature of these processes will be considered in more detail later.

3. LIQUID BREAKUP THEORY

In view of the importance of the aerodynamic breakup characteristics of the retardant on the area coverage, concentration and recovery of the dispersed retardant at ground level, and of the rheological properties of the retardant on its breakup characteristics, it is useful to review some of the present understanding of liquid breakup theory and the role of the physical properties of the liquid on the breakup process. More detailed application of some of this work will be considered later.

The aerodynamic breakup of liquids to form droplets is a complex process, and in the past has been subjected to considerable study. Most of these studies were devoted to the breakup of Newtonian liquids with well defined initial geometries such as drops and small diameter jets, but the general principles involved also apply to other geometries such as large globs, large diameter jets and other large liquid surfaces, the actual surface area undergoing the breakup usually being the largest uncertainty factor in the process. The droplet sizes produced by the breakup and the controlling physical properties are essentially the same in all cases.

In view that droplets are produced by the aerodynamic breakup of a glob of free-falling liquid retardant and that much of the available information regarding liquid breakup has been concerned with drops, it is desirable to first consider the idealized breakup behavior of individual liquid drops of a Newtonian liquid. The effects of other liquid geometries and non-Newtonian fluid properties will then be considered.

3.1 DROP BREAKUP MECHANISM AND BREAKUP TIME

The aerodynamic breakup of liquid drops has been subjected to considerable experimental study.⁴⁻¹¹ These studies have shown that if a drop is subjected to an air stream it will initially deform (flatten), and then undergo breakup provided that the airflow velocity is equal to or greater than some critical value that depends on the properties of the drop and the air density. The minimum air velocity required to breakup the drop can usually be estimated from an expression that equates the dynamic gas pressure tending to breakup the drop to the drop surface tension stress resisting the breakup, i.e.,

$$\frac{C_d \rho V^2}{2} = \frac{4\sigma}{d} \quad (1)$$

where

ρ is air density,

V is the relative velocity between the gas stream and the drop,

C_d is a drag coefficient,

σ is surface tension of the liquid drop, and

d is drop diameter.

Thus, for a specified relative velocity between the particle and the air, the maximum stable drop size is proportional to the surface tension of the liquid. Equation (1) is only approximate if the viscosity of the liquid is relatively large.

The breakup of a drop may occur in two general ways, depending on the conditions. Near the critical (minimum) air flow velocity the drop will be broken up by a so-called bag breakup mechanism, in which the drop is blown out in a concave manner into the form of a hollow bag which then breaks up into small droplets. At higher air velocities the drop always breaks by a stripping mechanism in which the outside surface of the drop is consecutively eroded (sheared) from the drop to form small droplets. The bag breakup mechanism has been attributed to pressure drag and the stripping mechanism to shear drag⁴, and it was shown experimentally that under suitable conditions the drop can apparently undergo both mechanisms simultaneously.

Equation (1) is a stability criteria for breakup, but does not give the time duration required for the breakup. For example, it is well known that a higher gas velocity will breakup a drop faster than will a lower velocity. Expressions for bag breakup time for certain limiting cases of liquid drop and

air flow properties were given initially by Hinze¹². A general expression for the bag breakup time, t , of a drop was derived by Gordon⁽¹³⁾ using Newton's second law, i.e.,

$$\frac{2(16\eta)^2}{\rho_1 d^2 (\rho V^2 - 16\sigma/d)} = \frac{16\eta t}{\rho_1 d^2} - \frac{1}{1 + \exp \frac{-16\eta t}{\rho_1 d^2}} \quad (2)$$

where ρ_1 is liquid density, η is liquid viscosity and the remaining symbols are the same as in Eq. (1). An extensive experimental study⁴ using shock tube and high speed photographic techniques of the breakup times of several kinds of liquid drops with different densities, viscosities, surface tensions and drop sizes under various velocity conditions by Andersen and Wolfe showed that Eq. (2) is in good agreement with the experimental data for both bag and stripping breakup except for a small, approximately constant factor that will be discussed subsequently.

Andersen and Wolfe⁴ derived the following expression for drop breakup time based on a parabolic velocity distribution across the drop,

$$t = \frac{d}{(A^2 + BP)^{1/2} - A} \quad (3)$$

$$A = 16\eta/d\rho_1; \quad B = 2/\rho_1 \quad (4a)$$

$$P = \frac{1}{2} \rho V^2 C_d - \frac{k\sigma}{d} \quad (4b)$$

Using values of $C_d = 1$, and $k = 2$, Eq. (3) was found to give good agreement with all of the experimental data except for a small approximately constant factor. The comparison is shown in Figure 1. It is noted that the theoretical breakup times are slightly larger than the experimental times, which was also true using Eq. (2). This factor arises largely from the manner in which the experimental breakup times were defined. In order to be consistent, the experimental breakup time was taken to be the time from the interaction of the gas flow with the drop until the drop just started to break. A comparable (but sometimes variable) time was then usually required for the drop to breakup completely. Thus the experimental breakup time should be multiplied by a small factor (about 2 to 3) to give a true breakup time, which causes the experimental breakup time to be in reasonably good agreement with Eqs. (2) and (3).

Other expressions are also available for calculating breakup times of drops, of which that of Mayer¹⁴ may especially be mentioned. This treatment considers the air flow to induce small capillary waves (instabilities) on the liquid surface which then break and are eroded from the drop. This treatment thus corresponds to the stripping (erosive) breakup mechanism. In this treatment the total breakup (stripping) time, t_s , is given by

$$t_s = \tau d/L \quad (5)$$

τ is the time required to form and break a wave with the mean wavelength L , where

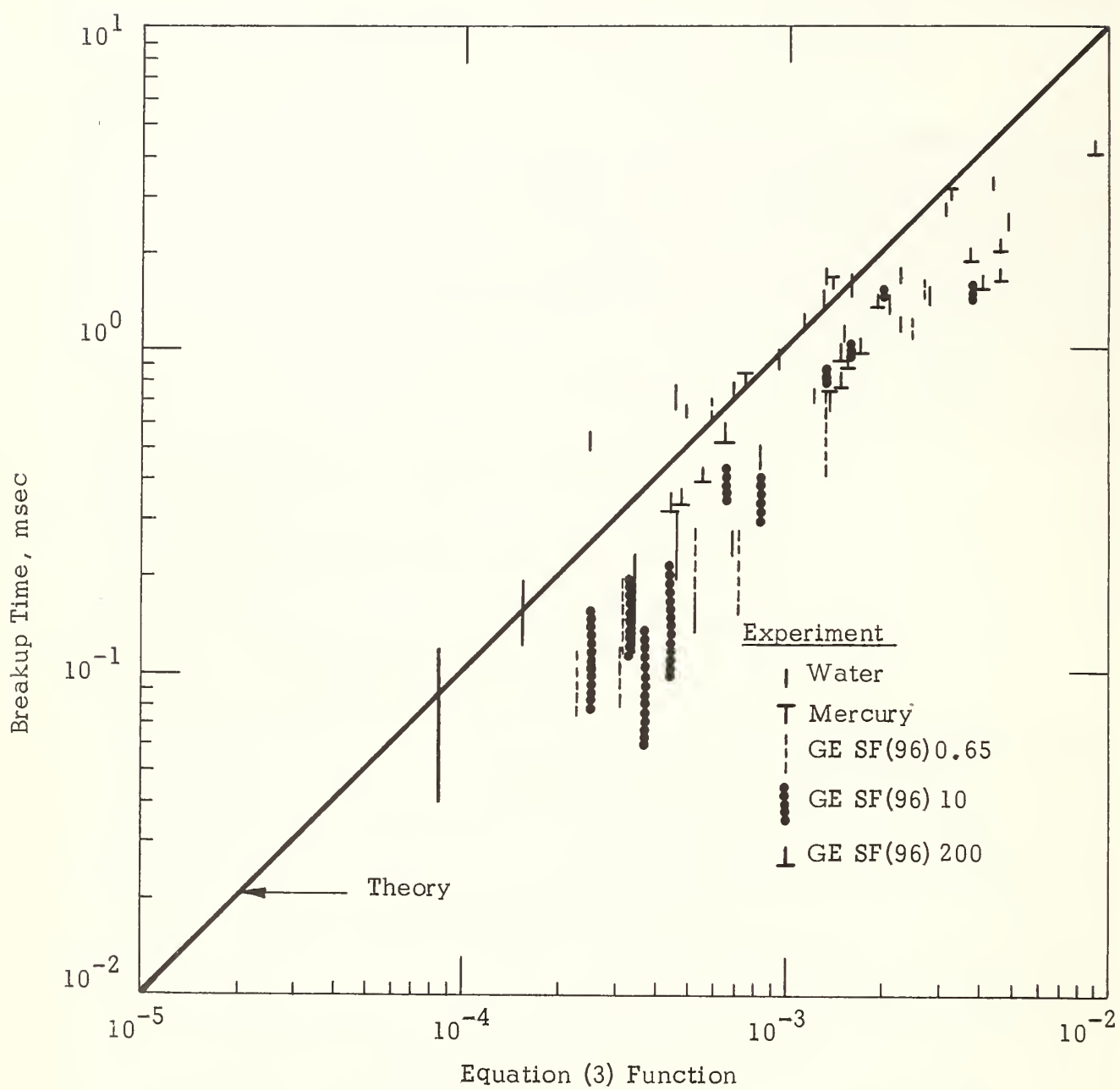


Figure 1. Comparison of Experimental Drop Breakup Times with the Andersen-Wolfe Equation.

$$\tau^{-1} = f/L^{1/2} - g/L^2 \quad (6)$$

$$f = (\pi/2\rho_1\sigma)^{1/2} \beta\rho V^2 \quad (7a)$$

$$g = 8\pi^2\eta/\rho_1 \quad (7b)$$

$$d = BL\beta^{2/3} \quad (7c)$$

The configuration parameter B has an experimental value of about 0.3. The sheltering parameter β is a function of velocity, but for the relatively low velocities encountered in the aerial dissemination of retardants its value is about 0.1. Equation (5) has also been found to be in reasonably good agreement with experimental data.

The preceding models allow the total breakup time of the drops to be estimated under specified conditions of drop size and composition, and gas flow. However, it is also possible to make estimates of the extent of breakup as a function of time. In the case of the Mayer theory it is possible to compute exactly the degree of liquid stripping (erosion) as a function of time. This will be discussed in more detail later.

Other theoretical discussions of the breakup of liquid drops are also available including those of Harper et al,^{15,16} Engle⁶, Hanson et al⁸, Jenkins and Booker⁹ and Ranger and Nicholls¹¹.

3.2 DROPLET SIZE

The sizes of the droplets produced by the aerodynamic breakup of liquid drops has received some consideration in the past. Andersen and Wolfe⁴ measured the size distribution of the droplets produced by the aerodynamic breakup of a single drop of the liquid known as 'bis', under a variety of conditions of air flow and drop size. Bis has a very low vapor pressure so that vaporization effects on the droplet sizes are negligible. Figure 2 illustrates some of the results. These investigators derived an expression for the mean diameter, d_m , of the droplets produced by the aerodynamic stripping of the drop, obtaining

$$d_m = \left[\frac{136\eta\sigma^{3/2} d^{1/2}}{\rho^2 \rho_1^{1/2} V^4} \right]^{1/3} \quad (8)$$

Figure 3 shows a comparison between the experimental values of mean droplet size and Eq. (8). The agreement is reasonable considering the crudeness of the model and the scatter in the experimental data. It is possible that the low value of the mass mean diameter obtained in the bag breakup cases may be due to the fact that only about one-third of the mass of the drop goes into the bag portion and two-thirds goes into the rim, which breaks into larger droplets. Equation (8) gives the same air velocity, viscosity and drop (injector) diameter dependence as found experimentally by Weiss and Worsham¹⁷ for liquid jets introduced into a gas stream.

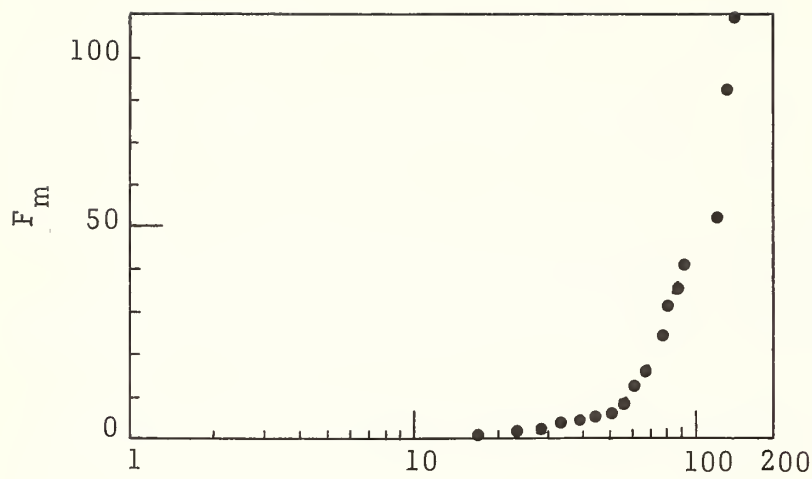


Figure 2(a). Cumulative Percent Mass vs Mass Median Diameter for Bag Breakup.

Test No. 57, $d_o = 0.6 \text{ mm}$
 $V = 66 \text{ ft/sec}$
 $d_m = 115 \mu$

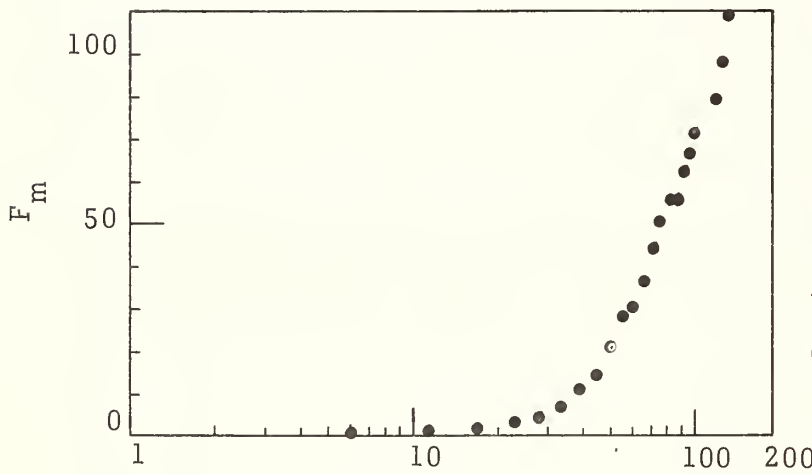


Figure 2(b). Cumulative Percent Mass vs Mass Median Diameter for Stripping Breakup at Low Velocity.

Test No. 21, $d_o = 1.6 \text{ mm}$
 $V = 130 \text{ ft/sec}$
 $d_m = 75 \mu$

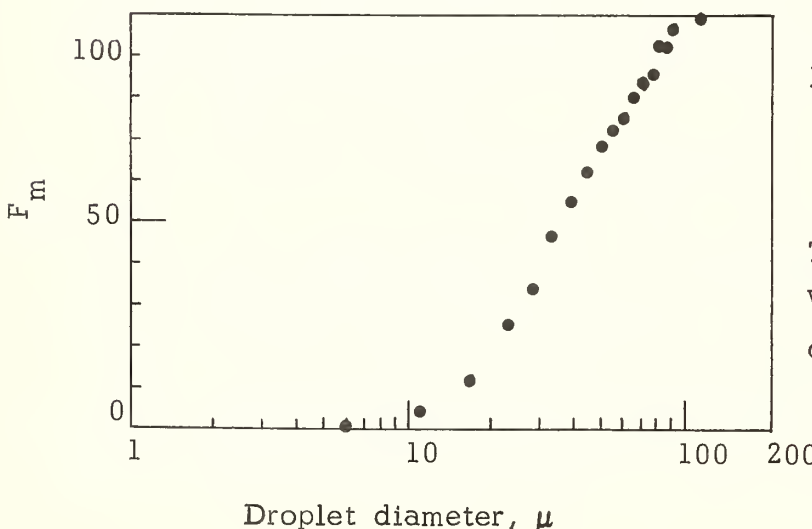


Figure 2(c). Cumulative Percent Mass vs Mass Median Diameter for Stripping Breakup at High Velocity.

Test No. 18, $d_o = 2.7 \text{ mm}$
 $V = 395 \text{ ft/sec}$
 $d_m = 34 \mu$

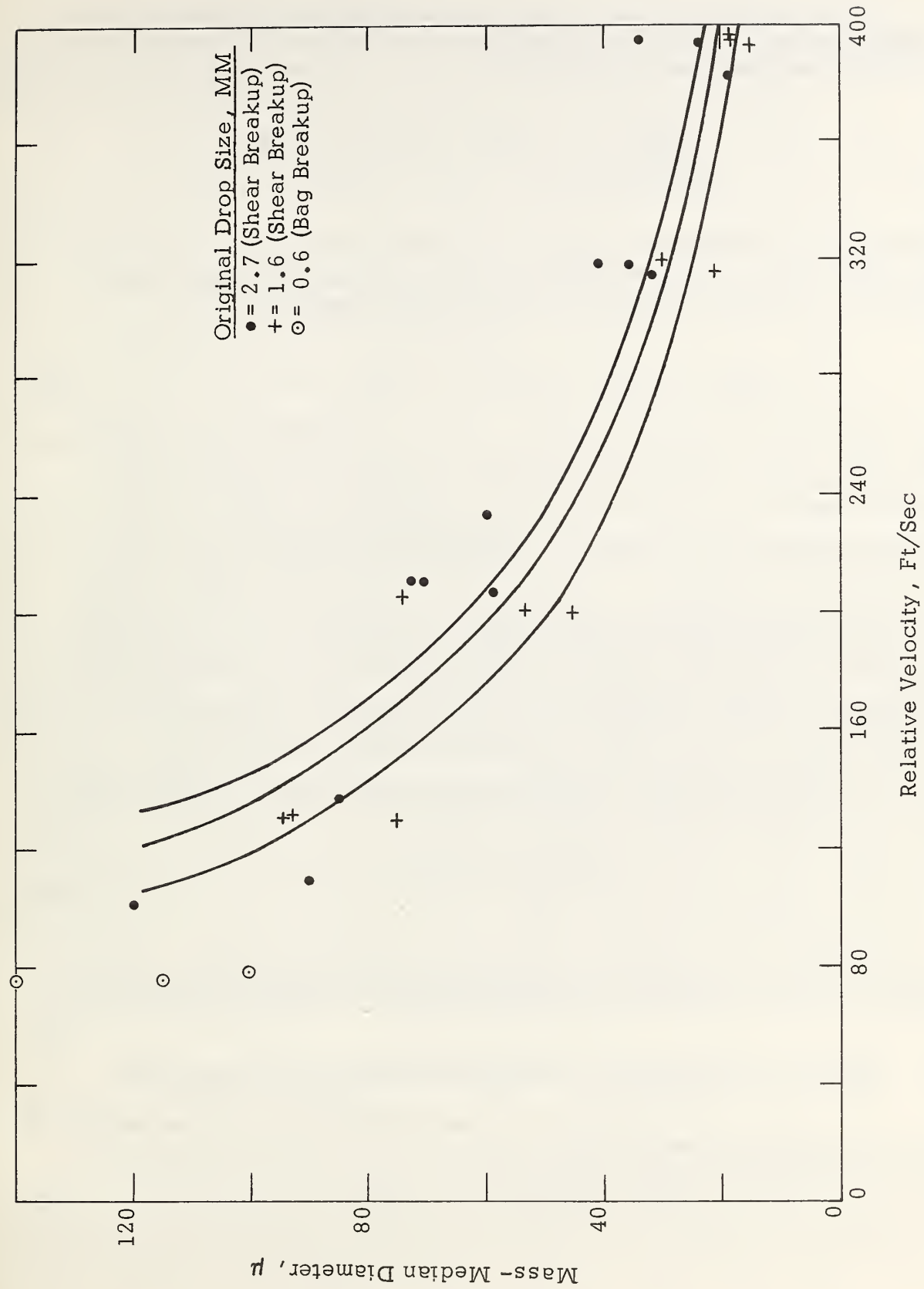


Figure 3. Comparison of Experimental Average Mass Droplet Sizes with Andersen-Wolfe Theory.

The distribution of the droplet size produced by the droplet breakup can be estimated using the logarithmic normal probability distribution function, as has been discussed by Brown^{18,19} i.e.,

$$F_P = \frac{100}{(2\pi)^{1/2} \ln \sigma} \int_0^{d_i} \exp \left\{ -\frac{(\ln d - \ln d_{gm})^2}{2 \ln^2 \sigma} \right\} d' \ln d \quad (9)$$

where F_P is the percentage of drops with diameters from 0 to d_i , d' denotes differential, and σ is the standard deviation of the geometric mean droplet diameter d_{gm} , which is related to the mass mean diameter d_m by

$$\ln d_{gm} = \ln d_m - 2.5 \ln^2 \sigma \quad (10)$$

d_{gm} corresponds to a value of 50 for F_P . The solution of Eqn. (9) requires the values of d_m and σ , and gives a straight line when plotted on logarithmic probability paper. The value of d_m can be obtained using Eqn. (8) or an equivalent equation. The value of σ generally lies between 1.7 to 1.9^{17,19} and the minimum droplet size, which has the value $2d_m/9$ when the Mayer equation is used to define d_m , will fall in the F range of 0.01 to 1; and the maximum drop size will then be about $9d_m/2$ and will fall in the F range of 99 to 99.9. A knowledge of d_m thus enables the drop size distribution to be estimated by choosing an F_P value for $2d_{gm}/9$ that falls between 0.01 to 1, e.g., 0.1, and drawing from it the line that passes through the point d_{gm} .

The theory of Mayer¹⁰ also provides an expression for mean droplet size produced by aerodynamic stripping, i.e.,

$$d_m = 22.7 \pi B \left[\frac{\eta (\sigma/\rho_1)^{1/2}}{\rho v^2} \right]^{2/3} \quad (11)$$

This expression has the same air density and velocity dependence as does Eqn. (8). It is also possible to generate the entire droplet size distribution by this theory, and this will be discussed later.

3.3 EFFECT OF GEOMETRY AND NONIDEALIZED FLUID PROPERTIES

A variety of investigations have been conducted on the breakup of liquids with initial geometries other than drops. The breakup of liquid jets has in particular been studied extensively.

One of the most important investigations of jet breakup in a high velocity gas stream was that of Weiss and Worsham¹⁷, who studied the drop sizes produced by the breakup of a jet liquid wax in a hot airstream. The mass median diameter (mmd) of the drops was found to be given by

$$d_m = k V^{-1.33} v_i^{0.08} D_i^{0.16} \eta^{0.34} (1 + \rho_o / \rho) \quad (12)$$

where

- k is a constant,
- V is a relative gas velocity,
- v_i is injector velocity,
- D_i is jet diameter,
- η is liquid viscosity,
- ρ is normal air density, and
- ρ_o is air density at 300°F.

This expression gives the same air velocity, viscosity and injector (drop) diameter dependence as given in Eqn. (8) for drops. Weiss and Worsham concluded that: "The atomization of liquids by large, high velocity airstreams occurs by direct action of the airstreams on the exposed liquid surface. Therefore the relative velocity between the liquid and the airstreams is of primary importance. Physical properties of the fluids do affect spray fineness, but their net influence is less critical. The exact way in which the liquid is introduced into the air, i.e., the geometry and operation of the injector, is of least importance, particularly at very high air velocities and for the customary range of variables." This statement together with the similarities of Eqns. (8), (11), and (12) indicate that the breakup of liquid drops and jets as well as other geometry liquids occur by essentially the same mechanism as long as conditions are such that the liquid breakup occurs by an erosion (instability) process at its surfaces. Hence the effect of gas properties (velocity and density) and liquid properties (density, viscosity and surface tension) on the breakup time and droplet diameter should be essentially the same for the erosive breakup of a liquid with any geometry.

Other studies of the breakup of liquid jets and of other geometry liquids are given in References 10, 20-26. In general the results of these studies support the previous conclusions.

The results of the theoretical and experimental studies of liquid breakup described throughout this section have in general applied to ideal, i.e., Newtonian liquids. Little information, either experimental or theoretical, is available on the breakup behavior of non-Newtonian liquids which undergo such behavior as shear thinning or viscoelasticity.^{27,28} However, some of the models used for

Newtonian liquids can also be used to describe the breakup of non-Newtonian fluids, provided that the effects of the strain rate dependence of the viscosity, and the fluid elasticity are incorporated in the equations.²⁹ This will be discussed in more detail later.

4. BREAKUP THEORY OF LIQUID RETARDANTS

As bulk liquid fire retardant undergoes free fall from an aircraft it is subjected to aerodynamic (wind) forces which deform (flatten) the liquid, and simultaneously shears (erodes) the liquid on its exposed surfaces in contact with the airflow into droplets of various sizes. The deformation of the liquid by the frontal drag causes the liquid to undergo both lateral spreading and thinning. After appreciable thinning, instabilities (known as Taylor instabilities) are induced in the front surface of the liquid, and grow rapidly once initiated. When the amplitude of the instabilities (waves) becomes essentially equal to the thickness of the deforming liquid, the liquid breaks into a large number of individual particles or globs. These particles may then undergo further breakup into smaller droplets by mechanisms such as surface erosion as they continue their fall trajectory.

There are thus two separate breakup mechanisms which occur during the free fall of bulk liquid (e.g., salvo drop) from an aircraft, viz., Taylor instability (or deformation) breakup which frontally breaks the deforming bulk liquid into smaller particles, and surface (wind) erosion which breaks (strips) droplets from the exposed surface of the initially ejected bulk liquid before it undergoes Taylor breakup, and from the liquid particles produced subsequently by the Taylor breakup of the bulk liquid.

A summary of the equations that were developed during the program to describe the preceding processes will now be given. Application of the equations to the breakup of real fire retardant solutions as well as the development of certain subsidiary relations necessary in their solution will be given later.

4.1 SURFACE EROSION BREAKUP

A glob of liquid retardant moving rapidly through the air will be subjected to wind friction at its exposed surfaces, and this friction will shear (erode) mass from appropriate surfaces of the glob. On a fundamental basis the wind causes small disturbances (instabilities) or waves to grow on the surface. These disturbances break when their amplitude is comparable to their wavelength, and are shed from the glob as particles or droplets. A variety of wavelengths are excited and grow at different rates. Thus a distribution of particle sizes are produced by the surface erosion. Small wavelength disturbances grow at a rate limited largely by viscosity (for a specified relative velocity), while large wavelengths are limited by inertia.

A model that can usefully be used to describe these events is that of Mayer¹⁴, whose basic results are given in Eq. (6) - (7c). However, Mayer only developed the average particle size produced over a long time period (Eq. (11)), and it may be desirable to include both the effects of

particle size distribution and time, depending on the case under consideration. The appropriate equations have been developed in ref. 30, where effects of gravity wave formation were also considered. Only capillary wave formation is of importance here.

The rate of formation of droplets per unit surface area of the eroding liquid in a differential wavelength range is given by¹⁴, $\dot{N} dL = (f/L^{5/2} - g/L^4) dL$. Consequently the mean rate of droplet formation per unit surface area from waves having wavelengths between L_1 and L_2 is given by

$$\dot{N}_{12} = (L_2 - L_1)^{-1} \left[\frac{2}{3} f (L_1^{-3/2} - L_2^{-3/2}) - (g/3) (L_1^{-3} - L_2^{-3}) \right] \quad (13)$$

The mean size L_{12} between L_1 and L_2 is given by

$$L_{12} = \left[\dot{N}_{12} (L_2 - L_1) \right]^{-1} \left[2f(L_1^{-\frac{1}{2}} - L_2^{-\frac{1}{2}}) - (g/2)(L_1^{-2} - L_2^{-2}) \right] \quad (14)$$

where

$$f = (\pi/2 \rho_1 \sigma)^{1/2} \beta \rho V^2 \quad (15)$$

$$g = 8\pi^2 \eta / \rho_1 \quad (16)$$

$$d = B \beta^{2/3} L \quad (17)$$

In these equations ρ_1 , σ and η are the density, surface tension and viscosity of the liquid, ρ is air density, V is the relative (wind) velocity between the liquid and the air stream, d is the diameter of the liquid particle produced by the breakup of a capillary wave with wavelength L , B is a parameter whose experimental value is about 0.3, and beta is the sheltering parameter. The value of beta has in the past - when only low viscosity liquids were under consideration - been regarded as either a constant, or a function whose value decreases with increase in air velocity. Studies on this program have shown it to also depend on liquid viscosity, and this will be discussed later.

The mass rate of formation ($gm/cm^2 sec$) of particles, \dot{M}_{12} , per unit surface area having diameter, d_{12} , is given by

$$\dot{M}_{12} = (\pi d_{12}^3 / 6) \rho_1 \dot{N}_{12} \quad (18)$$

provided that L_1 and L_2 in Eq. (13) and (14) are chosen over a sufficiently small increment. In this case the total mass per unit time of the particles formed per unit surface area is the sum of the mass formation rate of all the particle sizes, i.e.,

$$\dot{M} = \sum \dot{M}_{ij} \quad (19)$$

In the general case, however, the mean mass formation rate of liquid particles, \dot{M}_{12} , eroded from the liquid glob, from waves having wavelength sizes between L_1 and L_2 is given by

$$\dot{M}_{12} = \frac{\rho_1}{(L_2 - L_1)} \left[\frac{2}{3} f(L_2^{3/2} - L_1^{3/2}) - g \ell n(L_2/L_1) \right] \quad (20)$$

where the mean size L_{12} between L_1 and L_2 is given by

$$L_{12} = \frac{\frac{2}{5} f (L_2^{5/2} - L_1^{5/2}) - g (L_2 - L_1)}{\frac{2}{3} f (L_2^{3/2} - L_1^{3/2}) - g \ell n (L_2/L_1)} \quad (21)$$

The preceding equations were obtained assuming a uniform (Heaviside) probability density for the wave formation, as is commonly done for problems of this nature. A more realistic assumption may be to make the probability proportional to the frequency of wave (ligament) formation, but this would much further complicate the analysis. Generally speaking, experimental data on liquid erosion are not usually sufficiently detailed or accurate enough to distinguish the detailed form of the distribution function (hence the probability density), and in many cases the semi-emperical logarithmic normal probability distribution function discussed previously has consequently been used to further simplify the problem without general loss of accuracy. The mean droplet size for use in this distribution function is, however, either obtained from the surface erosion model or from experimental data.

Mayer considered the steady state case of the wind erosion of a half-space of liquid, in which the total erosion time is large compared with the droplet formation time. In this case the minimum droplet size is produced by those instabilities having $1/\tau = 0$ (Eq. 6), and consequently the minimum wavelength, L_{\min} , is given by

$$L_{\min} = (g/f)^{2/3} \quad (22)$$

He considered the maximum wavelength, L_{\max} , to be infinite. Substitution of these values in Eq. (14) gives the mean wavelength, $L_m = (9/2)L_{\min}$, which when combined with Eq. (17) gives the mean droplet size shown in Eq. (11).

The wind erosion of a liquid glob takes place over a finite time, and is thus transient in nature. In this case the minimum and maximum wavelengths excited during a time t is given by the minimum and maximum wavelength roots of the equation³⁰

$$L^2 - ft L^{3/2} + tg = 0 \quad (23)$$

It can be estimated that for the high velocity wind erosion of a low viscous fluid, the effect of using the minimum and maximum wavelength computed by this equation on the resultant size distribution of the eroded particles is generally of negligible importance, but as wind velocity is decreased and fluid viscosity increased there are computed differences when compared to

the Mayer limits. Of potential consequence also for the wind erosion of a liquid particle with finite size is that the maximum wavelength excited cannot exceed some effective fraction of the particle size.³¹ This also has negligible effect for the case of high wind velocity and low viscosity fluids, but for low wind velocity and high viscosity fluids it may be of considerable importance.

Equation (23) also shows that a liquid must be subjected to wind flow for a minimum time, t_m , before any particles are eroded from it, where

$$t_m = 2.116 (g/f^4)^{1/3} \quad (24)$$

This general behavior is observed experimentally, such as during the aerodynamic breakup of a liquid drop or jet by a shock wave.

The preceding equations have been shown to be in reasonably good agreement with breakup times and droplet sizes produced by the aerodynamic breakup of liquid drops and jets. In practice the theory can be fit (correlated) with experimental data as accurately as desired by considering B and β to be arbitrary constants. This procedure is valid since their values are only approximately known, and are largely based on the results of experiment.

4.1.1 Effect of Non-Newtonian Viscosity

The preceding equations assume Newtonian liquid viscosity, i.e., that the viscosity is independent of the shear rate of the liquid. However, in principle these equations can also be used to describe the breakup of a non-Newtonian, e.g., shear thinning or shear thickening (dilatant) liquid provided that the effect of shear rate on the effective viscosity of the liquid that controls the shear rate is included in the solution of the equations. The relation between shear rate, \dot{S} , and viscosity must generally be determined experimentally, and for a shear thinning liquid is often of the form³²

$$\eta = a + (b/\dot{S}) \sinh^{-1}(c\dot{S}) \quad (25)$$

where a , b and c are experimental constants.

The average effective shear rate, \dot{S} , of the liquid while undergoing surface erosion may be estimated as follows. Replacing the roughly sinusoidal behavior of an instability with wavelength L by a triangle gives the following expression for the average shear rate of the liquid during the growth of the instabilities,

$$\dot{S} = \frac{dv}{dr} = \frac{v}{(L/2)} = \frac{2v}{L} \quad (26)$$

where r is lateral distance, and v is the velocity of wave growth. Since the liquid ligament breaks when the wave amplitude is comparable to its wavelength, $v = L/\tau$, where τ is the particle formation time from a wave with wavelength L and is given by Eq. (6), i.e.,

$$\tau^{-1} = f/L^{1/2} - g/L^2 \quad (27)$$

Substituting for v in Eq. (26) gives

$$\dot{S} = \frac{2}{\tau} \quad (28)$$

Thus breakup calculations involving a non-Newtonian liquid must include Eq. (25) (or its equivalent) and (28) in the solution. It may be seen that the effective viscosity of different wavelength disturbances is different, and hence shear thinning or fluid dilatancy will affect the general form of the size distribution of the droplets produced by liquid breakup, as well as the average size.

The normal low shear rate (e.g., Brookfield) viscosity of various fire retardants vary widely, and range from about 0.01 poise for water to 15-25 poises for Phos-Chek XA and Fire-Trol 100. However water is a Newtonian liquid and its viscosity is independent of shear rate, whereas real retardants are thickened liquids and their viscosity usually decreases with increase in shear rate. For example Phos-Chek XA is a gum thickened solution while Fire-Trol 100 is a clay thickened solution. Liquid breakup rate and resultant droplet size both depend on the viscosity of the liquid. However under the dynamic conditions of breakup experienced by a liquid undergoing free fall from an aircraft, the effective viscosity controlling the breakup of the liquid is the shear thinned value consistent with the shear rate of liquid, rather than the low shear rate value. It may thus be seen that the relation between viscosity and shear rate of the retardant is of considerable importance in determining the breakup behavior of the liquid retardant, and the relative Brookfield values of different liquid retardants may or may not be indicative of the relative qualitative breakup behavior of the retardants under conditions experienced in free fall from an aircraft.

4.1.2 Effect of Fluid Elasticity

Another potentially important dynamic property of liquids that may affect liquid breakup is elasticity, and fluids may be either viscoelastic or elastoviscous in nature. The properties (e.g., elasticity) of viscoelastic fluids are time-dependent and involve hysteresis. Viscoelastic fluids that are also Newtonian often obey the Maxwell equation, i.e.,

$$P_{xy} + (\eta/G) \dot{P}_{xy} = \eta \dot{S} \quad (29)$$

where P_{xy} is shear stress and G is shear modulus. If the liquid is non-Newtonian, Eq. (29) may be considered to apply to the effective viscosity - which is shear-rate dependent - at any time.

Of more importance for the present studies are elastoviscous fluids, in which the elasticity is also manifested during the steady shear of the liquid. The practical significance of elasticity to aerodynamic breakup then is as follows. Elastic liquids when undergoing rapid shear develop a "normal stress" which acts as a tension in the direction of flow, and stores elastic energy. This energy acts as a stabilizing force on the shearing liquid

Thus in the case of viscoelastic liquid undergoing aerodynamic erosion, the liquid is stripped off initially in the form of threads²⁷, rather than discrete particles as occurs for an inelastic fluid. These threads ultimately break to form particles, but the particles are larger than if the elasticity were not present.

Liquid surface subjected to wind stress develops instabilities which grow and are eventually eroded from the surface of the liquid to form droplets. During its shearing growth, the liquid develops an elastic stress. This stress later decays as the aerodynamic forces subside on the shearing liquid. Breakup of the liquid may not occur until the relaxation of the stress. If the relaxation time, t_r , for stress relaxation of the liquid is small compared to, τ , the droplet formation time (given for inelastic liquids by Eq. 27), then the elasticity of the liquid should have no affect on the breakup characteristics of the liquid. However if t_r is comparable to τ , then fluid elasticity will affect the breakup characteristics, and in particular should decrease breakup rate and increase droplet size. Thus the magnitude of the stress relaxation time in comparison with the droplet formation time under the local wind conditions should be a measure of the importance of fluid elasticity on the breakup characteristics of the liquid.

The stress relaxation time can be expressed in several ways,³³⁻³⁵ i.e.,

$$t_r = \eta/G = s/\dot{S} = \eta s^2/P_n \quad (30)$$

where η is viscosity, G is shear modulus, \dot{S} is shear rate, s is the elastic strain (recoverable shear), and P_n is the normal stress. The elastic properties of a liquid are described by its values of s and P_n . For an inelastic liquid the recoverable shear is zero. In general all of the properties in this equation are shear rate dependent.

The effect of elasticity on the stability of a fluid undergoing shear can be expressed by the addition of an appropriate term describing the elasticity to the viscosity (non-Newtonian or Newtonian) of the liquid at the specified shear rate, so as to give an effective viscosity which incorporates both viscous and elastic effects. In particular the effective viscosity, η_e , is given by*

$$\eta_e = \eta (1 + s) \quad (31)$$

*The applicability of this equation was pointed out to the authors by Dr. P. J. Blatz of Shock Hydrodynamics, who also derived it using tensorial methods. The treatment is rather complex, and is given in Appendix II.

where η is the viscosity and s is the recoverable shear of the fluid. Note that both η and s may be shear rate dependent. For a nonelastic liquid, $s = 0$, and $\eta_e = \eta$. For a Newtonian liquid, $\eta = \text{constant}$, and is independent of shear rate. For a non-Newtonian liquid, η can either decrease or increase with increase in shear rate - depending on whether the liquid is a shear thinning or dilatant fluid. It may be seen from this equation that the effective viscosity of an elastic, shear thinning liquid at high shear rates is generally greater than the effective viscosity of a shear thinning nonelastic liquid, due to the presence of the term $(1 + s)$, and the fact that s always increases with increase in shear rate.

As noted in the preceding footnote, Eq. (31) can be derived on a rigorous basis but the treatment is relatively complex. The relation between viscosity and elasticity of liquids has been discussed extensively in the literature, and an equation with the limiting form of Eq. (31) has been used to describe the elongational viscosity of viscoelastic liquids.³⁶⁻³⁹ An equation of this form has also been used extensively in describing rubber elasticity, the term $(1 + s)$ then being called the stretch factor, λ . In this case it is often used in the form, λ^n , where n is an empirical constant that is used to correlate experimental data with theory.

The expression for effective viscosity, Eq. (31) can be naively obtained by recalling that in an elastic shearing liquid, the normal (elastic) stress ($P_n = P_{11} - P_{22}$) acts as a pull or tension in the direction of shear flow, and that the elastic energy must be supplied by the forces driving the fluid flow. The effective shear stress, P_{xye} , of the flowing fluid is then given by

$$P_{xye} = P_{xy} + P_n \quad (32)$$

where the kinetic energy pressure is included in P_{xye} , P_n is the normal elastic stress, and P_{xy} is the conventional viscous shear stress given by $\eta \dot{S}$, where η is the viscosity (which may be a function of shear rate, \dot{S}). The effective shear stress can be expressed in a similar manner, i.e., $P_{xye} = \eta_e \dot{S}$, where η_e is the apparent or effective viscosity of the elastic liquid. From Eq. (30), above, $P_n = \eta \dot{S} s$, where s is the recoverable shear. Substitution of these values in Eq. (32) gives Eq. (31).

4.1.2.1 Significance of the Effective Viscosity on the Liquid Breakup Characteristics.

Equation (31) is of great practical importance since it combines and clearly identifies the individual roles and relative importance of the viscosity and the elasticity of a liquid on the effective viscosity that controls the breakup characteristics of the liquid. Thus the non-Newtonian viscosity and the fluid elasticity of the liquid are the dominant rheological properties that control the stability of the liquid to breakup, and their combined effects are as given in Eq. (31). Thus correlations involving these rheological properties of a liquid should be based on Eq. (31) rather than the individual rheological properties. In use the viscosity term given in the surface breakup model

just discussed, and the deformation (Taylor breakup) model to be discussed subsequently should be replaced by the effective viscosity, i.e., Eq. (31), which encompasses all types of fluids, i.e., Newtonian, non-Newtonian, elastic and non-elastic fluids. It should be noted that changing the viscous or elastic properties of a fluid will also change the effective shear rate of the breaking liquid.

4.1.3 Secondary Droplet Breakup

The surface erosion of a liquid by wind flow produces a distribution of droplet sizes, as given by Eq. (13). The larger of these particles after formation may, under suitable conditions, undergo further breakup during descent. The potential effect of this breakup can be examined using one of the drop breakup models discussed in Section 3, including effects of shear thinning and fluid elasticity according to the shear rate dependence required in the model. However since the wind velocity is relatively low once the primary droplets are formed, it is likely that the shear rate is sufficiently small that the viscosity will be large enough to greatly impede the breakup. Hence secondary droplet breakup is probably of small or negligible importance for most viscous fire retardant solutions.

4.2 DEFORMATION (TAYLOR INSTABILITY) BREAKUP

As noted previously, as bulk liquid retardant is released from an aircraft it undergoes deformation by aerodynamic forces, which results in a thinning and lateral spreading of the fluid. After significant thinning, instabilities (waves) are induced in the front surface of the liquid and grow catastrophically - which results in the fracturing of the liquid into smaller pieces.

The importance of the Taylor breakup process on the dispersion characteristics of aerially delivered fire retardants has been emphasized by Swanson and Helvig^{40,41} who stated that the peripheral stripping of the liquid before Taylor breakup has only minor effect on the meaningful ground pattern of the dispersed retardant. They developed a model based on Bond number considerations for estimating the gross effect of the aircraft velocity and retardant load (gallons) on the breakup time of the retardant subsequent to its release from the aircraft. However the model did not provide any details regarding the nature of the dispersed retardant.

In this section a more comprehensive analysis is made on the Taylor breakup process from which the effects of the controlling parameters such as aircraft velocity, tank and gating system and the rheological properties of the fluid on the breakup characteristics of the liquid retardant can be estimated. These effects will be considered in more detail later.

As just noted, Swanson and Helvig^{40,41} simulated the deformation and Taylor instability breakup processes by replacing the retardant tank volume by an equivalent sphere, and utilized an equation developed at the Bell Telephone Laboratories^{42,43} to estimate the breakup time of the liquid as a function of aircraft velocity and retardant load. This equation-based on Bond number-was originally developed for estimating the breakup time of a small liquid drop by Taylor instability, and certain constants in it such as the drag coefficient were evaluated from experimental data obtained in a shock tube. In order to obtain good agreement between this theoretical equation and the experimental breakup times which were obtained from the photographic records of the aerial drops of several different sized loads of fire retardant, Swanson and Helvig found it necessary to reduce the value of a certain constant in the theoretical equation. Alternatively, the value of the drag coefficient - which was assumed to have a constant value of 2.5 - could presumably have been increased to obtain the agreement.

4.2.1 Deformation Rate of the Liquid

In order to separate the effects of the length, L_o , of the aircraft tank containing the fire retardant from its cross sectional area, the volume V_o , of the tank is replaced by an equivalent cylinder with length L_o and radius R_o , where

$$\pi R_o^2 L_o = V_o \quad (33)$$

The shear, γ , of the liquid at time, t , when subjected to aerodynamic forces with stagnation pressure, P , is given by*

$$t = A\gamma + 2\eta_d\gamma/P \quad (34)$$

$$A = \left[\frac{\rho_1 (2L_o^2 + R_o^2)}{2P} \right]^{\frac{1}{2}} \quad (35a)$$

$$P = \frac{1}{2} C_d \rho V^2 \quad (35b)$$

*This equation was obtained by Dr. P. J. Blatz of Shock Hydrodynamics. Its derivation is given in Appendix III.

where

$$\frac{dy}{dt} = \dot{s}$$

\dot{s} is the shear rate of the fluid,

ρ_1 is liquid density,

ρ is air density,

V is the relative velocity between the liquid and the air stream (the aircraft velocity),

C_d is the drag coefficient, and

η_d is the effective viscosity of the liquid during its deformation by the air flow.

η_d will hereafter be called the deformation viscosity of the liquid.

As the liquid undergoes deformation, it thins and spreads laterally. The thickness or length, L , of the liquid at any time during deformation is given by

$$L = L_0 \exp (-\gamma) \quad (36)$$

where L_0 is its initial thickness, which is equal to the length of the tank (the difference between the tank length and door length will not be distinguished in the present analysis). The effective radius, R , of the liquid at any time during deformation is given by

$$R = R_0 \exp (\gamma/2) \quad (37)$$

where R_0 is the initial effective radius of the liquid, and is related to tank volume and length by Eq. (33).

4.2.1.1 Effect of Shear Rate on Viscosity

For a Newtonian liquid retardant such as water, the deformation viscosity, η_d , in Eq. (34) is the normal viscosity of the liquid. For a non-Newtonian retardant, however, the value of η_d will be the effective viscosity,

η_e , evaluated at the shear rate experienced by the deforming liquid, where η_e is given by Eq. (31).

The shear rate of the deforming liquid may be estimated as follows. It can be shown that for the present purposes the term containing η_d in Eq. (34) is always small compared to the first term (For most purposes it can be neglected, but is retained here to show its effect). Neglecting the η_d term initially and solving for γ and then substituting back into the complete equation gives, $\gamma^{1/2} = t/A - 2\eta_d t^2/A^3 P$. Since $\dot{S} = d\gamma/dt$, it is seen that the shear rate is time dependent. The average value, \dot{S}_d , is adequate for the present purposes, and is given to good approximation over a time period, t_d , by

$$\dot{S}_d = \frac{t_d}{A^2} - \frac{4\eta_d t_d^2}{A^4 P} \quad (38)$$

In order to include Eq. (38) in the solution of the equations, it is necessary to utilize the experimental relationship between the shear rate and the effective viscosity of the liquid.

4.2.2 Growth Rate of the Instabilities

During the deformation of the liquid and after significant thinning has occurred, two dimensional instabilities (waves) are induced in the front liquid surface that interacts with the air flow. These instabilities- once initiated-grow rapidly, and when their amplitude is essentially equal to the thickness of the liquid, the liquid fractures into smaller pieces. In actual practice, instabilities with several different wavelengths may be initiated and grow simultaneously in the deforming liquid. High speed photographs of the aerial delivered free falling retardant show that in some cases during the breakup of the liquid one or more relatively large globs of liquid are formed that appear to become detached and break away from the remainder of the liquid cloud. That is, in some cases one or more relatively large liquid globs are formed whose trajectory differs (runs ahead) of the main body of the cloud. These globs may be the result of imperfections (or perturbations) in the breakup of the liquid due to the particular instantaneous manner in which the flowing liquid is ejected from the tank, or of large wave length instability growth superimposed on the more rapidly growing smaller wavelength instabilities. It is believed that the formation of these large globs in general represents a perturbation on the idealized (or average) behavior of the system. In any event it is not possible to account for their presence at this time, and the present treatment considers the average breakup of the liquid to occur as a result of the fastest growing instability growing to an amplitude equal to the thickness of the deforming liquid.

Keller and Kolodner⁴⁴(KK) have investigated analytically the growth rate of the fastest growing (Taylor) instability produced by a wind interacting normally with a non-viscous liquid with finite surface tension. They developed expressions for the time required to breakup a sheet of specified thickness by this mechanism (KK, Eq. 40), and the size of the resultant liquid pieces (KK, Eq. 39). Their solutions contain the wave number of the fastest growing

instability (KK, Eq. 35) which is a function of the liquid properties and its surface acceleration.

Bellman and Pennington⁴⁵(BP) investigated the growth of the fastest growing Taylor instability for the cases of a non-viscous liquid with surface tension, a viscous liquid without surface tension, and a viscous liquid with surface tension. For the non-viscous liquid with surface tension they obtained the same solution for the wave number of the fastest growing disturbance (BP, Eq. 3.9) as was obtained by Keller and Kolodner. Their results for a liquid with both viscosity and surface tension (BP, Eq. 4.7-4.10) are complex and cannot be expressed in closed form. It was shown however, that the presence of surface tension generally has negligible effect on the wave number of the fastest growing disturbance, and that this wave number is viscosity controlled. The principle effect of viscosity is to retard the growth rate of the disturbances and shift the fastest growing disturbance to a longer wavelength. This would result in larger particles being produced by the breakup of the liquid by this mechanism. The approximate solution of the wave number obtained by Bellman and Pennington for a viscous fluid without surface tension (BP, Eq. 2.35) was consequently used in the growth rate and particle size equations obtained by Keller and Kolodner, i.e., the wave number for a non-viscous liquid with surface tension in the KK equations was replaced by the wave number for a viscous liquid obtained by BP. The resulting expression for the breakup time, t_i , of a sheet of liquid with thickness, L, by Taylor instability growth is given by

$$t_i = 2(\rho_1 \eta_1)^{1/3} (L/P) \ln(L/A_i) = (BL/P)^{1/3} \ln(L/A_i) \quad (39)$$

where η_1 is the viscosity of the liquid while undergoing instability growth, P is given by Eq. (35b), \ln is natural logarithm, and A_i is the initial amplitude of the instabilities just as they start to grow.

4.2.2.1 Wavelength and Particle Size

The wavelength, λ , of the fastest growing instability is given by⁴⁵

$$\lambda = 4\pi \eta_1^{2/3} \left[\frac{L}{\rho_1 P} \right]^{1/3} \quad (40)$$

The equivalent spherical diameter, D, of the particles or globs formed by the Taylor breakup of the deformed (thinned) liquid with thickness L is given by

$$D = (24\pi)^{1/3} \left[\frac{L^{2.5} \eta_1^2}{\rho_1 P} \right]^{2/9} \quad (41)$$

This expression is based on the assumption that the liquid breaks at the nodal lines (where the octahedral shear stress is a maximum) and which are a distance $(\lambda/2)$ apart. The volume of a liquid particle is then given by $(\lambda/2)^2 L$. On the

other hand if the air bursts through the deformed liquid at the points of maximum liquid displacement, the volume of a liquid particle is given by $(\lambda^2 L)$, and D would be given by a factor of $4^{1/3} = 1.588$ greater than that given in Eq. (77). No experimental evidence is available as to which case actually occurs, and technical opinion seems divided as to which case occurs. A part of the controversy stems from the fact that the general behavior of the back surface of the liquid (opposite to the surface that interacts with the air flow) during the instability growth is not known, and this surface may either remain planar or undergo wave growth in phase with the front surface. For the present analysis the equivalent diameter of the particles produced by Taylor instability breakup of the liquid is assumed to be given by Eq. (41), but it should be kept in mind that it may be larger by a factor of about 1.59.

4.2.2.2 Effect of Shear Rate on Viscosity

For a Newtonian liquid the viscosity given in Eq. (39-41) is the ordinary shear viscosity, and is then equal to η_d of Eq. (34). For a non-Newtonian liquid, however, η_1 in Eq. (39-41) will differ from Eq. (34) since the shear rate differs.

The average shear rate of the liquid during the growth of the instabilities may be estimated as follows. Replacing the roughly sinusoidal behavior of an instability by a triangle gives the following expression for the average shear rate, \dot{S}_1 , of the liquid during the growth of the instabilities,

$$\dot{S}_1 = \frac{dv}{dr} = \frac{v}{(\lambda/2)} = \frac{2v}{\lambda} \quad (42)$$

where λ is given by Eq.(40), r is lateral distance, and v is the velocity of the wave growth which is given by

$$v = L/t_i \quad (43)$$

Substituting gives

$$\dot{S}_1 = \frac{P}{4\pi \eta_1 \ln(\frac{L}{A_i})} \quad (44)$$

Utilization of this equation requires an experimental relationship between shear rate and viscosity.

4.2.3 Solution of the Equations

Equation (34)describes the deformation of the liquid by aerodynamic forces as a function of time in terms of the shear of the liquid, and Eq. (36) relates the shear to the instantaneous thickness of the deforming liquid.

Equation (39) gives the breakup time of the liquid by Taylor instability growth for any constant liquid thickness L . However the liquid thickness does not remain constant, but rather decreases during liquid deformation. The question arises as to how to combine Eq.(34) and Eq.(36) so as to obtain valid expressions of the breakup time of the deforming liquid and the properties of particles produced. What is most desired, of course, is a solution of Taylor breakup for the case where the cylindrical liquid is undergoing deformation, and the thickness is continually decreasing. However, such a solution is not available in the literature, and to obtain it rigorously represents a formidable problem.

An apparently very good approximation to the solution of the problem can be obtained as follows, which uses the essentially exact limiting solutions obtained for the case of the monotonic deformation of a liquid cylinder (Eq.34), and the Taylor instability breakup of a liquid sheet of constant thickness (Eq.36). It will be observed that as (deformation) time increases, the value of the liquid thickness, L , decreases, which causes the Taylor instability breakup time of the liquid to also decrease. For small deformation times the instability breakup times are large, whereas for sufficiently large deformation time the instability time becomes vanishingly small. A plot of the sum of the deformation time, t_d , plus the Taylor instability breakup time, t_i , versus time (and hence liquid thickness) should hence exhibit a minimum, and this minimum should define the effective thickness, L_e , of the liquid during its deformation that controls the breakup. Thus the Taylor breakup time, t_b , of the liquid subsequent to its interaction with the air stream is given by

$$t_b = t_d + t_i \quad (45)$$

where the deformation time, t_d is given by Eq.(34), and the Taylor instability breakup time, t_i , is given by Eq.(39). The effective value of liquid thickness, L_e , that is used to evaluate the individual expressions is obtained from

$$\left[\frac{dt_b}{dL} \right]_{L=L_e} = 0 \quad (46)$$

which gives

$$L_e^{2/3} = \frac{\left[\frac{A}{2(\ln L_o/L_e)^{1/2}} + \frac{2\eta_d}{P} \right]}{B \left[1 + \frac{2}{3} \ln \frac{L_e}{A_i} \right]} \quad (47)$$

Once L_e is evaluated from this equation, the breakup time is evaluated by substituting $L = L_e$ in Eq. (45), i.e.,

$$t_b = A \left(\ln \frac{L_o}{L_e} \right)^{1/2} + \frac{2\eta_d}{P} \ln \frac{L_o}{L_e} + BL_e^{2/3} \ln \frac{L_e}{A_i} \quad (48)$$

The liquid instability wavelength (Eq. (40)), equivalent sphere particle diameter (Eq. (41)), liquid instability shear rate (Eq. (44)), and liquid deformation shear rate (Eq. (38)) all require the substitution of $L = L_e$ in their evaluation.

The radius, R_e , of the deformed liquid at breakup is given by

$$R_e = R_o \left(L_o / L_e \right)^{1/2} \quad (49)$$

The lateral motion of the liquid during its deformation causes the particles produced by the breakup to have a lateral velocity. This lateral velocity causes the particles to undergo further lateral spreading during their free fall - consistent with their drag properties. This causes the width of the ground pattern to increase with increase in aircraft altitude up to some limiting value. Turbulent diffusion also causes lateral spreading of the particles, but in this case only the very small particles (e.g., < 0.1 mm) undergo spreading during their fall.

The lateral velocity of the liquid at any time and position is given by dR/dt , where R is given by Eq. (37). Evaluating to obtain the lateral velocity of the particles at radius R_e at the time of liquid breakup gives

$$V_e = R_e \left[\frac{A}{\left(\ln \frac{L_o}{L_e} \right)^{1/2}} + \frac{4\eta_d}{P} \right]^{-1} \quad (50)$$

4.2.3.1 Further Comments

The present model used to describe the initial breakup of the liquid after ejection from the aircraft assumes the liquid to be in the form of a cylinder which undergoes aerodynamic deformation and then breakup due to the growth of Taylor instabilities. A rigorous solution that describes the combined deformation and instability growth is not available, and represents a formidable problem. What is available however, is a solution of the liquid deformation as a function of time, and an approximate solution of the Taylor instability breakup time of a liquid sheet with constant thickness.

Using these, the solution to the problem is obtained by assuming that the breakup time, t_b , of the liquid (Eq. (45)) is equal to the time, t_d , to deform the liquid from its initial thickness, L_0 , to some effective thickness, L_e , plus the time, t_1 , for the Taylor instability growth to break the liquid with thickness L_e . The unique value of L_e is obtained by the minimization procedure given in Eq. (46).

The preceding problem of the deformation and Taylor instability breakup of a liquid is analogous to the problem of the surface heating and ignition of a combustible material such as a propellant. In this case the heating of the propellant surface by some suitable means, such as by thermal radiation, causes the temperature of the surface to rise with increase in time. An exact analytical solution of this temperature rise is available for the case that the surface does not undergo thermal decomposition reaction. The heating of the inert surface is analogous to the deformation (without instability growth) of the liquid, except that the temperature increases with increase in time whereas the liquid thickness decreases. Analogous to the Taylor breakup time at constant liquid thickness, a solution of the decomposition reaction time leading to ignition is available for the case of an initially constant reaction temperature. However during the surface heating the temperature continually increases, which ultimately causes fast thermal decomposition which culminates in ignition.

An analytical solution of the preceding surface ignition problem was obtained earlier⁴⁶ in a manner similar to that used here for the Taylor breakup problem. The ignition time was considered to be given by the time for the surface heating (considered inert) to raise the surface temperature to some effective value, plus the time for the thermal decomposition (ignition-producing) reaction to occur at that temperature. The unique effective temperature was obtained by the minimization procedure given in Eq. (46).

However, unlike the Taylor breakup problem, numerical solutions of the surface heating and ignition equations were available.^{47,48} It was shown in reference 46 that the analytical solution obtained on the basis of the preceding minimization technique was in very good agreement with the numerical solution as closely as could be determined. Moreover the results of the numerical solution were consistent with an ignition criterion based on the minimization technique.

There is thus considerable evidence that the method used here to solve the equations describing the deformation and Taylor instability breakup of the liquid is a good approximation to the true solution of the problem, and will give useful results.

5. MEASUREMENT OF RHEOLOGICAL PROPERTIES

Experimental studies were conducted to measure the rheological and physical properties of presently used liquid fire retardants that are of importance in describing the dispersion and impaction behavior of the retardants. The retardants studies included Phos-Chek XA, Fire-Trol R100 and Fire-Trol R 931 (LC). The properties of interest included viscosity as a function of shear rate, surface tension, yield stress and fluid elasticity.

The viscosity of a thickened or viscoelastic fluid is usually a function of shear rate, and as discussed previously it is to be expected that shear thinning and elasticity has a significant effect on the breakup characteristics of most viscous fire retardant solutions. The viscosity of Newtonian fluids is independent of shear rate; whereas for shear thinning fluids the viscosity decreases with increase in shear rate, but at sufficiently high shear rates may either become constant or increase again. For a dilatant liquid the fluid viscosity increases with increase in shear rate.

On the program measurements were made by Shock Hydrodynamics of the viscosity of the retardants at shear rates between 1 and 1400 sec⁻¹ and yield stress, using a Haake Rotoviscometer which was obtained on loan from the Forest Service. Independent measurements of viscosity over a more extended shear rate range and of fluid elasticity were made by the Flame and Incendiary Research Laboratory of the U. S. Army Edgewood Arsenal in Edgewood, Maryland, under subcontract to Shock Hydrodynamics. The Rotoviscometer is a rotating viscometer, whereas the Edgewood Arsenal instrument is a high pressure capillary tube viscometer. Measurements were also made of retardant surface tension.

5.1 ROTATIONAL VISCOMETER TECHNIQUE

The fire retardants studied were prepared in a Proctor-Silex Model 8040 blender, which has seven speeds. The maximum and minimum speeds are 21,000 and 12,000 rpm. The mixing propellor has four blades, each 1.0 in. long and approximately 0.26 in. wide.

The retardant solutions were prepared as follows. To 500 ml of distilled water was added 68.4 grams of powdered Phos-Chek XA (obtained from Monsanto Corp.). The mixture was mixed for 0.5 min. at the lowest blender speed and then for 2.5 min. at the highest speed. The mixing procedure for Fire-Trol 100 (the Fire-Trols were obtained from Chemonics Co.) included the addition of 167.5 grams of the powder to 500 ml distilled water, and blending the mixture for 2.5 min. at the No. 2 speed level. Fire-Trol 931 (LC) was diluted in distilled water, mixing ration 1:4, and stirred vigorously to obtain a homogeneous solution.

For purposes of quality control, the apparent viscosity of each mixture was measured using a Brookfield LVF viscometer, at 60 rpm using spindle 4 for the Phos-Chek XA and Fire-Trol 100 and using spindle 2 for the Fire-Trol 931. The readings were taken after the spindles turned for 1 min. The mixtures were suspended in a 20°C water bath in a 300 ml beaker and allowed to obtain temperature equilibration with the bath before the viscosity was determined.

The Haake Rotovisco was employed for measurements of viscosity as a function of shear rate. A water bath was connected to the temperature controlled assembly using a submersible pump. The exterior wall of the MV beaker containing the sample was coated with glycerine so as to establish good thermal contact with the wall of the tempering vessel. Rotors MVI, MVII and MVIII were employed and measurements were made at the ten speeds between 3 and 486 rpm.

Using the lowest speed and the MV rotors, the instrument was calibrated by suspending known weights between 10 and 50 grams from the rotor using light weight thread, and measuring the scale reading, S_C . The force exerted by the weight results in a torque moment on the rotor which is defined by the weight, G , and radius, r , of the rotor. The values of scale sensitivity, a , were determined by

$$a = G r / S_C, \text{ grams-cm/scale division} \quad (51)$$

The ratio of the experimental values obtained to the values quoted on the Rotovisco calibration certificate were 4.78/(4.978), 4.92/(4.868), and 4.87/(4.869), grams-cm/scale division, respectively, for the MV I, II, and III, which represents a maximum uncertainty of 4.1% and an average error of 1.7%. The instrument constants a , B and k used in estimating apparent viscosity, shear rate and shear stress are shown in Table I.

TABLE I. INSTRUMENT CONSTANTS FOR HAAKE ROTOVISCOMETER*

Rotor	Rotor Radius (cm)	a	B	k
MV I	2.004	4.978	1370	2.38
MV II	1.84	4.868	529	6.93
MV III	1.52	4.869	259	20.49

*Beaker radius = 2.10 cm; Rotor length = 6.00 cm.

The formulae used in estimating the shear stress at the rotor, σ_r , the uncorrected shear rate, \dot{S}_u , and apparent viscosity, η_{app} ; are,

$$\sigma_r = AS_C, \text{ dynes/cm}^2 \quad (52)$$

where $A = k B/100$, and S_C is the scale reading of the instrument,

$$\dot{S}_u = B/U, \text{ sec}^{-1} \quad (53)$$

where U is the gear position of the Rotovisco, and

$$\eta_{app} = U S_C k. \quad (54)$$

5.2 EXPERIMENTAL RESULTS

The results obtained on each of the three fire retardant mixtures are shown in Figures 4 - 6. The effect of temperature variations on the apparent viscosities of Phos-Chek XA and Fire-Trol 100 were also studied, and the results obtained at 20° and 30° C are reported in these figures. In each case different samples of the same prepared mixture were used in making these determinations since it was found that variations in mixing and other uncontrolled test variations could be comparable to the variations caused by temperature changes. Examples of the magnitude of these test variations are shown in Figures 7 and 8 where the apparent viscosities of three different Phos-Chek XA mixtures are given.

The apparent viscosities obtained for the retardant solutions using the Brookfield LVF viscometer are estimated to be 1050-1650, 2075-2490, and 130-160 centipoise, for Phos-Chek XA, Fire-Trol 100, and Fire-Trol 931 (LC), respectively. The calculated shear rate under the operating conditions of the 'Brookfield' is 12.5 sec^{-1} for these measurements. These calculated shear rates are based on an empirical formula⁴⁵

$$\dot{S} = (0.209) \cdot (\text{rpm of spindle}), \text{ sec}^{-1} \quad (55)$$

5.2.1 Data Correction

The shear rates and viscosities obtained by Eqns. (53) and (54) are only "apparent" viscosities and apparent shear rates, since these terms are derived from the Newtonian expression for rate of shear at the wall of the inner cylinder³³. A more correct estimate of apparent viscosity and shear rate can be made by correcting for non-Newtonian behavior at the wall of the inner rotating cylinder, i.e., at the bob. The treatments of Krieger and Maron⁵⁰ and Krieger and Elrod⁵¹ were utilized, whereby the flow behavior of non-Newtonian fluids is defined by the functional relationship, g , between the viscosity gradient (or rate of shear) dv/dy , and the shearing stress, σ ,

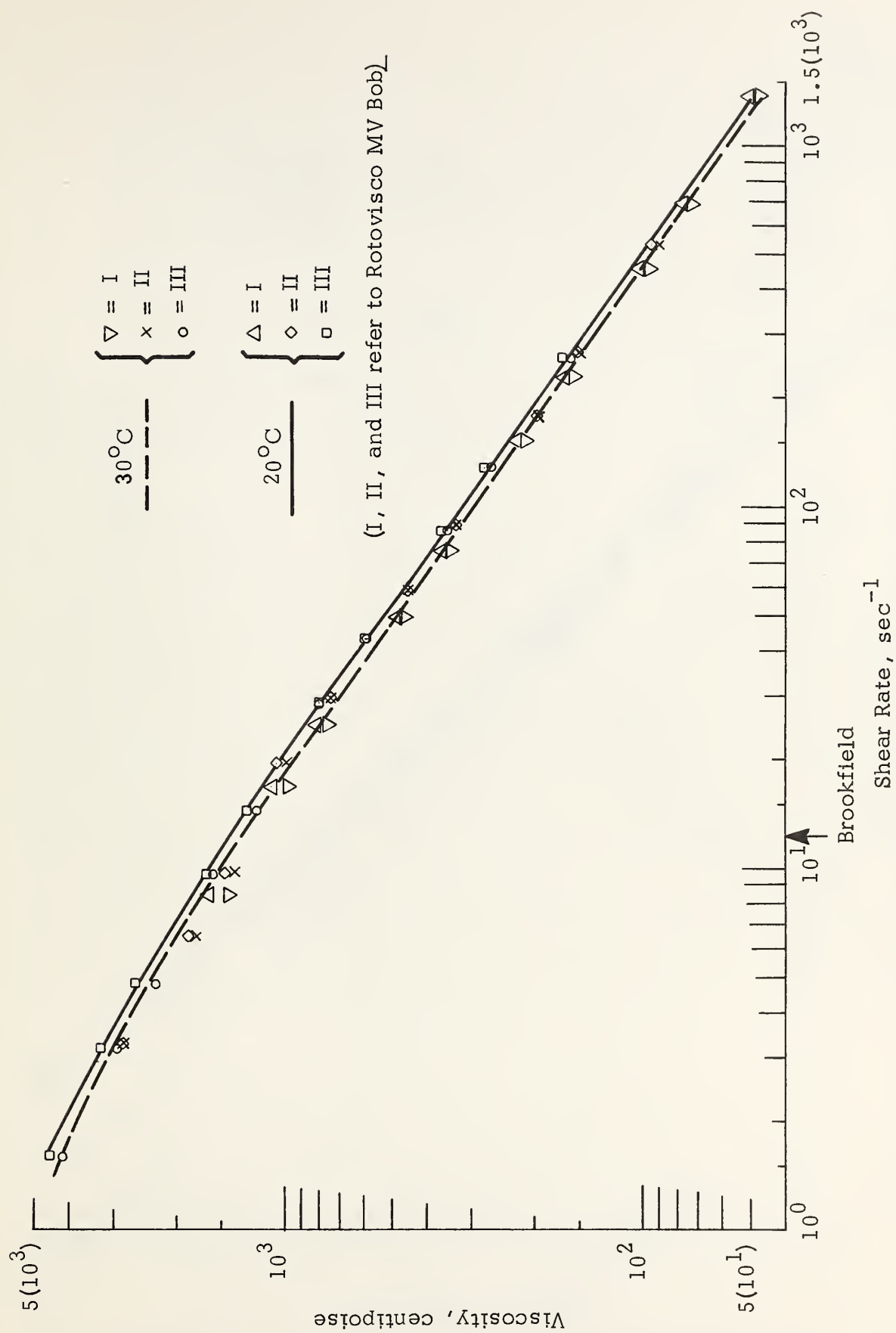


Figure 4. Apparent Viscosity of Phos-Chek XA as a Function of Shear Rate (Uncorrected).

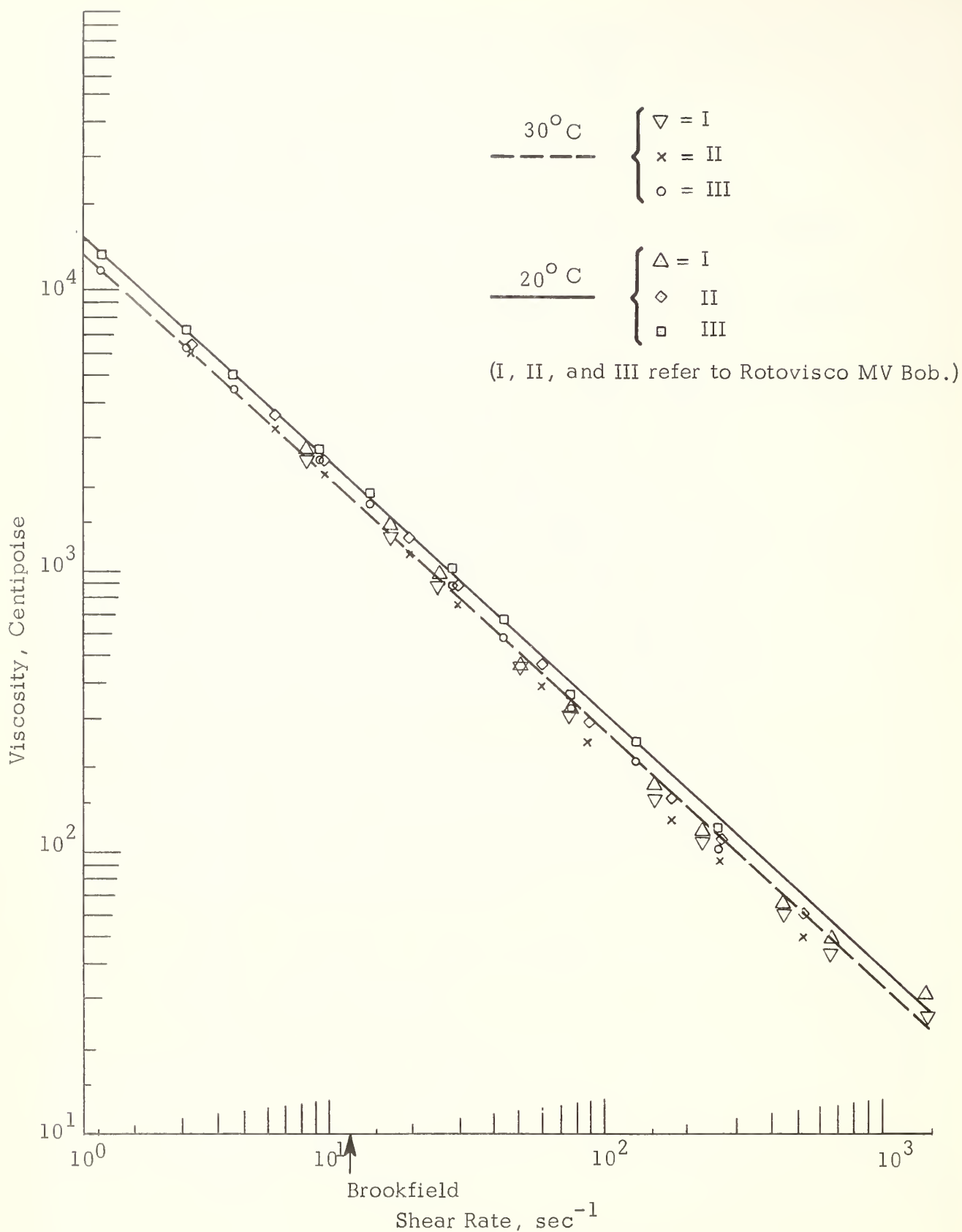


Figure 5. Apparent Viscosity of Fire-Trol 100 as a Function of Shear Rate (Uncorrected).

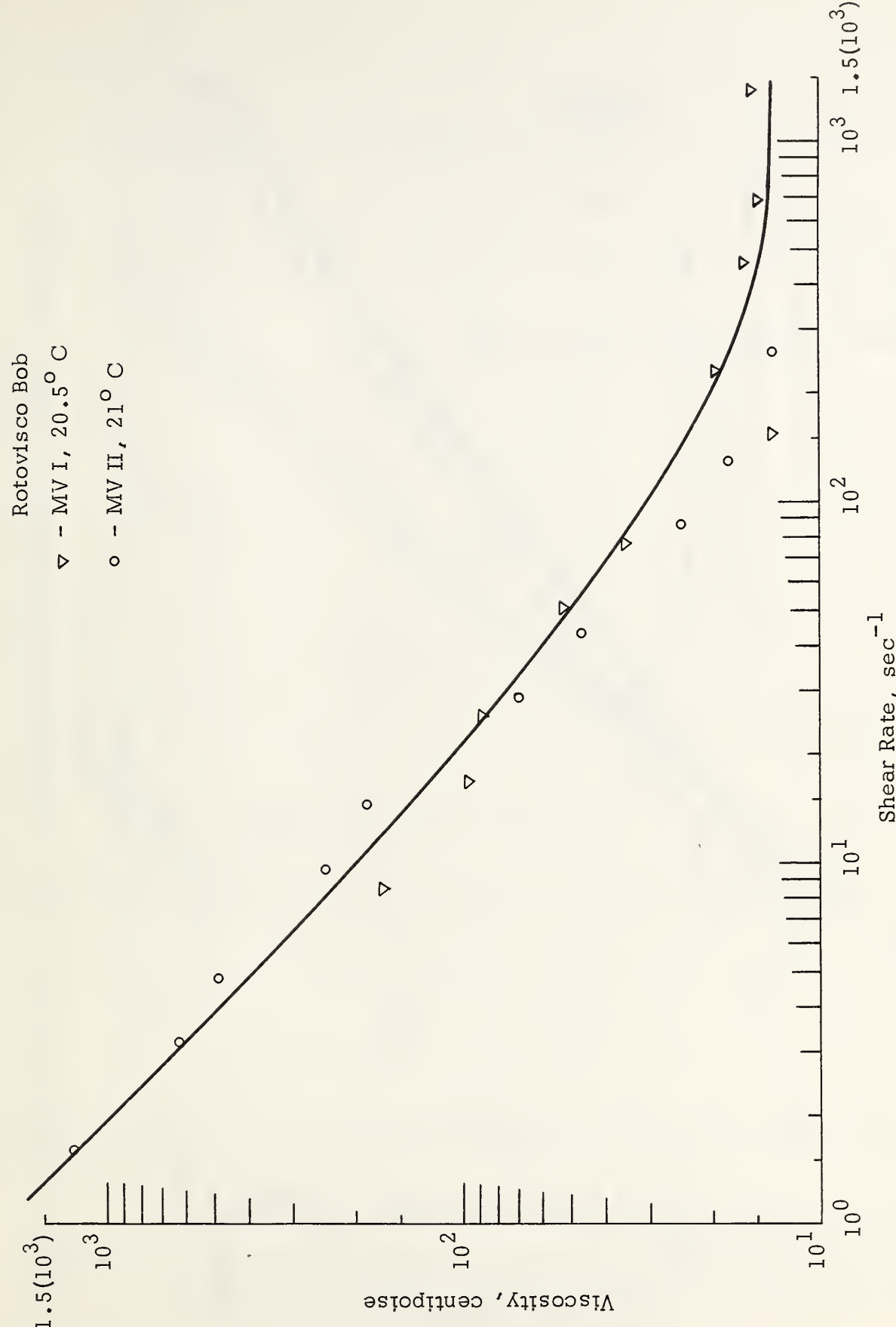


Figure 6. Apparent Viscosity of Fire-Trol 931 (LC) as a Function of Shear Rate (Uncorrected).

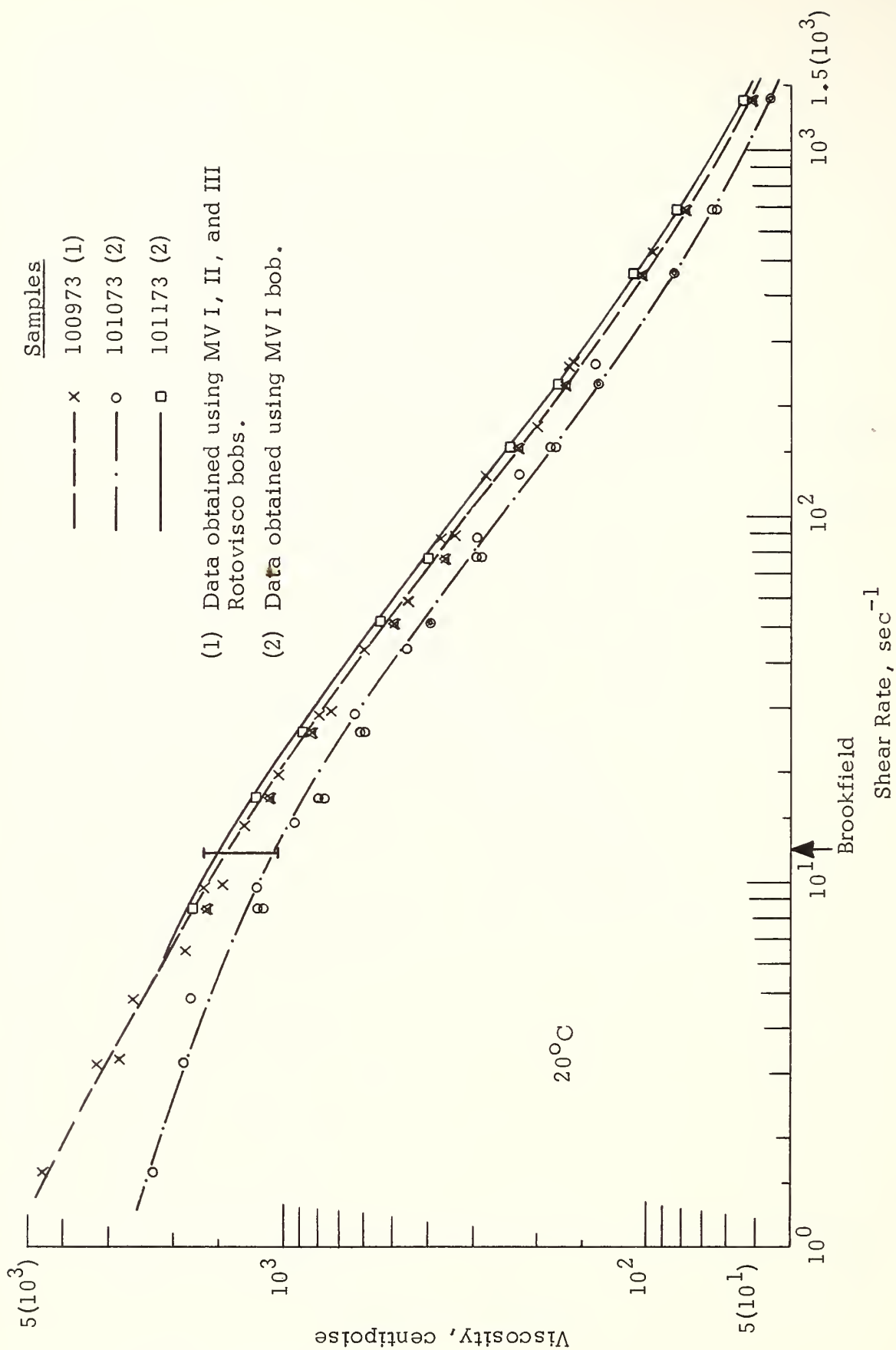


Figure 7. Apparent Viscosity of Phos-Chek XA Retardant Solutions as a Function of Shear Rate. Differences Between Solutions Reflect Variations in Sample Preparation.

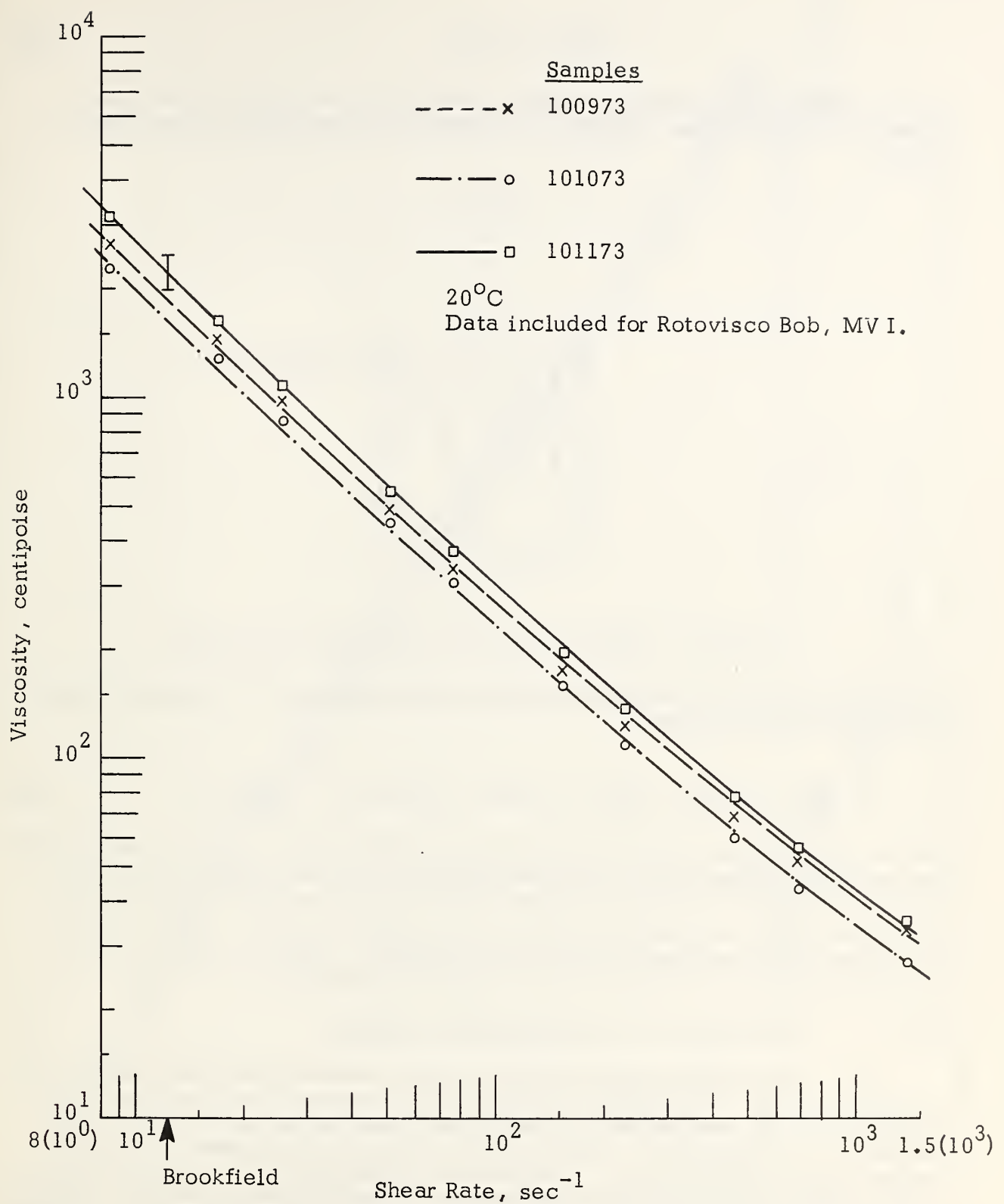


Figure 8. Apparent Viscosity of Fire-Trol 100 Retardant Solutions as a Function of Shear Rate. Differences Between Solutions Reflect Variations in Sample Preparation.

$$\frac{dv}{dy} = g(\sigma) \quad (56)$$

and the clearance between the walls of the sample cup and the rotor bob is taken as an independent variable (see Figure 9 for description of the viscometer).

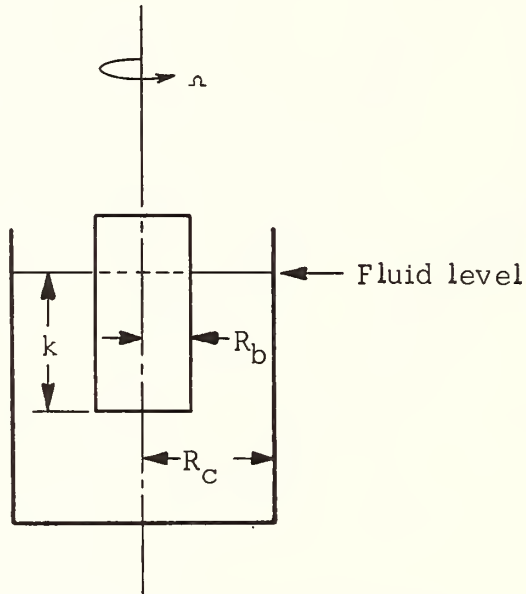


Figure 9. Model of Concentric Cylinder Viscometer.

From the mathematical model developed by these workers the corrected expression for the rate of shear is

$$\dot{\gamma}_{corr} \equiv g(\sigma_r) = \frac{\nu}{\ell n \epsilon} [1 + m \ell n \epsilon + \frac{1}{3} (m \ell n \epsilon)^2 + \frac{m'}{3} (\ell n \epsilon)^2] \quad (57)$$

where ν is the angular velocity of the rotor (radians/sec), ϵ is the ratio of the cup or beaker radius to the rotor (bob) radius, m is the slope of the $\log \nu$ vs $\log \sigma_r$ data and m' is the second derivative of $\log \nu$ vs $\log \sigma_r$. In order to obtain the values of m and m' at the various shear stresses, a least square polynomial was computed for each set of data (i.e., $\log \nu$ vs $\log \sigma_r$). A computer program was written to make these calculations.

5.3 DISCUSSION OF EXPERIMENTAL RESULTS

The experimental data for the three fire retardants were corrected using the Krieger-Maron-Elrod treatment. The corrected data are shown in Figures 10 to 16, and reflect the corrections made by the application of this treatment. In Figures 10-12 are shown log-log plots of apparent viscosity versus corrected shear rate. A comparison of these figures with Figures 4-6 shows that the effects of the corrections are generally small. Figure 13 shows a comparison of the viscosity versus shear rate of the three retardants. Figures 14-16 show log-log plots of shear stress versus corrected shear rate of the retardants.

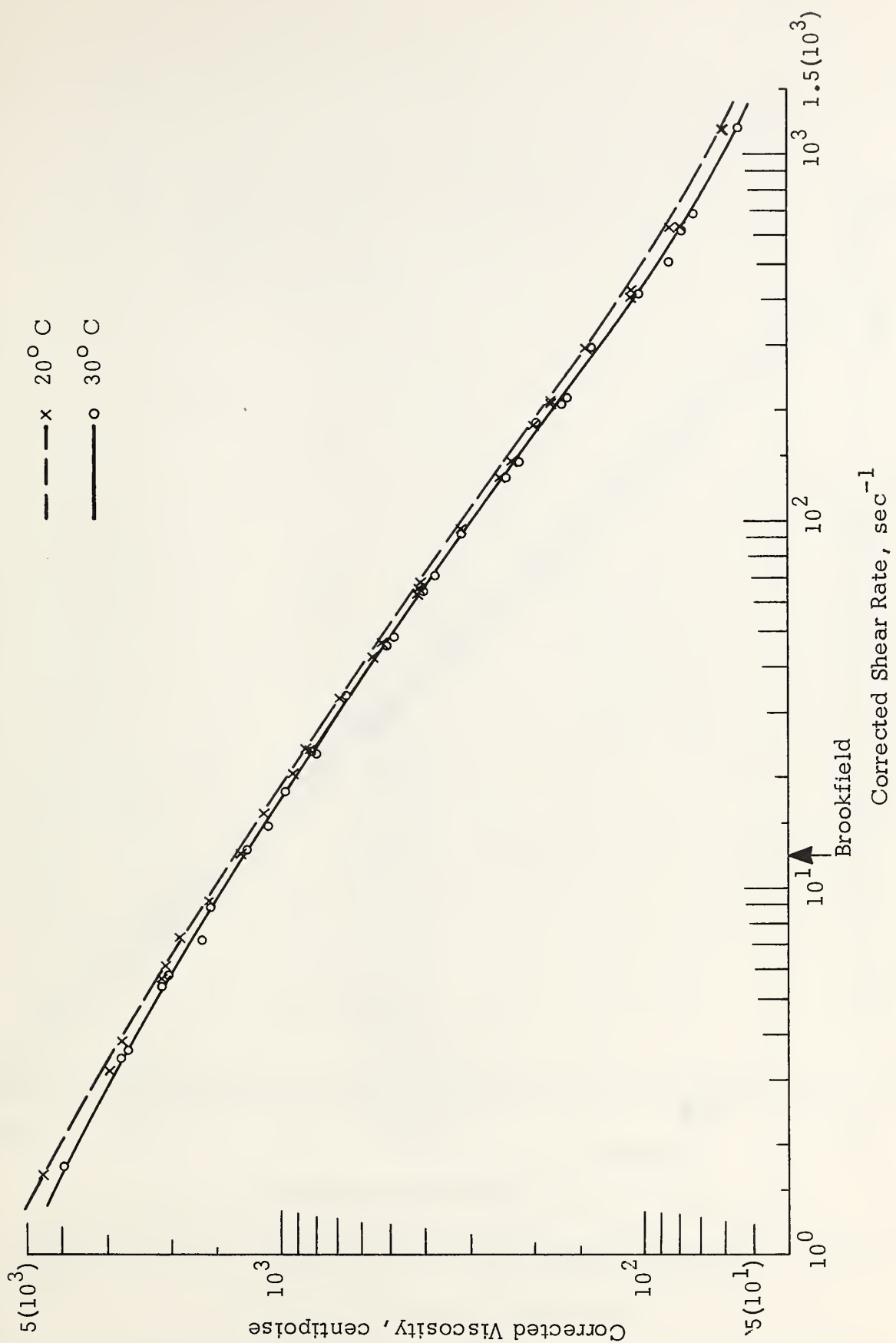


Figure 10. Corrected Apparent Viscosity Versus Shear Rate for Phos-Chek XA at 20° C and 30° C .

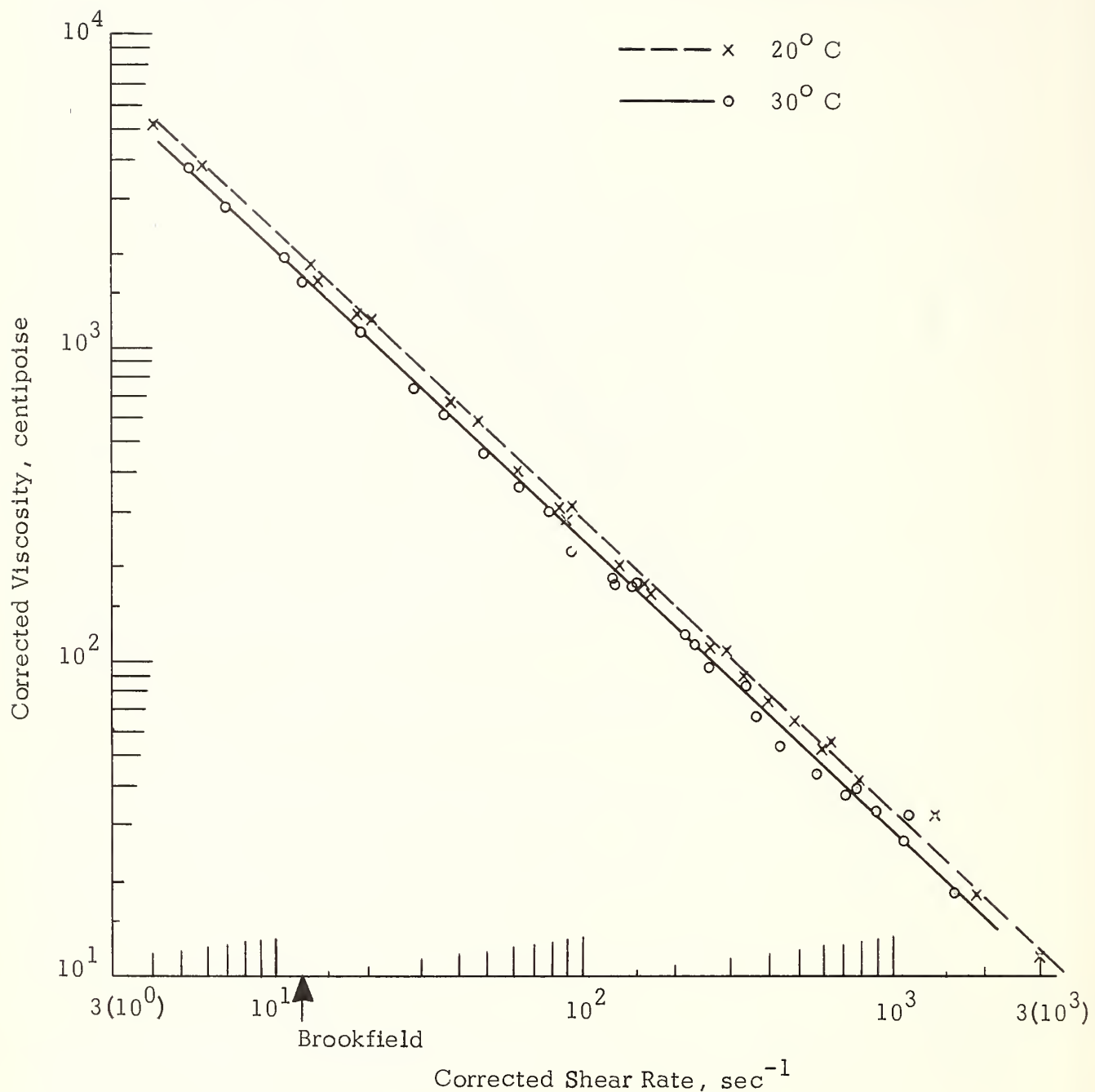


Figure 11. Corrected Apparent Viscosity Versus Shear Rate for Fire-Trol 100 at 20°C and 30°C .

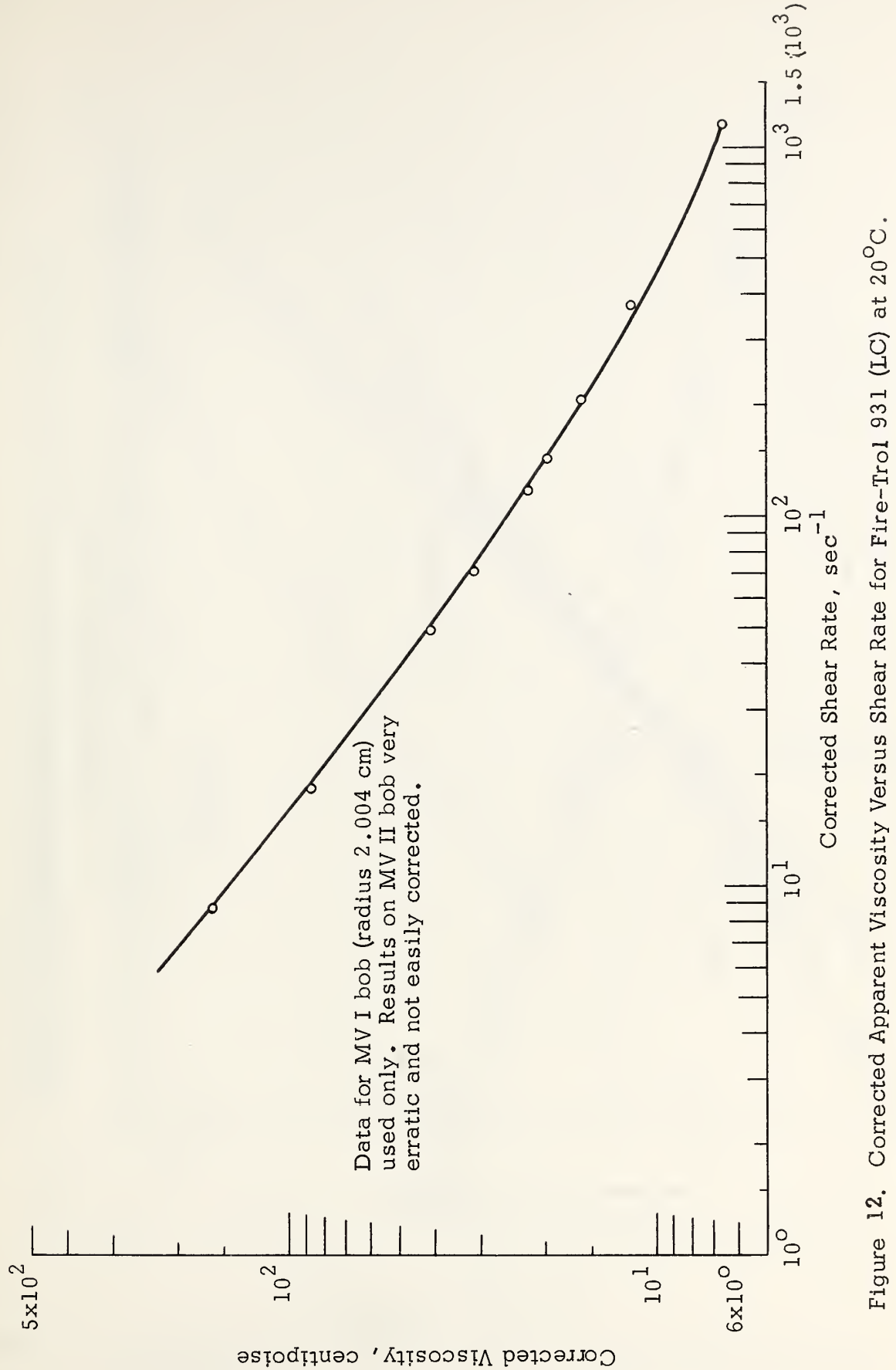


Figure 12. Corrected Apparent Viscosity Versus Shear Rate for Fire-Trol 931 (LC) at 20°C.

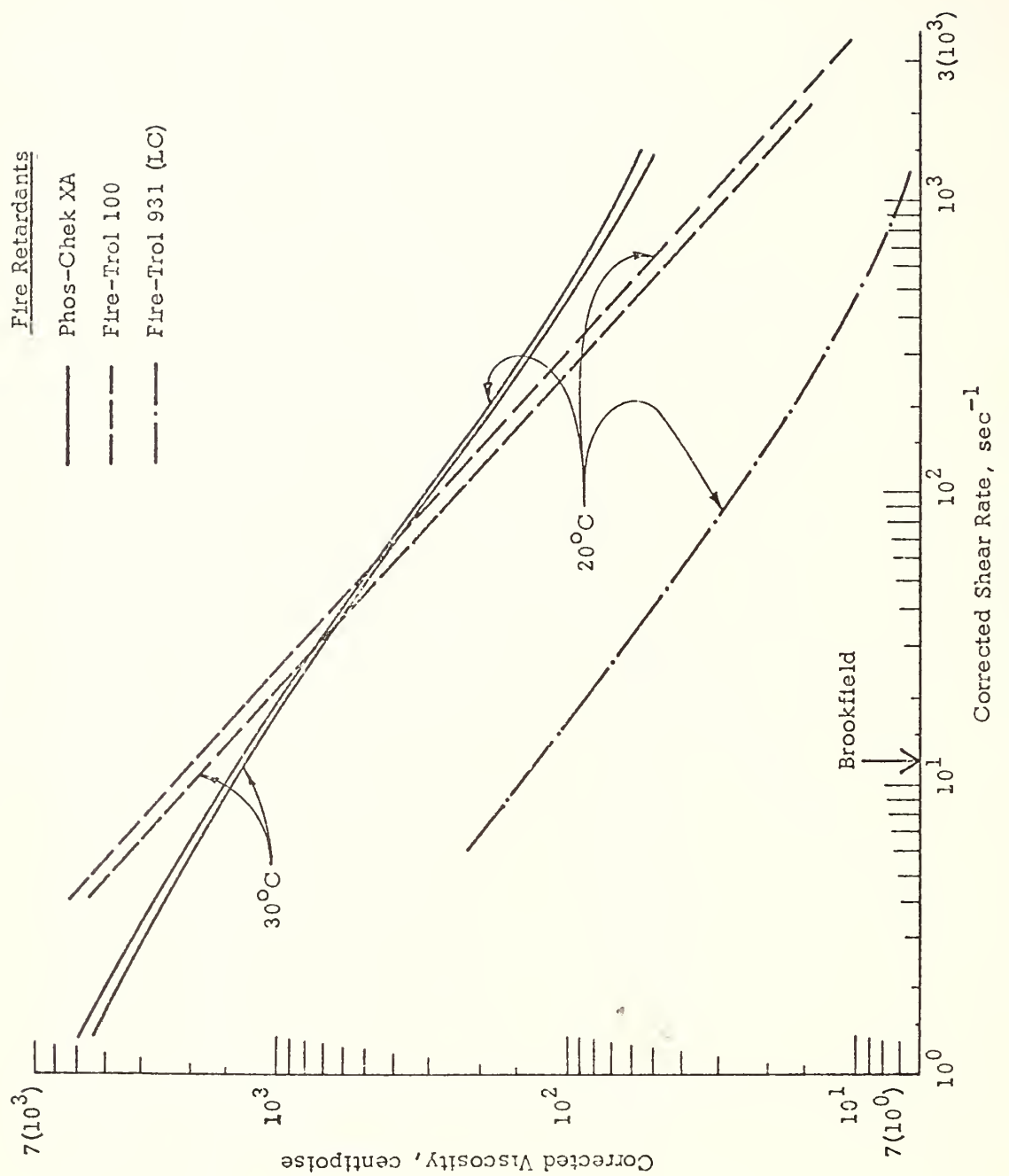


Figure 13. Comparison of the Corrected Viscosity as a Function of Shear Rate of the Three Fire Retardant Solutions.

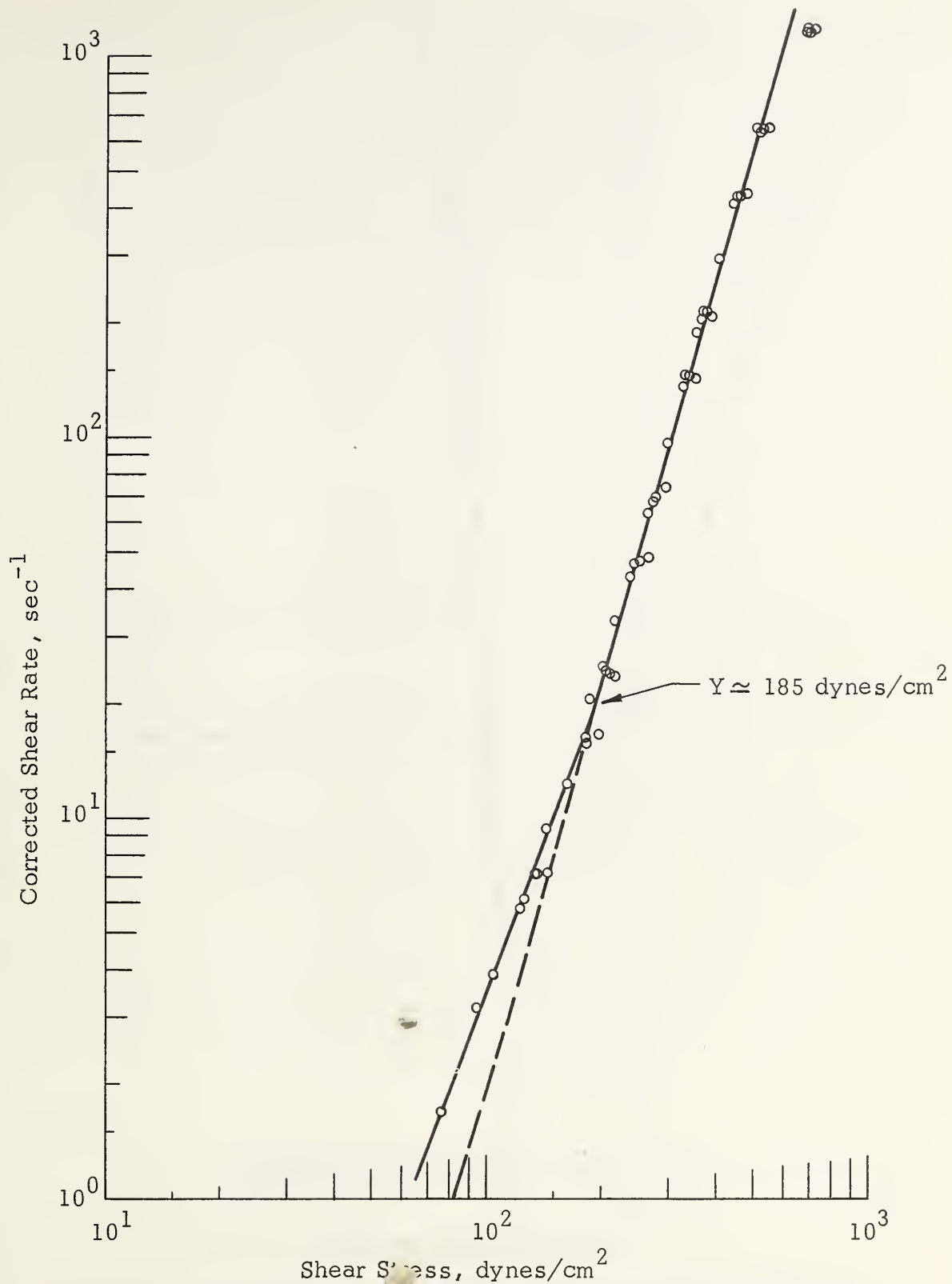


Figure 14. Power Law Plot of Shear Stress Versus Shear Rate for Phos-Chek XA at 20° C.

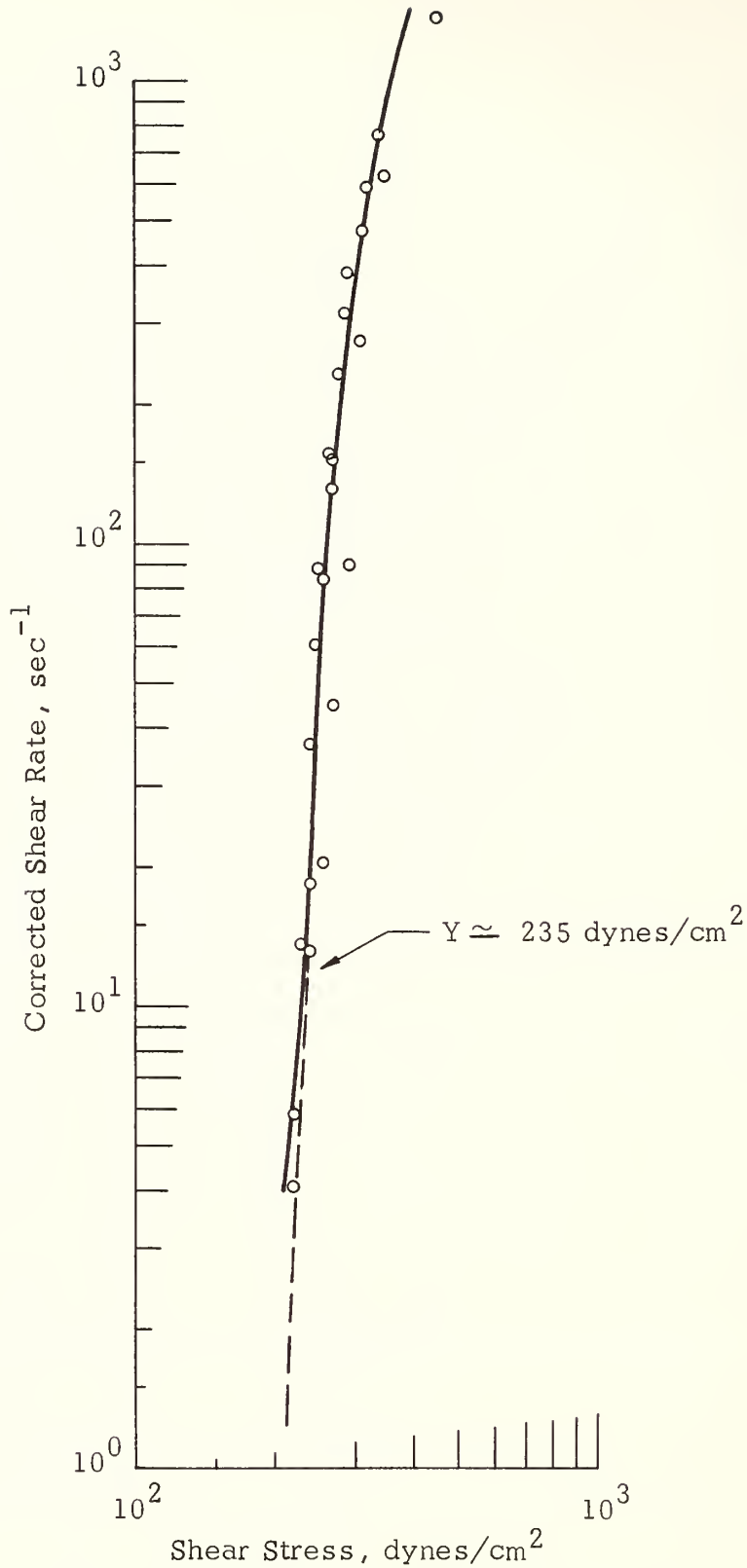


Figure 15. Power Law Plot of Shear Stress Versus Shear Rate for Fire-Trol 100 at 20°C.

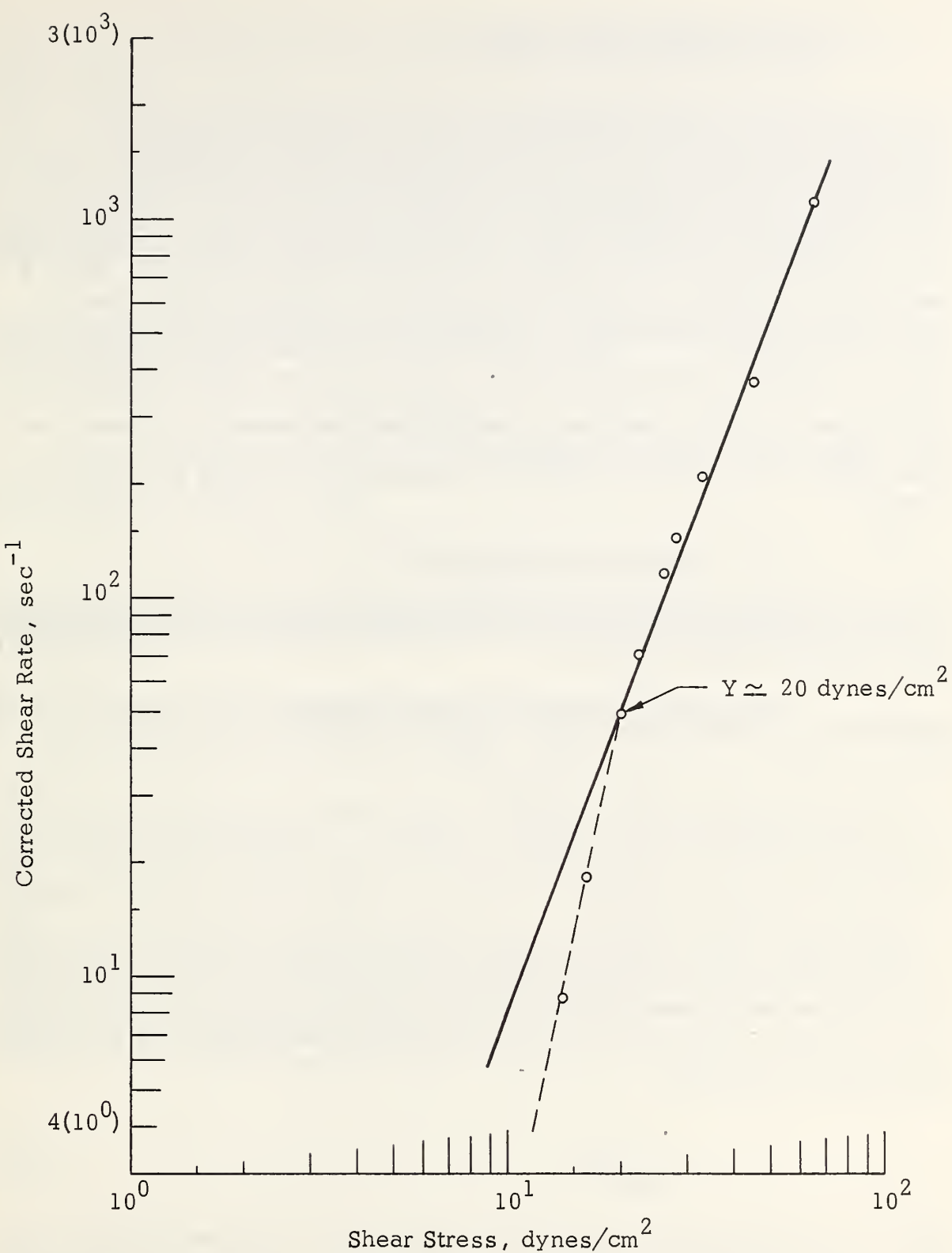


Figure 16. Power Law Plot of Shear Stress Versus Shear Rate for Fire-Trol 931 (LC) at 20°C.

5.3.1 Effect of Shear Rate

It can be seen from both the uncorrected and the corrected data that Fire-Trol 100 is much more sensitive to shear rate than is Phos-Chek XA, and a crossover in the apparent viscosities of the two retardants occurs at a shear rate of approximately 50 sec^{-1} . Thus at the lower (e.g., Brookfield) shear rates Phos-Chek XA has a higher apparent viscosity than Fire-Trol 100; whereas at shear rates greater than about 50 sec^{-1} the apparent viscosity of Phos-Chek XA is lower than that of Fire-Trol 100. This general behavior appears reasonable since Phos-Chek XA is a gum thickened material, whereas Fire-Trol 100 is a clay thickened material. It also appears that the viscosity of Fire-Trol 931 becomes essentially independent of shear rate at shear rates exceeding approximately $2000\text{-}4000 \text{ sec}^{-1}$. If this is true then the viscosity curves of the two Fire-Trol retardants would also cross. In this case the apparent viscosity of Fire-Trol 100 would be less than that of Fire-Trol 931 at sufficiently high shear rates. There is some uncertainty regarding the experimental curvature of the $\log \eta$ versus $\log \dot{S}$ plot at the highest shear rates for Fire-Trol 931, and it is necessary to have higher shear rate viscosity data in order to resolve this question.

5.3.2 Estimated Yield Stress

The Krieger-Maron-Elrod treatment does not include a consideration of the yield stress. However, from the data obtained, an attempt has been made to estimate yield stress, Y .

It has been observed that many viscoelastic fluids obey the power law although its use is often questioned on the basis of dimensional analysis⁵², i.e.,

$$\eta = \frac{\sigma}{\dot{S}} = k \dot{S}^{n-1} \quad (58)$$

$$\sigma = k_1 \dot{S}^n \quad (59)$$

In Figures 14-16 it is evident that over a relatively broad range of shear rates the power law is obeyed for both Phos-Chek XA and Fire-Trol 100, and for Fire-Trol 931 it is obeyed over a lesser range. When the shear stress (σ_r) within the gap between the rotating bob and stationary cup falls below the yield stress it would be expected that the fluid flow would be drastically altered. This shear stress is given by

$$\sigma_r = \frac{M}{2\pi k r^2} \quad (60)$$

where r is the radial distance from the rotating axis of the bob to some point between R_b , the bob radius and R_c , the cup radius, k , is the effective length of the bob in the fluid, and M is external torque on the bob. At the point where $\sigma_r < Y$, "plug flow" should occur, that is, in the part of the gap close to the cup wall where the yield value is not exceeded there exists a non-moving body of material, while across the remaining gap the same material exhibits laminar flow in the region where the stress exceeds the yield value.

It would be expected the slope, n , of the power law relationship (i.e., $\log S$ vs $\log \sigma_r$) changes when the shear stress at the bob approaches the yield stress.

As shown in Figures 14-16 there does appear to be a sharp enough transition to permit the estimation of the value of the yield stress, Y . The values estimated for Phos-Chek XA, Fire-Trol 100 and Fire-Trol 931 (LC), at 20°C are 185, 235, and 20 dynes/cm², respectively, using the corrected data obtained from the Rotovisco instrument under conditions where the largest bob (i.e., MVI, radius 2.004, cup radius 2.10 cm) was used.

The Reiner-Rivlin model for a plastic body or Bingham body³³ was also employed for the estimate of yield stress. This model which is based on Newtonian flow, i.e.,

$$\eta = (\sigma - Y) / (-dv/dr) \quad (61)$$

where σ is given by Eqn. (60) and M is the external torque on the rotating bob (see Figure 9). Assuming that

$$-dv/dr \approx r dw/dr \quad (62)$$

where w is the angular velocity and integrating between $w = \omega$ at the bob wall (radius R_b) to $w = 0$ at the interface laminar and plug flow (radius R) there is obtained

$$\omega = \frac{-dv/dr}{(\sigma - Y)} \left[\frac{M}{2\pi k} \left(\frac{1}{R_b^2} - \frac{1}{R_c^2} \right) - Y \ln \left(\frac{R_c}{R_b} \right) \right] \quad (63)$$

It can be shown that the curve ω versus σ approaches the stress axis at the yield stress tangentially (i.e., $d\omega/d\sigma \rightarrow 0$) because the gap distance (R_b/R) within which laminar fluid flow occurs approaches zero. Thus if one assumes Newtonian flow the yield stress, Y , can be estimated from a best fit of $d\omega/d\sigma$ versus σ or by graphical means at $d\omega/d\sigma = 0$. Following this procedure, yield values were obtained for the two viscous retardants Phos-Chek XA and Fire-Trol 100 at 20°C of between 124-182, and 181-199 dynes/cm². Since this model assumes Newtonian flow, however, the agreement between the latter values and those estimated graphically from the power law relationships (Figures 9-11) may be fortuitous.

5.4 CAPILLARY VISCOMETER TECHNIQUE

A comparison of the results obtained for the viscosity as a function of shear rate for the three retardants using the Model MV Haake Rotoviscometer is shown in Figure 13. Since the shear rate range encompassed by this instrument is lower than that possibly encountered during aerodynamic breakup, independent measurements of viscosity over a more extended shear rate range and of fluid elasticity were conducted under subcontract by the U. S. Army Edgewood Arsenal. These measurements were made without knowledge of the results obtained with the Rotoviscometer.

The Edgewood Arsenal viscometer is a high pressure capillary tube viscometer that was designed and constructed in-house. It is similar to that described in references 34, 35, 53, where the theory of operation - including fluid elasticity determination - is also discussed. Additional discussion is given in references 33 and 54.

The high pressure capillary tube viscometer is a gas pressure-operated apparatus consisting of a stainless steel capillary tube mounted between two filled reservoirs containing the test fluid. The fluid is pushed alternatively from one chamber to the other, and measurements are made either of volume flow as a function of time or of time as a function of volume flow. The slope of the volume flow versus time curve during steady flow must be determined very accurately for reduction of the data, and an 1108 computer was used to determine the slope by least squares.

A series of capillary tubes with different diameters was used in the studies in order to help vary the shear rate. Each tube with measured length L had previously been calibrated with Newtonian liquids with known viscosity to obtain the effective (hydrodynamic) radius R of the tube-including the couette entrance effect. The reduction of the data also included the standard correction for flow kinetic energy. The shear stress, P_{xy} , at the capillary wall is then given by

$$P_{xy} = K_T P_C \quad (64)$$

where $K_T = R/2L$, which is known for each capillary tube, and P_C is the corrected (for kinetic energy) pressure drop across the tube. The shear rate, \dot{S} , at the wall is given approximately by*

$$\dot{S} = K_d a \quad (65)$$

where $K_d = 4/\pi R^3$, which is known for each capillary tube, and a is the slope of the volume flow versus time curve. The viscosity η at shear rate \dot{S} and

*A more rigorous equation is discussed in reference 35.

shear stress P_{xy} is then given by

$$\eta = P_{xy}/\dot{S} \quad (66)$$

If the flowing fluids exhibits elastic properties, then corrections must also be made for the elastic energy, and these corrections serve to define the elastic properties of the fluid. The elastic energy is imparted to the accelerated liquid at the entrance of the capillary, stored as elastic potential energy during stationary flow, and is then carried out of the capillary by the flowing liquid. The effect of elastic energy on the flow is given by the equation

$$P_C = P_{xyc} \left[\frac{2L}{R} + 2n + s \right] \quad (67)$$

where P_{xyc} is the corrected shear stress at the wall taking into account both the elastic energy and end effect, n is the couette (end) correction, and s is the recoverable shear and is related to the normal elastic stress and the stress relaxation time by Eq. (31). The value of $(2n + s)$ in the bracketed term is obtained by plotting P_C as a function of L/R at constant shear rate and determining the abscissa value of L/R , i.e., the value of L/R for $P_C = 0$. The value of $2n$ is small compared to s and can usually be neglected, especially since the Newtonian end correction is already included in obtaining R , and L is always much greater than R . Then*

$$s = \frac{-2L}{R} - 2n \approx \frac{-2L}{R} \quad (68)$$

In order to hold shear rate constant, the elastic properties are determined using capillaries of different lengths but with the same radius.

5.5 EXPERIMENTAL RESULTS AND DISCUSSION

The three fire retardant solutions studied were prepared in a manner consistent with that used for the Rotoviscometer studies. All three formulations were prepared and observed for a period of time before experimental work was initiated with the high pressure capillary viscometer.

5.5.1 Phos-Chek XA Solution

The viscosity of this formulation was investigated as a function of shear rate at three temperature, 10° , 25° , and 50° C. In addition fluid elasticity was determined as a function of shear rate at 25° C.

*A more rigorous equation is discussed in reference 54.

5.5.1.1 Viscosity Behavior

The viscosity is determined using capillaries with very large L/R ratios so that n and s are completely negligible. Figure 17 shows the resulting experimental data obtained for the viscosity as a function of shear rate at 25° C. This data was obtained using a single prepared solution of the Phos-Chek retardant. It was observed that the formulation performed as a homogeneous material when it was evaluated in the high pressure capillary viscometer. Steady flow rates were observed under all experimental test conditions with all capillaries. There was no evidence of any interference of flow by any solid particles or foreign material or by heterogeneity. Small particles and foreign material in solutions usually demonstrate their presence in test solutions by causing irregular flow or stoppage of flow in the small diameter capillaries. In fact, in some cases test solutions are filtered to permit conduct of these viscosity determinations. An interesting observation noted was that Phos-Chek solutions become heterogeneous approximately three to four days after they have been prepared as demonstrated by the fact that steady flow rates cannot then be obtained in the high pressure capillary viscometer.

The viscosity was determined over a range of five decades of shear rate, the extent of the test equipment. the viscosity decreases from about 10 poise at 10 sec^{-1} shear rate to about 0.06 poise at 10^6 sec^{-1} shear rate at 25° C. A comparison of the data curve given in Figure 17 with that obtained with the Rotoviscometer (Figure 10) shows quite good agreement over most of the shear rate range common to both instruments ($10^1 - 10^3 \text{ sec}^{-1}$). The very small difference in the two sets of data is probably not generally statistically significant in view of the experimental scatter in the data and that different test samples were involved (e.g., see Figure 7). However, in the low shear rate range of 10 to 30 sec^{-1} where the viscosity measured by the Rotoviscometer is greater than that measured by the HP capillary (e.g., 50% greater at 10 sec^{-1}) the difference is probably significant, and the Rotoviscometer data appears most valid in this range since this data is supported by the Brookfield viscometer measurements.

The general agreement between the viscosity data obtained for Phos-Chek by the two viscometer measurements is of some interest since the two techniques differ appreciably in certain ways. Generally speaking the experimental scatter in the data is less for the Rotoviscometer than for the high pressure capillary viscometer and the data is much easier to obtain by the Rotoviscometer. However the high pressure capillary viscometer can attain much higher shear rates than can the Rotoviscometer.

The viscosity of Phos-Chek XA was also determined at 10° and 50° C. A different (second) prepared solution was used in these measurements than in the 25° C measurements. Curves describing the test results together with the curve obtained at 25° C are given in Figure 18. It will be observed that the viscosity data obtained at 10° C lie above that obtained at 25° C - as expected - but that the data obtained at 50° C lie above the 10° C data rather than below the 25° C data. The reason for this latter behavior is not known. Edgewood speculated that since the Phos-Chek is not a simple solution, the combination of increased temperature and shear rate may possibly impose a dominant effect on the polymer and not on the remaining ingredients, and that the reason the 10° C viscosity data was above the 25° C data was then due to sample differences. However the temperature effect found using the Rotoviscometer was normal, i.e., the 20° C data was below the 30° C data (Figure 10). Also the 10° C data obtained using the high pressure capillary viscometer is below the

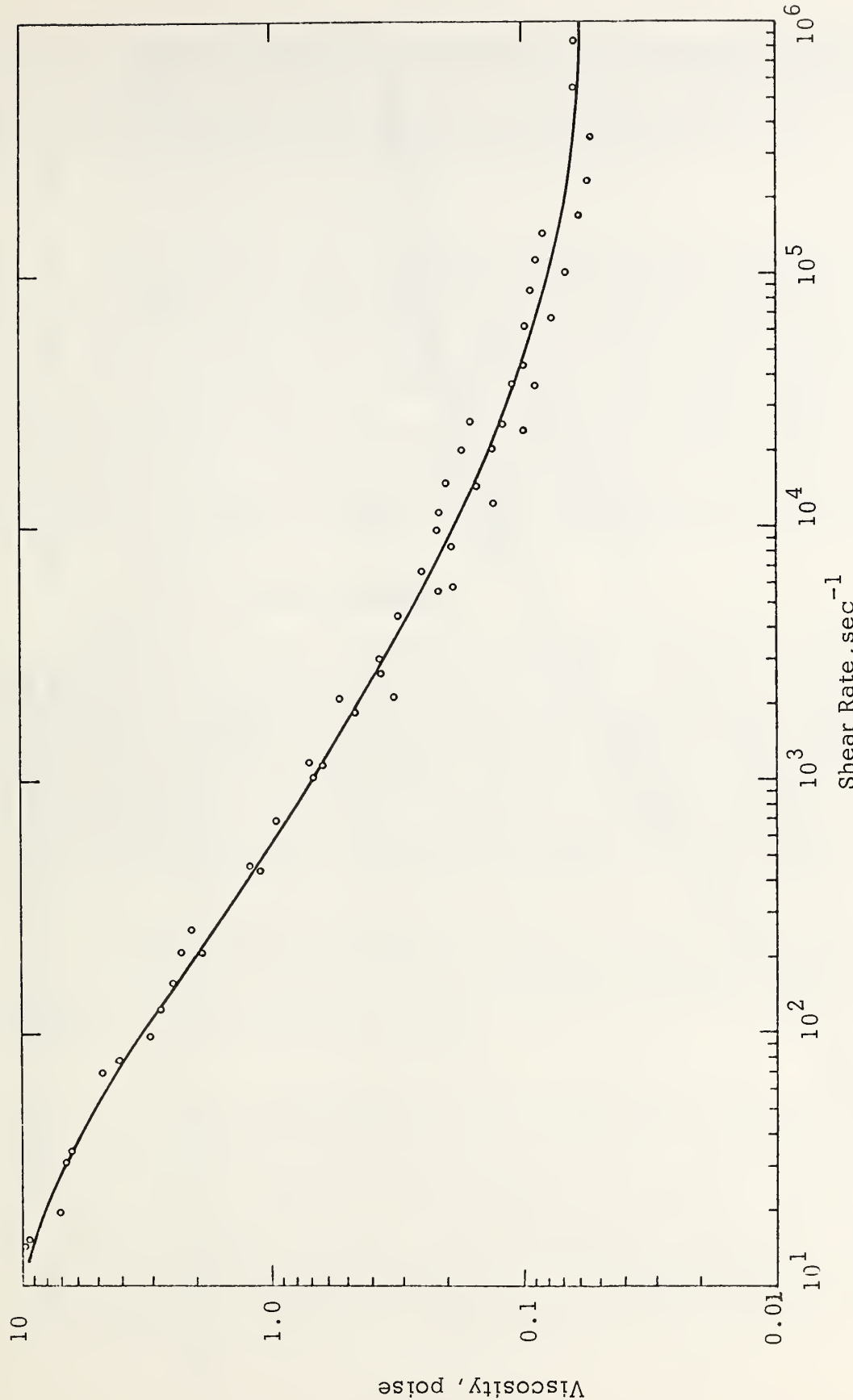


Figure 17. Experimental Viscosity Versus Shear Rate for Phos-Chek XA at 25°C Determined by the High Pressure Capillary Tube Technique.

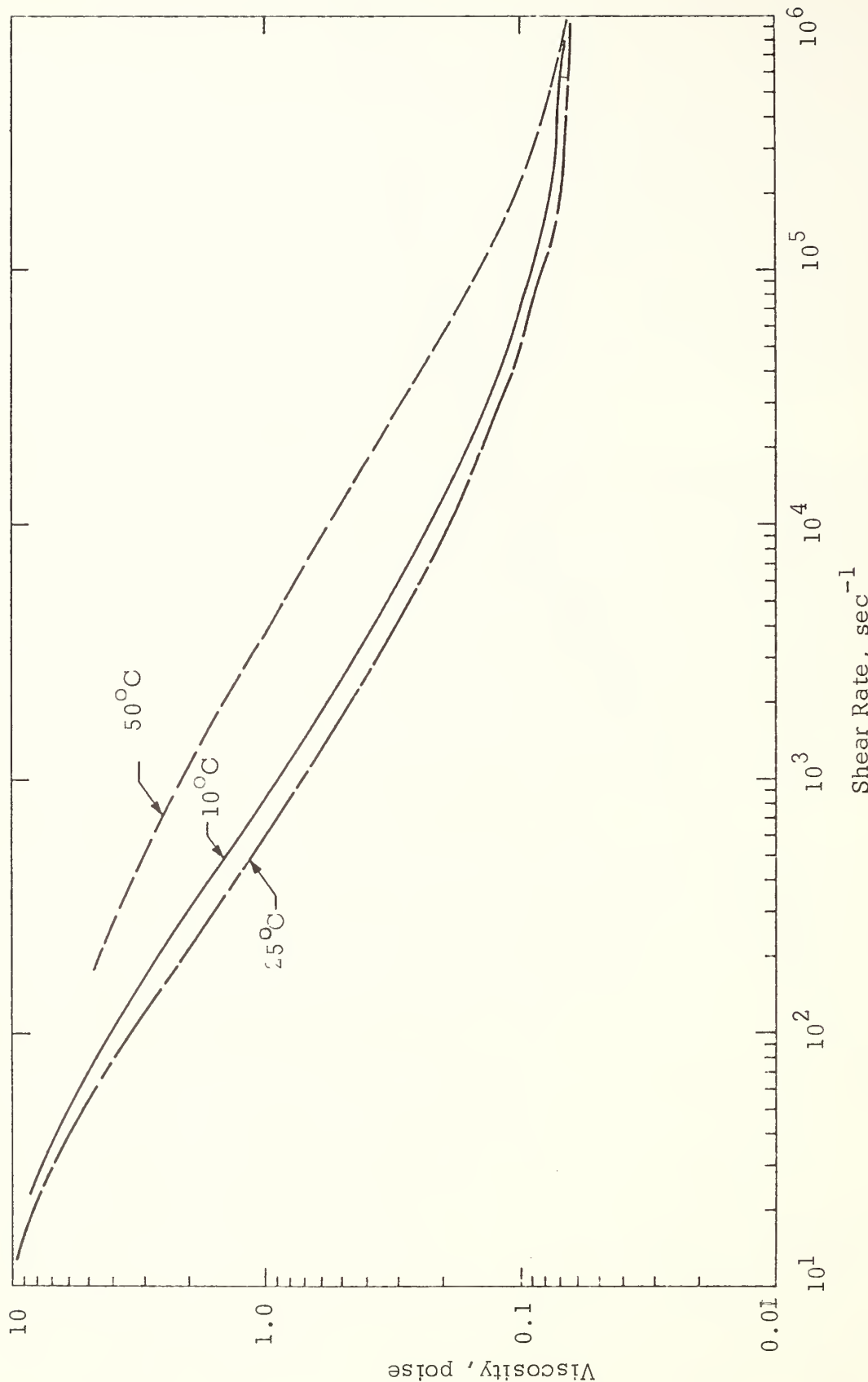


Figure 18. Viscosity Versus Shear Rate for Phos-Chek XA at Various Temperatures. From High Pressure Capillary Viscometer Experiments.

20°C data obtained using the Rotoviscometer, as would be expected. It would therefore appear that the 50°C data obtained with the capillary viscometer is either in error for some unknown reason, or else that at some temperature greater than 30°C the temperature effect reverses for some unknown reason. This latter possibility could be checked using the Rotoviscometer.

5.5.1.2 Elasticity Behavior

The elasticity of the Phos-Chek formulation was determined at 25°C in conjunction with the viscosity studies at that temperature (the same solution was used). Figure 19 illustrates the type of data used to estimate the elasticity based on Eq. 67. Figure 20 shows the resultant elasticity properties as computed using Eq.(68), and expressed in terms of recoverable shear as a function of shear rate. The recoverable shear is related to the normal elastic stress and the stress relaxation time by Eq. (30) . It is evident that Phos-Chek possesses significant elasticity during rapid shear, and this elasticity should act as a stabilizing force during the aerodynamic breakup of the liquid-particularly with regards to surface erosion-as discussed previously. The recoverable shear increases with increase in shear rate, with a leveling off at approximately 10 sec^{-1} and a potential complete leveling off at 10^3 sec^{-1} .

5.5.2 Fire-Trol Solutions

Studies were also conducted to measure the viscosity of the Fire Trol formulations as a function of shear rate at 25°C . It was found that the Fire-Trol formulations were very difficult to work with in the high pressure capillary viscometer, due primarily to the fact that they tended to undergo channeling during their evaluation. Channeling is evidenced by blow-through of the driving gas through the solution when significant amounts of solution are still in the test chamber. It occurs for solutions or conditions in which the effective flow viscosity is very small, and often for heterogeneous systems. No elasticity measurements were made on the Fire-Trol solutions, but on a physical basis these solutions should not possess any significant elastic properties.

Figure 21 shows the experimental viscosity data obtained for Fire-Trol 100. The viscosity was determined over a shear rate range of about 1 to 2000 sec^{-1} . It was not possible to obtain experimental data beyond this limit. The data differ somewhat from that obtained using the Rotoviscometer, and this discrepancy will be discussed shortly.

Figure 22 shows the experimental viscosity data obtained for Fire-Trol 931. This solution demonstrated the most rapid settling characteristics of the three retardants, and to insure valid test results the container holding this solution was agitated between each test run. It was only possible to obtain data over about 1.5 decades of shear rate for this solution. It will be noted that there is appreciable scatter in the data obtained at the lower shear rates ($2000\text{-}6000 \text{ sec}^{-1}$) using the high pressure capillary technique. An extrapolation of the data obtained with the Rotoviscometer in the shear rate range of $10^1 - 10^3 \text{ sec}^{-1}$ to the higher shear rates achieved with the high pressure capillary viscometer is also shown.

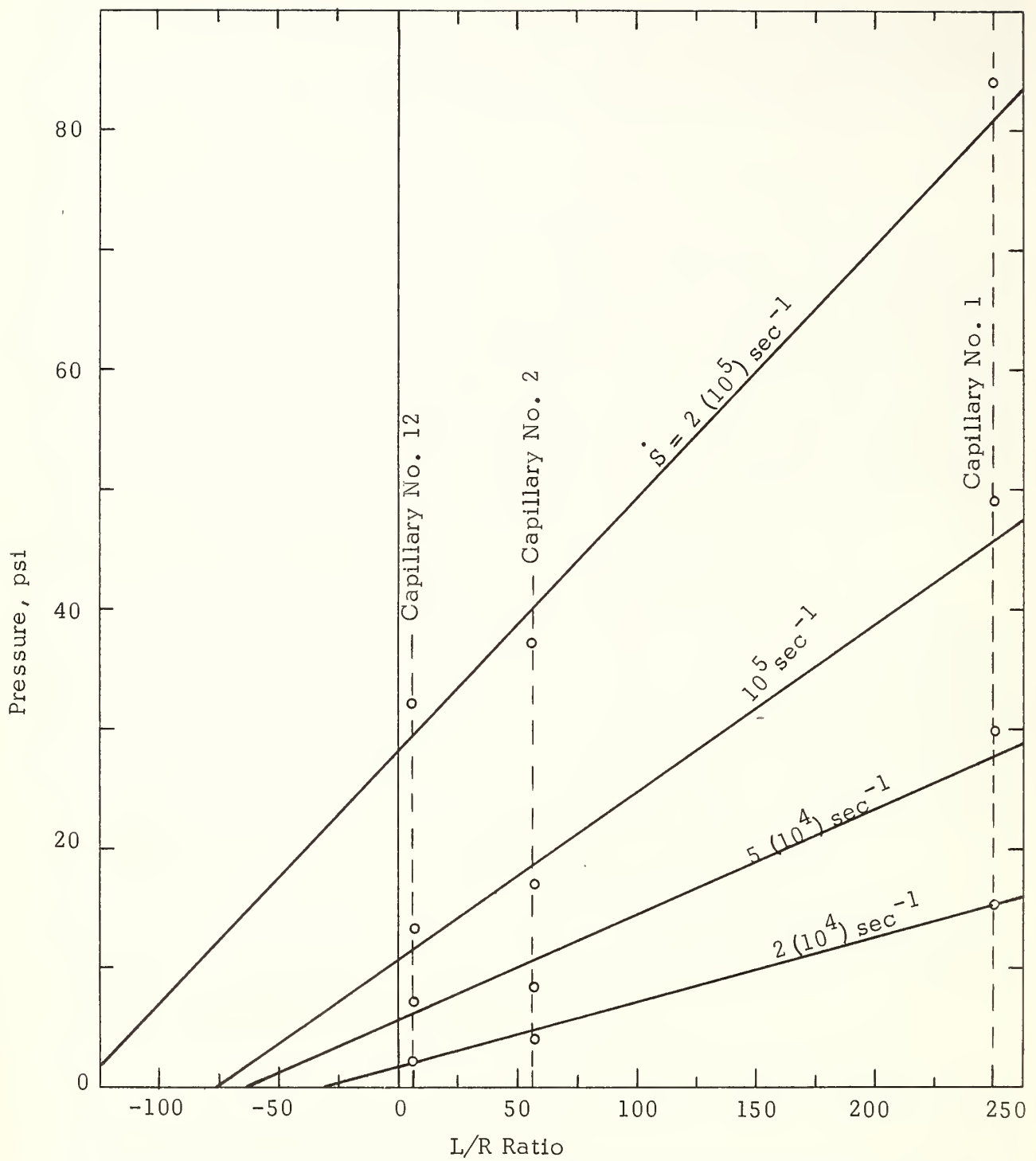


Figure 19. Plot of Pressure Versus L/R Ratio for Phos-Chek XA at 25°C at Various Shear Rates. The Abscissa Intercept Indicates the Recoverable Shear.

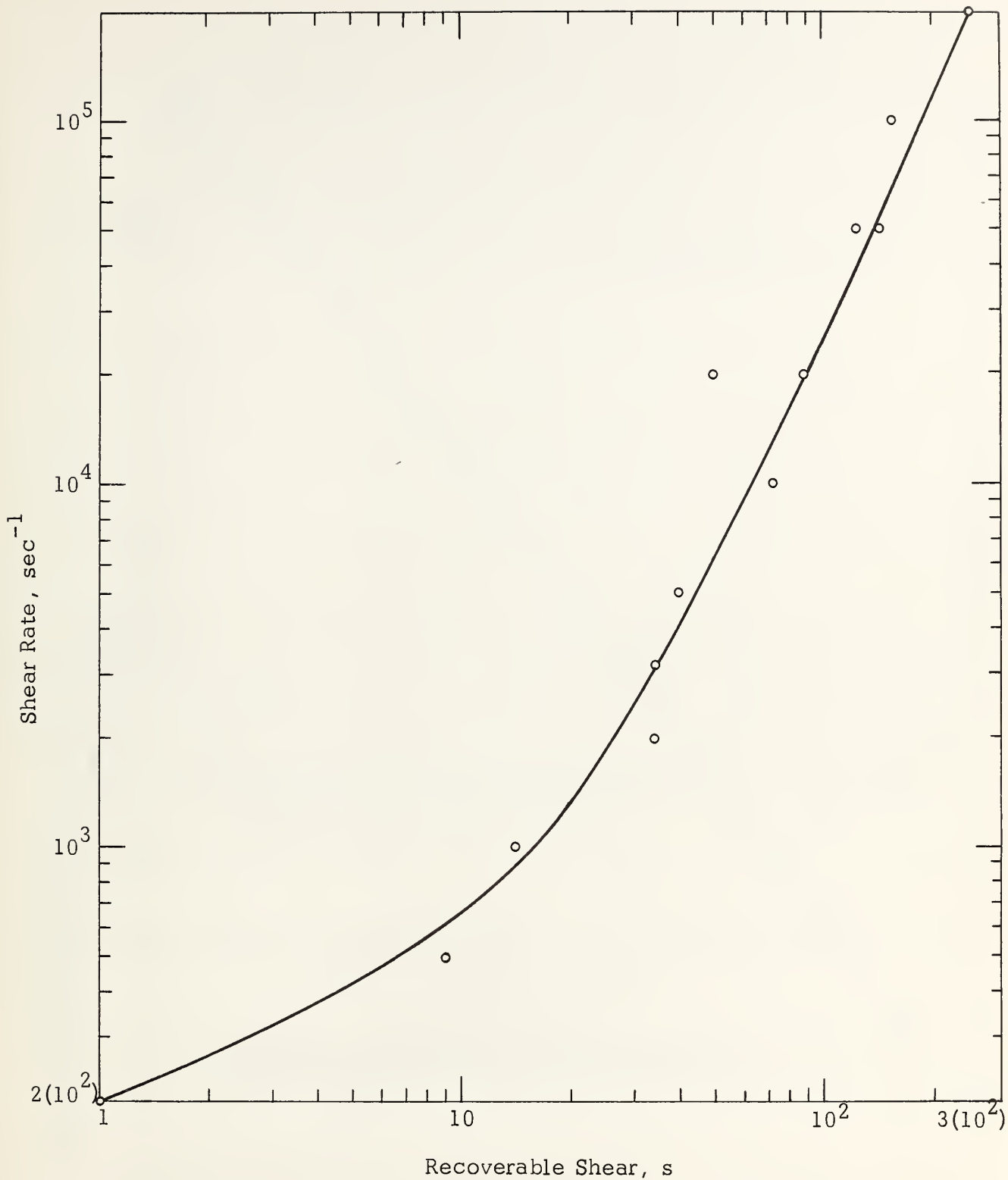


Figure 20. Recoverable Shear of Phos-Chek XA as a Function of Shear Rate at 25°C . (From pressure vs L/R plots).

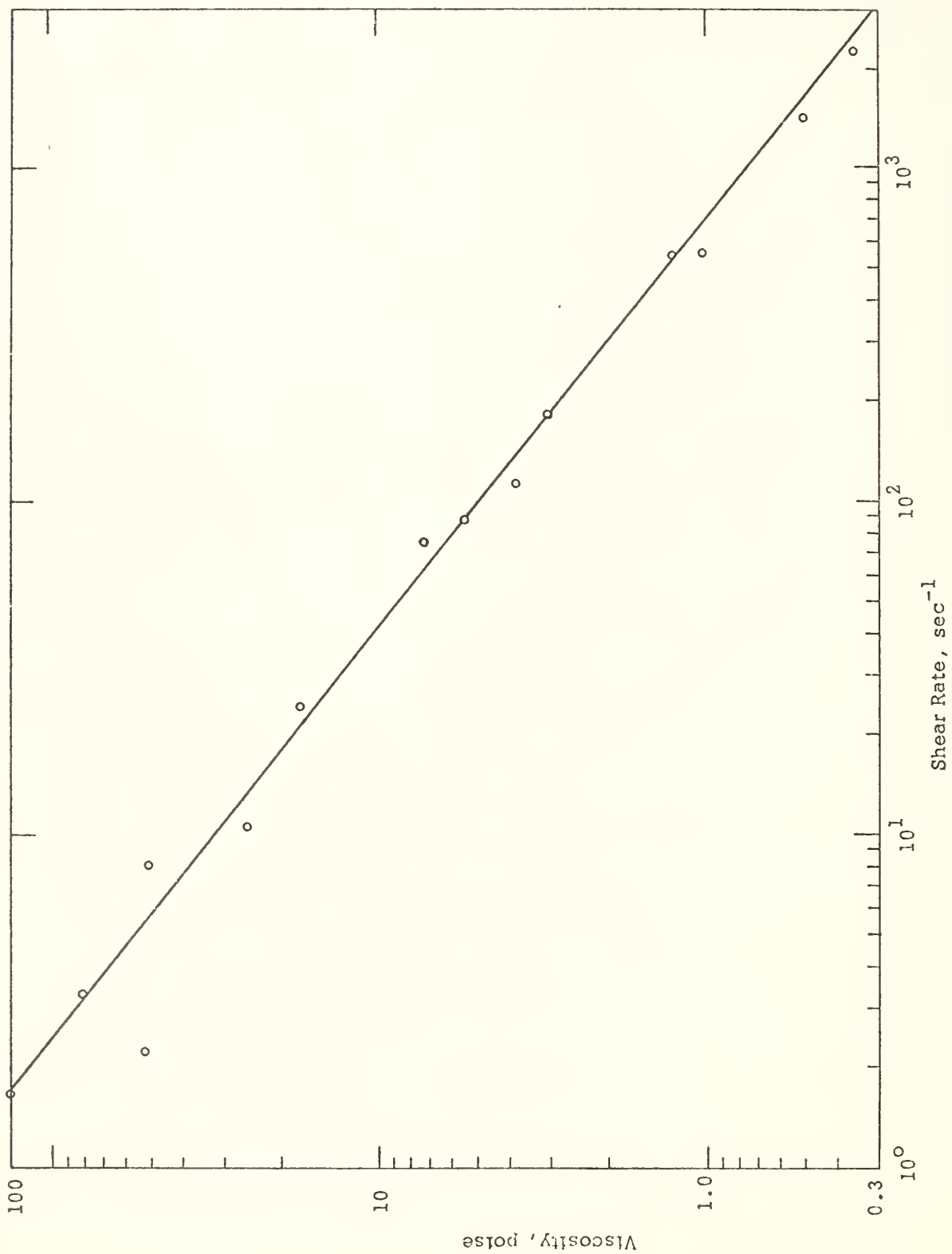


Figure 21. Viscosity Versus Shear Rate for Fire-Trol 100 at 25°C from High Pressure Capillary Viscometer Experiments.

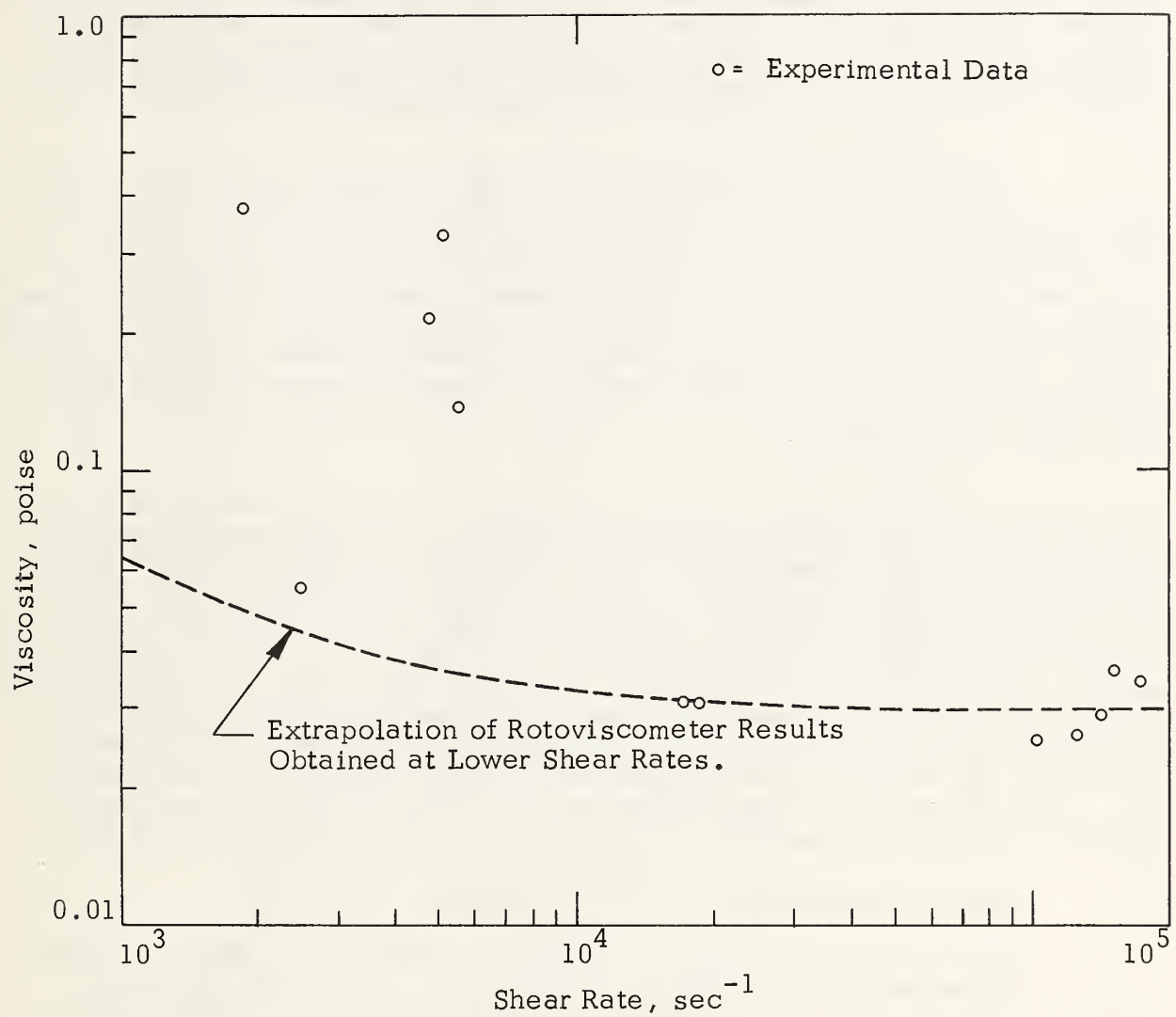


Figure 22. Viscosity Versus Shear Rate for Fire-Trol 931 at 25°C from High Pressure Capillary Viscometer Experiments.

5.5.3 Comparison of Data

Figure 23 shows a comparison of the experimental apparent viscosity data obtained for the fire retardants at 25°C using the Rotoviscometer and high pressure (HP) capillary tube techniques. As noted earlier the data obtained by the two different techniques for Phos-Chek XA is in good agreement over most of the shear rate range common to both techniques. There seems little doubt that the data curve given in this figure is a good representation of the viscosity behavior of Phos-Chek. Changes in temperature will alter this curve slightly, as may also changes in solution preparation as was discussed previously. At low shear rates the Rotoviscometer data should be used.

The data curve obtained for Fire-Trol 100 by the Rotoviscometer technique lies a little below that obtained by the HP capillary viscometer. It is not known whether this difference is real since different solutions were used in obtaining the data. In any event the difference is not very large and hence not of much significance. The important result found by both techniques is that the viscosity of this formulation decreases more rapidly than that of Phos-Chek and hence is lower at large shear rates. The slopes of the two viscosity curves of Fire-Trol using the two different measuring techniques are about the same, but since they are displaced from one another they cross the Phos-Chek curve at different shear rates.

The viscosity data obtained for Fire-Trol 931 by the two different techniques was over different shear rate ranges, and it can be seen that there appears to be some inconsistency in the data curves obtained. Nevertheless if the lowest viscosity data points obtained between $2(10^3)$ and $2(10^4)$ sec $^{-1}$ shear rate by the HP capillary technique (shown in Figure 22) are assumed to be valid, it is possible to join the data points obtained by the two different techniques by a smooth curve extrapolation, as shown in the figure. This procedure appears valid since there was wide scatter between the few points obtained in this shear rate range. Edgewood also believes this procedure and the results obtained to be valid since they experienced many difficulties in obtaining this data. They believe the asymptotic values to be correct however, and this is consistent with an extrapolation of the data obtained by the Rotoviscometer.

5.6 EFFECTIVE VISCOSITY OF FIRE RETARDANT SOLUTIONS

The solution of the breakup equations for the various liquid retardants requires a knowledge of the effective viscosity, η_e , of the retardants as a function of shear rate, \dot{S} . For Newtonian liquids the effective viscosity is merely the normal viscosity, which is constant and independent of shear rate. For non-Newtonian, non-elastic liquids such as Fire-Trol 100 and 931, the effective viscosity is merely the viscosity - which is a function of shear rate. Clay-thickened liquids are usually both non-elastic and non-Newtonian in behavior. For non-Newtonian, elastic liquids, such as Phos-Chek XA, the effective viscosity is given by $\eta_e = \eta (1 + s)$, where η is the non-Newtonian viscosity and s is the recoverable shear of the liquid. The recoverable shear is a measure of the elasticity of the liquid, and both η and s are functions of shear rate. Gum thickened liquids are usually both non-Newtonian and elastic in behavior.

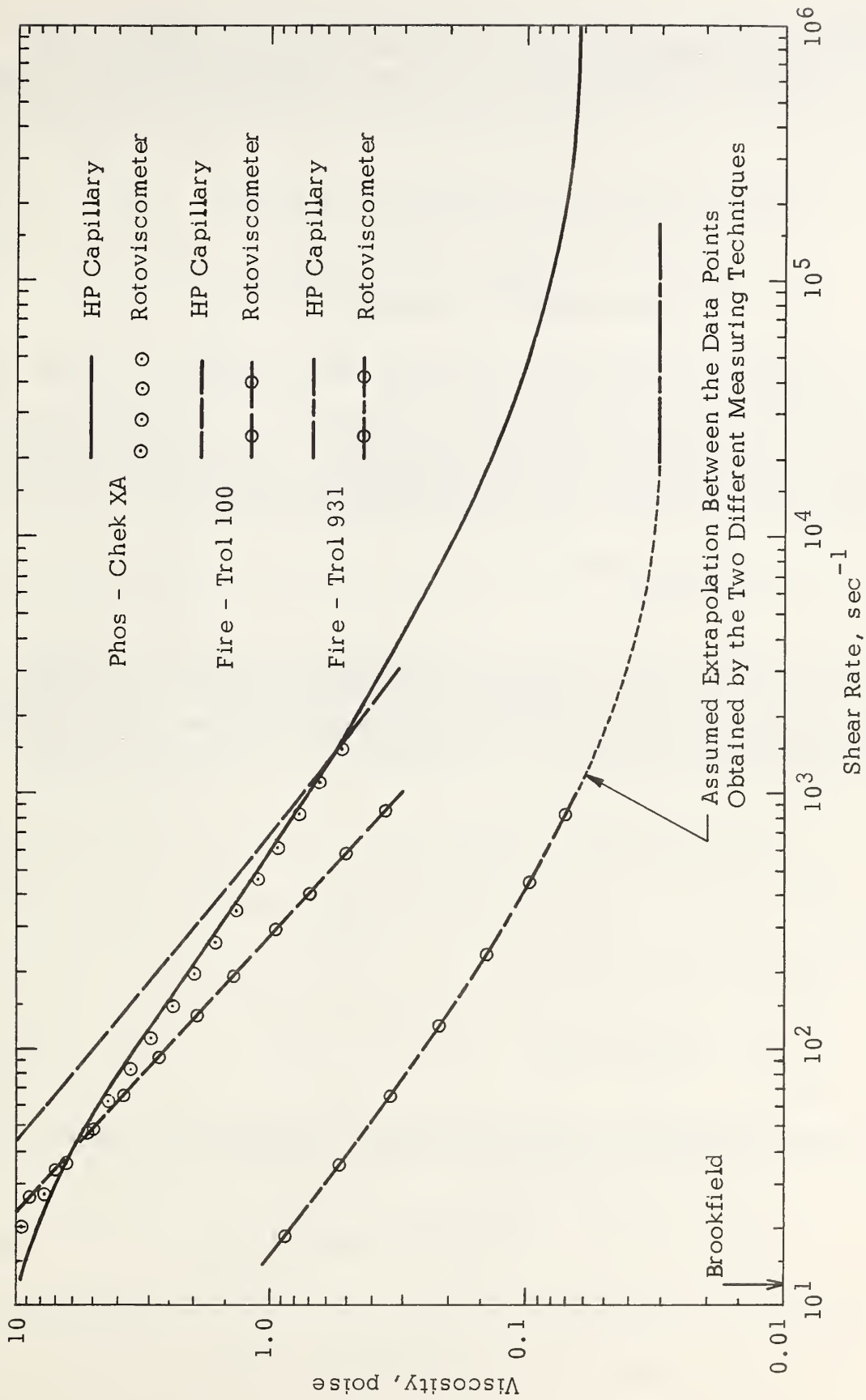


Figure 23. Comparison of the Viscosity Versus Shear Rate Curves of the Fire Retardant Solutions at 25° C. Determined by the two Different Experimental Measuring Techniques.

The effective viscosity of the various fire retardants were previously determined experimentally, and will be summarized analytically here. The effective viscosity of Phos-Chek XA in the shear rate range of 10 to 2(10^5) sec $^{-1}$ is shown in Figure 24. A reasonably good empirical analytical expression of this curve is

$$\begin{aligned}\eta_e = & -51.24 + 234.7 \log \dot{S} - 291.5 (\log \dot{S})^2 \\ & + 161.4 (\log \dot{S})^3 - 44.47 (\log \dot{S})^4 \\ & + 5.979 (\log \dot{S})^5 - 0.3131 (\log \dot{S})^6\end{aligned}\quad (69)$$

where η_e is in poise, \dot{S} is in sec $^{-1}$, and log is common logarithm. Below 10 sec $^{-1}$ the effective viscosity curve is the same as the non-Newtonian viscosity curve. This low shear rate range is that experienced by the liquid during its deformation prior to breakup by Taylor instabilities. Consequently the viscosity in the range of 1 to 10 sec $^{-1}$ is given by a separate equation which is designated as the deformation viscosity, η_d , which for Phos-Chek XA is

$$\eta_d = 60 \dot{S}_d^{-0.602} \quad (70)$$

For Fire-Trol 100 the viscosity curve obtained by the roto-viscometer is assumed to be most valid. The data were extrapolated in a manner that the viscosity becomes constant (0.045 poise-independant of shear rate) for shear rates greater than about 6(10^4) sec $^{-1}$. The equation for effective viscosity between 10 and 6(10^4) sec $^{-1}$ is

$$\begin{aligned}\log \eta_e = & 2.033 - 0.5089 \log \dot{S} \\ & - 0.2292 (\log \dot{S})^2 + 0.03937 (\log \dot{S})^3\end{aligned}\quad (71)$$

while that between 1 and 10 sec $^{-1}$ is

$$\eta_d = 184 \dot{S}_d^{-0.746} \quad (72)$$

For Fire-Trol 931 the effective viscosity is constant (0.031 poise) above 2(10^4) sec $^{-1}$. Between 10 and 2 (10^4) sec $^{-1}$ the equation is

$$\begin{aligned}\log \eta_e = & 0.9574 - 0.7583 \log \dot{S} - 0.0558 (\log \dot{S})^2 \\ & + 0.02315 (\log \dot{S})^3\end{aligned}\quad (73)$$

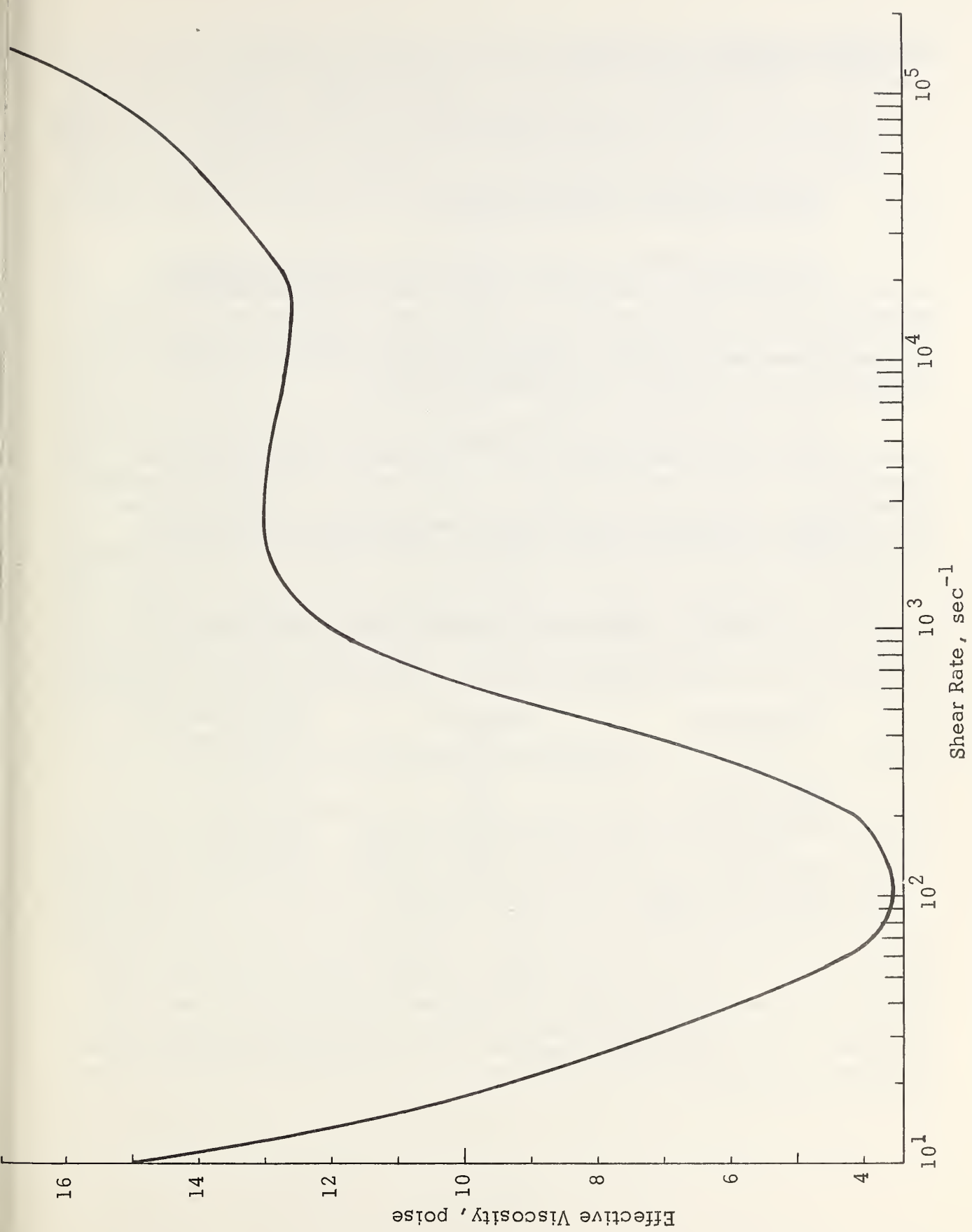


Figure 24. Effective Viscosity Versus Shear Rate of Phos-Chek XA

while that between 1 and 10 sec⁻¹ is

$$\eta_d = 10 \dot{S}_d^{-0.758} \quad (74)$$

5.7 SURFACE TENSION MEASUREMENTS

Measurements of the surface tension of the three fire retardant solutions at ambient temperature were made using a Fisher Surface Tensiometer, Model 120, which includes a du Noüy torsion balance and a platinum-iridium ring. Conventional procedures described in reference 55 were followed in making these measurements. The fire retardant solutions were prepared as before, according to Forest Service specifications.

The surface tension of the commercial distilled water used in the fire retardant mixtures was determined to be 73.7 dyne/cm at 22.5° C. This experimental value is slightly higher, by 1.8%, than the interpolated literature value⁵⁶ of 72.4 dyne/cm. The inverted ratio of these two values was used to correct (reduce) the surface tension measurements made on the retardants. These corrected values are shown in Table II. Some difficulty was encountered

TABLE II. CORRECTED* SURFACE TENSION ESTIMATES

Fire Retardant Solution	Temperature (°C)	Surface Tension (dyne/cm)
Phos-Chek XA	22	46.3 ± 0.1
Fire-Trol 100	24	92. ± 2.
Fire-Trol 931	25	80.0 ± 0.5

*Relative to Water

with Fire-Trol 100. Because of the high viscosity of this solution, the instrument could not be zeroed, and the apparent surface tension was found to be close to the upper detection limit. At the upper force limit the distended film between the ring and retardant surface takes a considerable time period (minutes) to break away from the surface, and it is therefore possible that the composition of the film changed with time and was significantly different from the bulk composition.

Good agreement was found between the surface tension obtained for Fire-Trol 931 and the values reported by Van Meter⁵⁷ for solutions of Poly-N, 10-34-0 concentrate - the main additive ingredient of Fire-Trol 931. However the values obtained for Phos-Chek XA and Fire-Trol 100 differ from those reported by Van Meter. The lower reading obtained for Phos-Chek XA may be due to the presence of a surfactant in the composition of the dry retardant material mixture that was apparently not present in the material (Phos-Chek 202XA) used by Van Meter whom obtained a value of 67-71 dynes/cm.

5.8 EFFECT OF RETARDANT CONCENTRATION ON RHEOLOGICAL PROPERTIES

In addition to the studies conducted on the normal fire retardant solutions used in actual practice, experiments were also conducted for the purpose of estimating the effects of concentration variations on the rheological and physical properties of Phos-Chek XA. This can possibly be an important factor on the wetting out process, since under suitable conditions it is expected that significant water loss from the retardant particles can occur during particle settling.

The fire retardant solutions were prepared in a blender as before. Various amounts of Phos-Chek XA were mixed in distilled water. Nominal mixtures of 200, 150, 100, 75, 50 and 25 percent of the conventional mixture were prepared. That is, the conventional or 100 percent mixture consisted of 68.4 grams powdered Phos-Chek XA per 500 ml water. The amounts of Phos-Chek XA added per 500 ml water for the 200, 150, 75, 50 and 25 percent mixtures were, respectively 136.8, 102.6, 51.3, 34.2, and 17.1 grams. Each formulation was mixed for 0.5 min. at the lowest blender speed and then for 2.5 min. at the highest speed.

5.8.1 Effect on Viscosity and Yield Stress

The experimental results obtained for Phos-Chek - corrected for non-Newtonian behavior - are shown in Figures 25 and 26. In Figure 25 there are shown the corrected viscosity versus corrected shear rate data, and in Figure 26 there are shown the data of shear stress versus corrected shear rate. Problems were encountered in measuring the shear stress of the "25 percent" Phos-Chek mixture with the MV rotors because of the relatively high fluidity of this mixture (similar problems have been encountered with Fire-Trol 931 (LC)).

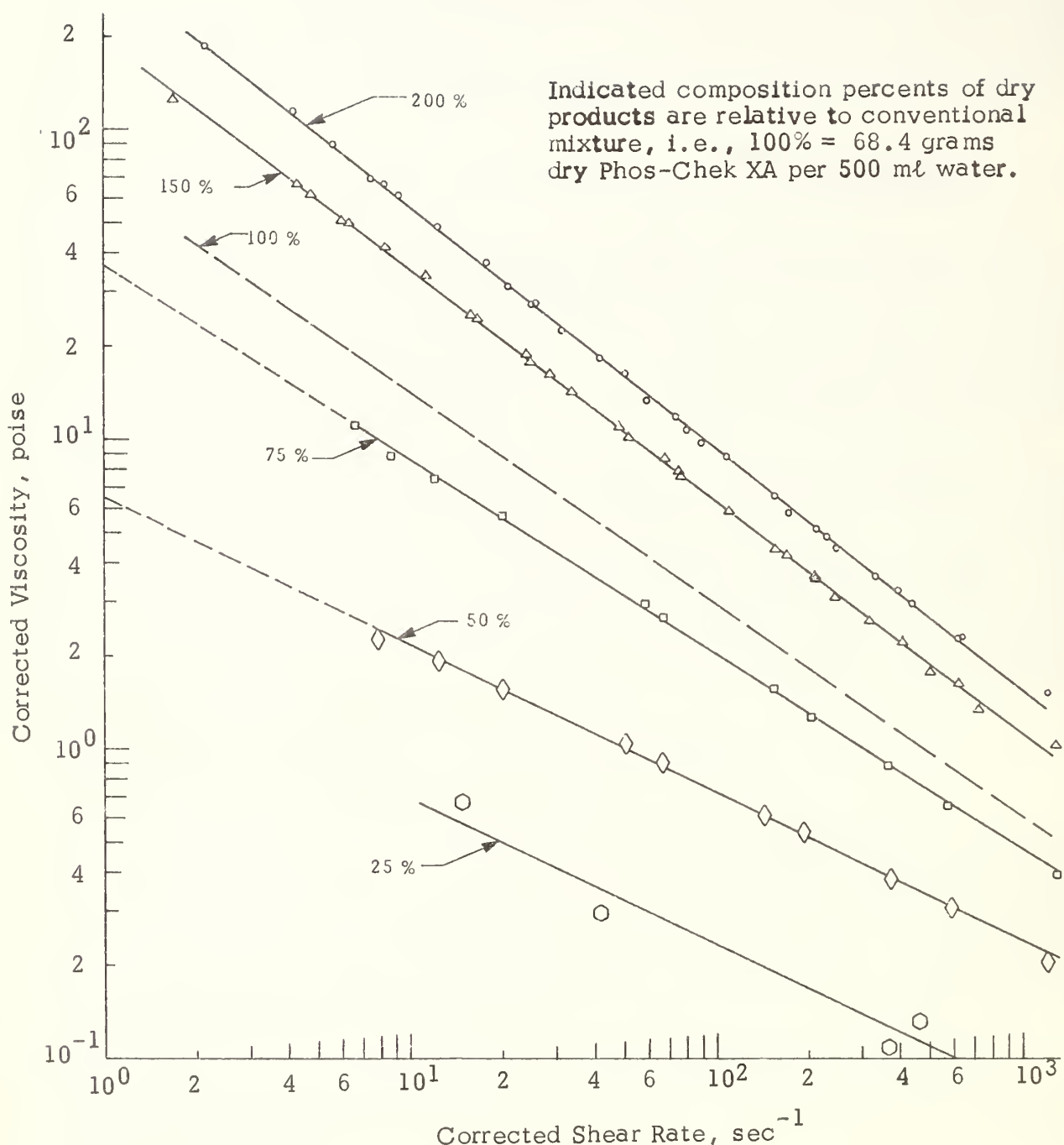
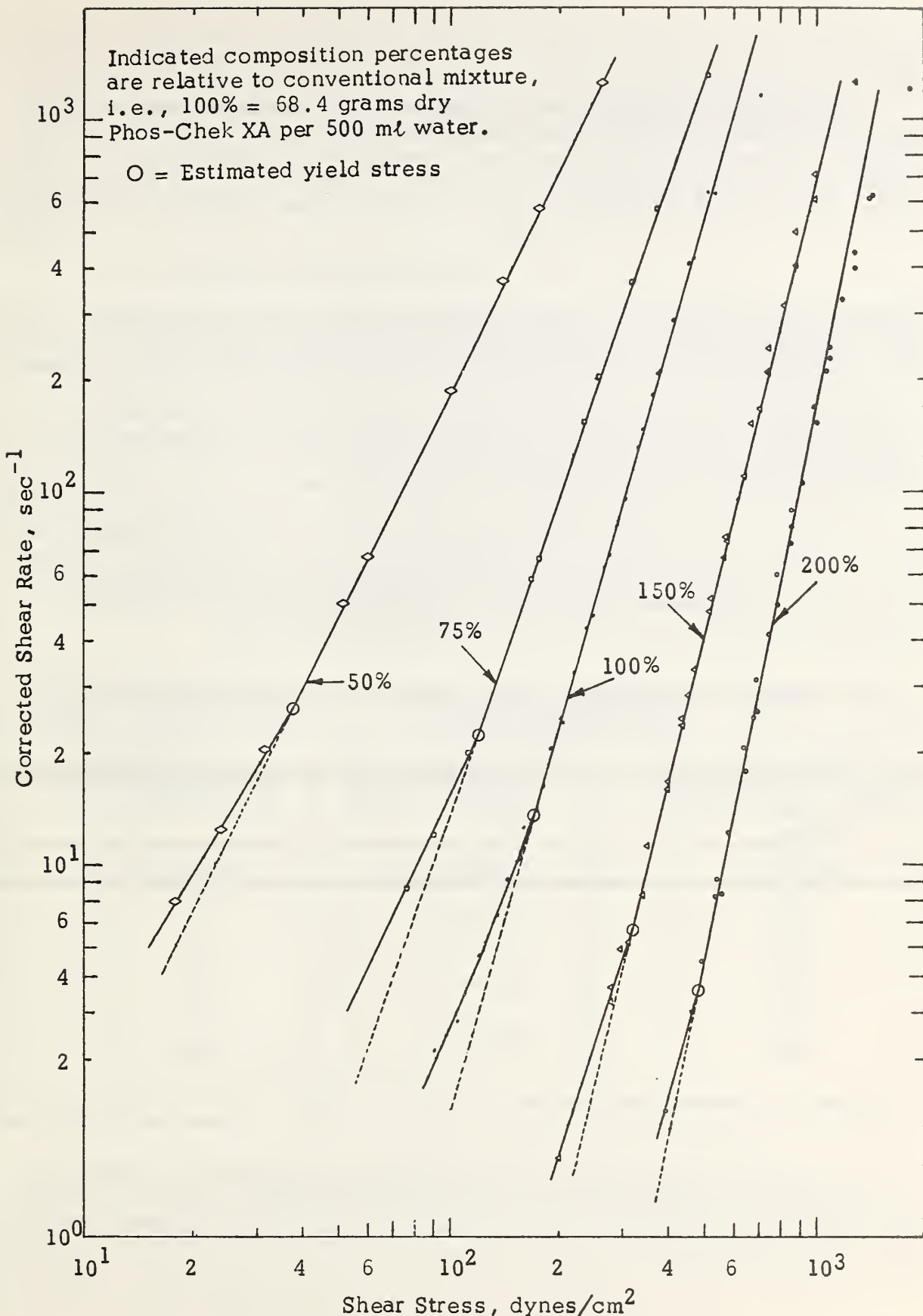


Figure 25. Corrected Viscosity of Phos-Chek XA as a Function of Dry Product Concentration and Shear Rate.



Each of the mixtures studied appear to obey a power law relationship between shear stress (and viscosity) and shear rate, i.e.,

$$\sigma = k, \dot{S}^\eta \quad (75)$$

$$\eta = \sigma / \dot{S} = k \dot{S}^{\eta-1} \quad (76)$$

Evidences of yield shear stress were obtained from the shear stress versus shear rate data shown in Figure 26. At the point along these curves where a departure from linearity occurs it is assumed that plug flow occurs between the rotating bob and the stationary cup. In the regions of "plug flow" the shear stress on the fluid falls below the yield stress and in that part of the gap close to the cup wall where the yield value is not exceeded there exists a non-moving body of material, while across the remaining gap the same material exhibits laminar flow in the region where the stress exceeds the yield value.

The approximate yield stresses estimated for these mixtures are listed in Table III. The yield stresses estimated are reported as upper limits since the exact location between the rotor and stationary cup where plug flow occurs, in each case, is not measured. The yield stress is taken as the measured shear stress at the rotor which is the largest stress within the gap.

TABLE III. ESTIMATED YIELD STRESSES FOR PHOS-CHEK XA MIXTURES IN WATER

Nominal Concentration of Phos Chek XA in Water (percent)*	Retardant Weight per Water Volume	Estimated Upper Limit of Yield Stress
	(grams/cm ³)	(dynes/cm ²)
50	0.068	38
75	0.103	121
100	0.137	187
150	0.205	320
200	0.274	486

*percent of conventional mixture

The very significant effect on fire retardant concentration on retardant fluidity could be an important factor in the lateral spreading and drop stability during impact. Gross alterations in retardant concentration and hence viscosity

and yield stress can be expected within the time period between dissemination and ground (or fuel) impact under fire conditions. The intense thermal environment of a forest fire can cause evaporative losses of water resulting in ground dispositions of retardant which are higher in solid content and thus more viscous. These evaporative losses probably do not occur at rates competitive with the aerodynamic breakup and therefore can be ignored in the liquid breakup estimates. Additional work however should be directed, in the future, to considerations of the vaporization kinetics and the impact behavior of the retardant as a function of concentration.

5.8.2 Effect on Surface Tension

Additional surface tension measurements were made on Phos-Chek XA mixtures for purposes of determining the effect of retardant concentration. The method employed to measure surface tension was previously described.

The results of these measurements are summarized in Table IV where it is shown that the surface tension of aqueous suspensions of Phos-Chek XA is independent of Phos-Chek concentration. The mean surface tension of concentrations between "25" and "200" percent is estimated to be $44.2 \pm 2.2 \text{ ergs/cm}^2$. This observed invariance of surface tension with retardant concentration is in agreement with similar observations made by Van Meter⁵⁷.

TABLE IV. SURFACE TENSION OF PHOS-CHEK XA-WATER MIXTURES AT 20°C

Nominal Concentration of Phos-Chek XA in Water (percent)*	Retardant Weight per Water Volume (grams/cm ³)	Surface Tension (ergs/cm ²)
0**	0.0	71.2
25	0.034	44.8
50	0.068	44.1
75	0.103	41.7
100	0.137	42.0
150	0.205	45.2
200	0.274	47.5

* percent of conventional mixture

** distilled water

It can therefore be hypothesized that, for the case of Phos-Chek XA mixtures in water, the surface restoring forces of the suspensions which oppose liquid deformation and fracture under aerodynamic and impact forces do not vary with Phos-Chek XA concentration. However, there is a very significant increase in apparent viscosity and yield stress with Phos-Chek XA concentration and these properties should affect differences in liquid instability.

6. SHOCK TUBE STUDIES

6.1 INTRODUCTION

In an earlier section of this report a summary was presented of the present knowledge and understanding of the aerodynamic breakup of liquids. It was shown that almost all previous experimental data has been obtained on Newtonian liquids, and the theoretical studies that have previously been conducted to describe breakup rate and droplet size in terms of the wind velocity and fluid properties have also been concerned with Newtonian liquids. Theoretical equations based on simplified models were consequently developed for describing the breakup of non-Newtonian liquids, since fire retardants of current interest are non-Newtonian in nature. The evaluation of these equations requires information on the viscosity as a function of shear rate, and the fluid elasticity of the liquids. Experimental data of this nature was obtained during the current program for the three fire retardants under study.

In order to check the analytical models experimentally and refine them if necessary so that they will have reasonable predictive capability, as well as possibly obtain further qualitative information regarding the breakup of fire retardants that may be useful for correlation purposes, it is necessary to obtain experimental information on the breakup of liquid retardants under controlled conditions. Consequently experimental studies have been conducted toward this end, and this report describes the results of these studies using two different techniques. In the first of these techniques - to be discussed in this section - a shock tube was used to produce a steady high velocity air flow over a liquid drop, and high speed photographic techniques were used to observe the breakup characteristics and breakup times of the drops. In later studies measurement of the droplet sizes produced by the breakup was subjected to preliminary study.

6.2 DESIGN OF THE SHOCK TUBE

The shock tube used for the studies was modified from a pre-existing one, and was redesigned especially for this program. It consists basically of two pieces of pipe (one closed at one end) which are separated by a diaphragm that can be opened (ruptured) within a very short time. The pipe with the closed end, called the compression chamber, contains air at a pressure higher than that in the other pipe, called the expansion chamber, which is open to the ambient atmosphere. When the diaphragm is ruptured a shock wave propagates into the expansion chamber, followed by a region of constant flow that lasts for a time dependent on the position of the shock and the lengths of the pressure and expansion chambers. The lengths of the two pipes comprising the shock tube used in the present experimental program were chosen to give a constant flow time in the test section of about 15 milliseconds.

A drawing of the shock tube is given in Figure 27. The shock tube is composed of:

- a. The compression chamber - which consists of a 9 ft. long piece of 4 inch-ID steel pipe with a cap and air inlet on one end and a bolt flange on the other end.

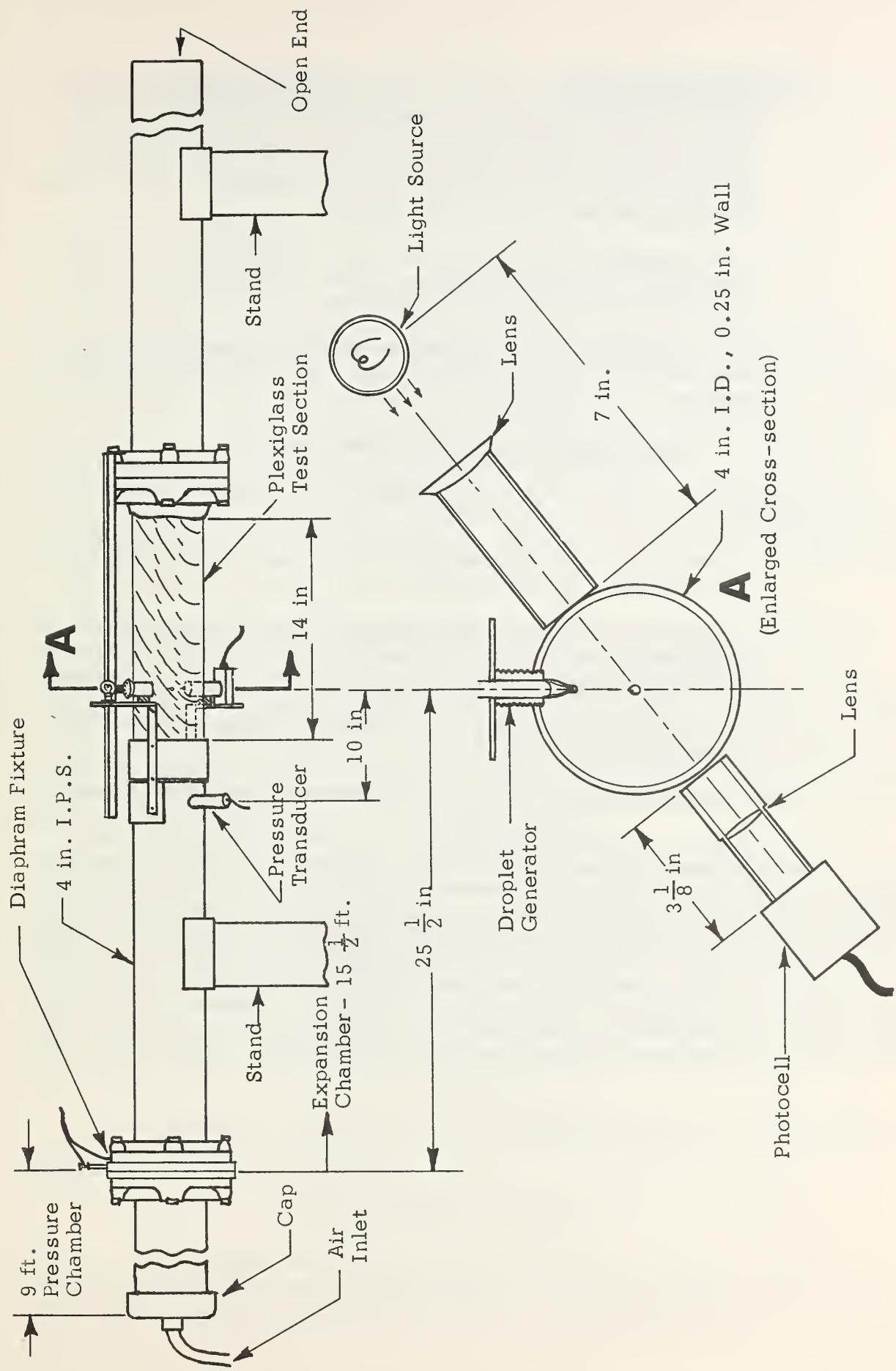


Figure 27. Shock Tube Used to Study the Aerodynamic Breakup of Liquid Fire Retardants.

- b. A diaphragm fixture - which consists of two plastic rings that hold the Mylar diaphragm between them. One of the plastic rings has electrodes through it which connects to the 3-mil exploding wire that cuts through the Mylar to open the diaphragms. The plastic rings are drilled to permit bolts from the flanges on either side to pass through.
- c. A test section - which is composed of a length of 4 inch-ID steel pipe for shock formation, which is connected to a transparent plexiglas observation tube that is flanged at the end.
- d. The remainder of the shock tube - which is 4 inch-ID steel pipe, which gives a total expansion chamber length of about $15\frac{1}{2}$ feet.

6.2.1 Shock Tube Instrumentation and Operation

The instrumentation for the shock tube was assembled to satisfy several objectives:

- a. to obtain high speed photographic coverage of the behavior of the liquid drop in the air flow,
- b. to detect the presence of a generated liquid drop at the desired position in the viewing area and produce a signal to trigger other instrumentation,
- c. to produce a high intensity illumination for the photographic sequences, and
- d. to provide a measurement of the flow field behind the shock.

A schematic of the instrumentation is shown in Figure 28. The operation is as follows. When a liquid drop is introduced into the observation portion of the test section (see crosssection "A" in Figure 27) it falls freely under gravitational forces toward the center of the tube. When it reaches the center of the tube it occludes a beam of light focused at the center of the tube and reduces the light reaching the photocell on the opposite side of the tube from the light source. The phototube (type 1P39) is connected to a Beckman Whitley Model 357 Electronic Flash Unit. The flash unit senses the drop in illumination and provides a power pulse to a flash lamp. The unit will supply single square pulses with the following durations and peak light output.

PULSE DURATION (milliseconds)	PEAK BEAM OUTPUT (candle power)
8.60	10^6
11.15	6.5×10^5
14.85	3.25×10^5
22.35	1.5×10^5

The flash unit also provides a pulse to trigger an oscilloscope and a high voltage fire pulse unit. When the high voltage fire pulse unit is triggered, it permits the discharge of an $8 \mu\text{f}$ capacitor charged to 1.5KV through a 25-30 μA , 3 mil Nichrome wire between the two 1 mil-thick Mylar diaphragms. The wire is arranged so that when it bursts and cuts through the diaphragms, it cuts out 4 inch-diameter circles except for a 1 inch-length of the circumference where the cut out circles remain attached to the rest of the Mylar sheet between the two flat rings of the diaphragm fixture. When the diaphragms are cut, the pressure in the pressure chamber causes them to flap open and the gas rushes down the expansion chamber. Within a travel distance equal to a few tube diameters, at the most, the flow forms into a shock wave followed by a region of nearly constant flow.

When the shock and flow behind the shock passes the pressure transducer located just before the beginning of the observation tube, the pressure in the flow causes the pressure transducer (Kistler Mod. 601A) to send a signal to a charge amplifier (Kistler Mod. 503) which produces a signal that is recorded on the oscilloscope, illustrated in Figure 29. When the shock wave reaches the liquid drop, the flow behind the shock reacts on the drop to accelerate it in the direction of the air stream and to also cause whatever drop deformation and breakup that is appropriate to the conditions. This is recorded with a Beckman Whitley Mod. 326 Dynafax Camera.

The Dynafax Camera is a continuous-writing framing camera, capable of framing rates of from 200 to 26,000 frames/sec with shutter speeds of 1.0, 2.5 or 5.0 μsec at maximum framing rate. This camera has a picture capacity of 224 frames of standard 16mm frame size on a 33-7/8-in. length of 35mm film. The total writing time available varies from 1.12 sec at 200 frames/sec to 8.62 ms at 26,000 frames/sec. Camera speed controlled by a variac in the camera base, and the framing rate is indicated by monitoring the frequency of an ac-voltage output from the camera with an EPUT counter. The frequency of the ac voltage is equal to the speed of the rotating mirror in the camera, and is directly related to the framing rate.

A Wollensak Raptar f/2.8, 3-in. Telephoto lens was used for all of the tests. Various lens-extension lengths were required to obtain the desired magnification and field of view.

6.2.2 Calculation of Wind Velocity

The studies were conducted by subjecting a liquid drop to the wind velocity present in the constant flow region, behind the shock, which had a duration of 15 millisec. The wind velocity was calculated from the pressure, P ,

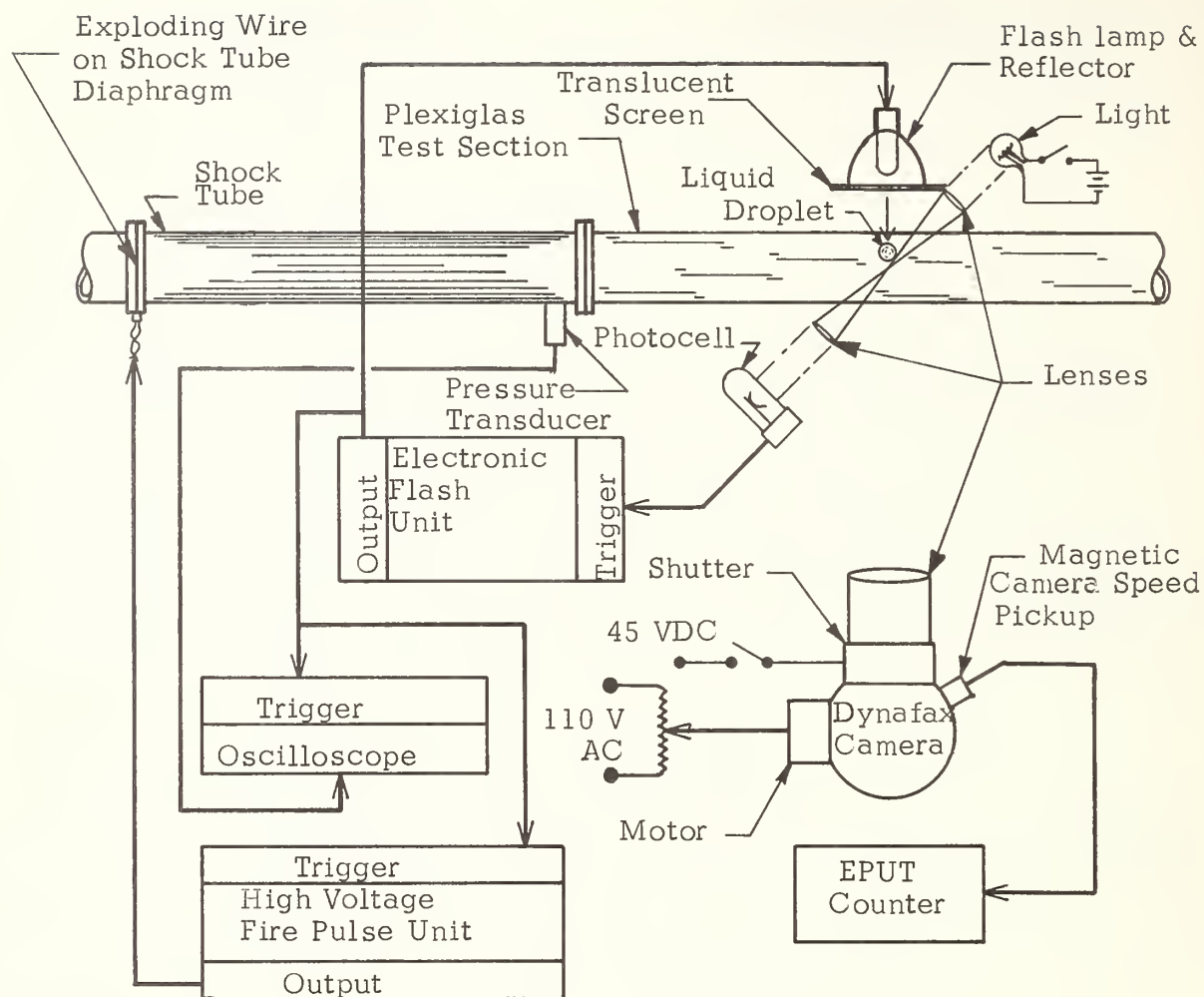


Figure 28. Shock Tube Instrumentation.

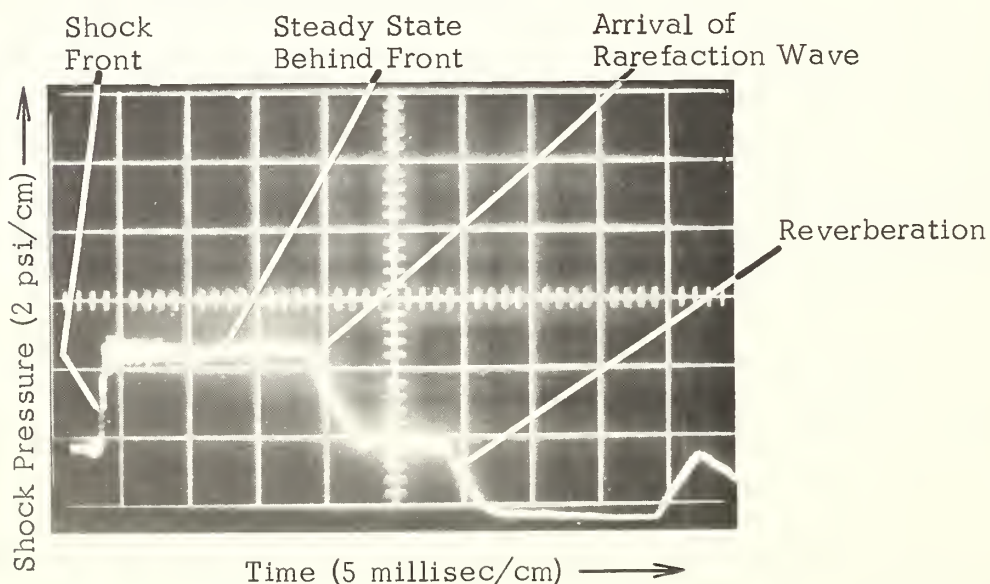


Figure 29. Oscilloscope Record of Pressure Transducer Signal.

of the constant flow region as recorded on the oscilloscope. If the pressure of the ambient air in front of the shock (and around the pressure transducer) is P_o , the absolute pressure, P_1 of the shock is

$$P_1 = P_o + P \quad (77)$$

The pressure ratio across the shock front is

$$P_{10} = P_1/P_o \quad (78)$$

The equations describing shock wave propagation gives the flow velocity, u , behind the shock front as

$$u = \frac{a_o (P_{10} - 1)}{\gamma[\beta(\alpha P_{10} + 1)]^{1/2}} \quad (79)$$

$$\alpha = \frac{\gamma + 1}{\gamma - 1}; \quad \beta = \frac{\gamma - 1}{2\gamma} \quad (80)$$

where a_o is the ambient sound velocity of the unshocked gas and γ is the adiabatic exponent of the gas. A graph of the wind velocity as a function of gas pressure is given in Figure 30 for air ($\gamma = 1.4$, $a_o = 1135$ ft/sec).

6.3 EXPERIMENTAL RESULTS

The experimental data obtained from the shock tube experiments consists of the observed deformation history and breakup behavior (including breakup time) of the liquid drops studied, as recorded by the camera for the particular wind velocity in the constant flow region behind the shock front. Typical frame sequences of the actual tests are given in Figures 31-33 for water, Phos-Chek XA, Fire-Trol 100 and Fire-Trol 931 at three different wind velocities each. The drop size (diameter) used in these studies was approximately 2 to 4 mm. The drops were generated by an ordinary eyedropper mounted in the wall of the test section. However the resulting drops were not uniformly the same size or even usually spherical in shape. Part of the reason for the non-uniformity was the fact that the eye dropper was squeezed remotely and thus it was difficult to maintain good control over the drop as it was forming at the end of the eye dropper. The drops were generally somewhat ellipsoid in shape except for the Phos-Chek drops. The Phos-Chek drops, as can be seen from the mounted framing sequences, came off the end of the eye dropper with a tear drop shape ending with a long filament back toward the tip of the eye dropper. This filament reacted with the air stream much faster than the bulk of the drop, due presumably to its lighter mass. The breakup analysis of Phos-Chek was based on the effects of the end of the drop opposite to the end with the filament.

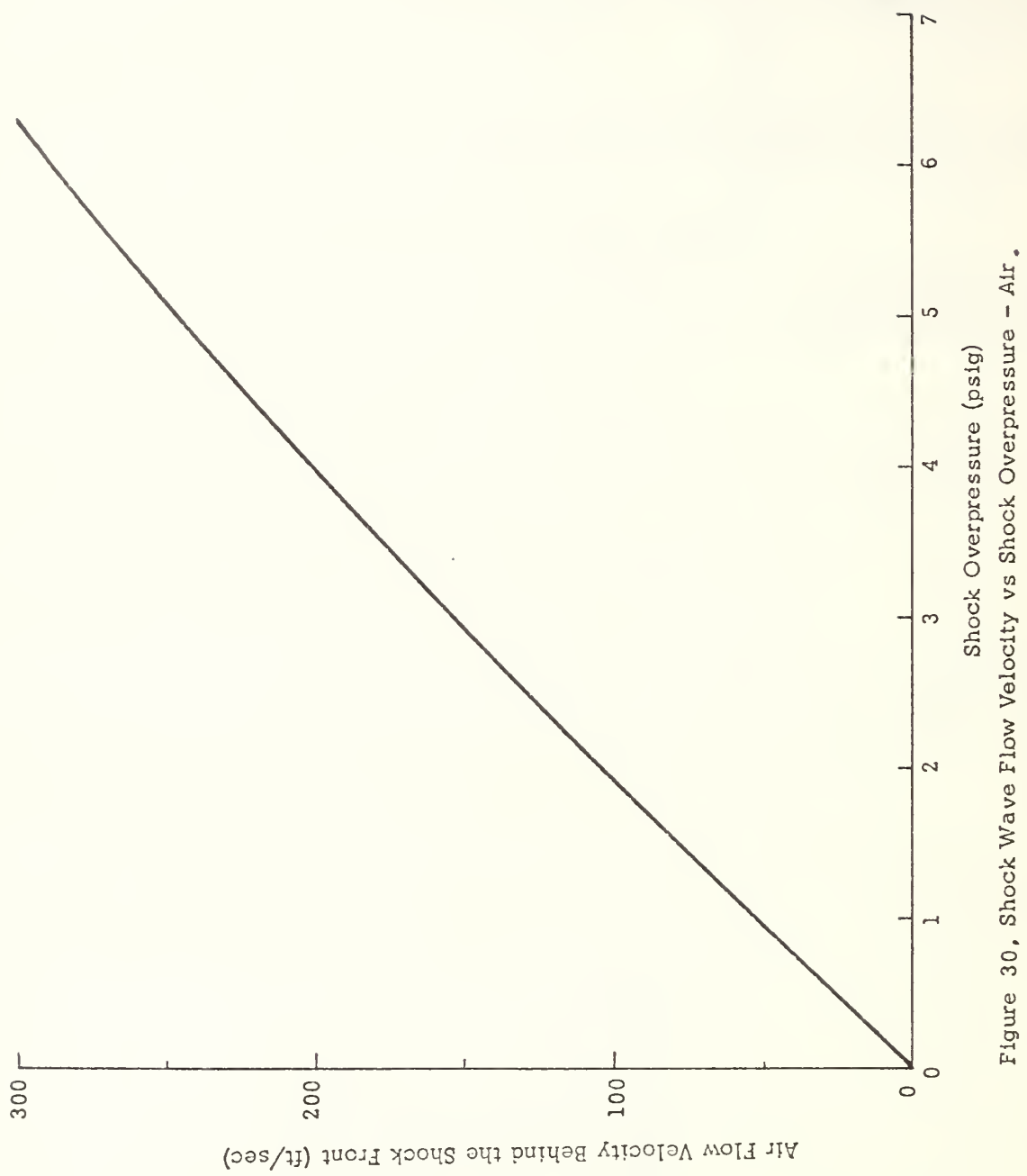


Figure 30, Shock Wave Flow Velocity vs Shock Overpressure - Air.

In the initial studies, of which the breakup sequence obtained from some of the experiments is shown in Figures 31-33 the magnification and camera speed used were such as to give sufficiently good pictures that the details of the deformation and initial breakup could be clearly observed while simultaneously allowing a good portion of the total breakup process to also be recorded. Later experiments in which longer time periods were observed (up to \sim 15 msec) resulted in smaller pictures of the breaking drops since a larger field of view was required. In the initial experiments the initial time at which the shock interacted with the drop was estimated by the first sign of flattening of the drop, as has been used in the past. This resulted in some uncertainty in some cases however, since the drops were not usually initially spherical. In later studies (the framing sequences are not given in the figures) a small piece of foil was mounted in the test section near the drop location, which enabled the interaction time of the shock with the drop to be clearly established.

6.3.1 General Behavior of Drop Deformation and Breakup

The general behavior of the liquid drops when subjected to wind flow of known velocity was obtained from the positive prints of the framing sequences. The framing sequences used included those given in Figures 31-33 plus a comparable number obtained at faster camera speeds (0.111 and 0.051 msec/frame) and in some cases longer observation times (up to 15 msec). Three wind velocity ranges were used in the studies, viz., 85-95 ft/sec (50-56 knots), 124-155 ft/sec (74-92 knots), and 276-288 ft/sec (164-171 knots). These will be referred to, respectively, as low, medium and high velocity.

Briefly, subsequent to the interaction of the wind flow at any velocity with a drop, the drop begins to undergo deformation (flattening). After a finite time delay the deforming drop begins to undergo breakup, and the breakup mechanism involved depends on wind velocity and the liquid involved. In general the liquids water, Phos-Chek XA, and Fire-Trol 100 undergo stripping (surface erosion) breakup at medium and high velocities, while Fire-Trol 931 undergoes stripping breakup at all the velocities. At the low velocity, water and Fire-Trol 100 undergo bag breakup. Generally speaking, the overall behavior of the breakup process for the three fire retardants for the preceding cases for both bag and stripping breakup is roughly similar (but retarded timewise) to that of conventional liquids (with the possible exception of Phos-Chek XA at the medium velocity). The breakup times of the liquids do differ however, at the same velocity, and this is due to differences in liquid properties. The effective viscosity of the fire retardant liquids during breakup are less than the Brookfield values, since otherwise breakup would not occur in the observed time periods.

The behavior of Phos-Chek XA at the low wind velocity, however, differs significantly from that of the other liquids. As mentioned previously the drops produced by the eye dropper contained a filament at one end, and during the interaction of the drop with the air flow this filament tends to become elongated but does not break. During the interaction also, the drop eventually deforms to produce a bag. However instead of bursting to give many small droplets as occurs by conventional bag breakup, the bag formed in the Phos-Chek drops apparently would develop a small hole and then slowly deflate, while another bag would form at another place on the deformed drop. In one sequence during the time the drop was in the camera viewing area, as many as three successive bags would form and slowly deflate without breaking into droplets.

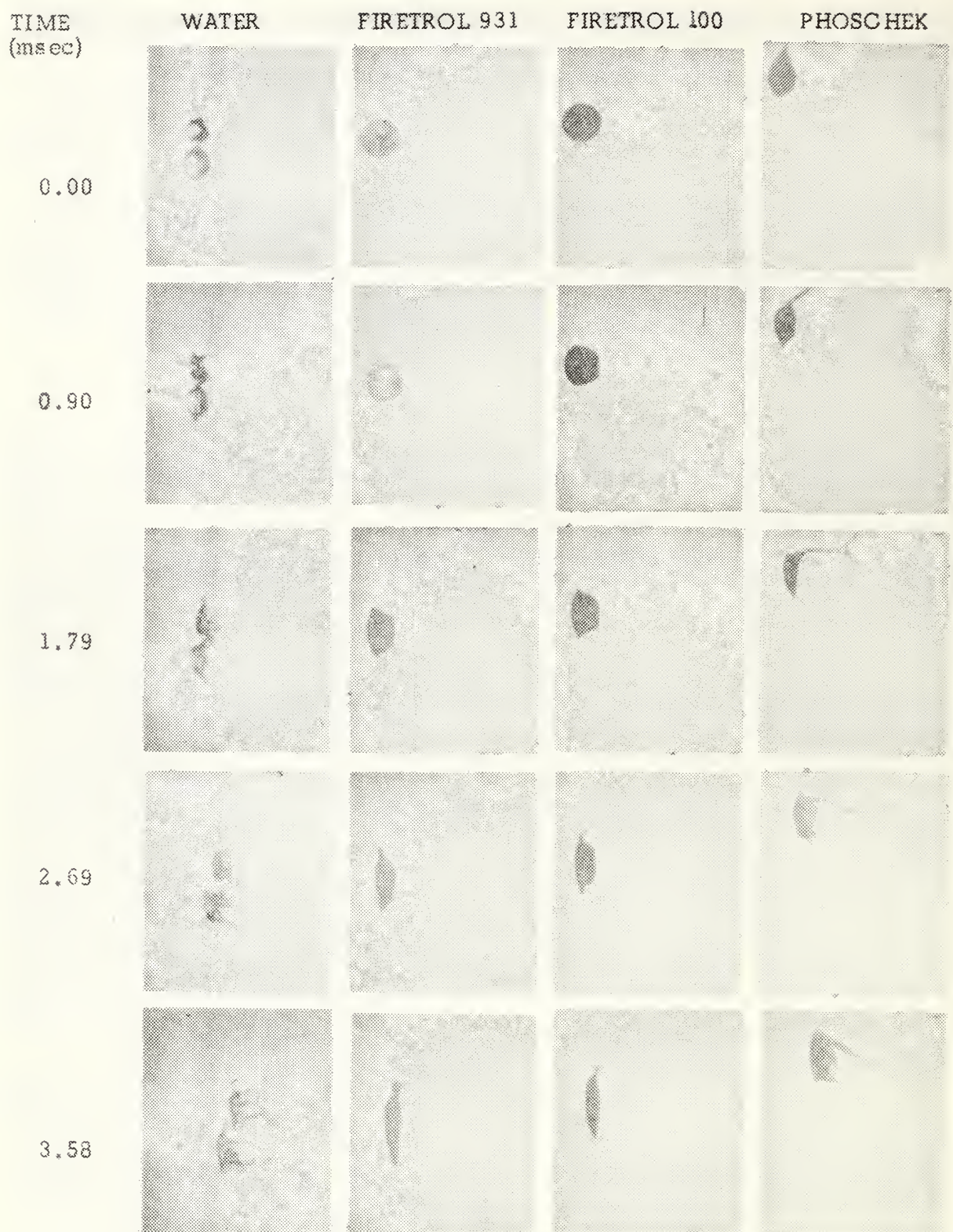


Figure 31. Selected Frames From Photographic Sequences of the Aerodynamic Breakup of 2 - 5 mm Drops of Various Liquid Retardants. Average Wind Velocity is 89 ft/sec.

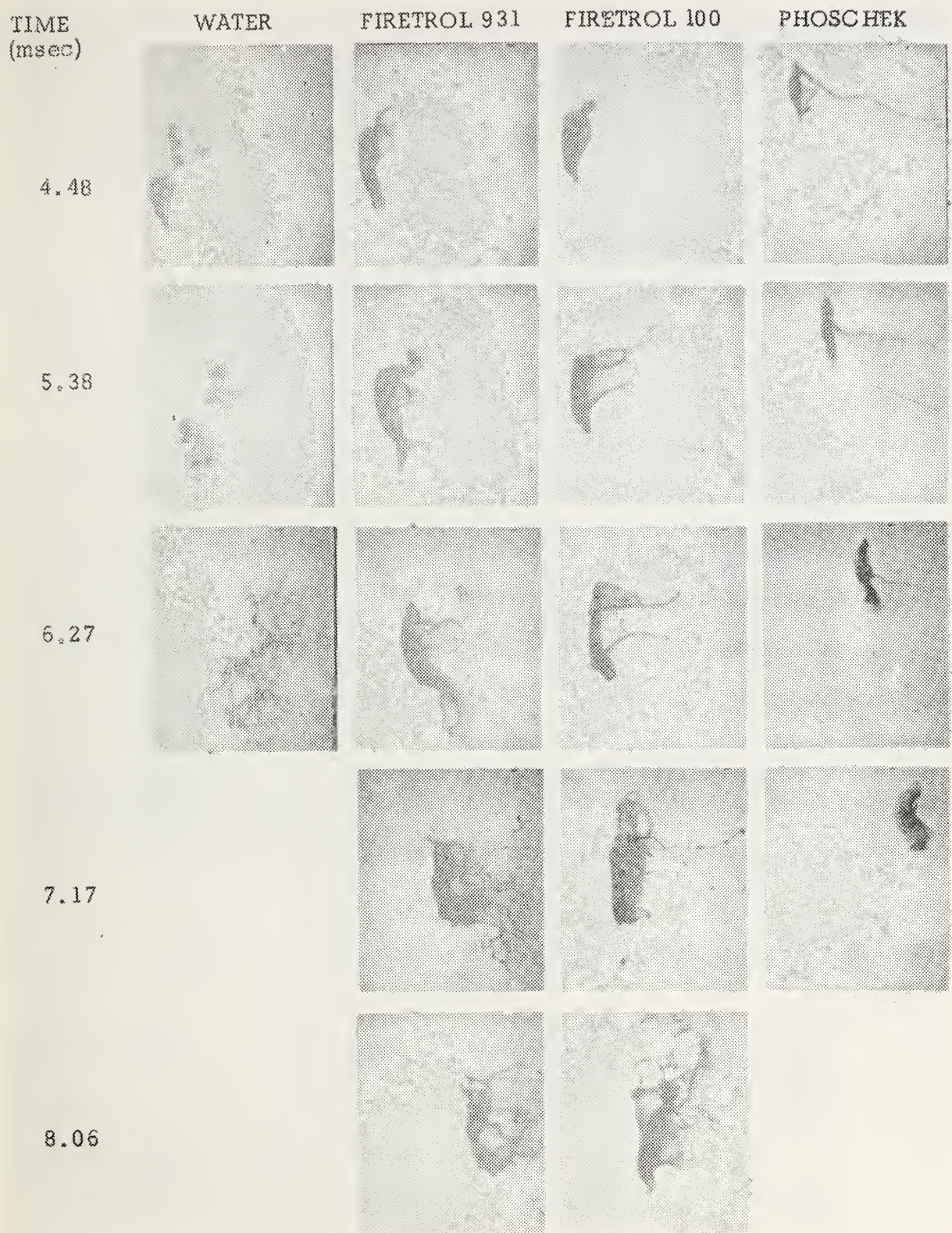


Figure 31. Continued.

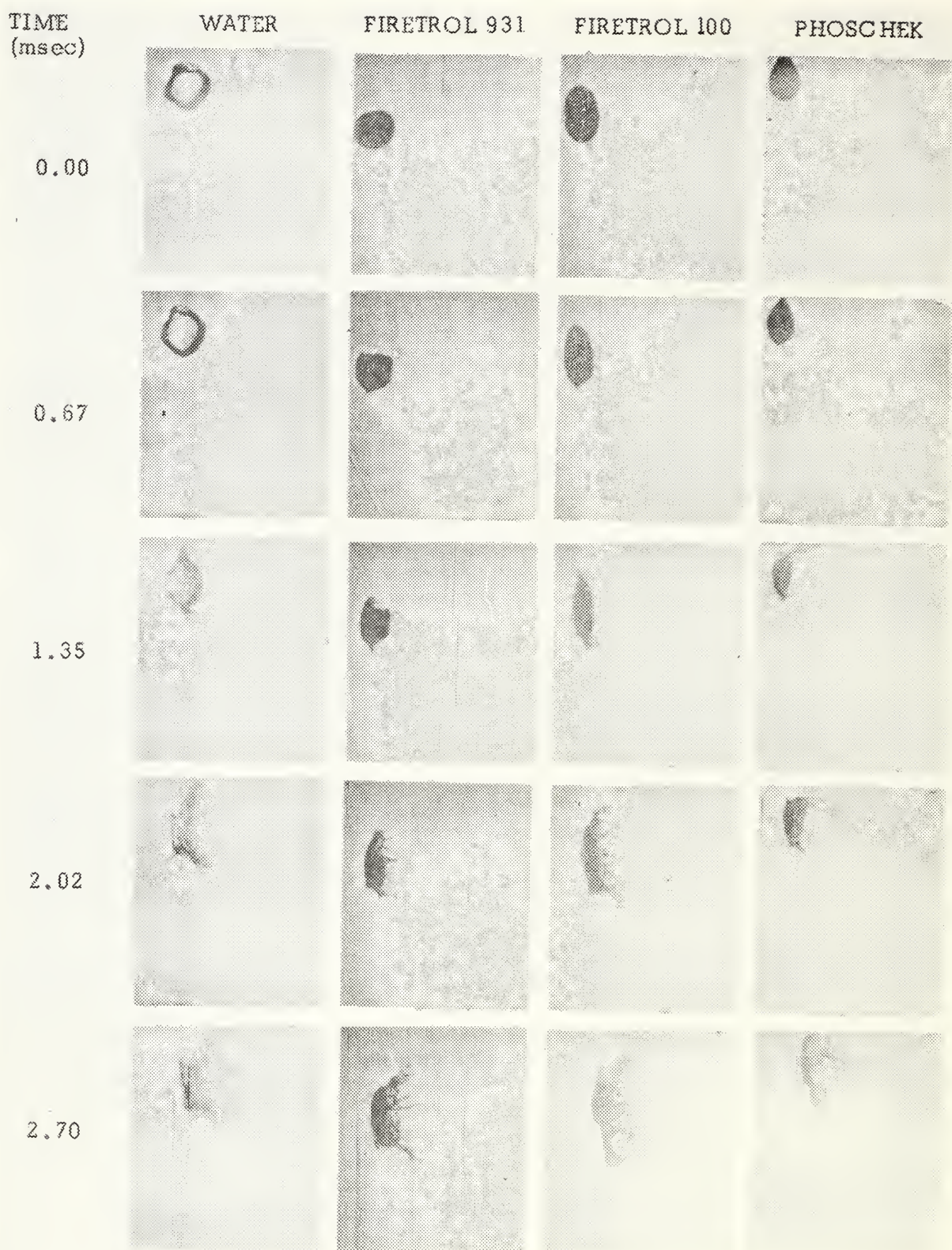


Figure 32. Selected Frames From Photographic Sequences of the Aerodynamic Breakup of 2 - 5 mm Drops of Various Liquid Retardants. Average Wind Velocity is 146 ft/sec.

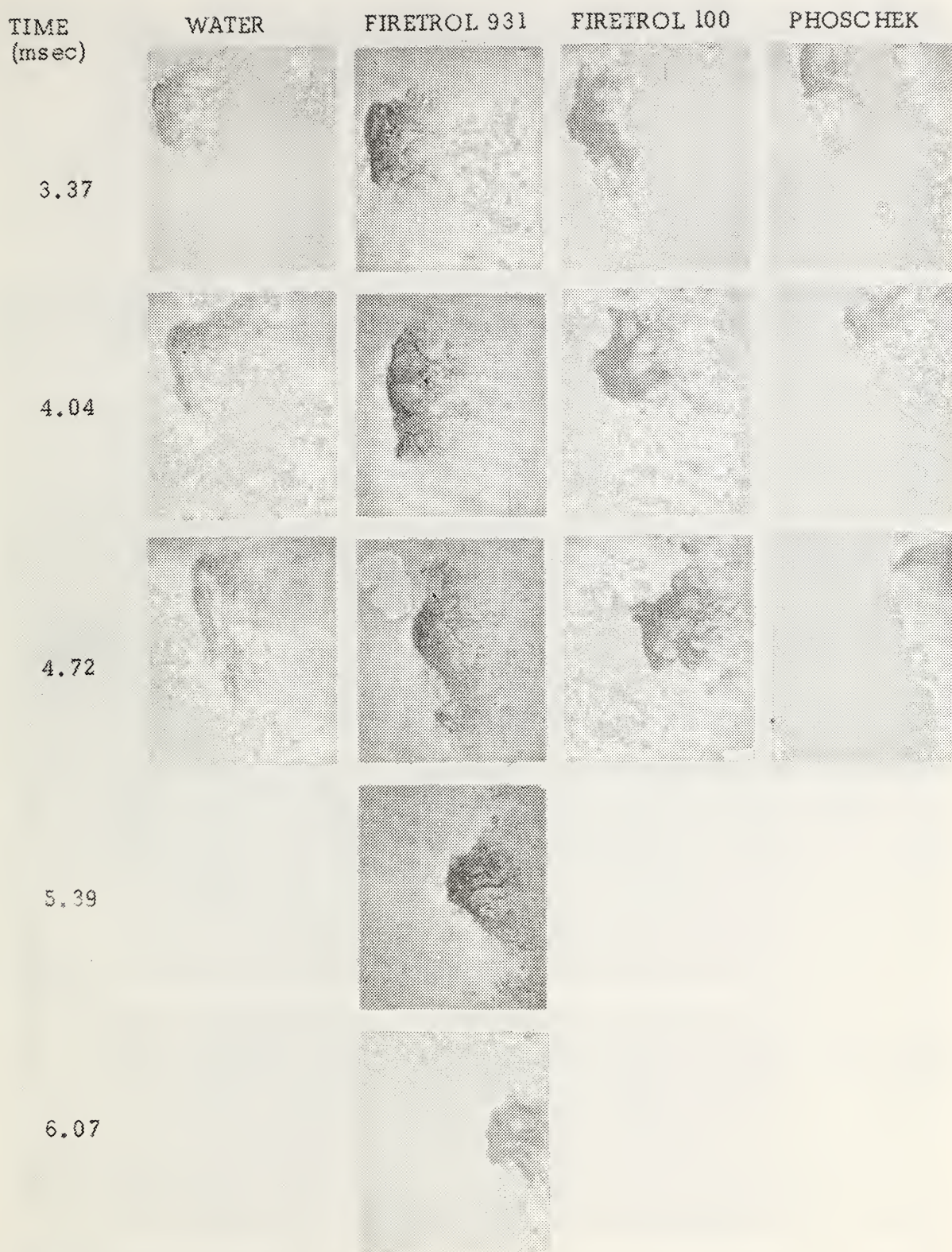


Figure 32. Continued.

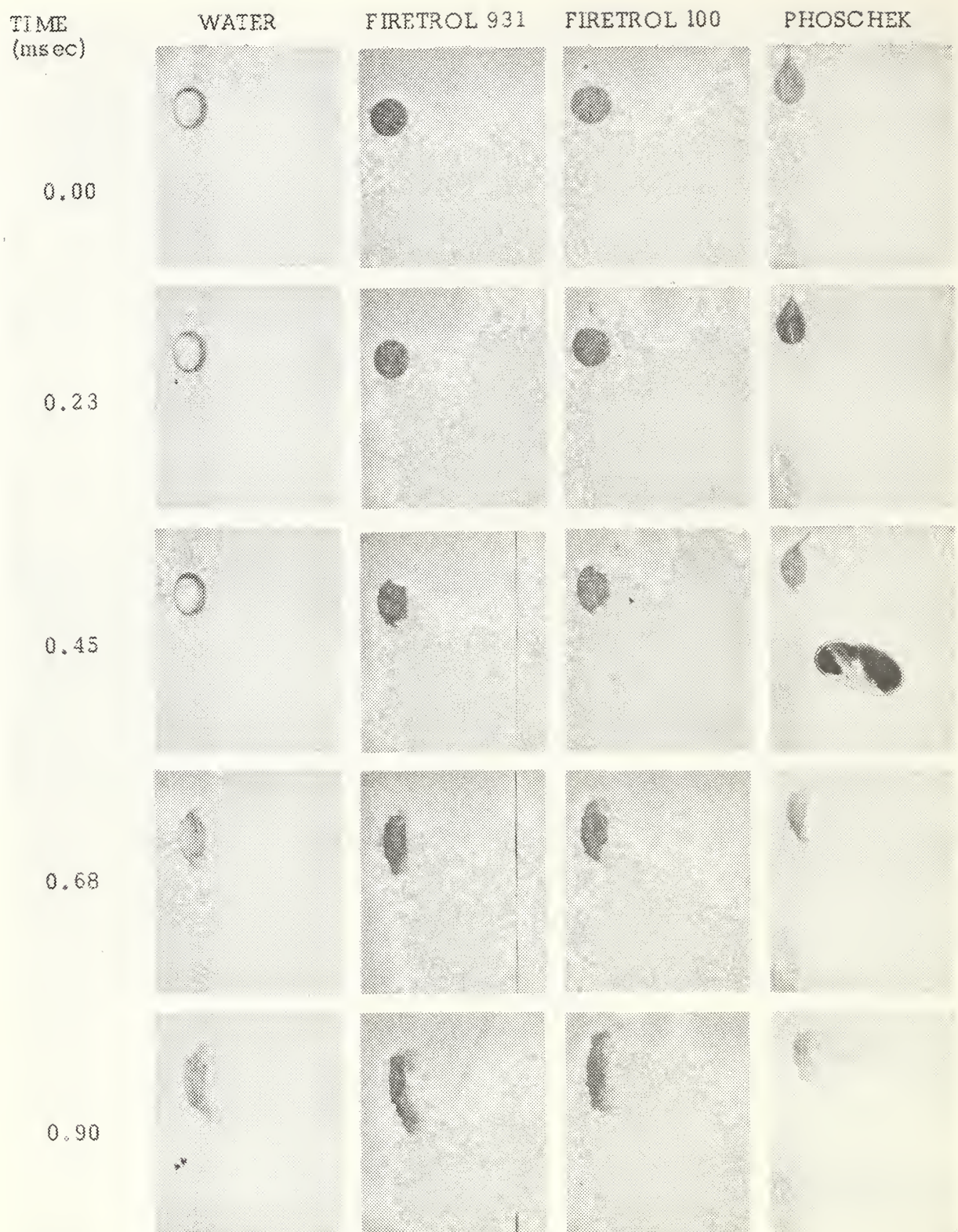


Figure 33. Selected Frames From Photographic Sequences of the Aerodynamic Breakup of 2 - 5 mm Drops of Various Liquid Retardants. Average Wind Velocity is 284 ft/sec.

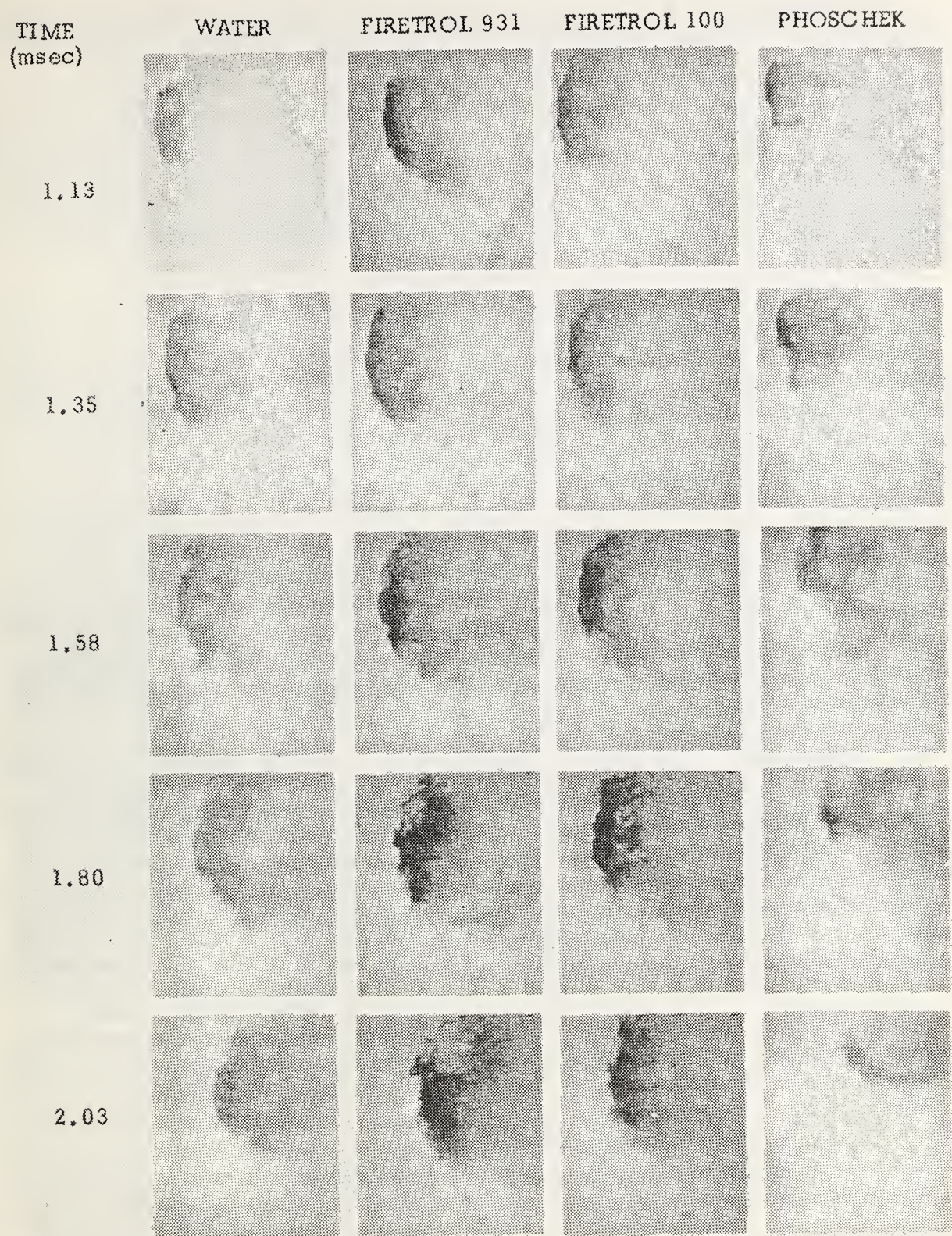


Figure 33. Continued.

The Phos-Chek thus exhibits unusual stability toward breakup at the low velocity, which may be partially carried over to the medium velocity, but not to the high velocity. This behavior together with elongation ability of the filaments and the non-shattering of the bag indicates that there is an internal strength component present in the deforming Phos-Chek. This should arise because the liquid exhibits elastic behavior during deformation, which is the case since it is a gum thickened material. Thus at low wind velocity the elasticity may give greater stability to the liquid toward breakup, whereas at higher velocity the shear stresses are too large for the elasticity to prevent breakup. The studies of the elastic nature of Phos-Chek provided further support regarding the validity of this hypothesis.

6.3.1.1 Large Drop Studies

Several preliminary experiments were conducted using relatively large drops (equivalent to about 1 inch diameter) of water. The drops were produced by a push-tube technique. The apparatus consists of a closed container of the liquid, with an open ended tube coming out the top at an incline. Near the bottom of the container is a movable diaphragm on which the liquid is resting. A small rapid displacement of the diaphragm causes a large drop of liquid to be ejected from the inclined tube. Another apparatus which was constructed to produce large drops consisted of a container which utilized a shutter with a hole in it at the bottom of the container. Rapid displacement of the shutter allows a large drop of liquid to be obtained. The size depends on the hole size and shutter speed. Neither of these techniques produced good spherical drops. It also did not prove possible to couple the drop forming device to the shock tube in a manner as to keep the entry hole closed, i.e., the hole in the test section of the shock tube through which the drop passed remained open during the passage of the shock.

The water drops used in the studies were roughly oblong or ellipsoidal in shape, with lengths that ranged from about 1.2 to 1.7 inches, and with widths of about 0.5 to 0.7 inches. The interaction of the shock with the drop produced drop deformation followed by stripping (surface erosion) breakup, as expected. However during the surface erosion process in one of the film sequences it was observed that corrugations appeared in the frontal surface of the liquid exposed to the wind flow, and breakup of the entire drop appeared to occur shortly thereafter. It is probable that this breakup process corresponds to Taylor instability breakup. If this is true then studies of the breakup of large liquid drops in the shock tube could provide information regarding this breakup mechanism. Further studies of this nature were deferred until analysis regarding the instability wavelength expected from Taylor instability can be conducted, since surface erosion studies using very large drops do not appear particularly useful.

6.3.2 Breakup Time Initiation

The total breakup time of a drop is the time from the passage of the shock front over the drop until the drop is completely broken up. The breakup time depends on wind velocity, drop size and liquid properties - especially effective viscosity. Some film sequences of the total breakup time of the drops have been obtained, and more should be obtained in order to best estimate the effective viscosity that controls the breakup, and compare it with the value

computed from theory using the experimental viscosity versus shear rate measurements. Fluid elasticity - when it is present - can also affect the breakup time as discussed previously.

The initial deformation of the drop preceding breakup also depends on the effective (shear thinned) viscosity. It may be shown that water and the three fire retardants studied have different effective viscosities during breakup initiation, and that these viscosities are consistent with the experimental effective viscosity versus shear rate curves. The problem can be considered from two different considerations, both of which lead to the same result.

A wind passing over liquid requires a finite time of passage before surface instabilities grow and surface erosion begins. This time, t_m , is given by Eq. (24). Thus t_m represents the initiation time for the surface erosion to begin, and may be considered to represent the time at which the drop just starts to break (or erode). According to Eq. (24), t_m should vary inversely as $V^{8/3}$, if all other factors remain constant, where V is wind velocity. The differences between the curves given by a plot of t_m versus $V^{-8/3}$ for the various liquids should thus reflect the differences in the effects of viscosity (or elasticity) of the liquids on the breakup initiation. Figure 34 shows a plot of some of the data obtained on the program. It may be seen that the magnitude of the breakup initiation times at a specified velocity decrease in the order, Phos-Chek XA, Fire-Trol 931, Fire-Trol 100, Water. This implies that the effective viscosity controlling breakup decreases for the liquids in approximately the same order. Water has the smallest breakup time and smallest viscosity, as expected. The figure shows that Phos-Chek has the largest effective viscosity, and this is consistent with the experimental viscosity data. The figure also appears to indicate - at first somewhat surprisingly - that the effective viscosity of Fire-Trol 931 during liquid breakup is greater than that of Fire-Trol 100. However this results because the parameter beta in Eq. (24) is a function of both wind velocity and viscosity, as will be discussed subsequently. When the value of beta is included in the correlation, the value of t_m at a specified wind velocity increases in the order H_2O , Fire-Trol 931, Fire-Trol 100 and Phos-Chek XA, and the effective viscosity increases in the same order. The figure also shows that the value of t_m for Phos-Chek at the low wind velocity is very long and out of line with the rest of the data. This results because of the effect of fluid elasticity, as discussed previously.

An alternative approach to the preceding viewpoint that a time t_m is required before the drop starts to break, is that the drop deformation time controls the time at which breakup initiation should occur. In this case it can be shown using the conventional expressions for drop breakup time (e.g., Eq. (3)) that the approximate correlating factor should be d/V , where d is drop diameter. A plot of t_m versus d/V (not given here) shows the same general behavior as Figure 33 (the curve separations are not as pronounced), from which the same conclusions are arrived at.

6.4 CORRELATION WITH THEORY

The experimental data obtained with the shock tube for water and the three fire retardant solutions was correlated with theory in the following manner.

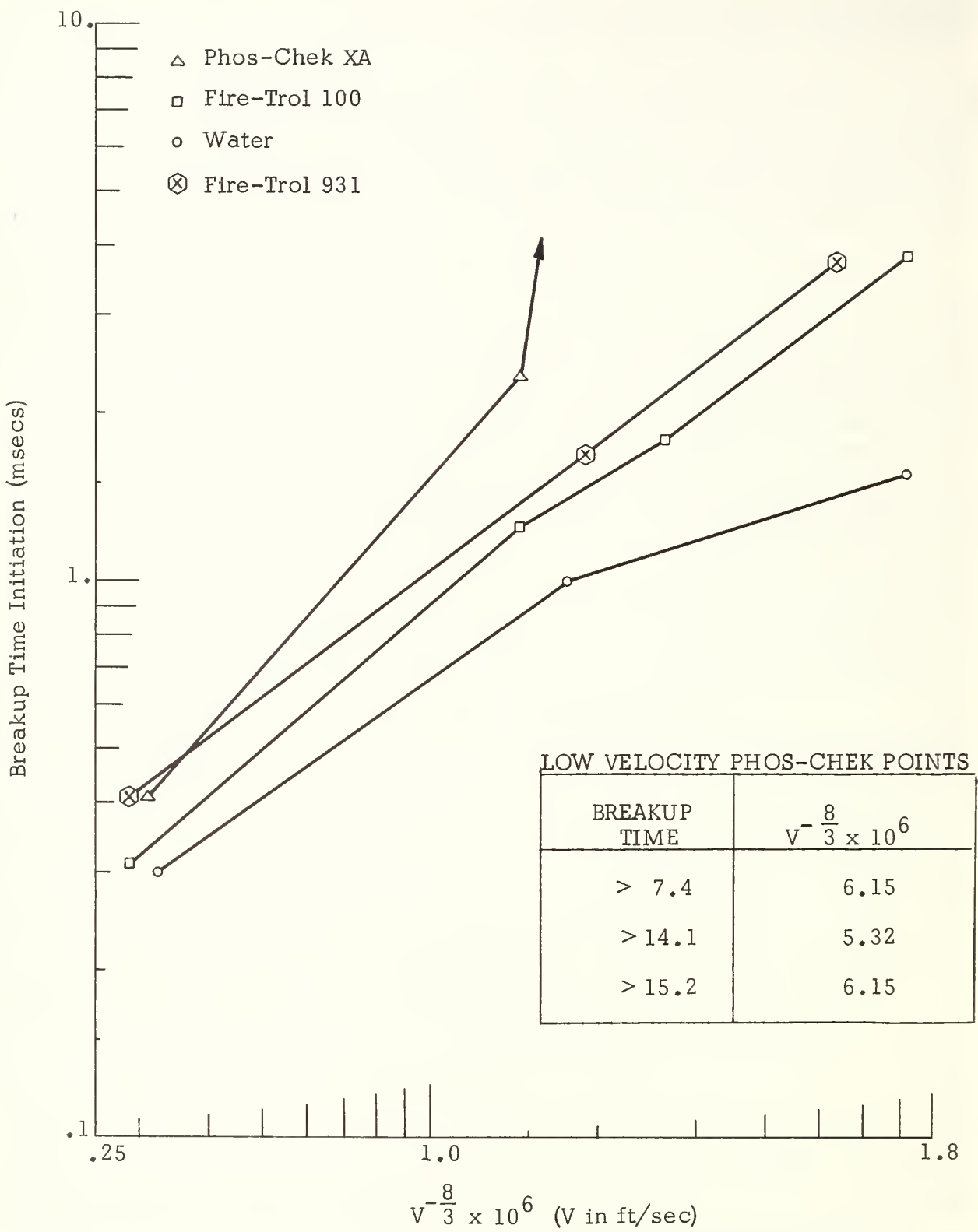


Figure 34. Experimental Time to Initiate Drop Breakup as a Function of Inverse Wind Velocity to the 8/3 Power.

The experimental value of the time for the liquids to begin breakup at each wind velocity was used in the theoretical expression (Eq. (24)) to compute a theoretical value of beta. The effective shear rate for evaluating effective viscosity was estimated from Eq. (28) with t_m replacing tau in the denominator.

Likewise the experimental value of total breakup time was used with Eq. (5) to compute beta, with the mean value of L and tau being used in that equation and Eq. (28) being used to compute shear rate. The total breakup time data of Morrell²² for water was also included using Eq. (5).

It was found that the value of beta depended on liquid viscosity as well as wind velocity. This was of some interest since previous studies have always considered beta to be either a constant¹⁴, or a function of wind velocity³⁰. The possibility that beta may depend on viscosity was, however, speculated earlier¹⁴. In view of these results the values of t_m obtained for large sized drops in reference 4 for water and three silicone fluids with different viscosities was included in the correlation. A rough fit of the data gave the following relation between beta, wind velocity (in cm/sec) and viscosity (in poise)

$$\log (\beta / \eta^{1/6}) = -0.4978 - 9.925 (10^{-5}) V + 1.53 (10^{-9}) V^2 \quad (81)$$

The absolute value of beta given in this equation at a specified velocity differs by a small factor from that given in reference 30 where R (drop radius) rather than d (drop diameter) was used in Eq. (5). It was found that the computed values of beta based on d were much more consistent with the values based on t_m than were values based on R. It may be also mentioned that an overall examination of the data subsequent to the preceding studies suggests that the value of beta may also depend slightly on drop size. It may be difficult to extract this dependence on the basis of available experimental data, but in any event this would require a complete re-evaluation of the experimental data. Further studies are in progress to evaluate the validity and usefulness of Eq. (81).

6.5 DROPLET SIZE STUDIES

In addition to the previous breakup rate studies, it is also desirable to obtain some measure of the droplet size distribution that characterizes the breakup of the different retardant solutions under various wind velocities, and during the present program studies of this nature were initiated. The determination of the droplet sizes produced by the breakup of the liquid drops has proven to be very difficult however, and it is useful to summarize some of the reasons for this.

Although the breakup measurements are performed under a constant velocity air stream, in reality the constant flow is temporary and lasts only 15 msec before it becomes nonsteady due to the arrival of rarefaction waves from both directions. Thus although the steady flow time is sufficient to allow total breakup of the drop (at sufficiently high wind velocities), it is not always possible to discern the individual small droplets that are produced by the breakup since they are still clustered together fairly closely. In the course of time, under a steady flow condition, the individual particles would tend to separate and enable improved discrimination. However, since the experimental conditions only give 15 msec of constant flow, the small droplets are subsequently subjected to a varying air stream for a time period that is relatively long compared to the original steady flow interval. This flow behavior leads to two possibilities. First, if the droplet size distribution is changed by the non-uniformities in the air stream, then any measurement or collection of the droplets must take place within the steady state interval, preferably at the end. On the other hand, if the size distribution of the droplets does not change significantly following the steady state period, then less hurried methods can be used in the collection and/or measurement.

6.5.1 Test Results

The first droplet collection experiments were designed under the second possibility since it was anticipated that this would give the simplest experimental configuration. It was not assumed that either possibility was the actual case, but the tests for the first possibility, i.e., the necessity for collection during the steady state period, would take longer to prepare and hence would naturally follow the easier test series.

There are several methods for obtaining droplet size distributions from a cloud of drops initially in the air. The simplest method is to allow the drops to settle out on a suitable surface so that the droplets can be counted and the droplet diameters determined. A complicating factor in the present tests was the variable wind velocities acting during the settling period of the droplets. Thus the velocities and even the direction of the wind was variable (due to rarefaction effects), and no accurate prediction regarding the trajectory of the droplets could be made. This is unfortunate in the sense that there are equations that relate the trajectory range of a droplet to its size. These cannot be used with this type of experiment so less elegant methods must be utilized. The experimental design chosen was to let the droplets fall on a long narrow horizontal strip of material on the bottom of the shock tube. The droplets that would be deposited on the strip could subsequently be examined, counted and measured to obtain a size distribution.

The first strip material used was white colored sheet plexiglas. The strip was 2" wide and 1/8" thick and was fastened to the bottom of the shock tube during a test. It was found that the resultant liquid deposits obtained on this material were in the form of streaks of material rather than round or nearly round deposits. This indicated that there was an appreciable horizontal component to the velocity vector of the droplet velocity and most likely many times that of the vertical component, especially for the smaller droplets. It was difficult to obtain a measure of the drop size from the streaks, and it appeared that the length of the streaks would not be a valid measure of the droplet size since the larger droplets fall faster and this tends to reduce the length of the streaks, whereas the smaller drops fall slower and this increases the length of the streaks. The width of the streaks was also variable so that this also

did not seem to be a reasonable criteria of droplet size. An additional difficulty with this method of evaluating drop size is the fact that it would be very difficult to calibrate the residue left on the strip with respect to known droplet size, since the known drop would have to attain a velocity vector comparable to that of the experimental droplets and this itself may produce changes in the drop before it hits the strip.

This difficulty is alleviated if the droplets can be made to give a circular residue. Since the plexiglas surface of the strip was very well polished, it was then considered that a somewhat rougher surface might control the streaking of the droplets. The first two materials tried were masking tape and plastic coated adhesive tape, which were stuck to the long plexiglas strip. Both of these materials were found to be unsuited for the test purposes. Next a more absorbent material, ordinary adhesive tape, was used to observe the droplet patterns. This was used for obtaining the droplet distribution for Phos-Chek at the three standard velocities used in the breakup tests, and the two Fire-Trol solutions at the medium velocity. The results showed that a large proportion of the droplets still gave streaks on the horizontal tape strip. The droplets were fairly well absorbed by the adhesive tape backing, however, so that in a relatively short time, the tape could be pulled up and folded without the danger of altering the droplet pattern. These tests gave good indications of the general horizontal distribution of the droplets for the various fire retardants for the three standard velocities. However, when considering the possibility of making actual measurements of droplet size, the adhesive tape did not give generally other than streak residual patterns of the droplets and these could not be reliably interpreted to obtain a droplet size.

In an effort to obtain maximum absorption of the droplet combined with minimum slickness of the surface, a horizontal strip of white desk blotter material was tried in a test with Fire-Trol 931 at a wind velocity of 155 feet/sec. The results from this test gave residual drop patterns that were substantially more circular than any of the other collector strips had given, but there were still a fair proportion of short streaks. During the test, the end (toward the open end of the expansion tube) of the strip came loose from the plastic support strip and apparently flapped with the wind currents in the shock tube. The residual droplet patterns left on the flapping end were almost entirely round and were also larger and more copious than those on the horizontal strip. The pattern was also on both sides of the flapping strip. These results would appear to indicate that the droplets move back and forth in the tube to some extent, and that the pattern obtained from a vertical collector in the cross section of the tube versus a horizontal collector along the bottom of the tube are likely to be different - with the vertical collector perhaps giving data that is easier to interpret although it may affect the wind flow to some extent.

Additional studies were conducted along the previous lines, but difficulties were experienced in measuring drop size-especially for the very small droplets. However definite patterns of droplet concentration along the horizontal distance of the shock tube could be discerned. In the last experiments a small vertical square (1" wide x 1 1/2" high) of cardboard backed by a flat steel support was set up about 4 ft away from the drop generator, and nearly circular drop patterns were obtained on the square. Although the square occupied a small fraction of the shock area, the drop patterns represented a large fraction of the material caught on both the small vertical and long horizontal blotters.

Further studies are needed to resolve the differences between the two methods of collecting drop size data - which inspite of difficulties show some promise. A method for determining the sizes of droplets while still in the shock flow was considered, but not tried. This method involves taking a short exposure flash picture of the broken-up drop down the tube from where the present framing sequences were taken. The optimum position would be determined by the maximum separation of the small droplets formed from the original drop while they are still in the shock flow field and not too near the tube walls. Examination of previous framing sequences have shown that towards the end of the sequence, individual droplets are just beginning to be discernable, so the method appears promising.

7. CONTROLLED LIQUID INJECTION STUDIES

A potentially useful technique for injecting liquid jets and slugs into air at high velocities was demonstrated during this program. This technique involves the use of an air gun to project a retardant filled container at controlled velocities. The container is impacted against a cushioned plate having a hole slightly smaller than the inner diameter of the cup. In the experiments performed to-date approximately 30mm diameter jets were generated. However, a wide range of jet diameters are possible by simply changing the gun barrel diameter and fluid container.

7.1 EXPERIMENTAL TECHNIQUE

A 1.5 in. (38mm) barrel was attached to one of the Shock Hydrodynamics gas guns. Pin probes were installed at a separation distance of 76mm at the end of the barrel and these probes attached to an electronic counter for purposes of timing the travel of the fluid filled cup within the 76mm flight path up the barrel (i.e., for velocity determinations). A 1.5 in. diameter, 2 in. long steel cup was employed as the liquid container and projectile.

The projectiles were impacted against a soft rubber cushioned steel plate, see Figure 35, having a 30mm orifice, permitting the liquid contents of the cup to be injected through orifice at velocities approximately twice the impact velocity. The projectile impact and liquid jet were photographed using a Beckman and Whitley Dynafax camera at a framing rate of 10,000 frames/sec. The maximum writing time for each frame at this framing rate is 5.4 μ sec and the frame separation is 100 μ sec; however, because the 16mm frames are staggered on a 35mm film strip the separation between adjacent frames is 200 μ sec. The field of view was illuminated by a linear array of G.E. FT 18 flash tubes.

7.2 OBSERVATIONS

Two velocity regimes were studied initially: jet velocities between (a) 350-400 ft/sec and (b) 600-650 ft/sec. Typical photographic frames are shown in Figure 36. In most of the photographic series, the cup containing the fluid can be seen just before impact against the cushioned orifice followed by jet formation and travel.

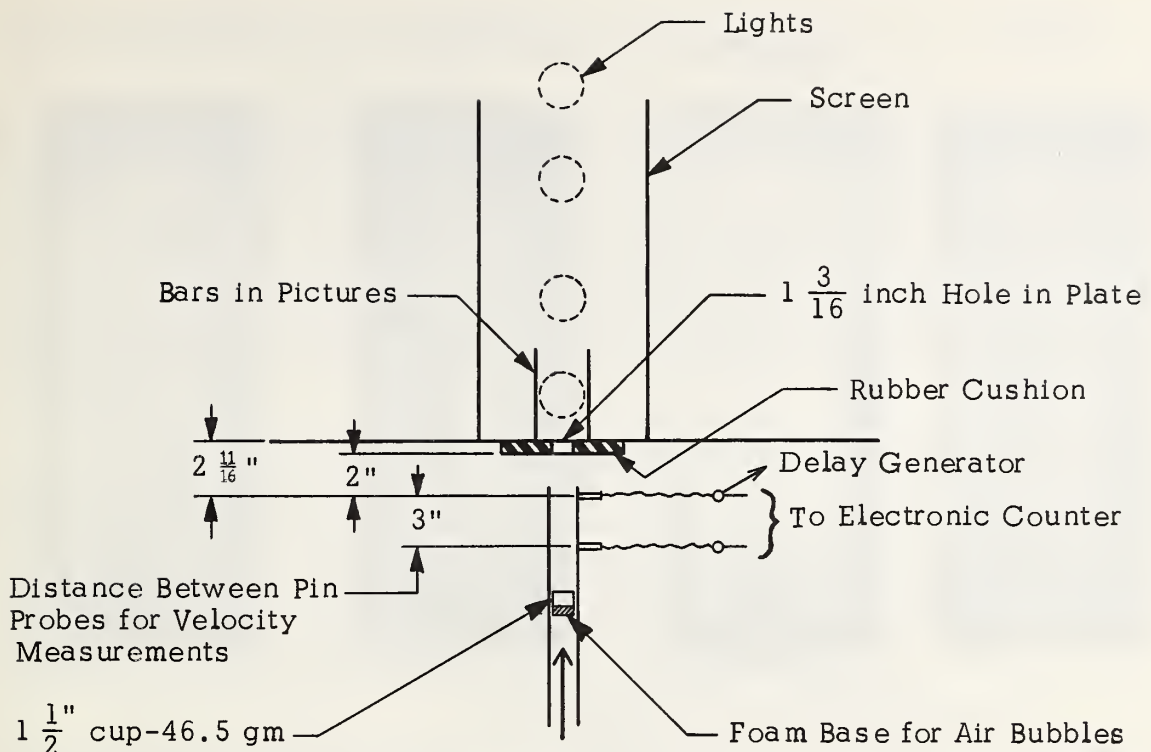
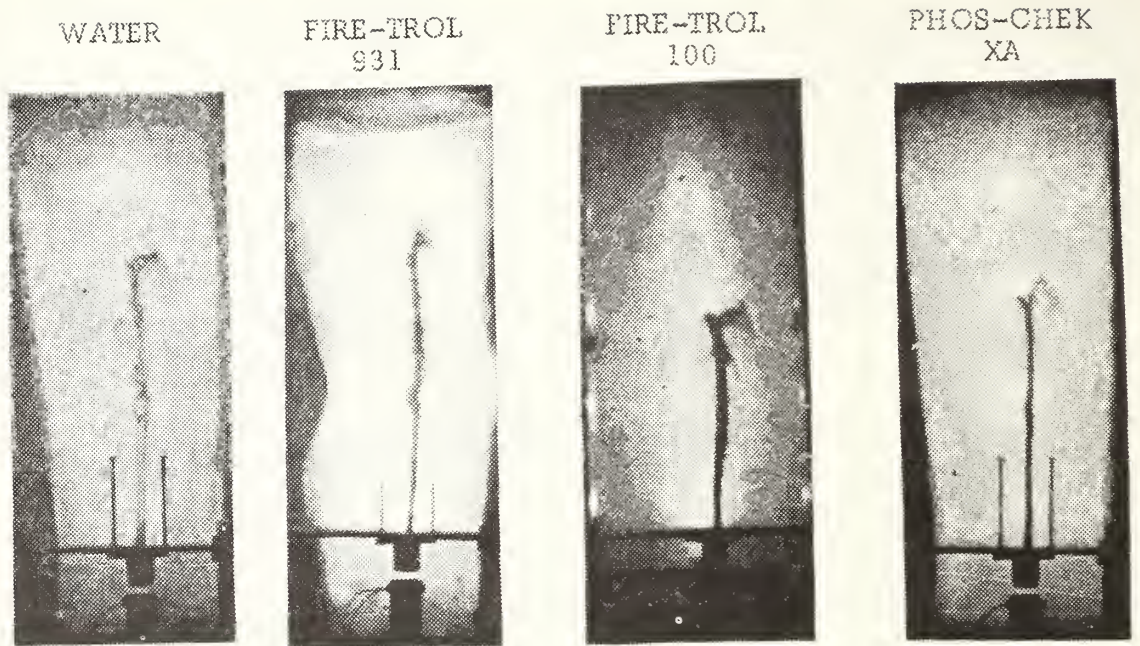


Figure 35. Test Set-Up for Liquid Jet Experiments.

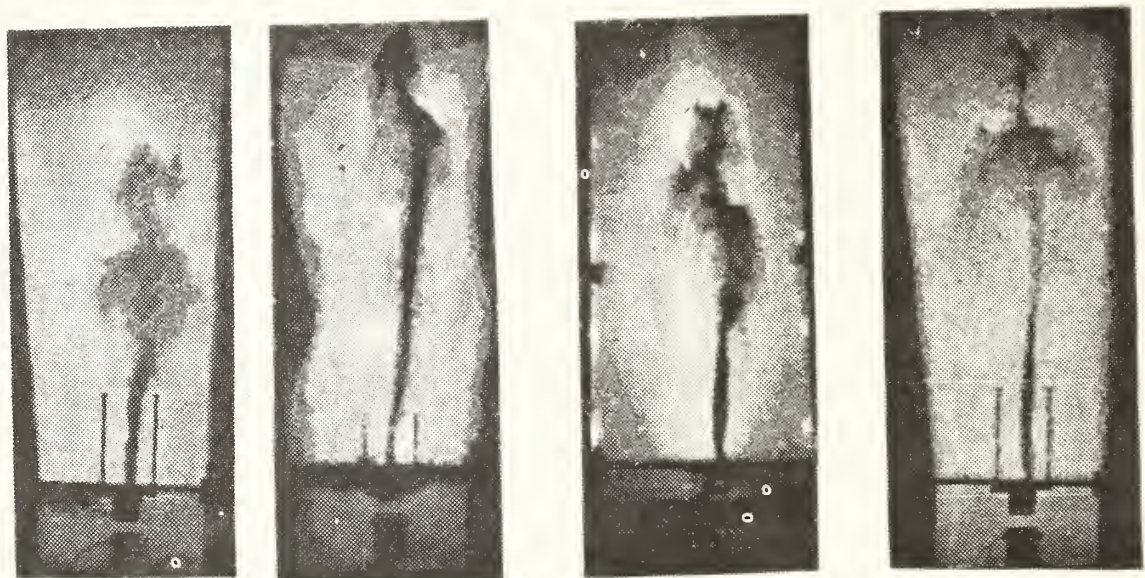
The retardants and water all form jets of varying stabilities as indicated by the general appearance of the jet, including the length that remains contiguous. In general some deformation and erosion occurs at the tip of all of the advancing jets, and behind the tip the jet exhibits various behaviors. Water forms the least stable jet. The jet is relatively broad, and the transition between the stable portion of the jet and the disturbed portion is reasonably sharp. The disturbed portion appears to be non-contiguous, and the jet spreads out with increase in velocity. Surface erosion occurs along the cylindrical surface of the disturbed portion of the jet.

Phos-Chek XA forms the most stable jet of the three retardants and water. The diameter of the jet at the lowest velocity is very narrow and sharp as though the jet were stretching, and the jet has the general appearance of a jet of a viscoelastic liquid. This agrees with the previous evidence that Phos-Chek XA exhibits elastic forces while undergoing acceleration. The base of the jet broadens at the higher velocity and necks down toward the jet tip. However the jet boundary remains sharp - indicating that no surface erosion occurs along the cylindrical surface. Erosion and deformation do occur at the jet tip, however, particularly at the higher velocity. The jet remains contiguous up to its tip for both high and low velocity.

The jet formed by Fire-Trol 931 is generally narrower than that of Fire-Trol 100, and is not as contiguous as that of FT 100 along the length of the jet. However the FT 100 appears to undergo a greater degree of breakup near the jet tip than does FT 931. Overall it appears that the jet of FT 100 is more stable than that of FT 931.



a. Initial Jet Velocity is 350-400 ft/sec.



b. Initial Jet Velocity is 600-650 ft/sec.

Figure 3C. Liquid Jet Injected Into Air Through a 30 mm Orifice.
Time is 4 msec After Injection.

8. LIQUID BREAKUP ANALYSIS AND CORRELATION

As discussed previously, as bulk liquid fire retardant is released from an aircraft it simultaneously undergoes both surface stripping (erosion) and deformation by aerodynamic (wind) forces created by the liquid moving rapidly through the air. The deformation results in a thinning and lateral spreading of the liquid. After significant thinning, Taylor instabilities are induced in the front surface of the liquid and grow rapidly until they penetrate the liquid-causing it to breakup into a large number of individual particles or globs. These particles may then undergo further breakup into smaller droplets by surface erosion or other mechanisms (e.g., bag breakup) as they continue their fall trajectory.

There are thus two separate breakup mechanisms which occur during the free fall of liquid retardant from an aircraft, i.e., Taylor instability breakup and surface erosion. The general characteristics of these breakup processes in conjunction with certain system parameters such as the aircraft velocity and altitude, and the rate of liquid ejection from the aircraft determines the area concentration distribution of the dispersed retardant that falls on the ground, the ground pattern (length and width) of the treated area, and the droplet size and impaction velocity of the retardant rain.

In section 4 of this report, equations were developed for describing both of these breakup mechanisms, while in section 5 measurements were made of fluid viscosity and elasticity as a function of shear rate and of surface tension, for use in the equations. In section 6 measurements were made in a shock tube of the surface erosion breakup of liquid drops of the three fire retardants of current interest and of water, for the purpose of estimating the values of a certain parameter that is contained in the breakup equations.

In this section an analysis is made of the breakup of the three conventional liquid fire retardants and water subsequent to their ejection from an aircraft. The effects of the controlling parameters such as aircraft velocity, tank and gating system, and the rheological properties of the fluid on the breakup characteristics of the liquid retardant are estimated. Discussion and correlations are also presented relating the liquid breakup and dispersion characteristics to ground pattern. These discussions and correlations as well as certain parts of the breakup analysis are preliminary, however, in that a more detailed comparison of the theory with existing experimental data could allow further refinement of the theory and enhance its predictive capability.

8.1 INITIAL BREAKUP BY TAYLOR INSTABILITY

8.1.1 Evaluation of the Breakup Equation Constants

The equations describing the Taylor instability breakup of the liquid contain two parameters whose values must be specified in order to use the equations for predictive purposes. One parameter is the drag coefficient, C_d , contained in Eq. (35b). Swanson and Helvig^{40,41}, in their treatment used the value 2.5 which was determined for small drops in a shock tube⁴³, although another study of this nature¹¹ gave a value of about 3.0. They emphasized that the drag coefficient may not remain constant over the entire deformation process, and may also be larger than that obtained in the shock tube with small drops. They found it necessary to reduce the value of a certain constant in the theoretical equation based on Bond number that they used to correlate breakup time, in order to obtain agreement with experiment. They could have alternatively increased the value of the drag coefficient to obtain the agreement. It can be estimated that this would result in a very significant increase in the effective value of the drag coefficient above that which they used.

In order to evaluate the liquid breakup equations the value of A_i , the initial amplitude of the fastest growing instability, must also be known. This can only be obtained by fitting the equations to experimental data. This apparent shortcoming, however, is almost always the case for problems involving instability growth⁵⁸. However, fitting A_i by experimental data helps insure that the model will give realistic predictions, and allows the elucidation of the important parameters - including rheological properties - that control the initial breakup of the liquid.

In the present studies the value of A_i was computed for several assumed values of the drag coefficient using the breakup equations and experimental values of the breakup time of the liquid, t_b , given by Swanson and Helvig for certain conditions. They gave values of 1.375 sec and 1.63 sec for the CL-215 aircraft dropping 700 gal ($V = 97$ knots) and 1400 gal ($V = 92$ knots) of Phos-Chek XA⁴¹, and 1.65 sec for the B17 aircraft (2000 gal, $V = 120$ knots) dropping Phos-Chek⁴⁰. These breakup times are times subsequent to the exit time of all the liquid from the tank. They considered the retardant breakup process to consist of a release phase during which time the liquid exits from the tank, followed by a deformation phase which culminates in breakup. The preceding experimental breakup times correspond to the deformation and breakup time of the liquid after the release phase is over with.

In the present studies in which the tank liquid is replaced by an equivalent cylinder, it was considered more realistic to consider the deformation of the liquid to begin when half of the liquid has exited the tank since the deformation of any element of the liquid begins immediately when it is outside the tank and in the airflow. In this case the preceding times should be increased to about 1.605, 1.86 and 2.05 sec, respectively. Actually solutions were obtained for both of the two preceding sets of times, as well as the case where the breakup time is considered to be the sum of the total liquid release time and the preceding deformation and breakup phase time. It was found that the most realistic drag coefficients

for use in the equations corresponded to breakup times whose values are with respect to the time that half of the liquid has exited the tank.

Using the breakup times evaluated relative to the time that half of the liquid exits from the tank, i.e., 1.605, 1.86 and 2.05 sec, the breakup equations were solved using the various parameters appropriate for Phos-Chek XA, and the results are shown in Table V. For any assumed value of drag coefficient and experimental breakup time there are the computed values of the other parameters. There are various characteristics that may be seen from these solutions. It will be noted that the average shear rate of the deforming liquid is of the order of unity (about 2 sec^{-1}). The shear rate increases with increase in the assumed value of the drag coefficient, C_d , which increases the initial lateral velocity, V_e , of the particles at breakup. However the value of the instability growth time, t_i , decreases with increased C_d and this causes the deformation time, t_d , to increase (for fixed breakup time, t_b). The latter results in a decrease in the liquid thickness, L_e , at breakup, and consequently also in particle size, D , and instability wavelength. The decrease in L_e , with increase in C_d causes an increase in lateral expansion ratio, R_e/R_o , and a decrease in the shear rate, S_1 , of the liquid while undergoing instability growth (Eq. 42). The value of η_d for Phos-Chek decreases with increase in S_d , while the value of η_l , increases with decrease in shear rate. However these variations are due to the particular functional relationship between effective viscosity and shear rate for Phos-Chek, and in the general case any variation can be obtained depending on the viscosity-shear rate relationship.

8.1.1.1 Initial Amplitude of the Instabilities

It will be observed from the table that the computed value of the initial amplitude of the instabilities, A_i , decreases with increase in C_d , and also apparently with increase in liquid load—especially at the higher values of C_d . The seemingly large changes in A_i are somewhat misleading however, since the value of A_i is a relatively insensitive parameter in the solution of the equations. Its value can vary widely under specified drop conditions without affecting the computed results strongly. For example if the value of A_i of $6.63(10^{-10})$ given for the first case for $C_d = 3.5$ in the table is used, the values of the computed parameters are as given. If now the value is changed to the value given for the third system, i.e., $7.9(10^{-17})$ — which is 7 orders of magnitude lower than the first value — but used to calculate the breakup properties of the first system, it is found that the computed breakup time differs from the correct value by less than 10%, and the computed particle size differs from the correct value by less than 40%. Thus the values of the computed parameters are relatively insensitive to several orders of magnitude change in A_i .

However, although the results are not strongly sensitive to the values of A_i , A_i does change with conditions — as indicated in the table. It was found that if

TABLE V. COMPUTED TAYLOR INSTABILITY BREAKUP CHARACTERISTICS OF PHOS-CHEK XA.

CL-215 Aircraft, 700 gal., $L_O = 155$ cm, $R_O = 73.8$ cm, $V = 97$ knots = 4990 cm/sec												
C_d	t_b (sec)	D^* (cm)	$\frac{R_e}{R_O}$	V_e (cm/sec)	A_i (cm)	L_e (cm)	t_d (sec)	\dot{S}_d (sec $^{-1}$)	η_d (poise)	S_1 (sec $^{-1}$)	η_1 (poise)	λ (cm)
2.5	1.605	6.02	2.24	239	1.56(10 $^{-5}$)	30.86	1.128	1.43	48.4	33.7	6.0	3.85
3.0	1.605	4.56	3.19	446	2.58(10 $^{-7}$)	15.19	1.235	1.88	41.0	22.8	8.5	3.61
3.5	1.605	3.49	4.48	765	6.63(10 $^{-10}$)	7.74	1.298	2.31	36.3	14.9	11.7	3.39
4.0	1.605	2.58	6.22	1258	7.94(10 $^{-14}$)	4.00	1.341	2.73	32.8	10.2	14.5	2.99
CL-215 Aircraft, 1400 gal., $L_O = 155$ cm, $R_O = 104$ cm, $V = 92$ knots = 4730 cm/sec												
2.5	1.860	6.43	2.70	406	1.53(10 $^{-5}$)	21.34	1.385	1.43	48.3	17.6	10.5	5.11
3.0	1.860	4.54	3.90	818	4.07(10 $^{-8}$)	10.19	1.480	1.84	41.6	12.2	13.2	4.39
3.5	1.860	3.15	5.58	1303	4.87(10 $^{-12}$)	4.97	1.540	2.23	37.0	8.6	15.4	3.63
4.0	1.860	2.11	7.99	2200	2.51(10 $^{-18}$)	2.43	1.583	2.63	33.6	6.2	16.3	2.84
B17 Aircraft, 2000 gal., $L_O = 231$ cm, $R_O = 102$ cm, $V = 120$ knots = 6180 cm/sec												
2.5	2.050	5.17	2.87	402	8.15(10 $^{-9}$)	28.14	1.537	1.37	49.6	34.2	5.9	3.20
3.0	2.050	3.97	4.25	765	7.19(10 $^{-12}$)	12.76	1.645	1.76	42.7	19.7	9.6	3.20
3.5	2.050	2.91	6.22	1320	7.90(10 $^{-17}$)	5.96	1.711	2.14	38.0	12.0	13.4	2.94
4.0	2.050	2.00	9.06	2320	4.09(10 $^{-25}$)	2.81	1.757	2.51	34.5	7.9	15.7	2.44

*The particle diameter will be a factor of 1.59 larger if breakup occurs at the points of maximum instability displacement rather than the nodal lines.

the values of certain parameters in the breakup equations are changed over a wide enough range without compensating changes in A_i , that a solution cannot be obtained for the equations, i.e., Eq. (47) has no solution because there is no minimum in the breakup time equation. This results, for example, for water-whose viscosity is three orders of magnitude less than for Phos-Chek-if the values of A_i deduced for Phos-Chek are used in the equations. This indicates that the value of A_i is a function of certain parameters-particularly load size and liquid viscosity.

An inspection of Eq. (47) indicates that in order for solutions to be obtained the value of A_i should be made a function of A, B, η_d and L_e . However the term containing η_d is always of negligible or of small importance, and the value of L_e depends on the value of C_d . This indicates that the values of A_i given in the table can be made a function of A/B for the various values of C_d . Evaluating and assuming that the relationship between a plot of $\log A_i$ and A/B is linear gives

$$A_i = a \exp(-bA/B) \quad (82)$$

where an eye fit to the curves gives values of a of 0.576, 2.46, 2.23 and 3.32 for drag coefficients of 2.5, 3.0, 3.5 and 4.0; and corresponding values of b of 0.0432, 0.0673, 0.1117, and 0.1758 respectively. It was found that the values of A_i given by this equation allows a solution of the breakup equations to be obtained under any condition (including water). Since the computed breakup characteristics of the liquid are relatively insensitive to the values of A_i as long as solutions can be obtained, the use of the preceding equation should give relatively reliable values. The value of A/B in the preceding equation is given by

$$\frac{A}{B} = \frac{\rho_1^{1/6} (2L_o^2 + R_o^2)^{1/2}}{2(2)^{1/2} \eta_1^{1/3} P^{1/6}} \quad (83)$$

It may be seen from this equation that the value of A_i depends primarily on the load size and liquid viscosity.

8.1.1.2 Selection of Drag Coefficient

The preceding analysis gives the value of A_i for any assumed value of C_d . The question then arises as to what value of C_d corresponds to a real retardant drop. The answer to this question requires information regarding the value of D (and the points where the liquid breaks), or L_e or R_e/R_o when breakup occurs. Swanson and Helvig indicated⁴⁰ that there was indirect (camera) evidence that the liquid expands nearly a factor of 10 for the B17 drop before breakup, but noted that erosion of small particles from the surface of the liquid in the air flow masks the true location of the deforming liquid. They also made an estimate of

the sheet thickness at breakup and obtained a value of 0.13 to 0.3 ft (3-9 cm). This value does not appear quite compatible with an expansion ratio of 10, which seems to imply a thinner sheet. Shock tube studies with small drops undergoing surface erosion give an expansion ratio of about three before breakup by Taylor instability.

Since the best value of C_d is not known at this time, for the present purpose a value of 3.5 was used to obtain solutions whose main purpose is to illustrate the effects of the various system and retardant parameters on the Taylor breakup of the aerially delivered retardant. This value gives a sheet thickness at breakup consistent with that estimated by Swanson and Helvig, but the expansion ratio is more in line with the shock tube studies. Additional studies on correlating the breakup of the particles with ground pattern lengths and widths as well as any other other findings may provide additional evidence that will be useful in determining the value of C_d that best describes the Taylor breakup of the liquid. For the present, however, the solutions showing the effects of the various system parameters and liquid properties have been based on a drag coefficient of 3.5.

8.1.2 Computational Results

A variety of solutions of the breakup equations were obtained to illustrate the effects of the various system parameters and retardant properties on the liquid breakup characteristics. In examining these breakup characteristics several things should be kept in mind. It will be recalled that the value of A_l was obtained by fitting the equations to experimental breakup time data. Because of this the computed breakup times should be relatively good (especially for viscous retardants) and their accuracy may be essentially comparable to that of the experimental data used in fitting the equations. On the other hand the absolute values of the other parameters depends to some extent on the value used for C_d , which was 3.5 as discussed previously. Table V illustrates the general effect of using other values of C_d .

It will also be recalled that the computed value of the equivalent spherical diameter, D , of the liquid particles produced by the breakup assumes that the liquid sheet breakup occurs at the nodal lines. If the breakup occurs instead at the points of maximum instability displacement, the diameter would be a factor of 1.59 greater. The computed particle diameter results from liquid breakup by the fastest growing instability. In reality however a distribution of sizes would be produced, and in this sense the computed diameter probably represents essentially the mean value. The distribution of sizes could probably be represented by a log probability distribution function, with the smallest particle size being about $2/9D$ and the maximum size about $9/2D$. In any case it should be remembered that the value of D represents the size (or mean size) of the particles produced by the Taylor instability breakup of the liquid ejected from the aircraft. It does not represent the final droplet size produced by the dissemination process because many of the particles produced by Taylor breakup will undergo further breakup before reaching a stable size.

In the computations, note that breakup time is measured with respect to the time for half of the liquid to be ejected from the aircraft.

8.1.2.1 Comparison of Retardants

Table V shows the computed Taylor breakup characteristics of Phos-Chek XA for three different conditions. It is of interest to compare these values with those of other common retardants, and Figure 37 shows the Phos-Chek (P-XA) data in comparison with the computed data for Fire-Trol 100 (FT-100), Fire-Trol 931 (FT-931) and water when dropped from the CL-215 aircraft using one or both tanks. The liquid breakup time of Phos-Chek is significantly greater than that of the other retardants at the larger load, and H_2O is smallest at the smaller load. Small seemingly reversals in the order of the retardants in some cases may not be real since the Phos-Chek data was computed by fitting to the experimental breakup times, whereas the other retardant data was calculated using the A_i curve generated from the Phos-Chek data. Since A_i changes a large extent in going from Phos-Chek to water, a small uncertainty in the slope of the $\log A_i$ versus A/B curve (discussed previously) can result in uncertainties of several hundredths of a second for low viscosity liquids.

The most interesting difference between the retardants is in the particle size produced. The particle size is largest for Phos-Chek, then FT-100, FT-931, and then water. The particle size of Phos-Chek is about a factor of 20 greater than that of water. The differences in particle sizes of the retardants results largely from the differences in their viscosities. The viscosities of Phos-Chek, FT-100, FT-931, and H_2O during breakup are about 14, 2, 0.5 and 0.1 poises, respectively. The corresponding instability shear rate, S_1 , are about 15, 42, 110 and 1588 sec^{-1} , respectively.

The relative lateral extent (radius) of the deforming liquid at breakup, R_e/R_o , and the initial lateral velocity of the outer particles, V_e , are also greatest for Phos-Chek and least for water. This appears to imply that the path width of the disseminated liquid is greatest for Phos-Chek and least for water. However because of droplet settling time differences due to particle size, the actual ordering is opposite.

8.1.2.2 Effect of Aircraft Velocity

Figure 38 shows the computed effect of aircraft velocity on the breakup characteristics of Phos-Chek dropped from the CL-215 aircraft. Increase in velocity decreases breakup time and particle size of the liquid in a significant manner, and increases lateral liquid velocity. It also decreases the relative radius of the deformed liquid but the effect is small.

8.1.2.3 Effect of Tank Length

Figure 39 shows the computed effect of tank length on the breakup characteristics of a liquid with fixed viscosity values (essentially those of Phos-Chek). Increase in tank length increases both breakup time and relative radius of the deformed liquid at breakup in a very significant manner, but has no effect on particle size. For sufficiently long tanks the lateral liquid velocity decreases mildly with increase in tank length.

8.1.2.4 Effect of Tank Cross Sectional Area

Figure 40 shows the computed effect of effective tank radius on the breakup characteristics of the same liquid. Breakup time increases with increase in radius but in a much slower manner than with the length. The particle size and

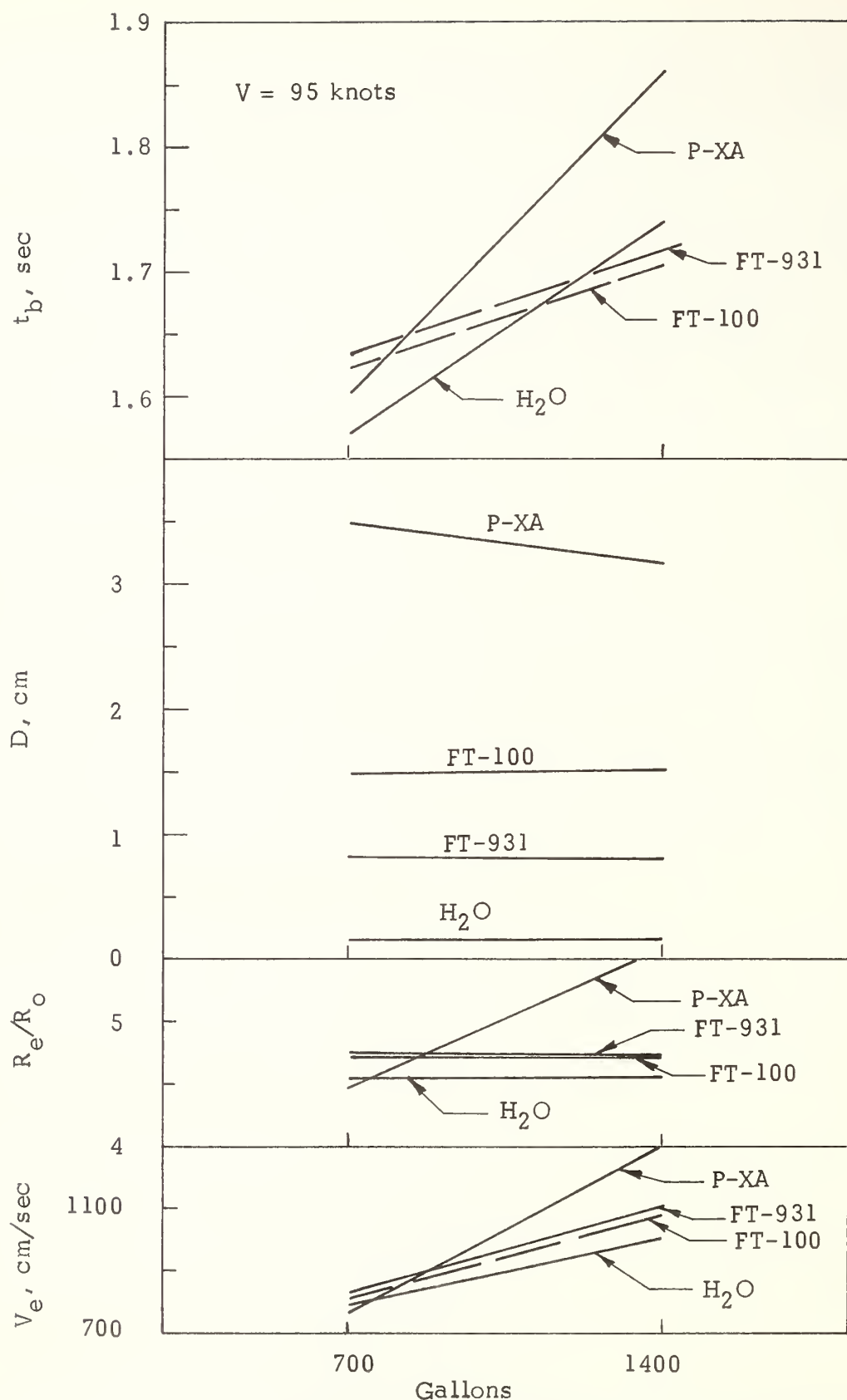


Figure 37. Computed Taylor Breakup Characteristics of Liquid Retardants in the CL-215 Aircraft.

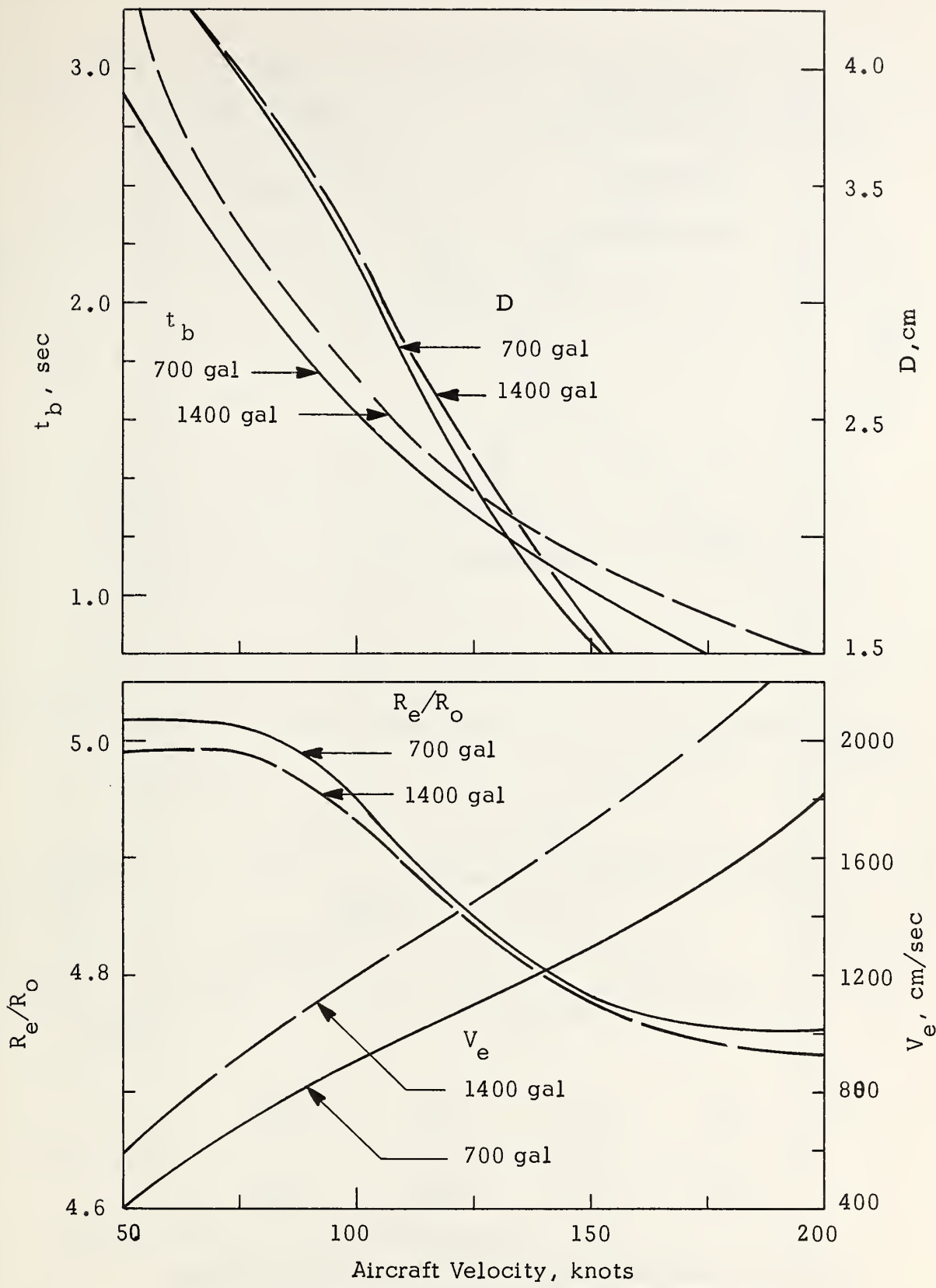


Figure 38. Computed Effect of Aircraft Velocity on the Taylor Breakup Characteristics of Phos-Chek XA from the CL-215 Aircraft.

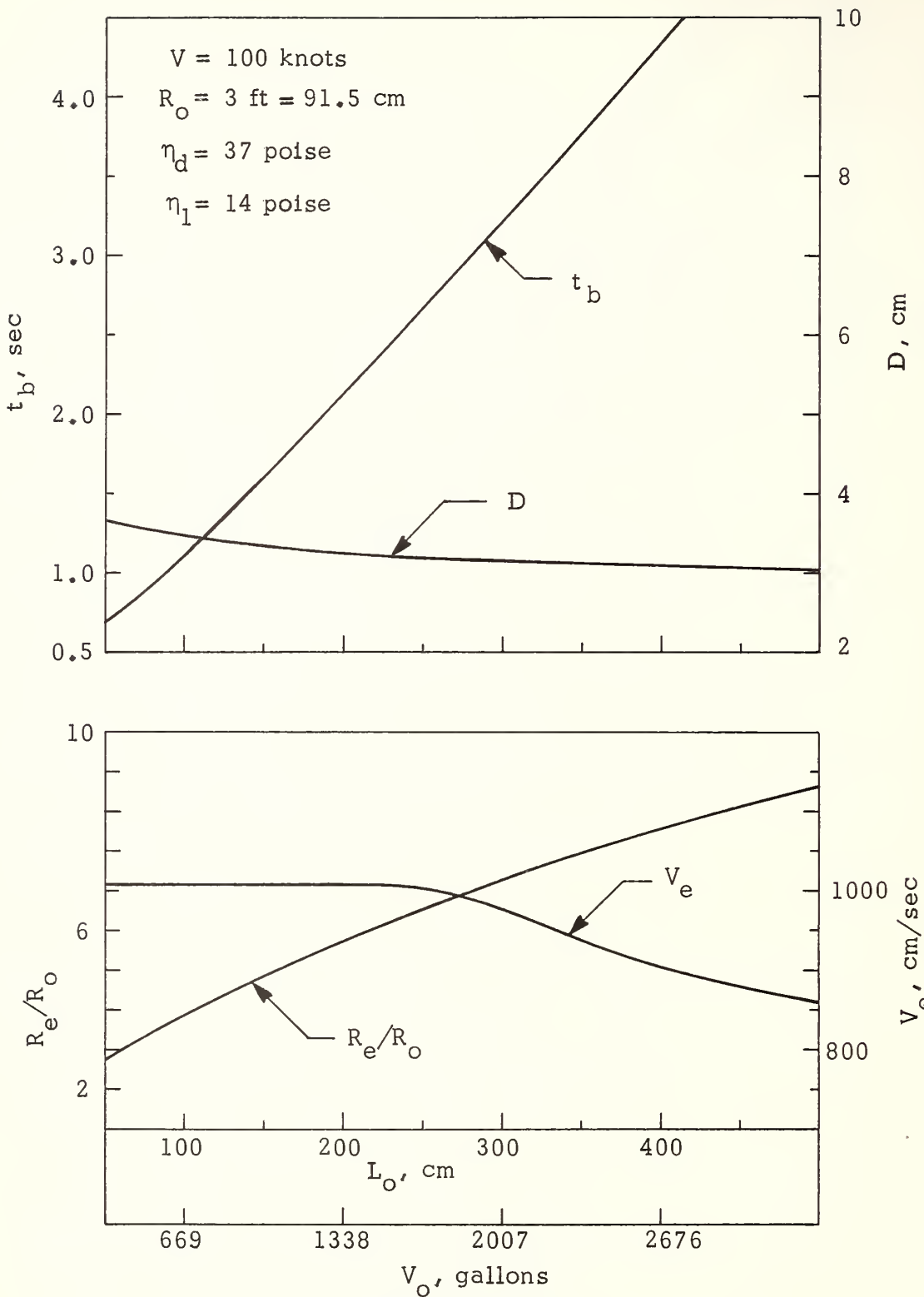


Figure 39. Computed Effect of Tank Length on the Liquid Breakup Characteristics.

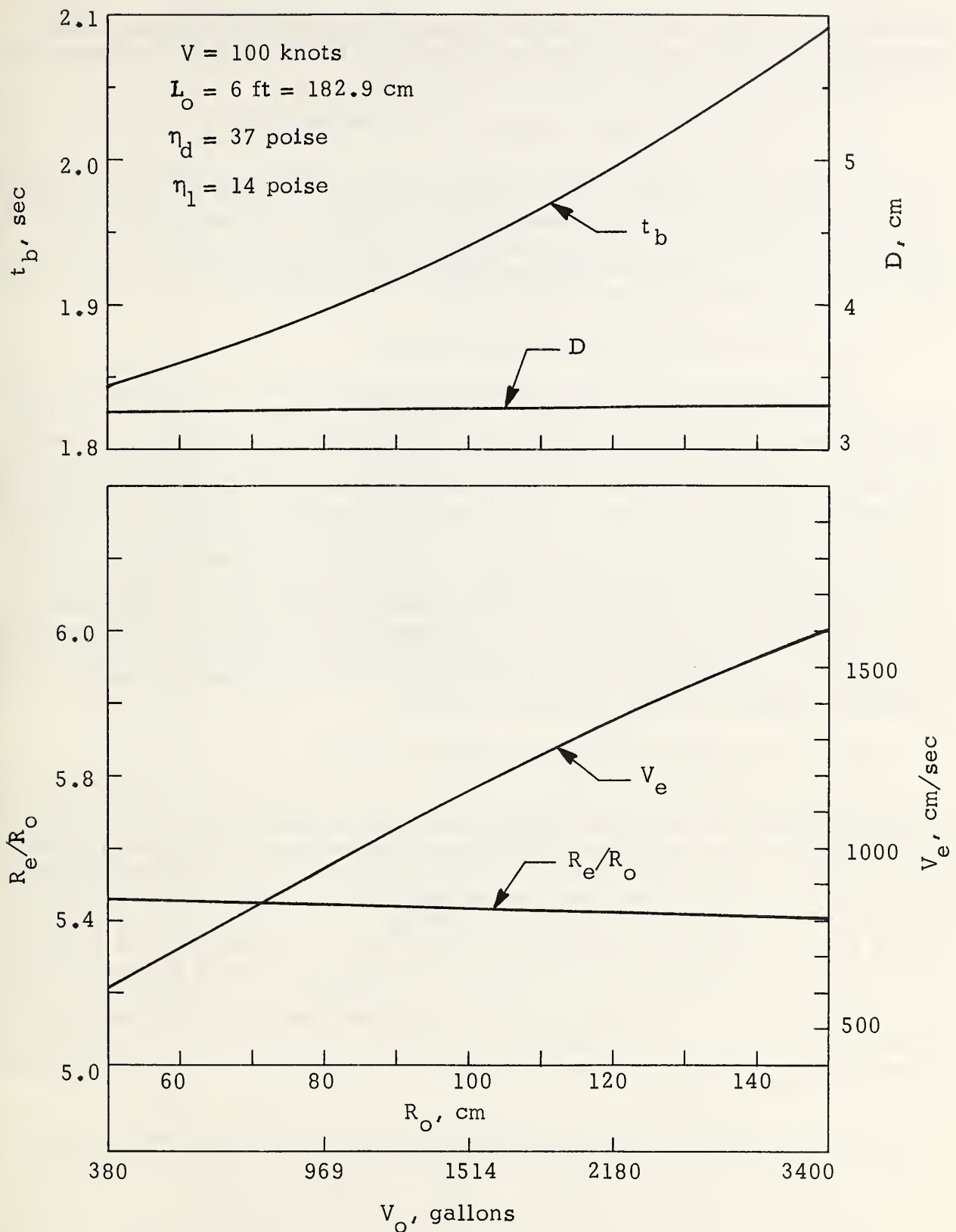


Figure 40. Computed Effect of Tank Radius on the Liquid Breakup Characteristics

relative liquid radius are independent of tank radius, but the absolute radius increases since tank radius increases. The lateral liquid velocity increases in a significant manner with increase in tank radius.

8.1.2.5 Effect of Tank Dimensions at Constant Volume

Figure 41 shows the computed effect of varying the ratio of tank length to radius, L_o/R_o , for a fixed volume of 2000 gallons for Phos-Chek. Breakup time increases significantly with increased L_o/R_o , as does relative liquid radius. The particle size exhibits a small maximum, but overall is essentially independent of L_o/R_o ratio. The most interesting effect is on lateral velocity, which decreases rapidly above some particular L_o/R_o ratio.

8.1.2.6 Effect of Deformation Viscosity

Figure 42 shows the computed effect of the viscosity of the deforming liquid on the breakup characteristics a liquid (Phos-Chek, CL-215 aircraft, one tank). This viscosity has no effect on the breakup characteristics unless it is greater than about 100 poises (for the specified conditions), above which value breakup time and particle size increase with increased viscosity, and relative liquid radius and lateral velocity decrease. The deformation viscosity of Phos-Chek, FT-100, FT-931 and water are about 37, 100, 5, and 0.01 poise, respectively. It therefore does not have any significant effect on the breakup characteristics of any of these retardants. On the other hand it could have significant effect on a suitably thickened or dilatant fluid. The average shear rate during deformation for any fluid under aircraft velocities of interest (75-150 knots) ranges from about 1 to 4 sec^{-1} . This value is lower than the Brookfield value (about 12 sec^{-1}), and hence the liquid viscosity should be measured in the low shear rate range to obtain information relevant to the deformation process.

8.1.2.7 Effect of Liquid Instability Viscosity

Figure 43 shows the computed effect of the viscosity, η_1 , of the liquid during instability growth on the breakup characteristics of a liquid (CL-215 aircraft, one tank). Breakup time increases with increase in viscosity but the effect is relatively small. On the other hand particle size increases very significantly with increase in viscosity. The effective viscosity of a non-Newtonian liquid (which may or may not be elastic) depends on the shear rate. During breakup the viscosity helps to determine the instability shear rate. For example, the instability viscosity, η_1 , of Phos-Chek, FT-100, FT-931 and water during Taylor breakup is about 14, 2, 0.5 and 0.01 poise, and the corresponding shear rates are 15, 42, 110, and 1500 sec^{-1} . Therefore the viscosity (and elasticity) of a retardant should be measured in the range of about ten to several hundred sec^{-1} to obtain the necessary information to evaluate the effective viscosity that controls the growth rate of the instabilities.

The relative radius of the deformed liquid and its lateral velocity also increase significantly with increase in viscosity.

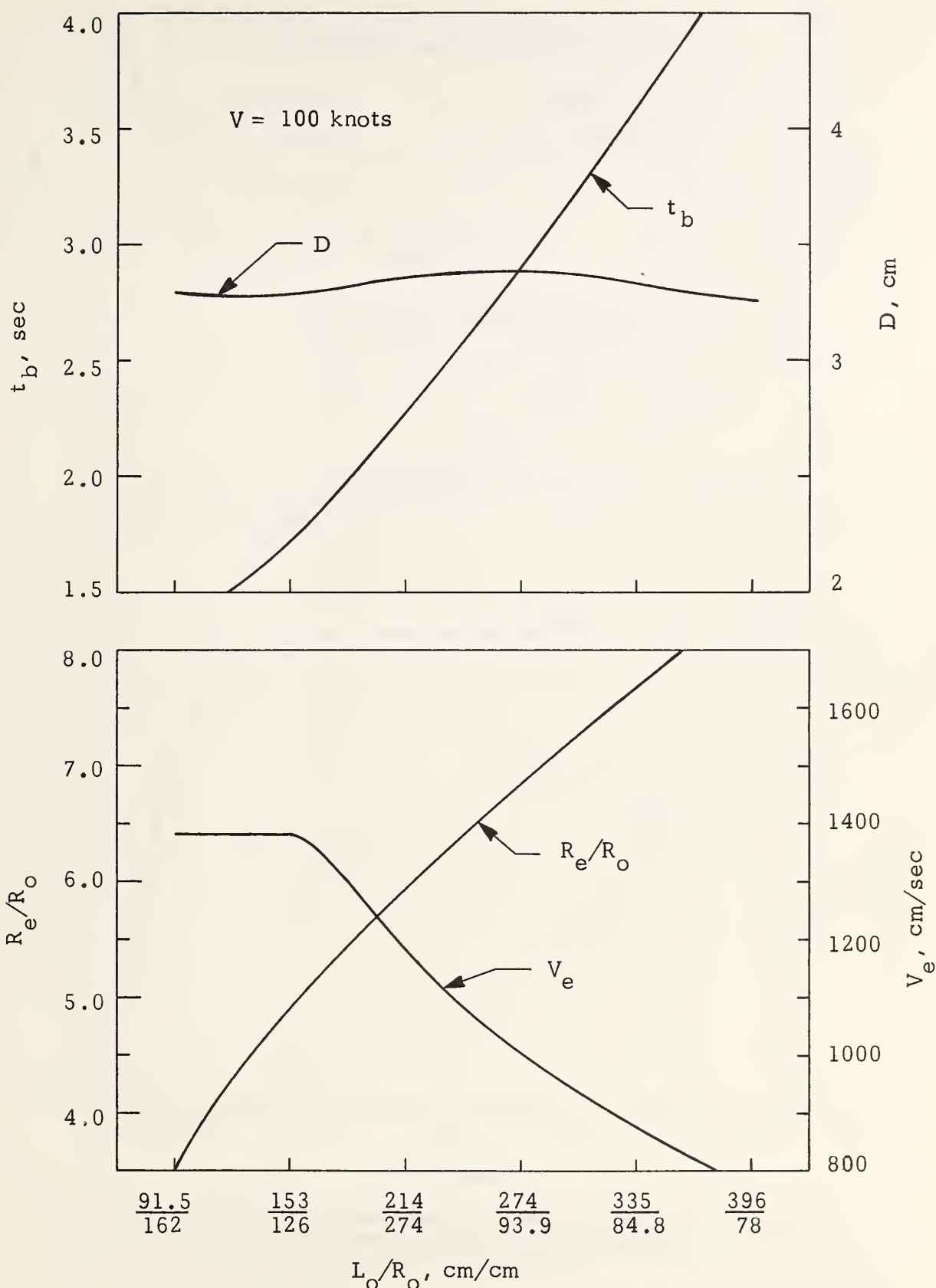


Figure 41. Computed Effect of Tank Dimensions on the Taylor Breakup Characteristics of 2000 gallons of Phos-Chek XA.

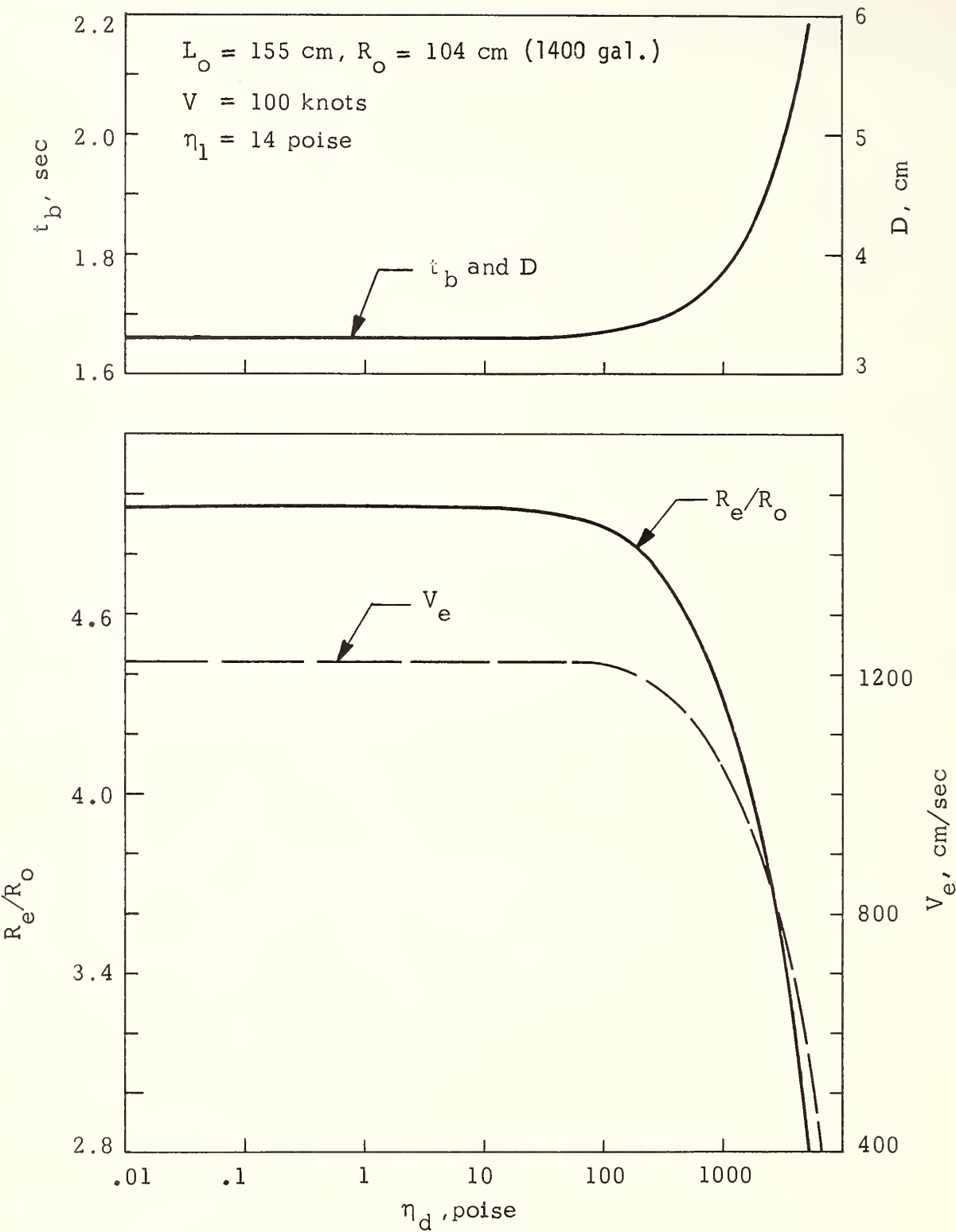


Figure 42. Computed Effect of Deformation Viscosity on the Liquid Breakup Characteristics.

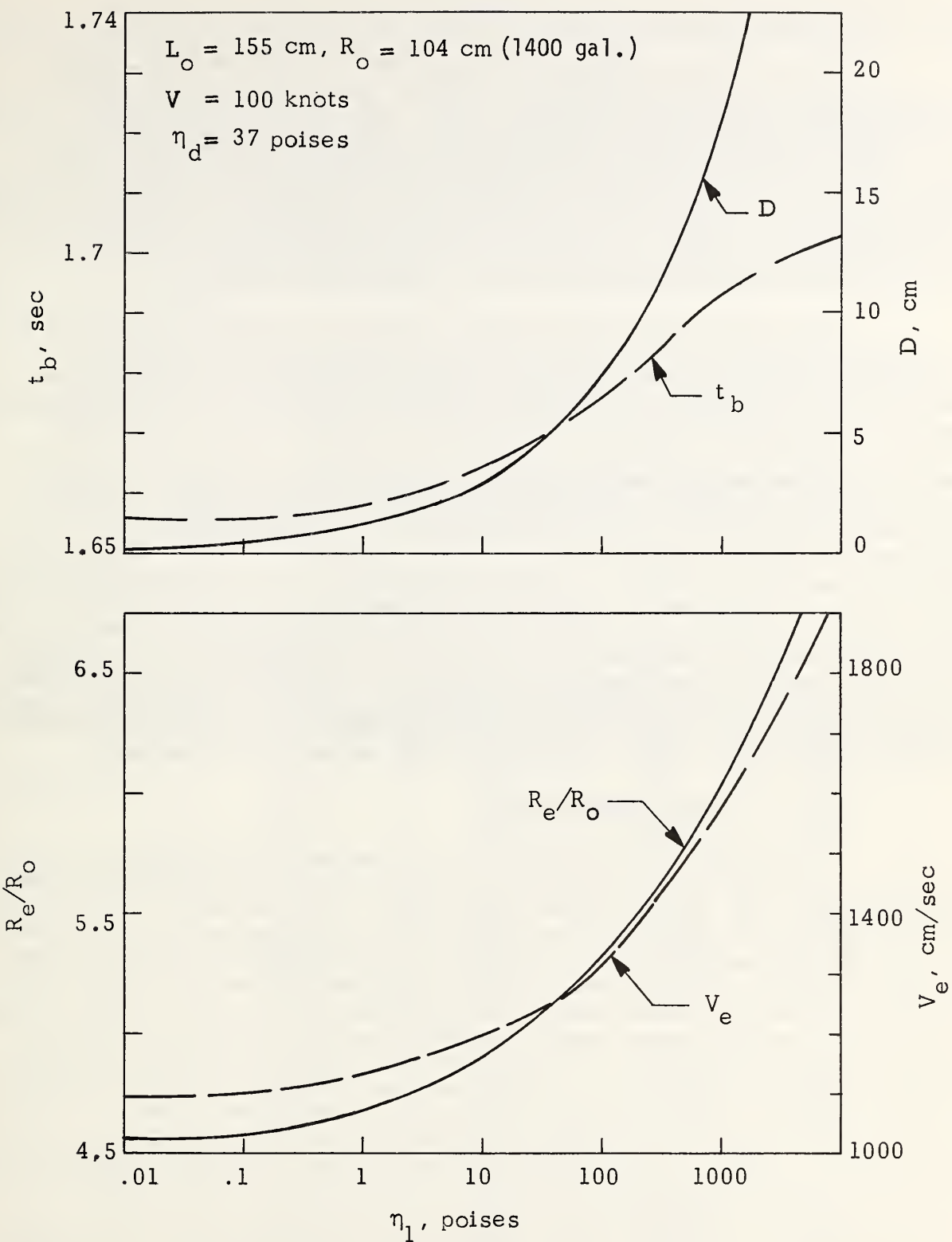


Figure 43. Computed Effect of Liquid Instability Viscosity on the Liquid Breakup Characteristics.

As bulk liquid retardant is released from an aircraft it undergoes surface stripping (erosion) before being broken up into many smaller particles by deformation and Taylor instability growth. These individual particles formed by the Taylor breakup process may then undergo further breakup by surface erosion (and possibly other mechanisms) during deceleration to their terminal velocity. The final droplet size of the broken-up retardant may thus be essentially determined by the surface erosion characteristics of the liquid under the local (time dependent) conditions of wind velocity and particle size - including the ability of the particles to undergo erosion under those conditions.

The surface erosion (stripping) of liquids is usually considered to occur by the growth and breaking of small waves (instabilities) induced in the surface of the liquid by the wind stress, and a model that has proven quite useful for low viscosity liquids was described in section 4.1. In principle the breakup of liquid particles should include a quantitative description of the surface stripping of a particle in conjunction with the velocity history of the particle as it is slowed down by air drag. Some effort along these lines to describe both the surface erosion (mass removal) rate and velocity history for the particles produced by the Taylor breakup was conducted during the current program. However several difficulties were experienced in these calculations, and it did not prove possible to conduct the analysis in the desired manner for this report. It is not useful to describe the details of these difficulties - which are at present unresolved. However it may be mentioned that it is possible that the surface erosion of a highly viscous liquid such as Phos-Chek at relatively low wind velocities should be considered in terms of classical liquid boundary layer stripping - such as discussed initially by Taylor^{6,11} rather than a model based on instability growth. The value of beta (Eq. 81) may also require some further modification. Further studies on these matters are in progress.

8.2.1 Average Droplet Size

In principle the size distribution of the particles produced by surface erosion of the liquid should be computed by using either Eq. (13) (for number distribution), or Eq. (20) (for mass distribution). The difficulties just mentioned prevented the performance of these computations. Consequently, for the present purpose the average drop size of the various retardants was estimated in the manner commonly used for low viscosity liquids and high wind velocity, i.e., by the mean drop size expression developed by Mayer, Eq. (11). The effective viscosity at the appropriate shear rate experienced by the liquid was used in the calculations however, i.e., shear rate was computed using Eq. (28) and the experimental effective viscosity versus shear rate expression was used to estimate the viscosity. A value of 0.3 was used for the parameter B, as is often the case for low viscous liquids. There is some reason to believe that B may possibly depend weakly on viscosity and velocity, but this potential dependence cannot be estimated at this time. In any event the use of Eq. (11) is an approximation since the effect of the particle size on the allowable wavelength excitation is not taken into consideration in the equation, and the effect of the shear rate vs viscosity relationship skewing the distribution curve is also not included. Thus the present calculations are approximate in nature, and should be regarded as a preliminary effort. In spite of the approximations involved however, it appears quite probable that the computations show essentially

the correct particle size behavior of the retardants - both as to absolute size and relative differences between the retardants, although it is believed that the computed values for Phos-Chek may be a little low.

One further point may be noted. The Mayer drop size expression, Eq. (11), is a number mean diameter. However the experimental value of 0.3 for B in this equation was obtained by comparing Eq. (11) with experimental drop size data based on liquid mass - not number of droplets. This in effect converts the Mayer equation into a mass mean diameter expression. The relation between mass mean diameter and droplet mean diameter - assuming a log normal probability distribution function - is given by Eq. (10). This equation shows that the mass mean diameter is usually roughly about twice the number mean diameter.

The results of the computations for the final average (mass mean) droplet diameter produced by the aerodynamic breakup of the various retardants as a function of aircraft velocity are shown in Figure 44 and Table IV.

TABLE VI. PRELIMINARY COMPUTED FINAL AVERAGE DROPLET SIZES PRODUCED BY THE SURFACE STRIPPING OF LIQUID RETARDANTS.

Liquid	Aircraft Velocity V (knots)	\dot{S} (sec ⁻¹)	η (poise)	d_m (mm)
Phos-Chek XA	50	263	5.20	5.77
	100	799	9.12	3.30
	150	1239	10.21	2.07
	200	1510	10.54	1.44
Fire-Trol 100	50	182	1.424	3.01
	100	692	0.437	0.538
	150	1139	0.289	0.238
	200	1420	0.242	0.144
Fire-Trol 931	50	272	0.130	0.589
	100	948	0.065	0.146
	150	1525	0.053	0.074
	200	1882	0.049	0.048
Water	50	405	0.0087	0.097
	100	1308	0.0087	0.038
	150	2058	0.0087	0.022
	200	2512	0.0087	0.015

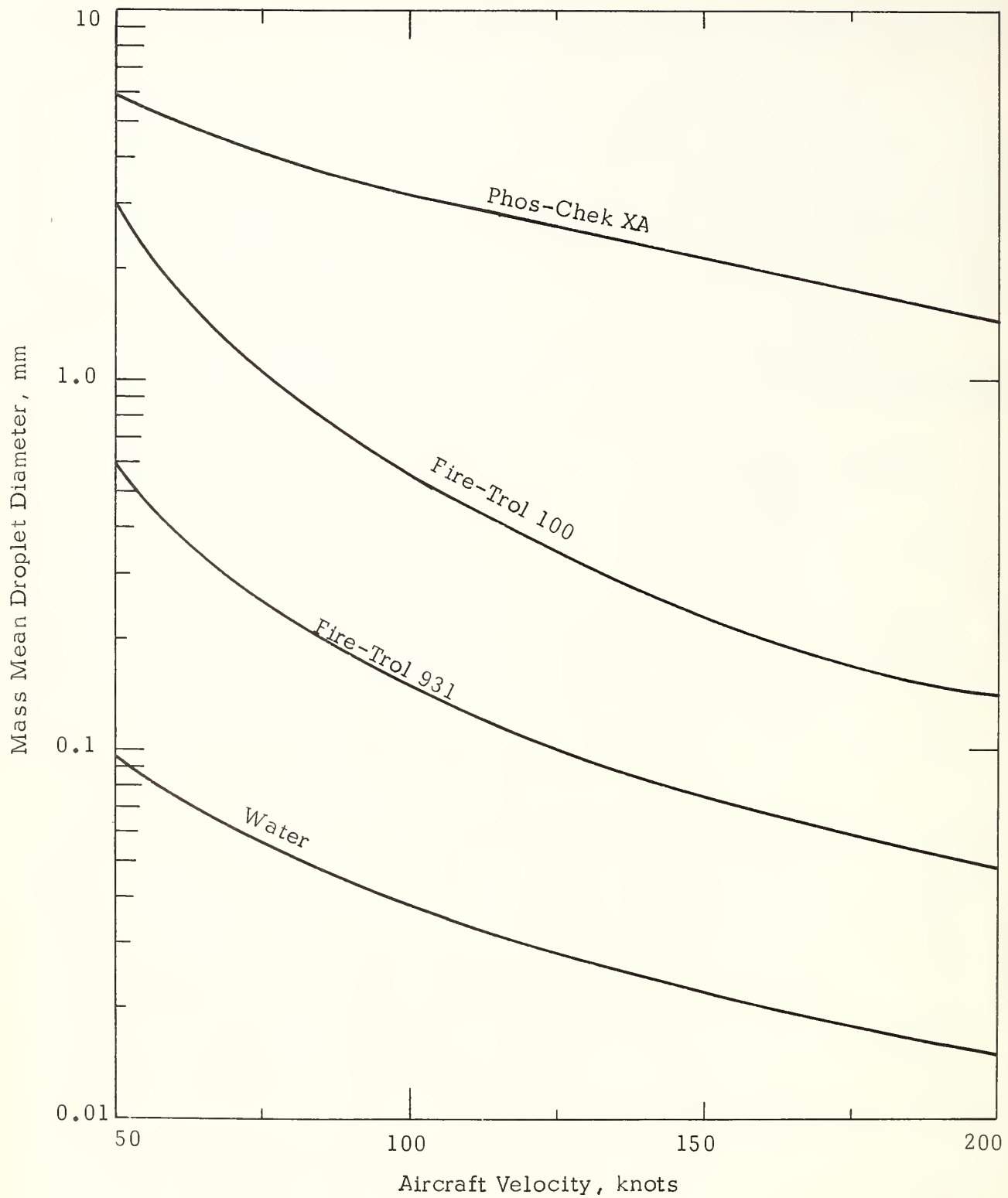


Figure 44. Preliminary Theoretical Estimate of the Final Average Diameter of the Droplets Produced by the Aerodynamic Breakup of Liquid Fire Retardants.

It will be seen that at any specified aircraft velocity the average particle size of the retardants increases in the order: water, Fire-Trol 931, Fire-Trol 100 and Phos-Chek XA. For example the mass mean diameter of the droplet produced by a 100 knot aircraft is: water-0.038 mm, Fire-Trol 931-0.15 mm, Fire-Trol 100-0.54 mm and Phos-Chek XA-3.3 mm. Thus the estimated mean particle size of Phos-Chek is roughly a factor of 100 greater than that of water.

It will also be observed that particle size decreases with increase in aircraft velocity, but there is less effect for Phos-Chek than for the other retardants. This is because the effective viscosity of Phos-Chek increases with increase in shear rate - due to its elasticity - whereas the two Fire-Trol solutions are (presumably) non-elastic, and shear thinning (Table VI). Table VI also gives the estimated shear rate of the liquid during surface erosion. The values range from several hundred to just under 2000 sec⁻¹. The values are larger than experienced by the liquid during its deformation and breakup by Taylor instability. The values are not exceeding large however, and are generally within the shear rate range of the Haake Rotoviscometer. This is of some interest since it indicates that future measurements on retardants for the present application can be obtained by the Rotoviscometer - which is a more rapid, easier and presumably more accurate technique than the high pressure capillary tube technique.

8.2.2 Particle Size Distribution

In order to make a rough estimate of all of the particle sizes, it was assumed that the sizes obey a log normal probability distribution (Eq. 9), as is usually the case for a low viscosity Newtonian fluid. Figure 45 shows the results of these computations for an aircraft velocity of 100 knots. It may be seen that a significant percentage (20%) of the Phos-Chek mass is present in particle sizes greater than 5 mm. This is consistent with the Honeywell statement⁴⁰ that "cloud terminal velocities estimated from films suggest Phos-Chek droplets on the order of 0.5 to 1 cm in the final region of the trajectory."

8.3 FURTHER DISCUSSION

The preceding models used to describe the breakup of aerial delivered fire retardants provide a basis for the elucidation of the important system parameters and fluid properties that control the dissemination of the retardant. The analyses that were conducted illustrated the effects of the system parameters on the breakup of the three chemical fire retardants of current interest and of water, and showed how the physical and rheological properties of these retardants affected the breakup rate of the liquid and the particle size of the dispersed retardant. It is evident that the breakup characteristics of the liquid has various implications regarding the dispersal of the liquid on the ground. A detailed and quantitative comparison of the results and implications of the theory with experimental data would require considerable effort however, and was not possible on the present program. For the purposes of this report a further brief discussion will be presented which attempts to summarize some of the ultimate effects of the system parameters and fluid properties on the dispersal of the retardant rain on the ground.

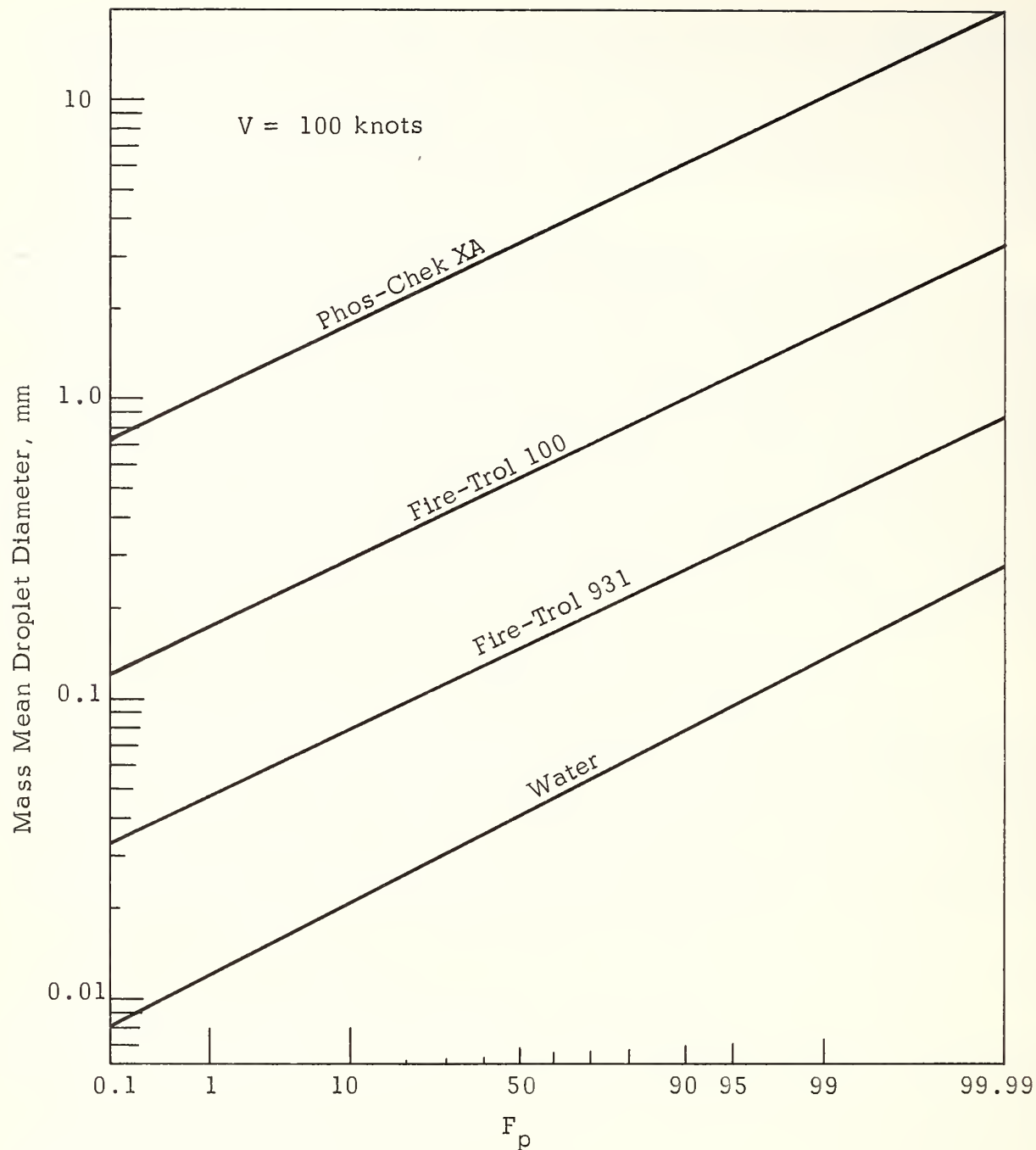


Figure 45. Preliminary Theoretical Estimate of the Final Size Distribution of the Droplets Produced by the Aerodynamic Breakup of Liquid Fire Retardants. F_p is the Cumulative Percentage of Liquid Mass.

8.3.1 Droplet Settling

After their formation by ultimate breakup of the bulk liquid—which has both horizontal and downward vertical motion during the breakup processes—the liquid droplets (particles) undergo settling. Depending on various conditions, many or all of the droplets reach their terminal velocity, v , by the time they reach the ground. Terminal velocity is attained when the drag force acting on the droplet is equal to the gravitational acceleration force, i.e., when

$$0.5C_d \rho v^2 A = (\pi d^3/6) \rho_1 g \quad (84)$$

where ρ is air density, ρ_1 is liquid density, A is the projected cross sectional area of the droplet, d is droplet diameter, C_d is the drag coefficient and g is the gravitational constant. The terminal velocity is thus given by

$$v = \left[\frac{4 \rho_1 d g}{3 \rho C_d} \right]^{1/2} \quad (85)$$

The value of the drag coefficient depends on the value of the Reynold's number, but for the present conditions is usually a little less than unity. It will be observed that droplet diameter is the most important parameter that affects the terminal velocity of the falling particles. It was previously shown that particle size is largely controlled by the effective viscosity of the liquid and the aircraft velocity. Large viscosity and small aircraft velocity produce large droplet size.

As an example consider ρ_1 and C_d to be constant and have values of 1.065 gm/cc and 0.7. The terminal velocities of the mean sized particles of the retardants given in Table VI for an aircraft velocity of 100 knots are then: Phos-Chek-748 cm/sec, Fire-Trol 100-302 cm/sec, Fire-Trol 931-157 cm/sec and water-80 cm/sec. The terminal velocity of Phos-Chek is thus about an order of magnitude larger than that of water. Larger terminal velocities imply shorter times in the air for the falling particles and hence less evaporation of the particles before they reach the ground. It would thus be expected that evaporation loss of the particles for constant conditions of aircraft velocity and altitude would be least for Phos-Chek, followed by Fire-Trol 100, Fire-Trol 931 and then water. It has been shown by George^{1,59} that this is indeed the ordering of the preceding retardants for air evaporation loss. It is also expected on the preceding basis that the time for the particles to reach the ground should be least for Phos-Chek and greatest for water, and the time for the droplet cloud to settle should also be in this order. Increase in aircraft velocity should increase cloud settling time. These conclusions are also consistent with experimental data.^{1,59} Increase in aircraft altitude increases evaporation loss since it increases the airborne time of the droplets.

8.3.2 Effect of Atmospheric Properties

The most important atmospheric effect on the droplet cloud is wind. It has been found that in general a cross wind moves the cloud as a whole, rather than separating particle sizes and significantly broadening the contour pattern.⁴⁰ Small droplets are acted on more strongly by the wind than larger droplets and also remain airborne for a longer period of time. Thus a droplet cloud produced from a liquid with a large effective viscosity (e.g., Phos-Chek) will be less affected by a wind than will a droplet cloud produced from a low viscosity liquid such as water. The droplets eroded from the liquid prior to its Taylor breakup are more subject to wind drift than are the droplets resulting from the Taylor breakup due to the fact that they are formed at a higher altitude and exposed to the wind flow for a longer period of time. The average particle size may also be smaller.

The change in air density with altitude will also in principle affect the liquid breakup characteristics, but the computed effect is very small. In general disseminating at higher altitudes (e.g., 1 or 2 miles) than sea level will decrease the Taylor breakup time and increase the final droplet size. It is doubtful if the effects are discernable experimentally however.

8.3.3 Ground Contour Pattern

The general ground pattern (specific area concentration) of the dispersed liquid retardant depends largely on the rate at which the retardant is released from the aircraft (including total load dropped), the aircraft altitude, and to a lesser extent on the aircraft velocity and the aerodynamic breakup characteristics of the liquid. As mentioned earlier, the concentration of liquid is not linear throughout the ground path length, but is generally low over approximately the first third of the path, increases to a maximum, and then decreases rather sharply. The low concentration over the initial part of the path length arises from the surface stripping of the liquid as it exits the aircraft. Later the deforming liquid breaks into many smaller pieces by Taylor instability growth which greatly increases the surface area available for stripping and also provides some droplets directly that do not breakup any further and whose trajectory is essentially straight downward. The Taylor breakup process provides the particles that lead to most of the meaningful (high concentration, $> 2 \text{ gal}/100 \text{ ft}^2$) ground concentration of dispersed retardant.

There are three general ground coverage parameters that are of interest in retardant dissemination studies, viz., area coverage, path length and path width. However the specific area concentration ($\text{gal}/100 \text{ ft}^2$) of dispersed retardant is not uniform in the disseminated area, and on a practical as well as a fundamental basis it is important to know the area concentration distribution within the disseminated area. For example it is known that a minimum of about $2 \text{ gal}/100 \text{ ft}^2$ of retardant is required to significantly impede the spread of fire in typical fuel stand, and concentrations of this magnitude and greater are consequently of most interest in aerial dissemination studies. The concentration of dispersed retardant produced by a typical aerial drop may vary in localized regions from less than 0.1 to about $10 \text{ gal}/100 \text{ ft}^2$. The distribution is generally not symmetrical, either longitudinally or laterally, and the disseminated area in some cases contain small localized regions where there is either no retardant at all, or else may contain relatively large globs or puddles. The normal pattern produced by the aerial dissemination process may in some cases be significantly

modified by the presence of wind.

The general ground pattern of a disseminated retardant produced by aerial dissemination and the effects of the various system parameters and fluid properties can be understood to a considerable extent in terms of the liquid breakup models discussed previously. A detailed examination would require an extensive effort however, and for the present report only a few generalizations will be considered.

8.3.3.1 Ground Coverage Area

The ground area having liquid concentrations of greater than 2 gal/100 ft² is usually of most importance, and liquid load size and drop height are the system parameters usually having the greatest effect on the area. Increases in load size and drop height generally increase the ground area. Increasing the drop height tends to increase the uniformity of the ground coverage, and this will cause the areas of localized regions with very large retardant concentrations to decrease and regions with smaller concentrations to increase. Increasing the drop height also enhances evaporation of the settling droplets, however, and this will eventually reduce ground concentration and the area having an effective concentration of retardant. The rate at which the load is released from the aircraft can also affect the area. The specific rate of release of the retardant usually varies throughout the discharge time period, and depends on such factors as tank geometry, door geometry, door opening rate, and venting. Depending then on the combined effect of various parameters, the ground area receiving a specified concentration of retardant can either increase or decrease as these parameters are varied independently. This may be seen in the plots given by George^{1,59} of area coverage vs drop height and wind speed for various retardants and various tank and gating systems.

The effective ($C \geq 2$ gal/100 ft²) area also is a function of retardant rheology. It has been found for example that for fixed conditions the effective coverage area of the four retardants under consideration decreases in the order: Phos-Chek XA, Fire-Trol 100, Fire-Trol 931 and water.⁵⁹ The area coverage is related to the rate of breakup of the retardant, to its lateral spread before ground deposition, and to the droplet size (including evaporation effects). Since there are various factors that contribute to area increase, there are also various potential ways in which area could be correlated. For example the figures in section 8.1.2 illustrate the effects of various system and fluid parameters on the factors relating to the lateral spread of the retardant ($R_e/R_o, V_e$), and for a specified retardant these factors could be used to help estimate the effect of drop height on path width. Certain shear rates and corresponding effective retardant viscosities were involved in these calculations. On the other hand the surface erosion rate and final droplet size are also involved in determining the area coverage, and a different shear rate and effective viscosity are involved in determining the values of these factors.

It is not clear as to the best manner in which area coverage should be correlated with retardant rheological properties, and in principle all the various factors involved should be considered rather than a single correlating factor. For illustrative purposes here, however, the ground area covered with 2 gal/100 ft² by the TBM aircraft has been plotted as a function of the effective viscosity for surface erosion of the retardant, and is shown in Figure 46. The data is a summary of some of the data given in ref. 59, and is rough in the sense that the

aircraft velocity was not exactly the same in all cases and the averages used for water at 100 ft altitude is not consistent with some of the data. It may be seen from this figure that the effective area coverage generally increases with increase in the effective viscosity of the retardant, and the relative ordering for the four retardants are as given by George.⁵⁹ In terms of total area coverage the lower viscosity retardants often produce larger total areas, but a larger fraction of this area has a very low (non-effective) concentration of dispersed retardant. This is consistent with the observation^{1,59} that gum thickened retardants produce more concentrated patterns. Figure 46 also shows that the area generally increases with increase in drop height. The very low value for water at the larger drop height probably results because of increased evaporation of water at higher altitudes.

8.3.3.2 Ground Path Length

Ground path length generally increases with increase in the effective viscosity of the retardant, and this effect for the four retardants is also illustrated in Figure 46. Thus Phos-Chek produces the longest effective path length of the four retardants. The path length from a specified tank and gating system is generally determined primarily by the flow rate from the tank, and superimposed on the flow rate effect is the rate of breakup of the retardant. In general, decrease in breakup rate increases path length. The flow rate from a specified tank has been found to be essentially independent of retardant type or composition, and hence is determined primarily by the tank and gating system design.^{41,59} The path length for the cases illustrated in Figure 46 decreases with increase in altitude, but in some cases drop height has no effect on length⁴¹, or may even increase it slightly. An increase in aircraft velocity should theoretically decrease the effective path length since it increases the liquid breakup rate. This effect has been found experimentally⁵⁹.

8.3.3.3 Ground Path Width and Shape

The width (lateral spread) of the ground pattern depends on drop height, tank and gating system design, aircraft velocity and retardant rheology. Figure 46 illustrates path width for the four retardants. The aerodynamic deformation of the retardant preceding its Taylor breakup causes a lateral spread of the liquid and gives an initial outward lateral velocity to the particles produced by the breakup (see section 8.1.2). The particles then continue their outward motion during their fall-consistent with their drag and surface erosion characteristics. Path width thus increases with increase in drop height up to some limiting value. Factors that decrease the Taylor breakup rate and the surface erosion rate-including increased effective viscosity for these processes (which depends on shear rate)-tend to increase path width. Likewise lower aircraft velocity and larger loads (or larger instantaneous volume release) tend to increase path width. The general shape of the path can under suitable conditions depend strongly on the wind.

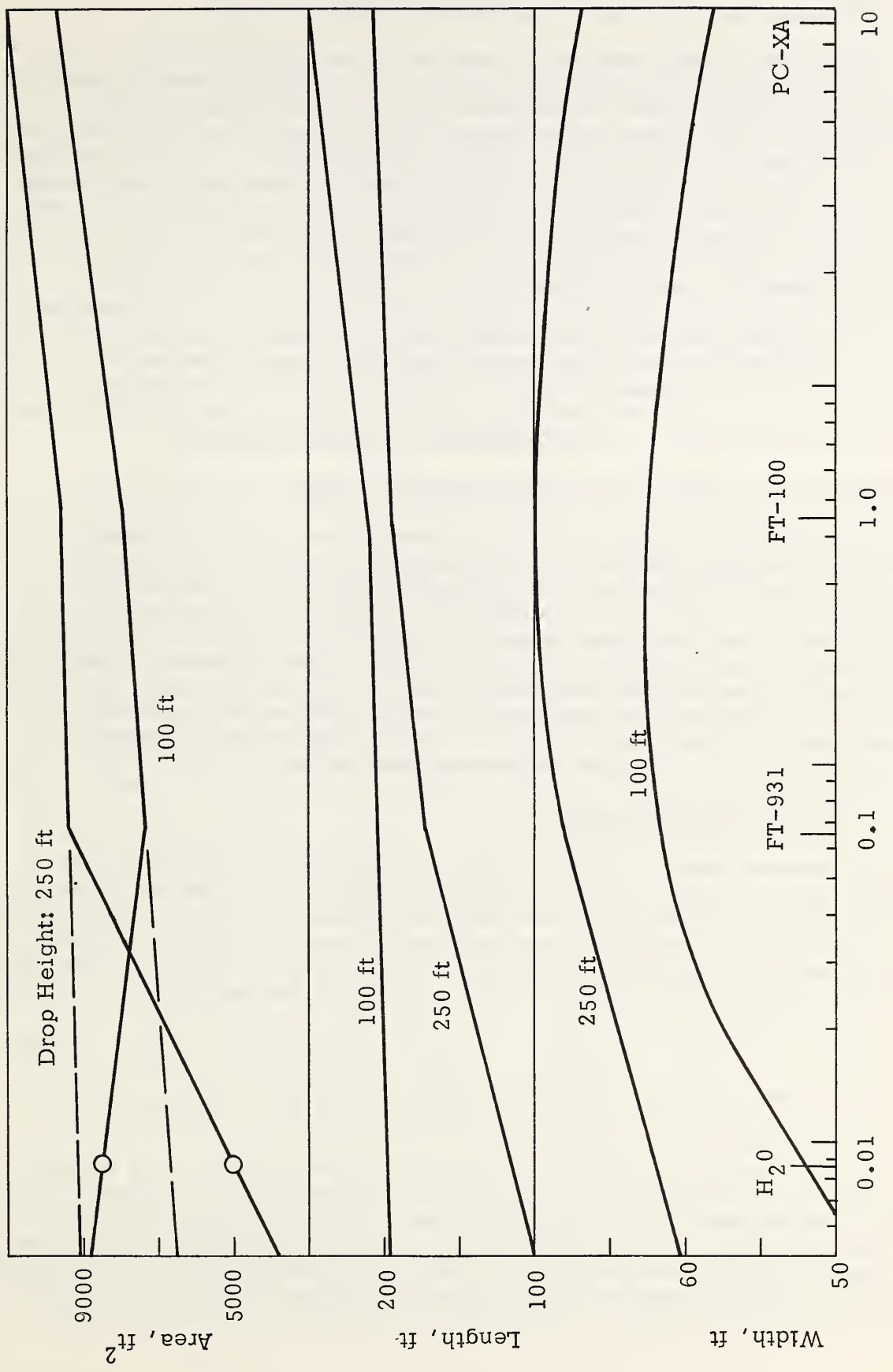


Figure 46. Correlation between Ground Pattern and Effective Viscosity of Retardants Dropped from the TBM Aircraft. $C = 2 \text{ gal}/100 \text{ ft}^2$. $V = 100 \text{ knots}$.

Subsequent to the aerodynamic breakup of the liquid fire retardant by various mechanisms after the retardant is ejected from the aircraft, a "rain" of the retardant particles is produced which falls upon the fuel elements (e.g., grass, brush or trees) present on the ground. The interaction of the falling liquid particles with the fuel causes a "wetting" of the fuel to various degrees--depending on the gross precipitation of disseminated retardant per unit ground area, and the properties of the liquid particles and the fuel elements. In order to make the most effective use of liquid retardant in various fire situations and for different fuel and retardant types, it is of importance to understand the penetration, retention, and distribution of the retardant as it interacts with representative fuels, and the effects of the various properties of the retardant such as size, impact velocity, and rheological properties, on the interaction process. Consequently during the present program a brief literature survey was conducted to determine what information exists on this general subject, and studies have been initiated to obtain further understanding of the wetting-out characteristics of typical fuels by various retardants.

9.1 WETTING OF FUELS BY WATER AND RETARDANTS

The ability of a dispersed liquid retardant to reduce or completely suppress an advancing fire front in a fuel complex depends on the ability of the dispersed droplets to wet or coat a large proportion of the fuel with a sufficient quantity of retardant salt. The salt deposited per unit area of fuel depends on the quantity of liquid retardant deposited on the fuel per unit ground area, the salt concentration of the retardant, the degree of spreading of the retardant over the fuel surface after droplet interaction with the fuel, and the degree of retardant retention by the fuel. The salt concentration of the droplets depends on the initial salt concentration of the retardant and the degree of water evaporation prior to droplet interaction with the fuel.

9.1.1 Fuel Characteristics

There are a variety of different types of fuel complexes that may be treated by a fire retardant, each of which may differ in its ability of undergoing wetting out or coating by the retardant because of geometric or configurational effects. General representative types include⁴⁰ a grass stand (several inches to a foot or more in height), chaparral field such as brush, thicket, or evergreen or short bushy trees (several feet in height), tall crowned trees (more than about 100 ft) such as Douglas fir, and litter or brush beneath crowned trees. The different fuel types also have different surfaces, and these surfaces may differ in their ability to wet out. The presence of moisture, cracks or other surface imperfections, bark roughness and whether the fuel is green or dry (or deciduous, or conifer and the time of year) are also factors in the wetting out process.

The geometry of the fuel helps to determine the portion of the settling droplets (which are of various sizes) that interact directly with the fuel, the amount of fuel surface that is subsequently wet by liquid running (drip) after droplet impaction on the fuel, and the amount of liquid retained as film storage on the surface. The surface composition and structure also helps to determine film storage on the surface, as well as liquid adsorption and running on the surface.

9.1.1.1 Retardant Requirements

The quantity of dispersed precipitated retardant that is required to effectively impede or prevent propagation of fire through a fuel complex depends on the ground concentration and various properties of the fuel, as well as on other factors such as retardant type, pattern width, and wind conditions. For orientation purposes, the following quantities of a typical conventional retardant expressed in gallons per 100 ft² of ground area (gpc) have been deduced to be representative of the effective levels of retardant coverage required for various diverse fuel types:⁴⁰ tall grass (0.5 to 1 gpc), chaparral (4 to 5 gpc), crowned trees (2 to 5 gpc) and forest litter (3 to 4 gpc). It has been shown that except for grass fuels, 2 gpc is the minimum concentration which will produce a significant reduction in the rate of flame spread in a light fuel complex.⁵⁹ Consequently the 2 gpc contour is of special interest in aerially delivered fire retardant studies, and except for grass stands, concentrations of two or more gpc of retardant are generally required for significant effectiveness.

9.1.2 General Mechanism of Fuel Wetting

The general mechanism of the wetting of a fuel such as brush or a tree crown by falling rain is well known.⁶⁰ Briefly, when the rain begins small drops with low impact velocity interacting with exposed regions of the fuel are largely retained intact by the fuel; whereas larger drops with higher impact velocity spatter during impact and flow to give liquid film and in some cases also smaller droplets. A portion of the falling rain drops pass directly through the fuel canopy without interaction with the fuel. As the rain continues, the small drops building up on exposed portions of the fuel (e.g., leaves or boughs) gradually coalesce with themselves and with liquid film formed by the larger drops. This enhances the spread of the liquid over both exposed and non-exposed areas of the fuel surface. Likewise the continuous spatter and running of the larger drops provides additional liquid for fluid flow and film formation over the fuel surface. When the liquid storage capacity of the partially exposed fuel elements becomes exceeded, the excess liquid forms miniature pools and rivulets which channel the liquid flow to the tips and edges of the fuel elements where -depending on conditions-the liquid will form drops which are removed by gravitational force. As these drops (or fluid flow) undergo free fall (drip) they interact with additional portions of the fuel below causing additional wetting, fluid flow and film formation, although a portion of the drops will fall unaltered through free spaces in the fuel to the ground. A small portion of the liquid may also be channeled from various fuel elements such as the boughs to the stem, where it is leaked to the ground by stem flow.

9.1.2.1 Liquid Storage on Fuel

Depending then on the intensity and duration of the rain, either all or a portion of the fuel will become wetted out by the rain. The liquid that can be stored on a thoroughly wetted fuel element during a rain is greater than that remaining on the fuel after the rain ceases since excess liquid not bound to the fuel is removed relatively rapidly from the fuel by drip (and evaporation) after discontinuance of the rain. Further removal of partially bound liquid from the fuel can be attained by shaking the fuel, or by wind. This will remove all liquid except that bound securely to the fuel in the form of film or absorbed liquid, which can only be removed by evaporation. Grah and Wilson⁶¹ used

the term "transitory storage" to describe the quantity of liquid that is initially lost by drip and evaporation from saturated fuel following discontinuance of a rain, and "conditional storage" to describe the additional liquid that can be removed from the fuel by wind or shaking. The remaining securely bound liquid that can only be removed by evaporation was called "residual storage". They developed an experimental technique for measuring these quantities in a relative manner. This technique consisted in following the weight of a fuel element that was subjected to wetting by a spray to saturation (constant weight), then discontinuing the rain and following the weight during the drip period to constant weight, and then shaking the fuel and weighing. For the study cases of small Monterey pine and Baccharis (an evergreen shrub) they found that the percentage of liquid held by the fuel in storage was roughly the same in each of the three storage conditions, i.e., about one-third of the total stored water under saturation conditions is subsequently lost by drip, an additional one-third is lost by shaking, and one-third remains firmly bound and can only be removed by evaporation.

9.1.2.2 Grah-Wilson Film Thickness

The results of the preceding experiments were further quantized by making an estimate of the total surface area of the fuels used in the studies, and converting the quantity of liquid held in conditional and residual storage into equivalent film thicknesses assumed to be uniformly applied over the surface area of the fuel. The value of these so-called Grah-Wilson film thicknesses represent a measure of the liquid that can be held by the fuel under various conditions. The values depend both on fuel type and liquid, and reflect different surface affinities and film properties.

9.1.2.3 Interception of Rain by Fuel

A partitioning of the rain fall on a fuel complex shows that the gross (total) precipitation of liquid, P , can be expressed by⁶⁰

$$P = T + D + F + S + E \quad (86)$$

where T is the precipitation passing directly through the fuel canopy, D is the drip from the fuel onto the ground beneath the fuel element, e.g., a tree, F is the flow of the liquid to the ground by stemflow, S is the quantity of liquid stored on the fuel, and E is the liquid loss from the fuel by evaporation. In forestry studies the gross precipitation is normally expressed in inches of rain. In fire retardant studies where the liquid load is fixed, the precipitation is more conveniently expressed as a surface concentration, usually gallons per 100 square feet of area (gpc). One gpc is equivalent to about 0.01604 inches of liquid.

The liquid from a rain of retardant that is available for coating a standing fuel is given by the interception loss ($S + E$) terms, but the E term is usually negligible or small. A measure of the S term is given by the conditional or residual storage film thickness - depending on conditions - provided that the fuel was initially essentially saturated by the dispersed retardant. The value of S is typically of the order of several hundredths of an inch

of liquid, which is equivalent to several gpc.

The liquid that is available for coating litter fuels located beneath standing fuel canopies is given by the throughfall ($T + D$) terms and the stemflow F . It has been shown that the role of stemflow in rain storms is usually of minor importance (1-15%).^{62,63} The precipitation passing directly through the fuel canopy, T , depends both on the concentration of fuel elements (e.g., leaves and boughs) in a specified fuel (e.g., trees) and the size of the falling liquid drops. A low fuel element (leaf or bough) concentration in a given fuel and a small drop size cause larger values of T . Studies have shown that under suitable conditions a significant fraction of a specified precipitation may pass through the fuel canopy without interaction with the fuel. For example Helvey and Patric⁶⁴ found for typical rainfall in hardwood forests that the value of T is given by

$$T = 0.901P - 0.031 \quad (87)$$

Other studies for other trees and vegetation have, however yielded much smaller values depending on conditions.⁶⁵ The intensity of the rain storm can have significant effect on the value of T , since more intense rainstorms have larger drop diameters. It has been found that throughfall ($T + D$) for a tree increases as the distance from the trunk increases, i.e., there is less throughfall near tree trunks than near the crown periphery.

9.1.3 Effect of Drop Size and Impact Velocity

The size and impaction velocity of the settling retardant droplets both affect the wetting of the fuel by the retardant. The angle of droplet impact with the fuel also may influence the overall wetting process, and this angle may be influenced by wind or wind gusts, as well in some cases by droplet trajectory. Thus the wetting out is to some extent a function of the method of application.

The effects of size and impaction velocity of the settling droplets on the wetting of fuel are to some extent interrelated. Very small droplets have low impaction velocities, and the isolated droplets are also relatively stable due to surface tension. Breakup of the droplet at impact cannot generally occur unless the dynamic pressure produced in the droplet during impact exceeds the stabilizing surface tension pressure in the drop, i.e., breakup cannot occur unless

$$\frac{1}{2} \rho_1 v_i^2 > 4 \gamma/D \quad (88)$$

where ρ_1 is liquid density, v_i is the impact velocity of the droplet, and γ and D are the surface tension and diameter of the droplet. Larger droplets have higher impaction velocities and lower stabilizing (surface tension) stress. Consequently the larger drops of retardant can undergo breakup and running during impact with the fuels.

The terminal velocity, v , of a falling spherical drop with diameter, D , is given by

$$v = \left[\frac{4 \rho_a D g}{3 \rho_a C_d} \right]^{1/2} \quad (89)$$

where g is the gravitational constant, ρ_a is air density and C_d is the drag coefficient. The drag coefficient varies with the Reynolds number. However liquid drops undergo some deformation and flattening during free fall - depending on their size, surface tension and viscosity - and this will affect (increase) the drag. Thus depending on conditions the drag coefficient of a falling drop may differ to some extent from that of a solid sphere. The value of the terminal velocities of various sized water drops has been determined experimentally, and representation values (summarized in ref. 40) are given below.

<u>D(mm)</u>	<u>v(cm/sec)</u>	<u>D</u>	<u>v</u>
0.1	27	2.0	651
0.2	72	3.0	801
0.5	204	4.0	880
0.75	305	5.0	914
1.0	403	6.0	923

It can be estimated using the preceding equations that falling water drops smaller than about 2.3 mm should be stable (not undergo breakup and spreading) during impact. The critical size will decrease with increase in temperature, since surface tension decreases with temperature increase.

In addition to impact pressure in falling drops or gravitational force on isolated drops resting on a surface, chemical forces may in some cases enhance the running or spreading ability of liquid drops. In this case the chemical composition of both the liquid and the fuel surface would affect the spreading characteristics. Liquid absorption by a fuel surface also affects spreading, as do factors that contribute to droplet coalescence. The size of the droplets can also affect the wetting characteristics of fuels in other ways. A cloud of very small particles (fog) can coat the fuel (including the underside of foliage), and if the individual small particles can eventually touch and undergo coalescence they will gradually run and spread on the fuel surface. It has been shown⁶⁶ that the rate of fall of very small (aerosol) particles due to gravity is usually small compared to that by normal turbulent diffusion processes of the atmosphere. However these very small particles are generally of little importance in fire retardant application. Studies have shown⁴⁰ that most fuels are most effectively coated by a combination of droplet impaction and subsequent run. However in the case of fine fuels such as tall grass the droplets may deflect the fuel and pass through intact.

9.1.3.1 Droplet Size Effect on Canopy Penetration

From statistical considerations it is evident that small droplets have a greater chance of directly penetrating foliage than do larger droplets. This penetration for the case of very small particles is enhanced by downdrafts.²⁰

In the general case however, a significant fraction of the liquid that eventually gets through the canopy arises from drip that is produced by droplet impaction with the canopy foliage. The sizes of the drip particles varies - depending on conditions - and the drip is usually distributed unevenly beneath the canopy.

The angle at which the falling droplets interact with the fuel can affect the extent of wetting of the fuel. Angular droplet impaction followed by vertical dripping does not achieve saturation on the leeward segments of the foliage, and thus a vertical rain (implying high altitude delivery) is best for retardant application.⁴⁰

9.1.4 Effects of Physical and Rheological Properties

The physical and rheological properties of the retardant droplet can affect its interaction with the fuel in various ways. Higher density retardants will have higher impaction velocities than lower density retardants for the same droplet size, but this effect appears to be of only small importance unless the droplet has undergone significant evaporation.

Of considerably more importance are the fluid viscosity and surface tension of the liquid. In general increases in surface tension and viscosity increase droplet stability, and decrease its ability to spatter on impact and run. This can result in lower coverage (wetting out) of the fuel, but in larger film thickness (retardant storage capacity) where coverage occurs. Viscosity also has a direct enhancing effect on fire extinguishment by water.⁶⁷ Decrease in viscosity and surface tension enhances the ability of the liquid to spread (run) on the fuel and penetrate to a limited degree into its surface (e.g., at cracks). Since increase in temperature decreases both surface tension and viscosity, droplets which are stable at normal temperatures may run at higher temperatures (if they don't evaporate first). The extent of water evaporation can sometimes have significant effect, since fluid viscosity (and possibly surface tension) may be a strong function of salt concentration in some cases.

The viscosity of a retardant is normally controlled by the use of a thickening agent. These materials are usually heterogeneous (e.g., clay thickened) or polymeric (e.g., gum thickened) in nature. Polymer based retardants apparently add strength and thickness to films applied to vertical fuel surfaces.⁴⁰ This may be of special importance since the effects of retardants are dominated by the fine fuels rather than the branchwoods.⁶⁸

Some retardants (e.g., Phos-Chek XA) are elasto-viscous in nature, and the elasticity of the fluid may possibly affect the nature of the impaction process, droplet breakup and liquid spreading (flow). For small impaction velocities (small droplets) the effective viscosity of thickened retardant would be that at low shear rate. For higher impaction velocity the effective (shear thinned) viscosity of thickened and elastic fluids may be less than the low rate value, and the fluid elasticity may add a stabilizing force so that the liquid undergoes some bounce during impaction. The thickened fluids may also exhibit increased cohesion with the fuel in some cases.

9.1.4.1 Viscosity Effect on Canopy Penetration

The ability of a retardant to run and drip affects both the wetting out of a fuel, and the penetration of canopy foliage by the retardant. Canopy

penetration is desirable in fighting fires in forest litter, but undesirable in crown fuel fires. Generally speaking, thinner retardants are best for litter fires since there is more canopy drip and more (probably) small particles that can penetrate the canopy directly without fuel interaction. Thicker retardants are better than thin ones in the treatment of crown fuels.

9.1.5 Vertical Fuel Coverage

Much of the present understanding of the wetting of fuels by a liquid rain has been obtained from many studies conducted over the years using normal rain storms. These studies have shown that fuel wetting involves droplet impaction with exposed fuel surface, which causes liquid spreading and run over the fuel surface, followed by drip and running over non-exposed fuel surface. Liquid is stored in the fuel after rain discontinuance largely in the form of film and drops, and the storage capacity depends on whether the fuel is shaken.

During the past few years studies have been conducted to attempt to understand the wetting of fuels by aerial delivered fire retardant rain. These studies showed that although the wetting of a fuel by a liquid retardant rain is apparently similar to that by an ordinary rain storm, there are various factors that require consideration when attempting to define the concentration of retardant that should be applied to a given fuel type under specified fire conditions. It is desirable from cost considerations that this concentration be known as accurately as possible and the factors that control it be understood.

The wetting of a fuel by a retardant rain may differ to some extent from ordinary water rain in that the duration of the retardant rain fall is relatively short (from several seconds up to several tens of seconds), the particle size distribution may be different and include many relatively large particles, and the viscous and other properties of the liquid may be appreciably different from ordinary water and may be shear rate dependent. This difference in rheological properties can cause the droplet impact and subsequent liquid run (spread) and drip processes to differ in behavior from that of ordinary water, and result in greater film thicknesses.

The studies that have been conducted, then, have been directed toward understanding the wetting of fuels by retardants in terms of the differences with rain wetting brought about by the retardant properties. Swanson and Helvig⁶⁸ developed a vertical fuel coverage model as a method of providing estimates of the vertical fuel effect on required retardant quantities. The model regards the vertical fuel structure as a series of geometrical segments which are described in terms of measured fuel parameters, geometry, surface area and volume. Retardant entering vertically either passes through the segment without interaction, or is captured and retained and eventually (when the segment is saturated) allowed to drip to the next segment. The model can be calibrated from experimental data, and provides estimates of the effect of the various retardant characteristics and properties on the wetting out of a vertical fuel. Swanson and Helvig also developed a model for the spread of liquid retardant on a vertical surface and concluded that the resultant film thickness produced by various retardants should differ by the square root of the ratio of their viscosities.

Anderson of the Forest Service has conducted studies of the actual

transmission of aerially delivered fire retardant through vertical fuels such as a tree crown.⁶⁹ He found that the proportion of retardant retained on the fuel increased as the fuel diameter and surface roughness of individual fuel elements increased. Equations were developed that described the retention, and it was shown that in the case of a tree crown the results were in agreement with previous studies on the transmission of rain through the crown.

9.2 EXPERIMENTAL STUDIES

Previous studies have shown that the wetting of a vertical fuel by a rain of liquid fire retardant involves liquid drop impaction (spatter) on the fuel, followed by liquid spreading, running and drip onto fuel sections beneath the spatter sections. The retained liquid after rain discontinuance is stored on the fuel in the form of film and drops. In order to further understand the various processes involved in the wetting out process - including effects of retardant and fuel properties - studies have been initiated during the present program on certain aspects of the problem.

9.2.1 Static Drop Spread

Experiments were conducted to obtain information regarding the effects of retardant and fuel properties on the spreading of retardant drops on fuels under gravitational force.

9.2.1.1 Experimental Technique

The experiments consisted in dropping a drop of the liquid retardant with an eyedropper from a height of about 1/2 inch (to allow drop formation) onto a fuel surface, and measuring the area of the equilibrium liquid after its spread over the fuel surface. The experiments were conducted at ambient temperature ($68^{\circ}\text{ F} \pm 5^{\circ}$). The fuel materials used in various studies were glass, paraffin, clear pine, clear redwood, fir (plywood), rough cedar (sanded) and manufactured pressboard. Both flat and inclined fuel surfaces were studied. Glass slides were used, the paraffin was melted and poured into petri dishes, and the wood samples were cut into conveniently handled sizes.

The initial diameter, D_o , of the drops used in the studies was determined as follows. For each liquid a known number of drops from the eyedropper were placed in a graduated cylinder and the volume was measured. It was attempted to keep the generation of each drop as consistent as possible. From this data the volume per drop was determined and the equivalent diameter of a spherical drop with that volume calculated. In the spreading experiments a sufficient number of drops (usually 6 to 10 or more) were studied in each case to obtain statistically reliable results.

The data obtained from the experiments was the final area of retardant coverage. The area produced by each drop was approximated by assuming the area to be an ellipse* and measuring with dividers and 1/100" ruler the major

*The major axis of the ellipse was usually in the direction of the grain of the wood.

and minor axes, compensating for assymmetries and such by eye. The product of these dimensions was statistically treated using an HP-45 calculator to give means and standard deviations. Finally, each mean spread area, A , was divided by the volume of the drop, V , producing it to give a "spread factor" type of number with dimensions $A/V = \text{cm}^{-1}$.

9.2.1.2 Experimental Results - Flat Surface

The experiments were conducted using Phos-Chek XA, Fire-Trol 100 and Fire-Trol 931, and in some cases also distilled water. The various fuel surfaces used in the studies were chosen for several reasons. Paraffin was selected because of its chemical inertness, as well as to partially simulate the waxy-like surface of many leaves. Glass is also inert but allows weak interfacial interaction by hydrogen bonding. In addition, both glass and paraffin are non-absorbant. The various wood surfaces were chosen to be representative of various real fuels, and for convenience. They also provide surfaces that have varying degrees of surface roughness, absorbtivity, and possibly interfacial tension. They are not necessarily the best materials for the present type of studies. However the results of the studies on these materials can serve as a basis for possible additional future studies.

Figures 47 and 48 show the results for the flat fuel surfaces, and the initial drop sizes used. For the wood materials the experiments were conducted on both dry and wet (saturated) surface materials.

It may be seen from the figures that wet surfaces produce better spreads than dry surfaces. In the cases of the wood surfaces, the drops tend to spread in the direction of the grain. The relative spread of the three retardants on paraffin is roughly consistent with their relative surface tensions, but water does not fit in the scheme. With the exception of water on paraffin, Fire-Trol 100 exhibited the least spread of all the retardants on all of the materials, both wet and dry. The spread of Phos-Chek and Fire-Trol 931 was about the same for pine and redwood surface, but for pressboard, fir and cedar the spread of Phos-Chek was greater. The general order of the surface materials for increased spreading is paraffin, pressboard, cedar, glass, redwood, pine and fir. This order results largely because of differences in water absorption by the surface material. For Fire-Trol 931, rough cedar absorbed water from drops fastest, as seen by the spread of a wet area around the drop, then plywood, pine and redwood. Pressboard doesn't absorb. For Phos-Chek, very little water is absorbed by the wooden surfaces. Cedar, the most absorptive, had only a very small water stain annulus about the drop. For Fire-Trol 100, only cedar exhibits the absorption of water. On glass, once the drop has completely dried, there was an irregular area of brittle, translucent, light green crystal around the central red area of the drop.

9.2.1.3 Experimental Results - Inclined Surface

The spreading of liquid retardant over inclined surface (same drop sizes) was studied using fir (plywood) at inclination angles (from horizontal) of 45° and 60° . The results, together with the flat (0°) surface results are shown in Figure 49. It is seen that spread area increases with inclination angle up to an approximately constant limiting angle near 60° . The retardant type order of spreading at inclined angles is the same as at 0° .

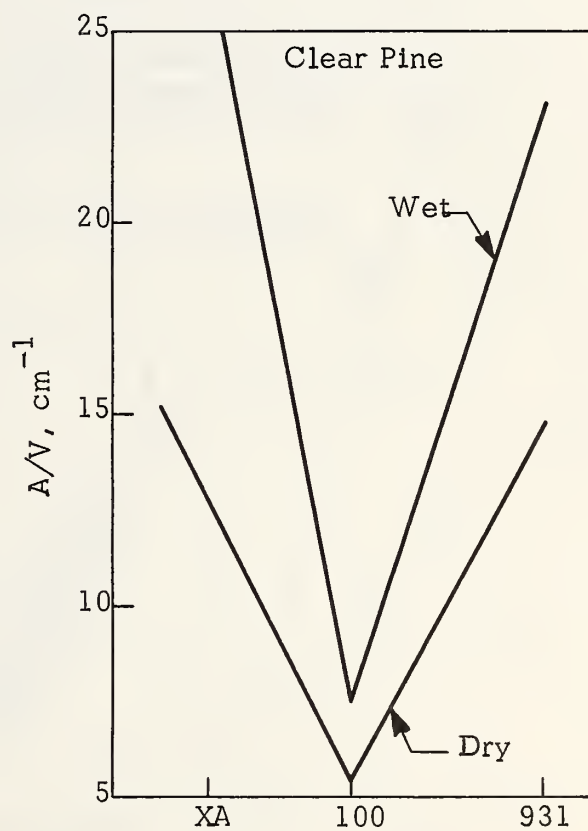
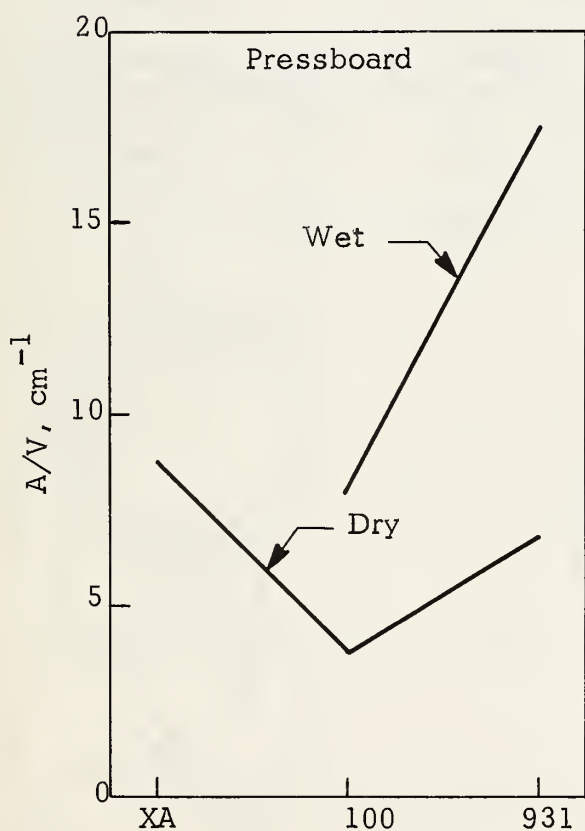
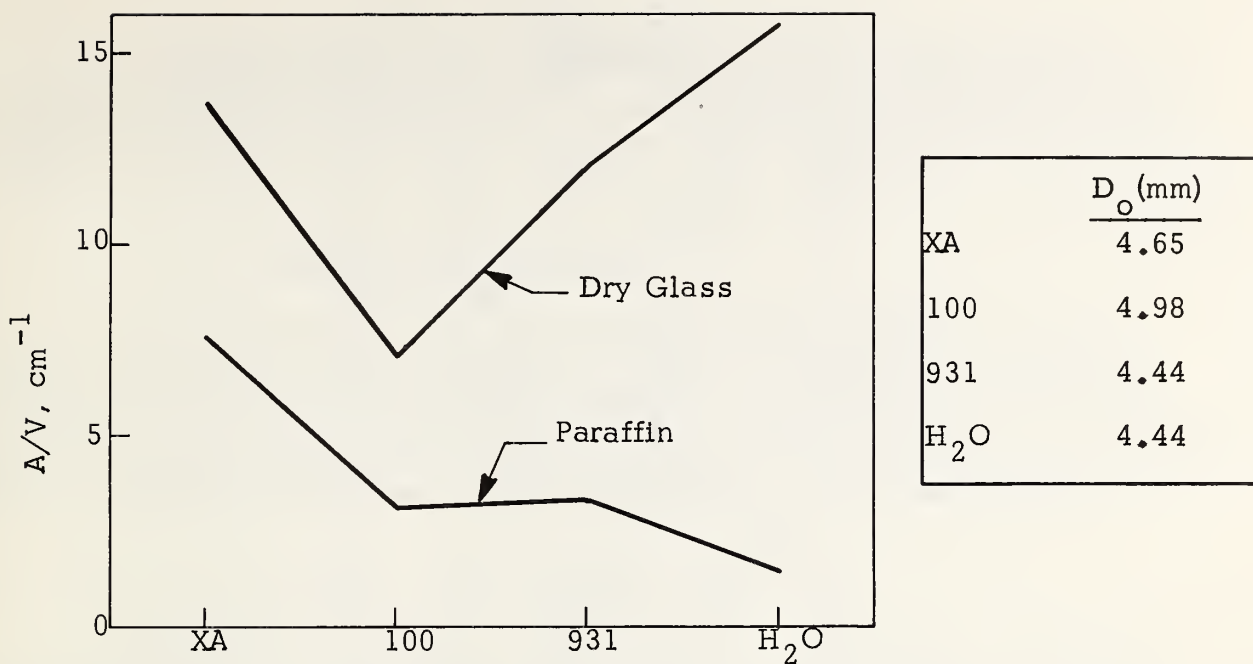


Figure 47. Static Spread of Liquid Retardant Drops Over Various Flat Material Surfaces.

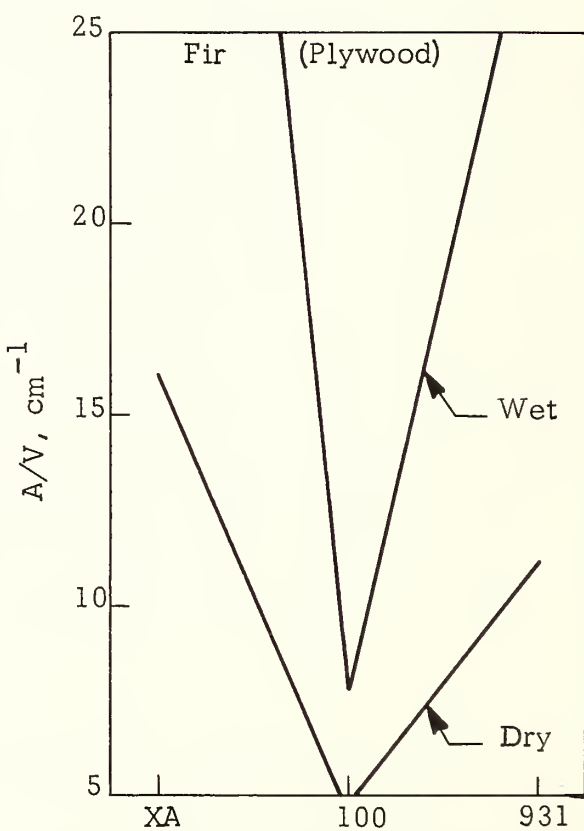
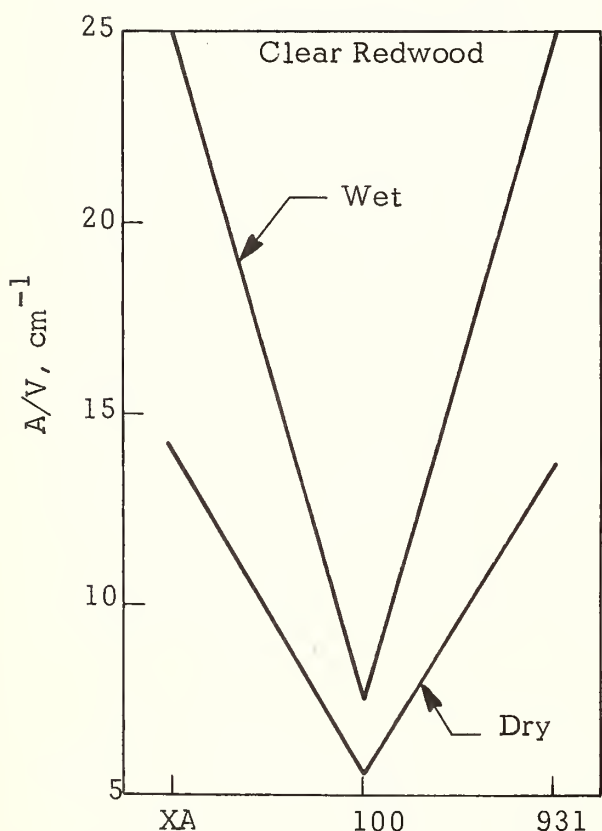
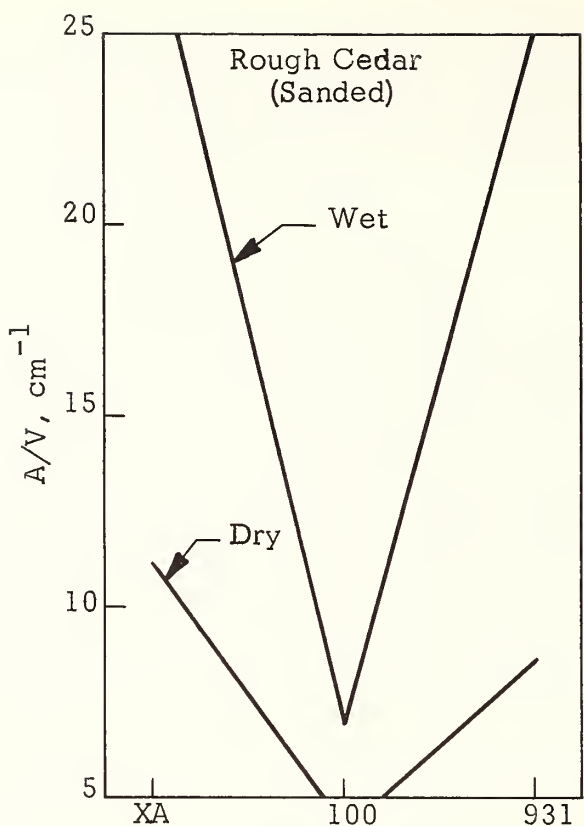


Figure 48. Static Spread of Liquid Retardant Drops Over Various Flat Material Surfaces.

The experiments were conducted with the grain of the wood both parallel and perpendicular to the incline. Small measurable differences were usually found between these two cases, but the effect of the grain direction was not consistent. The values given in the figure are averaged values of both cases.

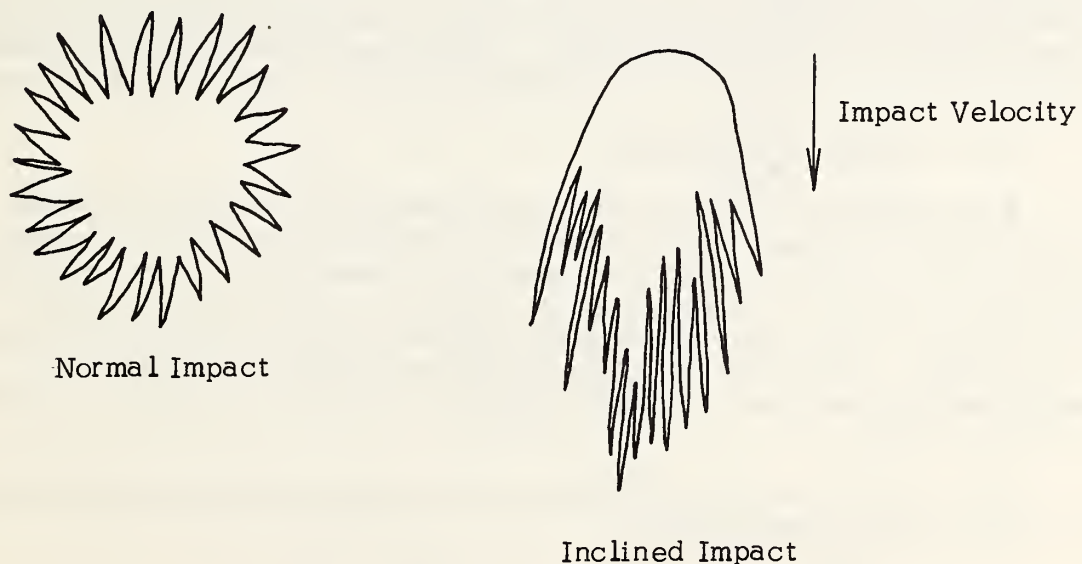
9.2.2 Drop Spread From Impact

In order to investigate the effects of impact velocity on droplet spread, experiments were conducted in which drops of the retardants (same size as in previous experiments) were dropped on fir (plywood) at different inclination angles from a height of 39'3". This height was used for convenience (it is a building height), but it can be estimated that drop velocities produced by this drop height should be a significant fraction of terminal velocity.

9.2.2.1 Splatter Patterns of Fire Retardants

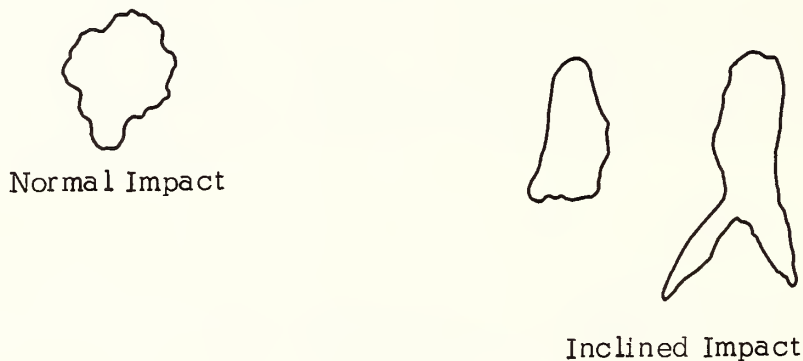
There are two distinct splatter patterns, depending on the type of thickener used in the retardant. The clay-thickened Fire-Trols 100 and 931, regardless of drop size, exhibit a starburst pattern of numerous striated rays emerging from a relatively large and well-coated central area. Target inclination was important in symmetry and predominant ray direction. Ten degree inclination yielded roughly circular patterns with rays emerging in all directions. With inclinations of 45 and 60 degrees, the patterns formed ellipses with elongations in the direction of the impact velocity vector. Rays emerged in predominantly this direction also, in a quasi-conical flared pattern. These general impact patterns are illustrated below.

SPLATTER PATTERNS OF THE FIRE-TROL SOLUTIONS



Gum-thickened Phos-Chek XA gave irregular, unsymmetrical patterns, with no striations or rays at any of the target inclinations. Instead, pseudopod-like extensions were in evidence. Drop signatures on inclined targets were elongated in the direction of impact velocity. Observations of this retardant during impact indicate that not all of the drop volume is deposited on the target; often, portions of the drop would rebound, or roll off the target. These general impact patterns are illustrated below.

SPLATTER PATTERNS OF PHOS-CHEK XA



9.2.2.2 Experimental Results

The results of the experiments are summarized in Figure 50. It may be seen that with the exception of Phos-Chek impacting the 60° inclined boards, the results are consistent with all the previous results, i.e., spread factors are smallest for Fire-Trol 100. The spread factor increases with increase in inclination angle, but the relative increase is much less than in the case of static spread. This indicates that the impact velocity produces essentially maximum spread at normal impact. The decrease in spread factors at 60° for Phos-Chek and Fire-Trol 931 is believed to be the result of liquid bounce from the surface rather than experimental error. The effect is particularly pronounced for the Phos-Chek and may relate to its elasticity under rapid loading conditions.

9.2.3 Effect of Drop Size

Some additional studies were conducted with Fire-Trol 100 using larger drops ($D_0 = 7.44\text{mm}$). The results are shown in Figure 51. A comparison of these results with those for the smaller (4.98mm) drops shows that the spread factors for the two cases are essentially the same within statistical scatter (the larger drop values are slightly smaller), except for the 60° case at 39 ft. drop height. These results imply that the spread areas observed are essentially maximum values, and that valid film thicknesses could be estimated from the spread areas.

Figure 52 shows typical pictures of the splotch patterns obtained on plywood in the various experiments.

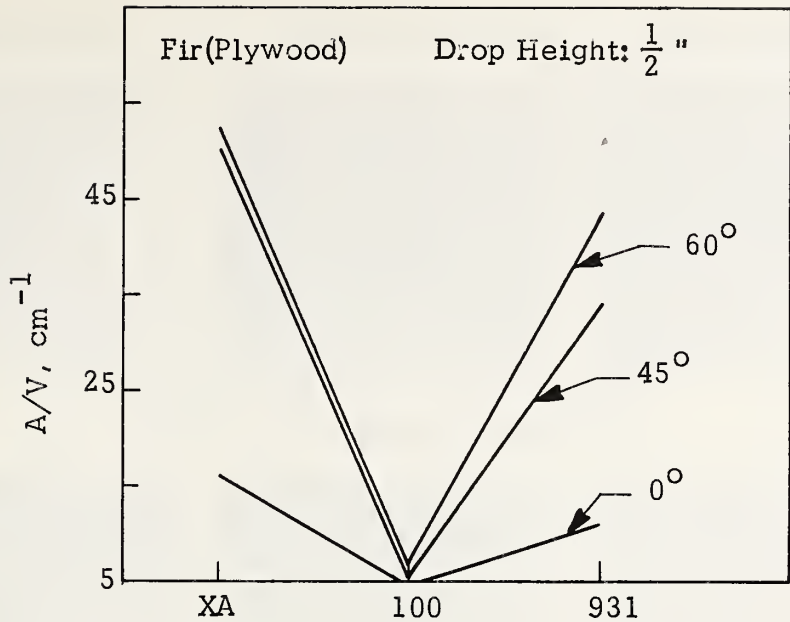


Figure 49. Static Spread of Liquid Retardant Over Flat and Inclined Plywood Surface.

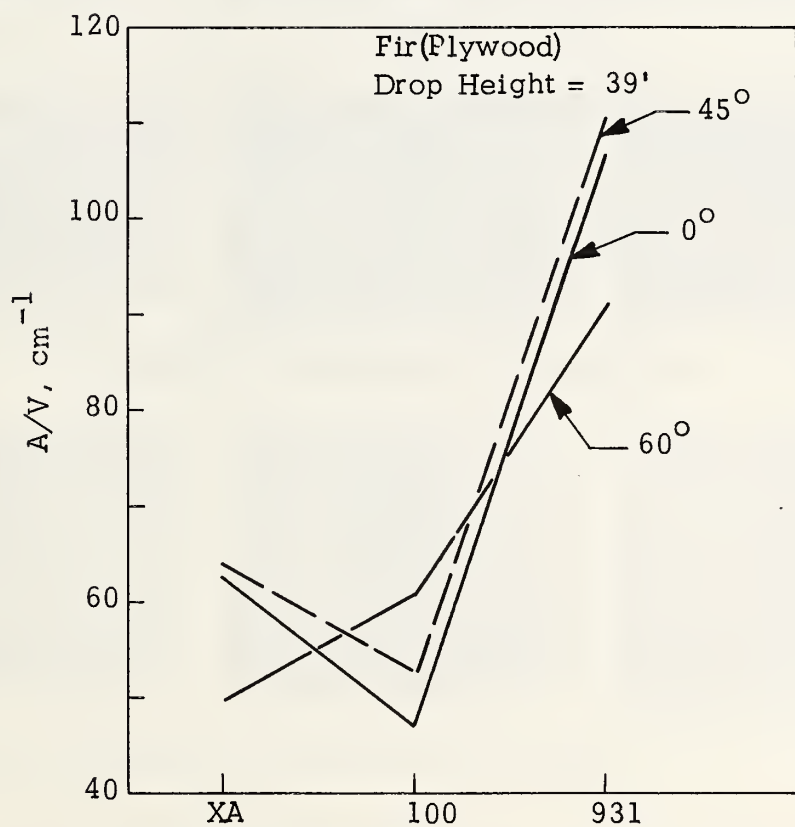


Figure 50. Dynamic Spread of Liquid Retardant Over Flat and Inclined Plywood Surface.

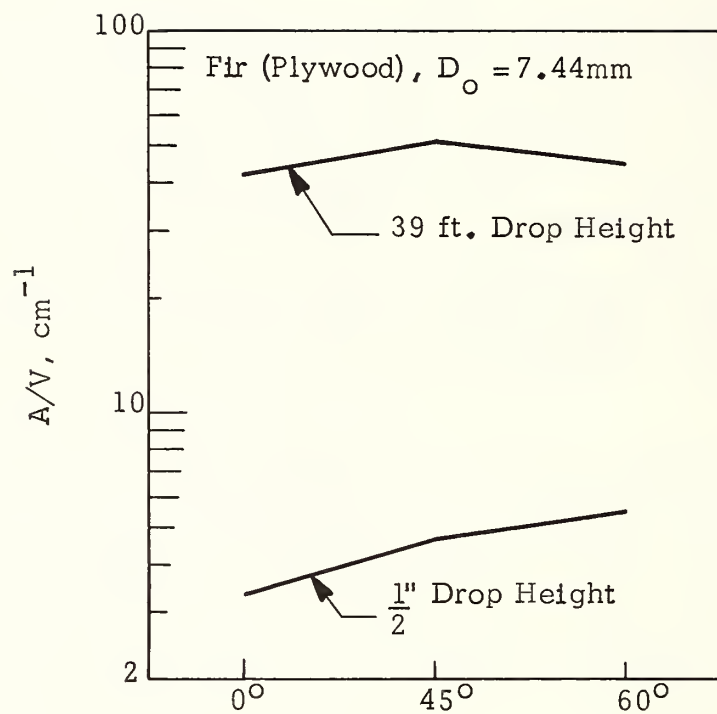
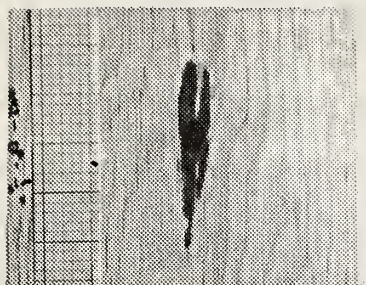
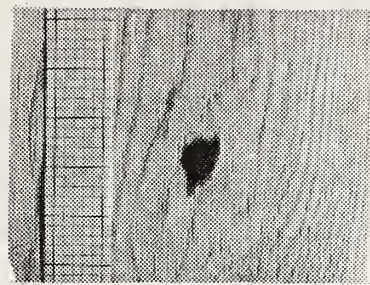


Figure 51. Static and Dynamic Spread of Large Drops of Fire-Trol 100 Over Flat and Inclined Plywood Surface.

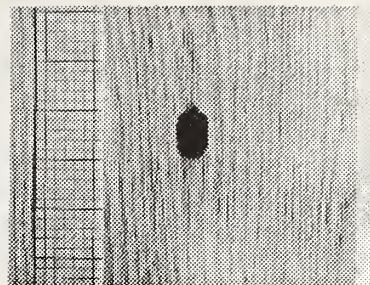
FIRE-TROL 931



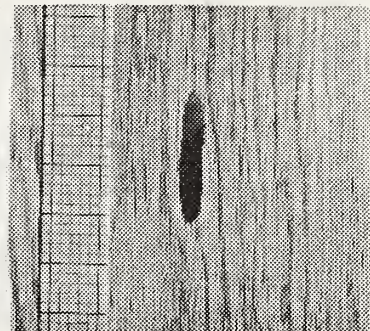
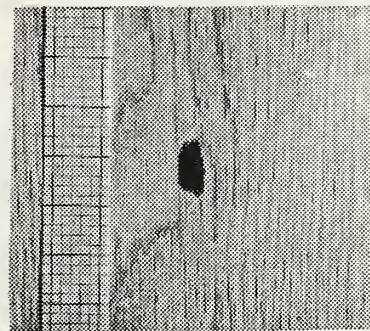
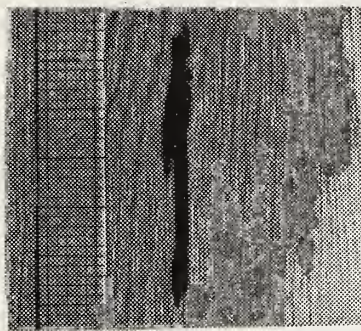
FIRE-TROL 100



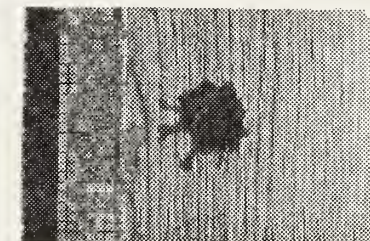
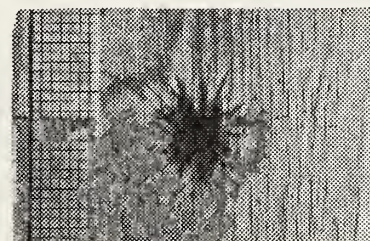
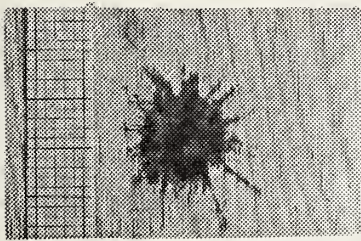
PHOS-CHEK XA



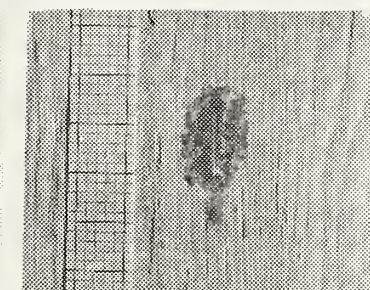
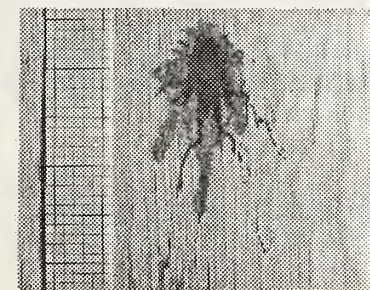
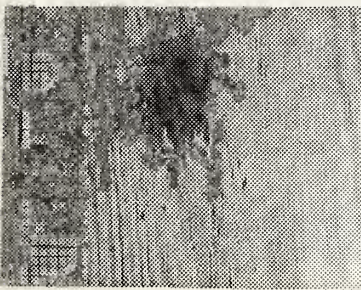
a. Static Spread Over Flat Surface (1 large division is $1/2"$)



b. Static Spread Over Inclined (45°) Surface



c. Dynamic Spread (39' Drop Height) Over Flat Surface



d. Dynamic Spread Over Inclined (45°) Surface

Figure 52. Splotch Patterns of Single Drops (4.5-5 mm) of Fire Retardant on Plywood.

9.2.4 Wetting Out of Fuels by Retardants

In order to obtain quick information regarding the relative abilities of retardants to be retained as stored liquid on a specified wetted fuel, a modified Grah-Wilson experiment was considered, and preliminary information obtained during the present program. The experiment consists in performing a Grah-Wilson experiment on the fuel in question-first with water and then (after suitable drying), with the retardant on the same fuel sample. This experiment gives the relative ability of the fuel to store the retardant with respect to water under the various conditions of the experiment, i.e., dynamic storage after fuel saturation is attained, static storage after drip, and static storage after fuel shaking. If the fuel sample can be suitably washed and dried after the retardant experiment, the experiment can be repeated with other retardants. Since the surface area of the fuel remains constant, the results of the experiments give the relative abilities of the retardants to adhere to the fuel as stored liquid with respect to water. If the fuel cannot be used again after treatment with the retardant, the experiment can be repeated with a different fuel sample for both water and a different retardant. Since the results of the retardant experiments are always with respect to water at constant fuel surface, various retardants can be rated relative to each other for various type fuels by conducting a series of relatively simple and rapid experiments. If the surface area of the fuel is known or the film thickness of water on the fuel is known, then the absolute film thickness of the retardant can also be estimated. However the estimation of the absolute surface area of a fuel element is generally subject to considerable error, and the estimation of the relative effectiveness of retardants to be retained as stored liquid appears to have considerable merit. During the program the preceding concept was subjected to preliminary study using water and Fire-Trol 100.

9.2.4.1 Experimental Procedure

For the experiments, two systems were constructed - one to deliver the liquid at a known flow rate onto the fuel, and the other to measure the added weight of the liquid as it is deposited onto the fuel. For the former system, a seven gallon, air-pressure driven spray paint reservoir can was converted to an overhand system of pipes and spray nozzle head. With known pressure within the reservoir, a constant spray was maintained. This spray formed a cone approximately 42 in. high and 30 in. wide at the base. To measure weight differences, a simple double - cantilever balance 36 in long was mounted on a strip of spring steel. As weight differences would tip the cantilever arms and flex the spring steel, strain gauges mounted on the spring steel would generate strain data which could be correlated to weight. A damper disc submerged in mineral oil was used to reduce the oscillations resulting from droplet impact against the fuel. The maximum excursion of the cantilever approximated a weight difference of about 300 grams, so that with proper counter-balancing beforehand, total weight changes of up to more than 800 grams could be measured. At highest sensitivities, weight differences of a gram could be detected. All weight data was recorded on a chart recorder.

A branch of oak, approximately 18 in. long and 9 in. in leaf diameter was chosen as the representative fuel. The branch was first allowed to dry in the air, then the test sequence performed using water. The branch was sprayed until a saturation weight was attained then allowed to drip without spraying to its lower equilibrium weight, and then shaken to a residual film weight. The branch was allowed to dry overnight, then the process repeated using Fire-Trol

100. During this latter test, the nozzle clogged before the dynamic saturation weight was necessarily achieved, making this weight rather uncertain. However, the percentage weight differences after drip and shake between Fire-Trol 100 and water demonstrated the utility of this technique in showing differences between the liquids.

9.2.4.2 Experimental Results

The results of the two experiments conducted are shown in Figure 53. It is evident that Fire-Trol 100 is much superior to water in its ability to be stored on the fuel under the conditions of the experiment. Thus the weight of the chemical retardant stored was about a factor of 6 to 7 greater than water for all three storage conditions, viz, dynamic, after drip, and after shaking. These values are slightly higher than those obtained by others⁶⁸, and further studies should be conducted to check the duplicatability of the experiments, and study other retardants and fuels.

10. CONCLUSIONS AND RECOMMENDATIONS

On the program analytical models were developed to describe the aerodynamic breakup of aerial delivered fire retardant. These models, together with shock tube and gas gun experiments, showed that the breakup characteristics-and hence the aerial dissemination characteristics - of liquid retardants depend significantly on the effective viscosity of the retardant. The effective viscosity describes the combined effects of fluid viscosity (which may be non-Newtonian) and fluid elasticity on liquid flow, and is shear rate dependent. Experimental measurements were made of the effective viscosity and surface tension of contemporary retardants, and the values used in the breakup models to estimate the breakup characteristics of the retardants under various conditions. It was shown that the breakup rate decreases and the droplet size increases as the effective viscosity of the retardant is increased. Particle size decreases in the following order for the retardants studied: Phos-Chek XA, Fire-Trol 100, Fire-Trol 931 and water. The ultimate ground effects of the aerial dissemination process such as effective ground pattern (area, length and width) and retardant recovery also generally decrease in the same order. It was concluded that the gum thickened retardant Phos-Chek is generally superior to the other retardants primarily because of its elastic nature-which allows it to maintain a high effective viscosity under aerial shear rate conditions. The large apparent viscosity of clay thickened Fire-Trol 100-as measured by conventional (Brookfield) methods-is somewhat misleading and is actually much reduced under aerial wind shear conditions so that the dissemination characteristics of this retardant are only slightly better than the shear thinning Fire-Trol 931, and water-which is Newtonian in behavior.

The breakup models showed that there are a number of interrelated (coupled) system parameters and fluid properties that control the aerial breakup of the retardant, and consequently its ground pattern-including particle size. On the program an examination was made of how many of these parameters and properties influence the breakup characteristics. However because of time limitations it was not possible to examine in detail the implications and predictions of the models in terms of existing ground pattern data on disseminated retardants, or vice versa. In order to make the most effective use of the models, such studies should be conducted. This would also allow potential improvement of the models as well as help to provide the best experimental values of certain constants that appear in the equations.

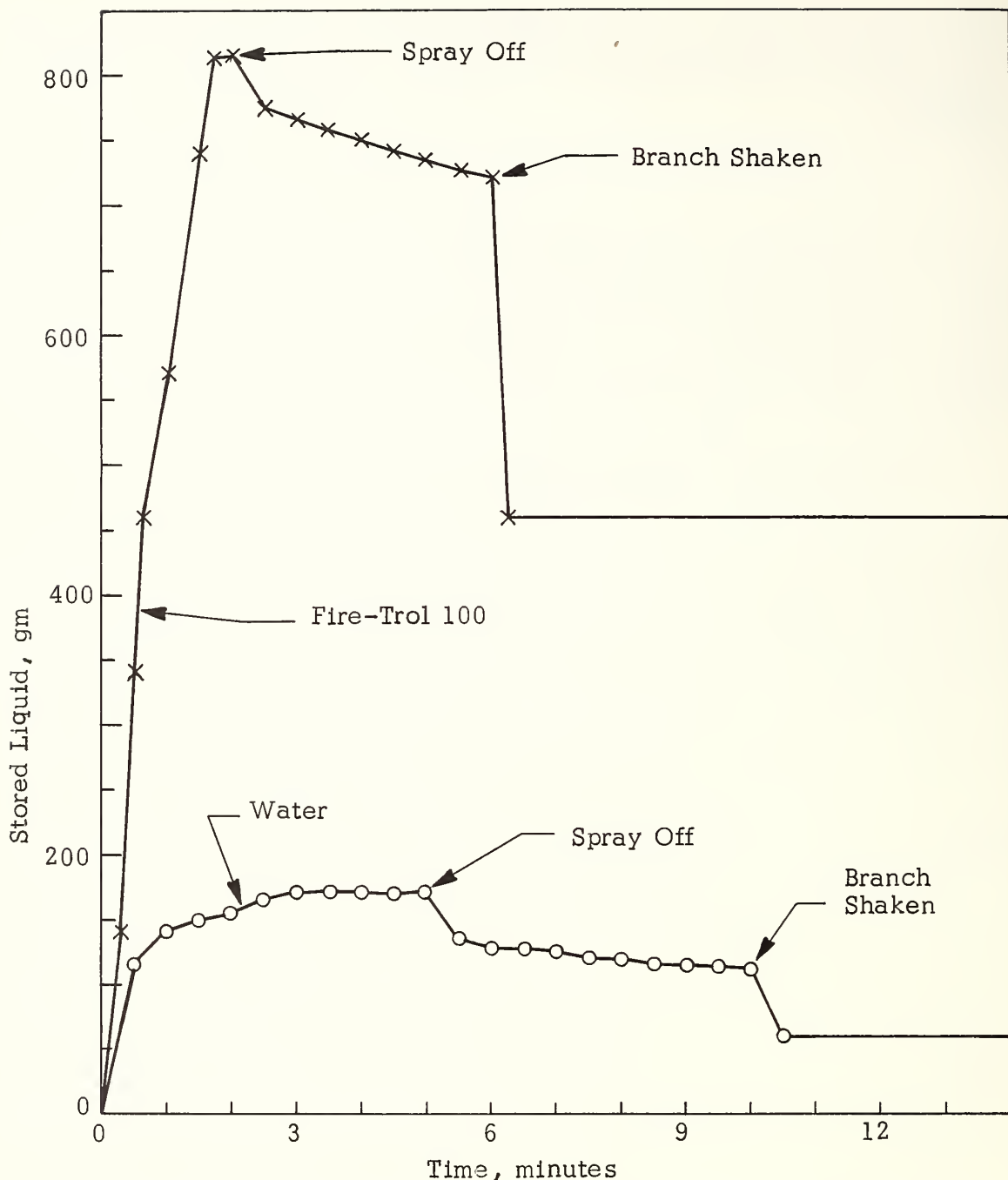


Figure 53. Results of a Grah-Wilson Experiment on a Common Oak Branch.

In view of the overall importance of elasticity to the breakup process it would also be desirable to investigate (both experimentally and analytically) the effect of gum thickener concentration (and type) on the rheological properties and aerodynamic breakup behavior of retardants. Also improved methods for measurement of fluid elasticity should be investigated since the high pressure capillary tube technique is relatively complex, time consuming, and only approximate in nature.

Preliminary studies on fuel wetting by retardants were also conducted on the program. These studies showed that the rheological properties of retardants have significant effect both on fuel wetting by dynamic droplet impaction, and on subsequent liquid storage by the fuel. Further studies leading to the development of analytical models that elucidate the important impact and fluid properties for impaction wetting and static film spread and storage should be conducted.

10.1 TEST PLANNING

In order to help check the analyses and predictions regarding the breakup of aerial delivered fire retardants conducted on the program, it is desirable that full scale tests be conducted that provide the necessary data for both checking the models and improving them. These tests should be conducted in a parametric manner, i.e., the important variables should be varied independently over a practical range with all other parameters being held constant. The parameters of most interest include aircraft velocity, drop height, liquid release characteristics (tank and gating system), and retardant rheological properties. Since wind effects represent a perturbation on the normal dissemination process, the preceding tests would best be conducted under no wind conditions. However since this is not generally feasible the effects of wind must be taken into consideration as is possible. The properties that should be measured in the tests include ground contour pattern (area, length, width and shape), retardant concentration distribution, retardant recovery, time for droplet impaction and cloud settling, and droplet (particle) size distribution.

However it will be observed that with the exception of the measurement of droplet size, the preceding tests are exactly of the type that the Forest Service has conducted in the past, and for which considerable data is available. Thus the measurement of droplet size under various conditions appears to be the most important new measurement that should be included in future tests. It would appear that for systems and retardants for which studies have been conducted in the past, that some of these tests could be usefully and relatively inexpensively be repeated by measuring only particle size in the tests. Before discussing droplet size measurement, a few further comments may be given regarding the tests and additional measurements that would be useful if found possible.

With regard to the tests themselves, aircraft velocity should be varied over a wider range than in the past if it is possible. Also the type or concentration of the thickening agents should be further changed in some cases so as to give additional values of deformation viscosity, Taylor breakup viscosity, and surface erosion viscosity in the tests (the rheological properties of these solutions would have to be measured in order to analyze the tests). Additional measurements (when or if they could be made) that would provide additional useful information include (1) measurement of the time of the initiation of the Taylor instability breakup of the deforming liquid, (2) measurement of the lateral

extent and/or thickness of the deformed liquid when Taylor breakup occurs, (3) measurement of the particle size produced by Taylor breakup, and (4) measurement of the lateral spread rate of the droplets during their settling.

10.1.1 Particle Size Measurement

The measurement of the droplet sizes of the rain produced by the aerial dissemination of a retardant is not easy. The problem has been examined by The Aerospace Corporation, whose report discussed various potential techniques.⁷⁰ They concluded-based on preliminary experimental studies-that a color photographic technique in which a grid with known spacing between the lines is photographed from some distance (30-40ft) with a telephoto lens at 200 frames/sec during droplet settling potentially represents a simple and inexpensive method for obtaining quantitative information regarding droplet sizes and shape. In the tests, all but four feet of drop zone nearest the grid in the camera's view is to be covered so that only those droplets within 4 ft of the grid are photographed. In this manner the size of the photographed droplets represents essentially the real size with respect to the grid spacing. Unless a relatively large camera-to-grid distance is employed and the droplet fall restricted to a short distance in front of the grid, the location of the droplets between the grid and camera can have a significant effect on the size of the droplet image that the camera records. In this case two synchronized cameras could be used to triangulate the droplet position, or a series of grids with known distances apart could be used to identify the position of some of the falling droplets.

In the studies, the measurement of particle size within the meaningful (high concentration) part of the ground pattern is of most importance. This region corresponds to the ground-pattern produced by the Taylor instability breakup of the liquid. However in some cases the particle size should also be measured in the ground pattern region preceding Taylor breakup. There may be differences in the particle sizes in the two regions since in the beginning region the particles arise only from peripheral stripping (surface erosion) of the bulk liquid; whereas in the meaningful part of the ground pattern they arise from Taylor breakup of the bulk liquid followed by surface erosion of the particles produced by the Taylor breakup.

REFERENCES

1. C. W. George and A. D. Blakely, "An Evaluation of the Drop Characteristics and Ground Distribution Patterns of Forest Fire Retardants," USDA Forest Service Res. Paper INT-134, IFR Experiment Station, Ogden, Utah, March 1973.
2. A. M. Kanury, "Ignition of Cellulosic Solids - A Review," Fire Research Abstracts and Review, 14, 24 (1972).
3. W. H. Andersen, Comb. Sci. Tech. 2, 213 (1970).
4. W. H. Andersen and H. E. Wolfe, "Aerodynamic Breakup of Liquids Drops," Proc. Fifth Shocktube Symp., NOL, April 1965; also Report 0395-04(18)SP, April 1964, AD 437340.
5. W. R. Lane, Ind. Eng. Chem. 43, 1312 (1951).
6. O. G. Engel, J. Res. NBS 60, 245 (1958).
7. E. Rabin, A. R. Schallenmuler and R. B. Lawhead, "Motion and Shattering of Burning and Nonburning Propellant Droplets," AFOSR-TN-59-129, March 1959; AFOSR-TR-60-75, March 1960.
8. A. R. Hanson, E. G. Domich and H. S. Adams, Phys. Fluids 6, 1070 (1963).
9. D. C. Jenkins and J. D. Booker, "The Time Required for High Speed Airstreams to Disintegrate Water Drops," C.P. No. 827, Ministry of Aviation, London, 1965.
10. C. C. Miesse, "From Liquid Stream to Vapor Trail," Proc. Gas Dynamics Symp., Northwestern Univ., 1956, pp 7-26.
11. A. A. Ranger and J. A. Nicholls, AIAA Journal 7, 285 (1969).
12. J. O. Hinze, App. Sci. Res. A1, 253, 273 (1949).
13. G. D. Gordon, J. App. Phys. 30, 1759 (1959).
14. E. Mayer, ARS Journal 31, 1783 (1961).
15. E. Y. Harper and G. W. Grube, "A Unified Theory of Raindrop Breakup," 8th Int. Shock Tube Symp., London, 1971.
16. E. Y. Harper, G. W. Grube and C. I-Dee, J. Fluid Mech. 52, Part 3, (1972).
17. M. A. Weiss and C. H. Worsham, ARS Journal 29, 252 (1959); Chem. Eng. Sci. 16, 1 (1962).
18. R. E. Brown, "The Atomization of a Solution of 2, 4-Dihydroxybenzophenone in Bis (2-Ethylhexyl) Hydrogen Phosphite," Report 0395-04(20)SP, Aerojet General Corp., Downey, Calif., May 1964.

REFERENCES (Continued)

19. R. E. Brown and K. L. Leonard, "Methods of Describing Droplet Size Distributions from Atomized Solutions," Report 0395-04(15)SP, May 1965.
20. A. C. Merrington and E. G. Richardson, Proc. Phys. Soc. 59, 1 (1947).
21. A. A. Putnam, et al., "Injection and Combustion of Liquid Fuels," WADC Tech. Report 56-344, March 1957.
22. G. Morrell, "Rate of Liquid Jet Breakup by a Transverse Shockwave," NASA TN-D-1728, Feb. 1963.
23. R. A. Dickerson, J. Spacecraft 6, 1306 (1969).
24. R. P. Fraser and P. Eisenklam, Trans. Inst. Chem. Engr. 34, 294 (1956).
25. B. J. Clark, "Breakup of a Liquid Jet in a Transverse Flow of Gas," NASA TN D-2424, Aug. 1964.
26. J. C. P. Huang, J. Fluid Mech. 43, 305 (1970).
27. N. Dombrowski, P. Eisenklam and R. P. Fraser, J. Inst Fuel 1, 399 (1957).
28. M. Goldin, J. Yerushalmi, R. Pfeffer and R. Shinnar, J. Fluid Mech. 38, 689 (1969).
29. W. H. Andersen and R. E. Brown, "Incendiary Munitions Analysis and Design Investigation," Report 6250-06 to Eglin AFB, Shock Hydrodynamics, July 1969.
30. W. H. Andersen and J. C. Tompkins, "Water Particle Loading of a Blast Wave Propagating Over a Water Surface," Final Report SHI-6055-04, To NOL, Shock Hydrodynamics, June 1968.
31. M. Adelberg, AIAA Journal 5, 1408 (1967); 6, 1143 (1968).
32. F. H. Ree, T. Ree and H. Eyring, Ind. Eng. Chem. 50, 1036 (1958).
33. J. R. Van Wazer, J. W. Lyons, K. Y. Kim and R. E. Colwell, Viscosity and Flow Measurement, Interscience, N.Y. 1963.
34. F. H. Gaskins and W. Philippoff, J. App. Pol. Sci. 2, 143 (1959).
35. W. Philippoff and F. H. Gaskins, Trans. Soc. Rheology 2, 263 (1958).
36. R. B. Bird and T. W. Spriggs, Phys. Fluids 8, 1390 (1965).
37. M. C. Williams and R. B. Bird, Phys. Fluids 5, 1126 (1962).
38. A. B. Metzner and A. P. Metzner, Rheologica Acta 9, 174 (1970).

REFERENCES (Continued)

39. T. Kotaka, M. Kurata and M. Tamura, J. App. Phys. 30, 1705 (1959).
40. D. H. Swanson, "High Altitude Retardant Drop Mechanization Study," Final Report, Vol. 1, to Northern Forest Fire Laboratory, Missoula, Montana, Honeywell, April 1973.
41. D. H. Swanson and T. N. Helvig, "Extended High Altitude Retardant Drop Mechanization Study," January 1974.
42. E. Y. Harper, G. W. Grube and I. D. Chang, J. Fluid Mech. 52, 565 (1972).
43. P. G. Simpkins and E. L. Bales, J. Fluid Mech. 55, 629 (1972).
44. J. B. Keller and I. Kolodner, J. App. Phys. 25, 918 (1954).
45. R. Bellman and R. H. Pennington, Quart. J. App. Math. 12, 151 (1954).
46. W. H. Andersen, Comb. Sci. & Tech. 2, 213 (1970); 5, 43 (1972).
47. B. L. Hicks, J. Chem. Phys. 22, 414 (1954).
48. A. D. Baer and N. W. Ryan, AIAA Journal 3, 884 (1965).
49. Private communication from D. W. Howard, Brookfield Engineering Laboratories, Inc.
50. J. M. Krieger and S. H. Maron, J. Appl. Phys. 23, 147 (1952); ibid., 25, 72 (1954).
51. J. M. Krieger and H. Elrod, J. Appl. Phys., 24, 134 (1953).
52. J. T. Bergen, ed., Viscoelasticity, Phenomenological Aspects, Academic Press, New York (1960).
53. F. H. Gaskins and W. Philippoff, Trans, Soc. Rheology 3, 181 (1959).
54. A. B. Metzner, W. T. Houghton, R. A. Sailor and J. L. White, Trans. Soc. Rheology 5, 133 (1961).
55. A. Weissberger, Ed., Physical Methods of Organic Chemistry, Vol. 1, Interscience, N.Y., 1945, Chapter 6.
56. R. E. Weast, Ed., Handbook of Chemistry and Physics, 46th Edition, The Chemical Rubber Co., Cleveland, 1965, P. F-27.
57. W. Van Meter, "Retardant Airdrop Simulation Pilot Study," Northern Forest Fire Laboratory, Missoula, August 1970.

REFERENCES (Continued)

58. S. Chandrasekhar, Hydrodynamic and Hydromagnetic Stability, Clarendon Press, Oxford, 1961.
59. C. W. George, "Effect of Drop Height on Retardant Ground Distribution Patterns from the CL-215," U.S. Forest Service Report, Missoula, Montana, Jan. 1973.
60. R. E. Leonard, "Mathematical Theory of Interception," Forest Hydrology, W. E. Sopper and H. W. Lull, Ed., Pergamon Press, 1967, pp. 131-136.
61. R. F. Grah and C. C. Wilson, J. Forestry 42, 890 (1944).
62. E. L. Hamilton and P. B. Rowe, "Rainfall Interception by Chaparral in California," Calif. State Board of Forestry, 1949.
63. G. K. Voight, Forestry Sci. 6, 2 (1960).
64. J. D. Helvey and J. H. Patric, Water Resources Res. 1, 193 (1965).
65. P. J. Zinke, "Forest Interception Studies in the United States," Forest Hydrology loc. cit., pp. 137-161.
66. H. F. Johnstone, W.E. Winsche and L.W. Smith, Chem. Rev. 44, 353 (1949).
67. C. S. Grove, S.T. Grove and A.R. Aidun, Fire Research Abstracts and Reviews, 4, 54 (1962).
68. D. H. Swanson and T. H. Helvig, "Capture of Retardants in Vertical Fuels," Final Report, Vol. 2 to Northern Forest Fire Laboratory, Missoula, Honeywell, April 1973.
69. H. E. Anderson, "Forest Fire Retardant: Transmission Through a Tree Crown," USDA Forest Service, Research paper in process of being published, 1974.
70. E. B. Anderson, et al, "Aerial Delivery Systems Program," Final Report, ATR-74(7299)-1, to U.S. Forest Service, The Aerospace Corporation, December 1973.

APPENDIX I
GLOSSARY OF TERMS

A	A constant given by Eq. (35a).
A_i	Initial amplitude of Taylor instability waves, cm; Eq. (39).
B	Dimensionless parameter having an experimental value of about 0.3, Eq. (7c). Also a parameter defined in Eq. (39).
C_d	Drag coefficient, dimensionless.
d	Liquid drop diameter, cm.
d_m	Mass mean diameter of droplets produced by the surface erosion of a liquid, cm.
D	Initial diameter of the particles produced by the Taylor instability breakup of a wind deformed liquid, cm, Eq. (41). Also, liquid droplet diameter, Eq. (89).
f	Parameter given by Eq. (15).
g	Parameter given by Eq. (16). Also the gravitational constant, Eq. (85).
G	Shear modulus of a liquid, dyne/cm ² , Eq. (30).
L	Wavelength of a capillary wave induced in a liquid surface by wind stress, cm, Eq. (6). Also the thickness of a liquid at time t during its wind deformation, Eq. (36).
L_e	Effective thickness of a wind deformed liquid when Taylor breakup occurs, cm, Eq. (47).
L_o	Length of the retardant tank on an aircraft, cm, Eq. (33).
\dot{M}	Mass formation rate of liquid droplets per unit area of liquid per unit time by the wind erosion (stripping) of the liquid, gm/cm ² sec, Eq. (20).
N	Droplet formation rate per unit area of a liquid per unit time by the wind erosion of the liquid, 1/cm ² sec, Eq. (13).
P	Stagnation pressure, dyne/cm ² .
P_n	Normal elastic stress in a shearing liquid, dynes/cm ² , Eq. (30).

R_e	Effective radius of the deforming liquid when Taylor breakup occurs, cm, Eq. (49).
R_o	Effective radius of the retardant tank on an aircraft, cm, Eq. (33).
s	Recoverable shear (elastic strain) of a liquid while undergoing steady shear, dimensionless, Eq. (30).
\dot{s}	Shear rate of a liquid, sec^{-1} . Also the shear rate of a liquid while undergoing surface erosion, Eq. (28).
\dot{s}_d	Effective shear rate of a liquid while undergoing wind deformation, sec^{-1} , Eq. (38).
\dot{s}_1	Effective shear rate of a liquid while undergoing Taylor instability growth, sec^{-1} , Eq. (44).
t	Time, sec.
t_b	Total breakup time of a liquid undergoing deformation and Taylor instability growth by wind stress, sec, Eq. (48).
t_d	Deformation time of a liquid by wind stress prior to its breakup by Taylor instability growth, sec, Eq. (34).
t_i	Breakup time of a liquid by Taylor instability growth subsequent to its deformation by wind stress, sec, Eq. (39).
t_m	Minimum time a wind must pass over a liquid surface before the wind stress causes wave growth and particle erosion from the surface, sec, Eq. (24).
t_r	Stress relaxation time of an elastic liquid, sec, Eq. (30).
t_s	The stripping breakup time of a liquid particle, sec, Eq. (5).
v	Liquid velocity induced by wind stress, cm/sec. Also the impaction or terminal velocity of a falling droplet, Eq. (89).
V	Air (wind) velocity, knots. Also the relative velocity between a liquid and an air flow.
V_e	Initial lateral velocity of the liquid particles formed by the Taylor instability breakup of a deforming liquid, cm/sec, Eq. (50).
V_o	Volume of the retardant tank on an aircraft, gallons, Eq. (33).
γ	Yield stress of a liquid, dynes/cm ² , p. 49.

β Sheltering parameter of a wind-induced capillary wave, dimensionless, Eq. (7a).

γ The shear of a liquid, dimensionless.

η Viscosity or effective viscosity of a liquid, poise.

η_1 Effective viscosity of a liquid undergoing Taylor instability growth, poise.

η_d Effective viscosity of a liquid undergoing wind deformation, poise.

η_e Effective viscosity of a flowing liquid, poise, Eq. (31).

λ Wavelength of a Taylor instability wave, cm, Eq. (40).

ρ Ambient air density, gm/cc. Also, shocked air density.

ρ_1 Liquid density, gm/cc.

σ Liquid surface tension, dyne/cm.
Also liquid shear stress (P_{xy}), dynes/cm².

τ The time required for wind to form and break a capillary wave with wavelength, L, from a liquid surface, sec, Eq. (6).

APPENDIX II

DERIVATION OF EFFECTIVE VISCOSITY EQUATION*

The following discussion presents a rational basis for the characterization of an elastoviscous medium. Starting with a power balance gives

$$P = \oint \vec{da} \cdot \vec{T} \cdot \vec{v} = \dot{U}_1 + \dot{U}_2 + D \quad (1)$$

where

da is differential area

T is the stress tensor

\vec{v} is the particle velocity,

U_1 is the strain energy ($U_1 = \int W dV$)

D is the dissipation, the dots represent material time derivatives

U_2 is the kinetic energy ($U_2 = \int K dV$), where

$$K = \frac{\rho_1}{2} v^k v_k \quad (2)$$

and ρ_1 is liquid density.

Converting the left hand member of Eq. (1) to a volume integral gives

$$\int \nabla \cdot (T \cdot \vec{v}) dV = \int dV (\rho_1 \vec{v} \cdot \vec{a} + D + \dot{W}) \quad (3)$$

or

$$(\nabla \cdot T) \cdot \vec{v} + T : \vec{v} \nabla = \rho_1 \vec{v} \cdot \vec{a} + D + \dot{W} \quad (4)$$

The first member of each side of Eq. (4) balance. A modified Stoke's law is now introduced,

$$T = -pI + 2\eta d \quad (5)$$

*This derivation was obtained by Dr. P. J. Blatz

where I is the unit tensor, and

$$d = \frac{(I + \tau \vec{v} \cdot \nabla) \cdot (I + \tau \nabla \vec{v}) - I}{2\tau} \quad (6)$$

Therefore

$$T : \vec{v} \cdot \nabla = \eta (\nabla \vec{v} + \vec{v} \cdot \nabla + \tau \vec{v} \cdot \nabla \cdot \nabla \vec{v}) : \vec{v} \cdot \nabla \quad (7)$$

or

$$T : \vec{v} \cdot \nabla = \eta d \cdot (I + \tau d) \quad (8)$$

Thus the work that goes into dissipation and strain energy increase consists of two parts:

(1) Strain energy increase, $\dot{W} = \eta d \cdot I$, and

(2) Viscous dissipation, $D = \tau \eta d \cdot d$

For one dimensional flow, the term $(I + \tau d)$ is equivalent to $(1 + s)$, where s is the elastic strain (recoverable shear) of the medium. Therefore the effective viscosity, η_e , of the medium is given by

$$\eta_e = \eta (1 + s) \quad (9)$$

APPENDIX III

DERIVATION OF LIQUID CYLINDER DEFORMATION RATE EQUATIONS*

Consider a cylinder of an incompressible liquid of density ρ_1 with an initial length L_o and initial radius R_o . The front surface of the cylinder is exposed to wind flow in the normal (z) direction, which exerts a pressure P at the stagnation point (axis) of the cylinder. The radial stress distribution over the front face of the cylinder is assumed to be parabolic, i.e., $-P + QR^2$; over the back face it is TR^2 , and along the cylindrical surface it is $-U$, where R is axial distance and P , T and U require determination.

The stress components in the liquid are given by

$$\sigma_r = \eta \dot{S} - p \quad (1)$$

$$\sigma_\theta = \eta \dot{S} - p \quad (2)$$

$$\sigma_z = -2\eta \dot{S} - p \quad (3)$$

where η is liquid viscosity, \dot{S} is shear rate and p is fluid pressure. Utilizing mass conservation it is assumed that

$$\dot{R} = u = \frac{\dot{S}}{2} R ; \quad R = R_o \exp(S/2) \quad (4)$$

$$\dot{z} = w = -\dot{S}z ; \quad z = L = L_o \exp(-S) \quad (5)$$

where S is total shear, and the dots indicate time derivatives. From the momentum balance equations**

$$\frac{\partial p}{\partial R} = -\rho_1 R \left(\frac{\ddot{S}}{2} + \frac{\dot{S}^2}{4} \right) \quad (6)$$

$$\frac{\partial p}{\partial z} = -\rho_1 z (-\ddot{S} + \dot{S}^2) \quad (7)$$

which integrate to give

$$p = p_o - \rho_1 \frac{R^2}{2} \left(\frac{\dot{S}^2}{4} + \frac{\ddot{S}}{2} \right) - \rho_1 \frac{z^2}{2} (\dot{S}^2 - \ddot{S}) \quad (8)$$

* This derivation was obtained by Dr. P. J. Blatz.

** The shear terms vanish by definition, and the viscous terms also drop out since it is postulated that u and w are linear in r and z , respectively.

Substituting Eq. (8) in Eq. (1) and (3) and evaluating the stress at the liquid boundaries gives

$$2U = -\rho_1 (\dot{S}^2 - \ddot{S}) \quad (9)$$

$$Q = \frac{\rho_1}{4} \left(\frac{\dot{S}^2}{4} + \frac{\ddot{S}}{2} \right) \quad (10)$$

$$T = -2\eta \dot{S} - p_o + \frac{\rho_1}{4} \left(\frac{\dot{S}^2}{4} + \frac{\ddot{S}}{2} \right) \quad (11)$$

Hence

$$-P = -3\eta \dot{S} + \rho_1 \frac{L^2}{2} (\dot{S}^2 - \ddot{S}) - \rho_1 \frac{R^2}{2} \left(\frac{\dot{S}^2}{4} + \frac{\ddot{S}}{2} \right) \quad (12)$$

Integrating Eq. (12) gives the shear, S , of the liquid as a function of time, t , and initial length and radius of the cylinder, i.e.,

$$t = \frac{1}{2KS^2} + \frac{2\eta}{P} S \quad (13a)$$

$$K^2 = \frac{8P}{\rho_1 (2L_o^2 + R_o^2)} \quad (13b)$$

The length, L , and radius, R , of the deforming cylinder at any time is related to the liquid shear by Eq. (4) and (5).

